Final Report

Site-Specific Seismic Hazard Analyses and Development of Time Histories for Resolution Copper's Proposed Skunk Camp Tailings Storage Facility, Southern Arizona

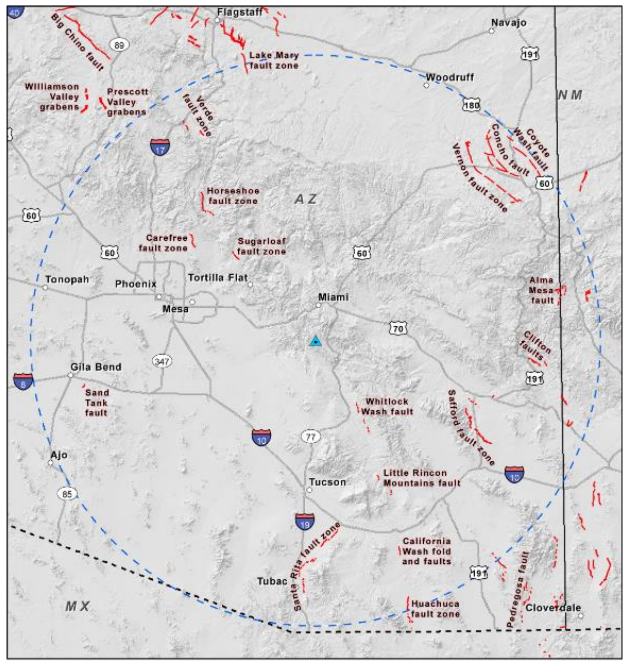

Prepared for:

Resolution Copper

Prepared by:

Ivan Wong, Patricia Thomas, and Nora Lewandowski
Lettis Consultants International, Inc.
1000 Burnett Ave Ste 350
Concord, CA 94520

Ross Hartleb
Lettis Consultants International, Inc.
27441 Tourney Rd Ste 220
Valencia, CA 91355

6 January 2020

TABLE OF CONTENTS

List of Tables

List of Figures

ABBREVIATIONS AND ACRONYMS

ABSMOOTH	LCI proprietary software that computes recurrence parameters from earthquake catalogs
BADCT	Arizona Mining Guidance Manual (Best Available Demonstrated Control Technology)
EPRI/DOE/NRC	Electric Power Research Institute/Department of Energy/ Nuclear Regulatory Commission
GMM	Ground motion model
HAZ45	PSHA computer program developed by Norm Abrahamson
KCB	Klohn Crippen Berger
MMI	Modified Mercalli intensity
M	Moment magnitude
m_b	Body-wave magnitude
M_D	Coda duration magnitude
M_I	Intensity-based magnitude
M_L	Richter local Magnitude
M_N	Nuttli magnitude
MASW	Multi-channel-anaylsis-of-surface-waves
NEHRP	National Earthquake Hazards Reduction Program
NGA	Next Generation of Attenuation
NSHM	National Seismic Hazard Maps
PEER	Pacific Earthquake Engineering Research Center
PGA	Peak horizontal ground acceleration
PSHA	Probabilistic seismic hazard analysis
SA	Spectral acceleration
SBR	Southern Basin and Range Province
UCERF2	Uniform California Earthquake Rupture Forecast, Version 2
UCERF3	Uniform California Earthquake Rupture Forecast, Version 3
UHS	Uniform Hazard Spectrum
USGS	U.S. Geological Survey
V_S	Shear-wave velocity
V_S30	Time-averaged V_S in top 30 m

Executive Summary

This report presents the results of a site- specific probabilistic seismic hazard analysis (PSHA) and deterministic seismic hazard analysis (DSHA) for the proposed Skunk Camp Tailings Storage Facility (TSF) site in southern Arizona. This study builds upon the site-specific hazard analysis performed for Resolution Copper's Near West site (Wong *et al*., 2017) 32 km to the northwest.

The objective of this study is to estimate the levels of ground motions that could be exceeded at specified annual frequencies (or return periods) and to compare the site-specific PSHA results with the results of a DSHA. The site is located in the Basin and Range Province of southern Arizona. Southern Arizona has a low level of seismicity compared to the rest of the western U.S. The Skunk Camp site is located about 52 km northeast of the Whitlock Wash fault zone which is the nearest Quaternary active fault capable of generating large earthquakes (**M** > 6.5).

In this study, geologic and seismologic data were used to evaluate and characterize potential seismic sources, the likelihood of earthquakes of various magnitudes occurring on those sources, and the likelihood of the earthquakes producing ground motions over a specified level. Uncertainties in models and parameters are incorporated into the PSHA through the use of logic trees. Based on the PSHA, Uniform Hazard Spectra (UHS), and time histories were developed. The study was performed considering Appendix E "Engineering Design Guidance" of the Arizona Mining BADCT Guidance Manual.

The inputs into the PSHA consist of a seismic source characterization model, ground motion models, and a range of site conditions corresponding to firm rock. The seismic sources include both crustal faults capable of generating large surface-faulting earthquakes and an areal source zone to account for background seismicity that cannot be attributed to identified faults explicitly already included in the seismic source model. All known Quaternary active or potentially active faults within 200 km of the site were included in the analysis. We also included longer, more active faults beyond 200 km in southern California and Baja California such as the San Andreas fault. A total of 47 faults are included in the seismic source model. For each fault, (1) rupture scenarios, (2) probability of activity, (3) fault geometry including rupture length, rupture width, orientation, and sense of slip, (4) maximum or characteristic magnitude and (5) earthquake recurrence including both recurrence model and rates were included in the seismic source model.

The Next Generation of Attenuation (NGA)-West2 ground motion models (GMMs) and one European GMM were selected based on the seismotectonic setting and used in the hazard analyses to estimate ground motions as a function of magnitude, distance, and site condition among other parameters.

The results of the PSHA in terms of peak horizontal ground acceleration (PGA) are tabulated below for a range of return periods. The probabilistic seismic hazard at the site is low consistent with the observations of low levels of tectonic activity and historical seismicity in the surrounding region.

Return Period (yrs)	PGA (g's)
475	0.04
2,500	0.08
5,000	0.11
10,000	0.16

A DSHA for a scenario **M** 6.9 earthquake on the Whitlock Wash fault, at a rupture distance of 52 km was performed. The 84^{th} percentile PGA was 0.09 g. Nine horizontal-component time histories for a 10,000 year return period were also developed.

1.0 INTRODUCTION

This report presents the results of a site- specific probabilistic seismic hazard analysis (PSHA) and deterministic seismic hazard analysis (DSHA) for the proposed Skunk Camp Tailings Storage Facility (TSF) site in southern Arizona.

1.1 Purpose

The objective of this study is to estimate the levels of ground motions that could be exceeded at specified annual frequencies (or return periods) and to compare the site-specific PSHA results with the results of a DSHA. The site is located in the Basin and Range Province of southern Arizona southeast of the town of Superior and south of Miami (Figure 1). Southern Arizona has a low level of seismicity compared to much of the rest of the western U.S. (Figure 2). The Skunk Camp TSF site is located about 52 km northwest of the nearest Quaternary active fault, the Whitlock Wash fault zone (Figure 3).

In this study, geologic and seismologic data were used to evaluate and characterize potential seismic sources, the likelihood of earthquakes of various magnitudes occurring on those sources, and the likelihood of the earthquakes producing ground motions over a specified level. This updated study builds upon numerous studies that have been performed for dams and other mining facilities in central and southern Arizona, including most recently the evaluation of Resolution Copper's Near West site (Wong *et al*., 2017). We included Quaternary faults within 200 km of the site in our hazard analyses. Due to the generally low seismic hazard, we also included more distant but more active faults in southern California (Figure 4).

The PSHA methodology is used in this study for assessing ground motion hazard. The evaluation of seismic hazard required the explicit inclusion of the range of possible interpretations of components in the seismic hazard model, including seismic source characterization and ground motion estimation. Uncertainties in models and parameters are incorporated into the PSHA through the use of logic trees (Figure 5). The following report presents the seismic source characterization, the ground motion models used in the PSHA and DSHA, the probabilistic and deterministic ground motion hazard results, calculation of Uniform Hazard Spectra (UHS), and development of time histories.

1.2 Scope of Work

The scope of work performed is described in as follows:

Task 1 – Seismic Source Characterization and Fault Reconnaissance

All local and regional active faults surrounding the project area that may be significant in terms of ground shaking hazard were included in the site-specific probabilistic seismic hazard analysis (PSHA). A seismic source model for southeastern Arizona was utilized. A field reconnaissance of the Dripping Springs fault, a normal fault which intersects the project area, was also performed to assess the likelihood of the fault being active in Quaternary period. We also evaluated other local faults around the Project area to determine whether the seismic source model needed to be updated. Fault parameters that were characterized included geometry and rupture dimensions, maximum earthquake, nature and amount of slip for the maximum earthquake, and rate and nature of earthquake recurrence. The hazard from crustal background seismicity was included in the analysis using regional seismic source zones and gridded seismicity.

Task 2 – Evaluation of Historical and Contemporary Seismicity

The historical and contemporary seismicity was evaluated in the Project region based on an updated seismicity catalog. Historical ground shaking in the Project area from past earthquakes was evaluated. Recurrence rates of the historical seismicity for defined regional seismic source zones were developed for input into the PSHA.

Task 3 – Site Characterization

The available geological, geophysical, and geotechnical information for the Project area was reviewed including shear-wave velocity (V_S) data so that a V_S30 (time-averaged V_S in the top 30 m) for the site can be computed. V_S30 is an input parameter into the ground motion models (GMMs). We assumed rock site conditions.

Task 4 – Probabilistic Seismic Hazard Analysis (PSHA)

Based on the seismic source model for the region and ground motion models, site-specific probabilistic hazard was calculated for the Project area. State-of-the-art ground motion models were used in the PSHA and deterministic seismic hazard analysis (DSHA) included the Pacific Earthquake Engineering Research (PEER) Center's Next Generation of Attenuation (NGA)-West 2 models.

Hazard curves and horizontal Uniform Hazard Spectra (UHS) for the return periods of 475, 2,500, 5,000 and 10,000 years at 5%-damping were calculated. The horizontal hazard was deaggregated at selected periods to characterize the controlling earthquakes. The probabilistic hazard was compared with the 2014 U.S. Geological Survey National Seismic Hazard Maps (NSHM), which are for a firm rock site condition (V_S30 of 760 m/sec).

Task 5 – Deterministic Seismic Hazard Analysis (DSHA)

A DSHA was performed for the most significant seismic sources to the Project area using the NGA-West 2 ground motion models. The ground motions from the controlling deterministic earthquakes were compared to the UHS from the PSHA.

Task 6 – Design Earthquake Ground Motions

Design Earthquake ground motions were selected based on the results of the PSHA and in consultation with KCB and in accordance with best practices.

Task 7 – Time Histories

Nine single-component horizontal time histories were developed by spectrally matching seed time histories to the selected Design Earthquake spectrum. Attention was paid to selecting seed time histories whose spectral shape, magnitude, duration, and Arias intensity are similar to the Design Earthquake properties.

1.3 ACKNOWLEDGEMENTS

This study was performed on behalf of Resolution Copper. Our thanks to Kate Patterson of Klohn Crippen Berger (KCB) for her project management support, Joseph Quinn (KCB) for his review of the draft report, and Tom White (Resolution Copper), Aaron Graham (Westland Resources), Christopher Kowalchuk (KCB), and Lillian Wavering (Resolution Copper) for their assistance in the field reconnaissance.

2.0 PSHA METHODOLOGY

The PSHA approach used in this study is based on the model developed principally by Cornell (1968). The occurrence of earthquakes on a fault is assumed to be a Poisson process. The Poisson model is widely used and is a reasonable assumption in regions where data are sufficient to provide only an estimate of average recurrence rate (Cornell, 1968). When there are sufficient data to permit a real-time estimate of the occurrence of earthquakes, the probability of exceeding a given value can be modeled as an equivalent Poisson process in which a variable average recurrence rate is assumed. The occurrence of ground motions at the site in excess of a specified level is also a Poisson process, if (1) the occurrence of earthquakes is a Poisson process, and (2) the probability that any one event will result in ground motions at the site in excess of a specified level is independent of the occurrence of other events.

The probability that a ground motion parameter "*Z*" exceeds a specified value "*z*" one or more times in a time period "t" is given by:

$$p(Z > z) = 1\text{-}e^{-\nu(z)\cdot t} \quad (1)$$

where $\nu(z)$ is the annual mean number (or rate) of events in which *Z* exceeds *z*. It should be noted that the assumption of a Poisson process for the number of events is not critical. This is because the mean number of events in time t, $\nu(z)\cdot t$, can be shown to be a close upper bound on the probability p(*Z* > *z*) for small probabilities (less than 0.10) that generally are of interest for engineering applications. The annual mean number of events is obtained by summing the contributions from all sources, that is:

$$\nu_k(Z > z) = \sum_n \nu_{kn}(Z > z) \quad (2)$$

where $\nu_{\kappa n}(Z>z)$ is the annual mean number (or rate) of events on source n for which *Z* exceeds *z* at site k. The parameter $\nu_{kn}(Z>z)$ is given by the expression:

$$\nu(Z > z) = \sum_n \alpha_n \left(M^0\right) \int_{M^0}^{M_n^u} f_n(M) \left[\int_0^\infty f_{kn}(r|M) \cdot P_{kn}(Z > z|M,r) \cdot dr\right] \cdot dM \quad (3)$$

where $\alpha_n(M^0)$ is the rate of all earthquakes on source *n* above a minimum magnitude, M^0; $f_n(M)$ is the probability density function of earthquake magnitude between M^0 and a maximum earthquake that source *n* can produce, M_n^u (i.e., recurrence model); $f_{kn}(r|M)$ is the conditional probability density function for distance from site *k* to an earthquake of magnitude *M* occurring on source *n*; and $P_{kn}(Z>z|M,r)$ is the conditional probability that, given an earthquake of magnitude *M* at distance *r* from site *k*, the ground motion (Z) will exceed the specified level *z*. Distance *r* is calculated as the closest distance from the rupture to the site.

Calculations were made using the computer program HAZ45 developed by Norm Abrahamson, which has been validated using the test cases in the Pacific Earthquake Engineering Research (PEER) Center-sponsored "Validation of PSHA Computer Programs" Project (Thomas *et al.*,

2010) as well as the follow-on PEER PSHA Computer Program Validation Project (Hale *et al*., 2018).

2.1 SEISMIC SOURCE CHARACTERIZATION

Two types of earthquake sources are characterized in this PSHA: (1) fault sources; and (2) areal source zones (Section 5.1). Fault sources are modeled as three-dimensional fault surfaces and details of their behavior are incorporated into the source characterization. Areal source zones are regions where earthquakes are assumed to occur randomly. Seismic sources are modeled in the hazard analysis in terms of geometry and earthquake recurrence.

The geometric source parameters for faults include fault location, segmentation model, dip, and thickness of the seismogenic zone. The recurrence parameters include recurrence model, recurrence rate (slip rate or average recurrence interval for the maximum event), slope of the recurrence curve (*b*-value), and maximum magnitude. Clearly, the geometry and recurrence are not totally independent. For example, if a fault is modeled with several small segments instead of large segments, the maximum magnitude is lower, and a given slip rate requires many more small earthquakes to accommodate a cumulative seismic moment. For areal source zones, only the areas, maximum magnitude, and recurrence parameters (based on the historical earthquake record) need to be defined.

Uncertainties in the seismic source parameters as described below were incorporated into the PSHA using a logic tree approach (Figure 5). In this procedure, values of the source parameters are represented by the branches of logic trees with weights that define the distribution of values. A sample logic tree for a fault is shown on Figure 5. In general, three values for each parameter were weighted and used in the analysis. Statistical analyses by Keefer and Bodily (1983) indicate that a three-point distribution of 5th, 50th, and 95th percentiles weighted 0.185, 0.63, and 0.185 (rounded to 0.2, 0.6, and 0.2), respectively, is the best discrete approximation of a continuous distribution. Also they found that the 10th, 50th, and 90th percentiles weighted 0.3, 0.4, and 0.3, respectively, can be used when limited available data make it difficult to determine the extreme tails (i.e., the 5th and 95th percentiles) of a distribution. Note that the weights associated with the percentiles are not equivalent to probabilities for these values, but rather are weights assigned to define the distribution. We generally applied these guidelines in developing distributions for seismic source parameters with continuous distributions (e.g., Mmax, fault dip, slip rate or recurrence) unless the available data suggested otherwise. Estimating the 5th, 95th, or even 50th percentiles is typically challenging and involves subjective judgment given limited available data.

Source Geometry

In the PSHA, it is assumed that earthquakes of a certain magnitude may occur randomly along the length of a given fault or segment. The distance from an earthquake to the site is dependent on the source geometry, the size and shape of the rupture on the fault plane, and the likelihood of the earthquake occurring at different points along the fault length. The distance to the fault is defined to be consistent with the specific GMM used to calculate the ground motions. The distance, therefore, is dependent on both the dip and depth of the fault plane, and a separate distance function is calculated for each geometry and each GMM. The size and shape of the rupture on the fault plane are dependent on the magnitude of the earthquake; larger events rupture longer and wider portions of the fault plane. The rupture dimensions were modeled following the magnitude-rupture area and rupture-width relationships of Wells and Coppersmith (1994).

Recurrence

The recurrence relationships for the seismic sources are modeled using the truncated-exponentially Gutenberg-Richter, characteristic earthquake, and the maximum magnitude recurrence models (Section 5.1). These models are weighted to represent our judgment on their applicability to the sources (Figure 5). For areal source zones, only a truncated exponential recurrence relationship is assumed to be appropriate.

The general approach of Molnar (1979) and Anderson (1979) was used to arrive at the recurrence for the truncated-exponential model. The number of events exceeding a given magnitude, N(m), for the truncated-exponential relationship is

$$N(m) = \alpha(m^o) \frac{10^{-b(m-m^o)} - 10^{-b(m^u-m^o)}}{1 - 10^{-b(m^u-m^o)}}$$

where $\alpha(m^o)$ is the annual frequency of occurrence of earthquakes greater than the minimum magnitude, m^o; b is the Gutenberg-Richter parameter defining the slope of the recurrence curve; and *mu* is the upper-bound magnitude event that can occur on the source. A m^o of **M** 5.0 was used for the hazard calculations because smaller events are not considered likely to produce ground motions with sufficient energy to damage well-designed structures.

The model where faults rupture with a "characteristic" magnitude on specific segments was included as described by Aki (1983) and Schwartz and Coppersmith (1984). For the characteristic model, the numerical model of Youngs and Coppersmith (1985) was used. In the characteristic model, the number of events exceeding a given magnitude is the sum of the characteristic events and the non-characteristic events. The characteristic events are distributed uniformly over a ± 0.25 magnitude unit around the characteristic magnitude, and the remainder of the moment rate is distributed exponentially using the equation (4) with a maximum magnitude 0.25 unit lower than the characteristic magnitude (Youngs and Coppersmith, 1985).

The maximum magnitude model can be regarded as an extreme version of the characteristic model and the model proposed by Wesnousky (1986) was used in the PSHA. In the maximum magnitude model, there is no exponential portion of the recurrence curve. The model is a normal distribution centered at the characteristic magnitude and truncated on the upper range at 2 standard deviations. The standard deviation used is 0.12 magnitude units.

The recurrence rates for the fault sources are defined by either the slip rate or the average return time for the maximum or characteristic event and the recurrence *b*-value. The slip rate is used to calculate the moment rate on the fault using the following equation defining the seismic moment:

$$M_o = \mu A D \quad (5)$$

where M_o is the seismic moment, μ is the shear modulus, A is the area of the rupture plane, and D is the slip on the plane. Dividing both sides of the equation by time results in the moment rate as a function of slip rate:

$$\dot{M}_o = \mu A S \quad (6)$$

where $\dot{M}_o$ is the moment rate and S is the slip rate. Mo has been related to moment magnitude, M, by Hanks and Kanamori (1979):

$$\mathbf{M} = 2/3 \log M_o - 10.7 \quad (7)$$

Using this relationship and the relative frequency of different magnitude events from the recurrence model, the slip rate can be used to estimate the absolute frequency of different magnitude events.

The average return time for the characteristic or maximum magnitude event defines the high magnitude (low likelihood) end of the recurrence curve. When combined with the relative frequency of different magnitude events from the recurrence model, the recurrence curve is established.

2.2 Ground Motion Prediction

To characterize the ground motions at a specified site as a result of the seismic sources considered in the PSHA and DSHA, empirical GMMs for spectral accelerations were used. The models used in this study were selected on the basis of the appropriateness of the site conditions and tectonic environment for which they were developed (Figure 5; Section 5.3).

Ground motions are generally assumed to be lognormally distributed. However, recent studies (e.g., GeoPentech, 2015) have demonstrated that ground motions deviate from the generally assumed lognormal distribution at epsilon (ε) values greater than about 2.5, where ε is the number of standard deviations above or below the median ground motion intensity. As part of the Southwestern United States Ground Motion Characterization SSHAC Level 3 study

(GeoPentech, 2015), residuals for the NGA-West2 models were examined at various epsilon values, and it was determined that the within-event residuals had “fat tails” in that there was a higher probability of extremes (at both high and low epsilon) than predicted by a lognormal distribution. To adequately model these fat tails, a mixture model was developed, which consists of two equally weighted lognormal distributions: one model having a mean of zero and log standard deviation of 0.8 times sigma and the second model having a mean of zero and log standard deviation of 0.2 times sigma. The mixture model was implemented for this study. However, due to the levels of ground motions of interest for this study that have low contributions from $\varepsilon > 2.5$ events, sensitivity analyses indicate the results are quite insensitive to use of the mixture model versus the lognormal model. Five standard deviations about the median value were included in the analysis.

3.0 SEISMOTECTONIC SETTING AND HISTORICAL SEISMICITY

The seismotectonic setting and historical seismicity of the Skunk Camp site are discussed below.

3.1 SEISMOTECTONIC SETTING

The Skunk Camp site is located in southern Arizona south of the town of Miami (Figures 1 and 2). Arizona is divided into three physiographic and seismotectonic provinces: the Colorado Plateau in the northeast, the Southern Basin and Range (SBR) in the south and southwest, and the intervening Transition Zone that is roughly 40 to 100-km-wide and northwest-southeast trending (Figure 6). All three provinces are characterized by relatively few late Quaternary faults and low rates of seismicity. These regions are bounded to the east by the Rio Grande Rift, and to the west by the Salton Trough Province (Figure 6). The site is located in the SBR Province near the boundary with the Transition Zone.

The SBR Province is a block-faulted terrain of alternating mountain ranges and intervening valleys, bounded by moderately to steeply dipping normal faults. The mountains comprise igneous, metamorphic, and indurated sedimentary rocks of Precambrian through Tertiary age; the valleys are filled with undeformed sequences of fluvial and lacustrine sediments of Oligocene to Pleistocene age. There are differing estimates on the timing of initiation of Basin and Range extension; McQuarrie and Wernicke (2005) suggest that deformation began at 25 Ma, whereas Menges and Pearthree (1989) indicate that deformation may have commenced during the Miocene at 15 Ma. However, there is general consensus that major extension ceased at some time in the late Miocene or Pliocene, and the modern landscape is dominated by geomorphological landforms that indicate tectonic inactivity (Menges and McFadden, 1981). Relative tectonic quiescence in southern Arizona is also reflected by the low levels of historical seismicity and sparse evidence for Quaternary faulting. The SBR Province is dominated by northwest-southeast-striking normal faults; however, the site region encompasses the transition from this northwest-southeast structural grain to a more north-south orientation as the province extends into northern Mexico.

The Transition Zone represents a tectonic transition from the relatively thin (~15 to 20 km) extended crust of the SBR to the thick (~40 km) crust of the Colorado Plateau. Bedrock in the region consists primarily of Precambrian metamorphic and granitic plutonic rocks and Paleozoic sediments. The composition of late Cenozoic basin-fill sediments reflects widespread Tertiary volcanism in the region. The Transition Zone is characterized by north- to northwest-trending mountain ranges and intervening basins related mainly to Miocene and younger normal faulting (Menges and McFadden, 1981; Mack *et al.*, 2003). The topography of the Transition Zone is more subdued than that of the SBR Province to the south: the ranges are less pronounced and the basins are smaller and less well-defined. The relatively subdued landforms, low to moderate levels of seismicity (Brumbaugh, 1987; Bausch and Brumbaugh, 1997), and relative lack of significant late Quaternary faulting (Pearthree *et al.*, 1983) have been interpreted to indicate geologically recent tectonic cessation of major extension in the region (Menges and McFadden, 1981). The few Quaternary normal faults that are mapped in the region generally trend northwest-southeast and are likely reactivated faults that originated during Basin and Range extension (Lockridge *et al.,* 2012). Based on reconnaissance mapping and limited paleoseismic studies, these faults have average recurrence intervals of tens to hundreds of thousands of years (Pearthree, 1998; Piety and Anderson, 1991).

The Colorado Plateau in northern Arizona is part of a large region that extends across southeastern Utah, northwestern New Mexico, and western Colorado. Physiographically and geologically distinct from the highly deformed Rocky Mountains to the north and east and the Basin and Range region to the south and west, the Colorado Plateau is characterized by relative tectonic stability and elevated topography dissected by rivers. Whereas major crustal deformation of the Colorado Plateau ceased at the end of Laramide orogeny (40 Ma), the region has been subject to about 2 km of epeirogenic uplift during the Cenozoic (Morgan and Swanberg, 1985). During uplift, the plateau acted as a coherent block, with only minor differential movements creating northerly-trending monoclines and associated structural basins. Contemporary seismicity in the Colorado Plateau Province is low to moderate, with widespread, generally small events that cannot be correlated with surface geological features (Wong and Humphrey, 1989).

The Salton Trough to the west of the Basin and Range marks the transition between ocean-floor spreading in the Gulf of California and right-lateral strike-slip faulting along the San Andreas fault zone. This region is one of the most seismically active areas in the western United States, characterized by right-lateral strike-slip faulting and elevated levels of contemporary seismicity with repeated events of **M** 6 to 7 during the period of historical record (Figure 4). Slip rates on faults in this region are as high as 30 mm/yr (Working Group on California Earthquake Probabilities, 2008).

3.2 HISTORICAL SEISMICITY

A historical seismicity catalog was compiled for an area that encompassed over 200 km around the site, extending from a latitude of approximately 31°N to 36.3°N and a longitude of approximately 115°W to 107.5°W (Figure 2). The catalog extends from 1830 to September 2019 and the majority of the catalog consists of the compilation presented in Wong *et al*. (2008). Primary data sources used in that compilation include the Northern Arizona University regional catalog (1830 through 2005) and the USGS Advanced National Seismic Service (ANSS) (1931 through 2019) catalog. The catalog was updated using the USGS ANSS catalog.

The site is located in the SBR in an area of low historical seismicity. This area, however, has had poor seismographic coverage. In addition to the SBR, the catalog includes seismicity to the north in the area of the Transition Zone as well as the southern Colorado Plateau (Section 3.1). The catalog includes 26 events of magnitude **M** 5 to 5.9, three events of magnitude **M** 6 to 6.9, and three events of **M** 7 and greater (Figure 2). One of the **M** 7 events is documented as having occurred in 1830, though it is based on one report made in the mid-1850’s and is therefore considered suspect and poorly constrained and documented (DuBois *et al.*, 1982). Wong *et al.* (2013) note that this event continues to be included in some catalogs but has been removed from the Arizona Geological Survey catalog because it is poorly dated, dubious, and because no physical evidence has been found to corroborate such a reportedly high intensity and relatively young event (Phil Pearthree, Arizona Geological Survey written communication to I. Wong, 2013). The event appears on Figure 2, but it was excluded from the earthquake recurrence calculations.

3.2.1 Significant Earthquakes

This section describes three significant historical earthquakes that have occurred in or near the Project region whose effects were likely felt at the site.

1887 Sonora Earthquake

The largest event in the catalog was an earthquake of **M** 7.4 that occurred on 3 May 1887 in northern Sonora, Mexico, approximately 330 km southeast of the site (Dubois *et al*., 1982; Suter and Contreras, 2002) (Figure 7). The earthquake ruptured three major normal faults (Otates, Teras, and Pitáycachi faults) and was felt throughout Arizona and New Mexico and as far south as Mexico City (Dubois *et al*., 1982; Suter and Contreras, 2002). The maximum felt intensity was between Modified Mercalli intensity (MMI) XI and XII and strong ground shaking, intensity MMI VI to VII, could have been observed at the site (Figure 7; DuBois *et al*., 1982).

1922 Miami Earthquake

In the historical seismicity catalog, the closest moderate-sized earthquake to the Project area was a **M** 5.0 event that occurred on 17 June 1922 in the vicinity of Miami, Arizona, north of the Project area (DuBois *et al*., 1982) (Figure 8). Although the felt intensity at the Project was not reported by DuBois *et al*. (1982), it likely would have been at least MMI IV based on the proximity to the MMI V contour. Although the event was felt throughout the town of Miami, no structural damage was reported (DuBois *et al*., 1982). Wong *et al.* (2008) noted that this event was recorded on a seismograph in Tucson and that the location and size of the event are highly uncertain.

2014 Southeastern Arizona Earthquake

A more recent **M** 5.3 event occurred on 29 June 2014 approximately 150 km east-southeast of the Project, near the town of Duncan, Arizona and near the Arizona-New Mexico border (Figure 9). This event was recorded on the USGS Did You Feel It website (http://earthquake.usgs.gov/earthquakes/eventpage/usc000rnfe#dyfi). The maximum reported intensity of MMI V was reported near the epicenter. Based on reported intensities surrounding the site, an intensity of at least MMI II to III would have been observed in the Project area (Figure 9). The earthquake occurred at a depth of 6.4 km and the moment tensor solution reported by the USGS shows that the event is consistent with northeast-striking oblique-normal faulting. Subsequent to this event, there were more than 40 likely aftershocks ranging in magnitude from **M** 2.0 to 4.0.

3.2.2 Local Seismicity

The largest event within 50 km of the site was the 17 June 1922 **M** 5.0 earthquake (Figure 10). This event is the third closest earthquake to the site in the catalog; the closest events were two **M** 3.5 earthquakes that occurred on 11 September 1963 and 21 October 1963, respectively, approximately 18 km east-northeast of the site (Figure 10). The other event within 50 km of the site was an **M** 3.8 earthquake that occurred on 25 December 1969 approximately 37 km northeast of the site.

4.0 RECONNAISSANCE-LEVEL FAULT INVESTIGATION

A reconnaissance-level fault investigation was performed in the Skunk Camp TSF Project area to evaluate surficial evidence for and against Quaternary-active faults and to determine whether any local faults should be included in the seismic source characterization. The fault investigation involved both desktop and field evaluations. The desktop evaluation included reviews of geologic maps, scientific literature and consultant reports, air photos, and high-resolution topographic data of the Project area. Field evaluations included three days of geologic reconnaissance at the site and surrounding area.

Specifically, the objectives of the reconnaissance-level fault investigation were to:

- Critically evaluate previously mapped faults in the Project area for which map relations suggest possible Quaternary activity.
- Observe geologic and geomorphic conditions in the Project area for possible evidence of previously unrecognized Quaternary-active faults.

The results of our reconnaissance-level fault investigation are consistent with the lack of Quaternary-active faulting in the Project area, and we conclude that Quaternary-active faults are highly unlikely in the site area. As such, we assess the surface fault rupture hazard at the Skunk Camp TSF site to be low.

4.1 Desktop Fault Evaluation

The east face of the Dripping Spring Mountains is a highly embayed mountain front with no triangular facets or other gross geomorphic features commonly associated with active mountain-front faulting. Active mountain fronts also are commonly associated with coalescing alluvial fans or bajada with distributary drainage networks. The drainage network in Dripping Spring Valley is an incised tributary network, suggesting the landscape has experienced a prolonged period of erosion without significant uplift along the mountain front.

Regional compilations of Quaternary-age structures (e.g., Menges and Pearthree, 1983; USGS and AZGS, 2019) do not show any Quaternary-active faults in the Project area and there are no known Quaternary-active faults in the vicinity. However, map relations shown on ca. 1960s–1970s geologic maps suggest possible Quaternary fault activity. For example, Cornwall *et al.*'s (1971) geologic map of the 7.5-minute Sonora quadrangle shows an unnamed, northwest-striking, northeast-dipping normal fault that roughly follows Dripping Spring Wash in the vicinity of the Project (Figure 11). Following the convention of KCB Consultants (2019), this unnamed fault is herein referred to as the "Dripping Spring fault." Along most of its length the trace of the Dripping Spring fault is shown by a dotted line, indicating that it is concealed (Cornwall *et al.*, 1971; Cornwall and Krieger, 1978). However, a few short sections of the Dripping Spring fault are shown by solid lines in map unit Tcg (Miocene- to Pliocene-age Tertiary conglomerate) basin-fill deposits and, surprisingly, in Qal (Quaternary alluvium) deposits in active washes (Cornwall *et al.*, 1971) (Figure 11).

Cornwall *et al*. (1971) map the Ransome fault on the Sonora quadrangle as a southwest-striking, west-dipping normal fault that extends northward out of basement rocks into Tertiary basin fill near Haley Spring and is truncated by the Dripping Spring fault (Figure 11). Along most of its length in Tcg basin-fill deposits, the Ransome fault is mapped as concealed (dotted), but short sections of the Ransome fault are shown by solid lines in Tcg basin-fill deposits and across map unit Qp (Quaternary pediment surfaces) (Cornwall *et al.*, 1971).

To the north, in the southwestern portion of the Pinal Ranch quadrangle, Peterson (1963) maps both east-west- and north-south-striking faults in Tertiary conglomerate and tuffaceous sandstone (Figure 11, near waypoints WP-15, WP-16, and WP-17). Due to the lack of younger Quaternary units mapped along these faults, it is not possible to determine the age of most-recent slip based on map relations alone.

More recently, Richard and Spencer (1998) compiled previous geologic mapping of the Ray–Superior area and reinterpreted some of the map relations to provide a better understanding of the geologic history of the area. Notably, Richard and Spencer's (1998) map shows the Ransome fault as confined to basement rocks and not extending north into Late Miocene to Pleistocene basin-fill deposits (their map unit QTs), and the Dripping Spring fault does not appear on their map. Near Captain Trap Spring north and east of Mill Creek, Richard and Spencer (1998) map an unnamed, approximately 0.5-km-long, northwest-striking, northeast-dipping fault in Miocene-age conglomerate (Tc) that is concealed beneath QTs basin-fill deposits (Figure 12, near waypoint WP-14). This unnamed fault does not appear on earlier maps by Peterson (1963) and Cornwall *et al.* (1971). Given its orientation and location, this unnamed fault could be associated with the Dripping Spring fault. Based on Richard and Spencer's (1998) map, there is no evidence for Quaternary activity on this unnamed fault.

Prior to mobilizing to the field, we evaluated aerial imagery and topography of the Project area, including high-resolution topographic data and orthophotographs with 1.5-ft precision provided to the project by PhotoSat (2019). We also inspected Google Earth imagery from 1992 to 2019. Specifically, we evaluated these data for topographic and tonal lineaments that could be evidence for possible active faulting. We identified no lineaments in Tertiary or younger deposits associated with mapped traces of the Ransome, Dripping Spring, or other unnamed faults in the Project area. We did, however, identify an approximately 1-km-long, north-south-trending topographic and tonal lineament located near waypoints WP-09 through WP-13 (Figures 12 and 13). This lineament is not coincident with any previously mapped fault, but we inferred that if the lineament is a fault, then it would have to be steeply dipping to vertical based on its linear trace that crosses moderate- to high-relief topography.

4.2 Geologic Field Reconnaissance

A geologic field reconnaissance was performed around and north of the location of the Project area from 4 to 6 November 2019, with a focus on areas where previous workers have mapped faults in basin-fill deposits and on the area where we identified a topographic and tonal lineament near waypoints WP-09 through WP-13 (Figures 12 and 13). The locations visited in the field were recorded by a handheld GPS device. GPS tracks and waypoints are shown in Figures 11 to 13, and specific observations and interpretations made at each GPS waypoint are summarized in Table 1.

Most of our field observations were made along Dripping Spring Wash and several unnamed canyons that flow east out of the Dripping Springs Mountains into Dripping Spring Wash. We also visited locations along Walnut Canyon, Cedar Creek, Mill Creek, and Mineral Creek.

In general, Tertiary and younger deposits are poorly exposed throughout much of the Project area. In spite of the moderate- to high-relief topography and several relatively deeply incised canyons, natural exposures along previously mapped faults are sparse and much of the landscape in the vicinity of the Project area is vegetated by desert scrub, interior chaparral, and semi-desert grasses. As such, it was not possible to definitively preclude the presence of faults in Tertiary basin-fill deposits by observing continuous, unfaulted deposits that overlie previously mapped fault traces (Table 1). However, where encountered we observed no evidence for faulting in Tertiary and younger deposits. Moreover, we observed no geomorphic features such as fault scarps, offset drainages, or offset ridgelines that would suggest active faulting.

We walked along and across the topographic and tonal lineament near waypoints WP-09 through WP-13 (Figure 13). Here, we observed no geomorphic or geologic evidence for Quaternary-active faulting. Instead, this lineament appears to be an erosional feature associated with the geologic contact between Precambrian diabase (db) and Tertiary basin-fill conglomerate (Tcg).

4.3 Fault Investigation Results

Our field observations are consistent with the lack of Quaternary-active faulting in the Project area, and we conclude that Quaternary-active faults are highly unlikely at the site. We did not observe any geomorphic evidence suggestive of active faulting. However, given the expected very low rates of faulting in the region, the rate of scarp formation or other surface deformation features could be masked by more rapid local rates of erosion. There were also limited exposures of Tertiary and younger deposits in the site area to completely rule out Quaternary faulting.

Based on the results of our desktop and field-based observations, we conclude that the Dripping Spring, Ransome, and other local unnamed faults near the Project area should be excluded from the seismic source characterization for the following reasons:

- The gross-scale geomorphology of the Dripping Spring Mountains and Dripping Spring Valley (e.g., embayed mountain front, lack of triangular facets, tributary drainage network) strongly suggests the absence of active tectonics.

- Evidence for Quaternary activity on the Dripping Spring and Ransome faults appears only on ca. 1960s to 1970s geologic maps. More-recent mapping published by the Arizona Geological Survey (Richard and Spencer, 1998) does not show these faults as possibly Quaternary-active.

- Neither the Dripping Spring nor Ransome fault is included in the U.S. Geological Survey's Quaternary Fault and Fold Database, nor are they included in tabulations of active faults developed by the Arizona Geological Survey.

- Our reconnaissance-level fault investigation is consistent with previous geologic reconnaissance performed for the Project by KCB Consultants (2019), which also did not identify evidence for Quaternary-active faulting in the Project area.

5.0 INPUTS TO ANALYSES

The following section discusses the characterization of the seismic sources and the GMMs selected and used in the PSHA and DSHA. The seismic source model used in this study was based on previous studies in the region performed by the authors over the past 20 years.

5.1 SEISMIC SOURCES

Seismic source characterization is concerned with three fundamental elements: (1) the identification, location and geometry of significant sources of earthquakes; (2) the maximum size of the earthquakes associated with these sources; and (3) the rate at which the earthquakes occur. The seismic source model includes crustal faults capable of generating large surface-faulting earthquakes (Section 5.1.1), and an areal source zone, which accounts for background crustal seismicity that cannot be attributed to identified faults explicitly included in the seismic source model (Section 5.1.2).

5.1.1 Crustal Fault Sources

Fault parameters required in the PSHA include: (1) rupture model (including independent single plane and potentially linked models); (2) probability of activity; (3) fault geometry including rupture length, rupture width, fault orientation, and sense of slip; (4) maximum or characteristic magnitude [Mmax]; and (5) earthquake recurrence including both recurrence model and rates. These parameters are generally discussed further below. Selected faults that contribute the most to the hazard are specifically discussed in subsequent sections. We have explicitly incorporated the uncertainties in each parameter through the use of logic trees, as exemplified in Figure 5.

All known active or potentially active faults were included in the analyses within 200 km of the site (Figure 3). We included known faults showing evidence for late Quaternary (≤ 130,000 years) activity or repeated Quaternary (≤ 1.6 million years) activity. We also included longer, more active faults in southern California and Baja California, such as the southern San Andreas fault, because from previous analyses in the region (e.g., Wong *et al*., 2013), we know that these major fault sources can be significant contributors to the hazard at longer periods, despite their great distances (Figure 4). The Pitaycachi fault, source of the 1887 Sonora earthquake, was also included in the hazard analysis because although it is distant (190 km away) and its slip rate is slow (< ~0.1 mm/ yr), it is the source of the largest earthquake in the region (Figure 4).

Faults are generally modeled as single, independent, planar sources, simplified from the complex zones shown on Figure 3. Table 2 shows the parameters for the faults. Our fault characterization is based on our previous probabilistic seismic hazard analyses in Arizona, the APS study, and from data compiled in the USGS Quaternary Fault and Fold Database (http://earthquake.usgs.gov/hazards/qfaults/) and sources listed in Table 2.

Maximum magnitudes were estimated for the local faults using the empirical relationships of: (1) Wells and Coppersmith (1994), for all fault types; (2) the Stirling *et al.* (2002) censored relationship for all fault types; and (3) Wesnousky (2008) for all fault types, as noted in the footnotes of Table 2. None of the local faults are blind, and minimum seismogenic depths were assumed to be 0 km. We assumed maximum seismogenic depths of 12 km (weighted 0.3), 15 km (weighted 0.5), and 17 km (weighted 0.2), primarily based on the maximum depth of historical seismicity in the region (e.g., Lockridge *et al*., 2012).

Fault dips are averages over the entire seismogenic crust. Although near-surface fault dip data are available for many of the faults, crustal dip data are lacking. We assumed default dips of 50° (weighted 0.6) ±15° (weighted 0.2) for all the local faults, which all show dominantly normal slip. This default fault dip distribution is after recommendations made by the Basin and Range Province Earthquake Working Group II (BRPEWGII; Lund, 2012; see Issue G4) to the USGS regarding crustal-scale dips for typical range-bounding normal faults in the Basin and Range Province. This distribution was based on focal plane and aftershock data for historical surface-rupturing earthquakes in the Basin and Range Province, as well as normal faults worldwide.

Recurrence models can significantly impact hazard calculations and we considered truncated exponential, maximum magnitude, and characteristic recurrence models for this analysis. Observations of historical seismicity and paleoseismic investigations suggest that characteristic behavior is more likely for individual faults, whereas seismicity in areal zones best fits a truncated exponential model (Schwartz and Coppersmith, 1984; Youngs and Coppersmith, 1985). The maximum magnitude model is an extreme version of the characteristic model (Wesnousky, 1986). We favored (weighted 0.6) the characteristic model for all local fault sources and assigned equal weights of 0.2 to the exponential and maximum magnitude models. Typically we assign a lower weight to the truncated-exponential model but some of the fault zones modeled in the PSHA may consist of multiple faults (e.g., Carefree fault zone) that could rupture in a range of earthquake sizes.

In assigning probabilities of activity for local fault sources, we considered both the likelihood that the fault is structurally capable of independently generating earthquakes, and the likelihood that it is still active within the modern stress field. We incorporated many factors in assessing these likelihoods, such as: orientation in the modern stress field, fault geometry (length, continuity, and dip), relation to other faults, age of youngest movement, rates of activity, geomorphic expression, amount of cumulative offset, and any evidence for a non-tectonic origin. Faults with definitive evidence for repeated Quaternary activity were generally assigned probabilities of being active (seismogenic) of 1.0 (Table 2). The probability of activity for faults that do not show definitive evidence for repeated Quaternary activity was individually judged based on available data and the criteria explained above. Resulting values range from 0.5 to 1.0 (Table 2) and the specific reasons for assigning probabilities less than 1.0 to a particular fault are generally given in the comments column of Table 2.

As is often the case, recurrence interval data are generally lacking for the local faults so we used slip rates to characterize rates of fault activity (Table 2). We considered all available long- (≤ 1.6 Ma) and short-term (≤ 130 ka) data in developing slip rate distributions, but we preferred short-term data whenever possible. In addition to the time period, we also considered the type and quality of data in determining rates. Preferred slip rates (generally weighted 0.6) are primarily based on data in the USGS Quaternary fault database and as noted in the comments column of Table 2. Maximum and minimum values (each generally weighted 0.2) are typically selected to represent 95th and 5th percentile values as previously discussed in Section 2, unless the available data suggest otherwise as noted in the comments column of Table 2. Note that from our previous hazard analyses in the area we found that none of the local faults contributed significantly to the hazard so we do not include detailed local fault specific discussions herein.

5.1.1.1 Whitlock Wash Fault Zone

At its closest approach, the Whitlock Wash fault is 52 km southeast of the mine (Figure 3). Very little is known about the fault and to our knowledge, no detailed paleoseismic investigations have been carried out. Pearthree (1998) includes the fault in his Quaternary fault database for Arizona and based primarily on the earlier work by Menges and Pearthree (1983) and Pearthree *et al.* (1988), the fault is also included in the USGS Quaternary Fault and Fold Database. The fault strikes north to northwest and is discontinuous along its estimated 23 km-length. Quaternary activity is suspected based on a prominent escarpment and observed faulting in Pliocene basin-fill deposits (Pearthree, 1998). However, no evidence of Quaternary displacement has been observed. Mapping at the southern portion of the fault revealed unfaulted lower to middle Quaternary deposits.

We assign a probability of activity of 0.9 because of the lack of definitive evidence for Quaternary displacement. Based on magnitude-rupture length relationships, we assign a Mmax of **M** 6.8 ± 0.3. A magnitude of **M** 6.9 was assumed for the DSHA. The slip rate for the fault is unknown but is estimated to be less than 0.02 mm/yr (Pearthree, 1998). We assign a best-estimate slip rate of 0.01 mm/yr with a very large uncertainty spanning an order of magnitude.

5.1.1.2 Southern California Faults

Based on previous analyses, we included the San Andreas, San Jacinto, and Cerro Prieto faults in the PSHA (Figure 4). These plate-boundary structures are all long, complex, and highly-active fault zones or systems that have been extensively studied. They are included because of their potential to generate very large (up to **M** 8 or larger) and relatively frequent events compared to the local faults (Figure 4). The source characterization of these faults follows that used by the USGS in the 2008 National Seismic Hazard Maps (Petersen *et al*., 2008). This seismic source model is referred to as the Uniform California Earthquake Rupture Forecast, Version 2 (or UCERF2), which was developed by the Working Group on California Earthquake Probabilities and was documented by Wills *et al*. (2008) and Field *et al*. (2008). The parameters of the more significant regional faults included here are summarized in Tables 3a through 3c. The UCERF2 model did not include the Cerro Prieto fault, but we added it here because it is a major transform structure south of the U.S.-Mexico border that appears to be accommodating significant slip comparable to the Imperial fault and is included in the UCERF3 model (Figure 4).

Cerro Prieto Fault

Our characterization of the Cerro Prieto fault is taken from Thomas *et al.* (2015). Although it is not included in either the USGS Quaternary Fault and Fold Database, or the California Geological Survey 2010 Fault Activity Map (http://www.quake.ca.gov/gmaps/FAM/faultactivitymap.html), the Cerro Prieto fault was included in Jennings' (1994) earlier Fault Activity Map of California and Adjacent Areas after original mapping by Gastil *et al*. (1975). It is now included in the UCERF3 model, which is the basis for the 2014 USGS NSHMs. The Cerro Prieto fault is a northwest-striking dextral-slip transform fault that extends for over 115 km and is part of where the East Pacific Rise comes onshore (Figure 4). It extends from the Wagner Basin spreading center in the Gulf of California to at least the Cerro Prieto spreading center (and volcano and geothermal field), near Mexicalli, Mexico. It is approximately 365 km southwest of the site. It has not been mapped or studied paleoseismically in any detail and the Southern California Earthquake Data Center lists the slip rate as uncertain with the fault being "difficult to trace in alluvium of the Colorado River delta" (http://www.data.scec.org/significant/cerroprieto.html).

The Cerro Prieto fault does have linear trends of associated microseismicity that extend northwest of the fault as mapped by Jennings (1994), well beyond the Cerro Prieto volcano, prompting Magistrale (2002) to suggest the fault extends another 35 km to the northwest into southern California. Based on this, the model includes two scenarios for the northern end of the fault (Table 3a): Scenario A, at the Cerro Prieto Volcano (weighted 0.6); and, Scenario B, extending into southern California after the microseismicity trend defined by Magistrale (weighted 0.4).

The Cerro Prieto geothermal field at the northern end of the fault has been the focus of much investigation, including the **M** 5.4 earthquake that occurred on 24 May 2006 and ruptured the Morelia fault, a small cross-fault at the northern end of the Cerro Prieto fault (Suarez-Vidal *et al*., 2007). There is also suggestion that multiple large historical surface ruptures (about **M** 7.1) have occurred on the southern Cerro Prieto fault, including one in 1915 and 1934, but they are not as well- documented (Biehler *et al*., 1964; Merriam, 1965; Allen *et al*., 1965). Due to lack of other published information on previous ruptures and the large uncertainties on rupture behavior, the model assumes a floating rupture model for the Cerro Prieto fault with a preferred characteristic magnitude of **M** 7.1 (Table 3a), but included a broad distribution (+0.5 and -0.3) due to the large uncertainties. The upper bound of **M** 7.6 allows the entire fault to rupture.

Rates are unknown for the Cerro Prieto fault. Several investigators have postulated that it is a principal plate-bounding structure, with slip from the San Jacinto fault being transferred to the Cerro Prieto fault via the Imperial fault (Magistrale, 2002; Suarez-Vidal *et al*., 2007; T. Rockwell, San Diego State University, written communication, cited in Table B-1 of Field *et al*., 2013). The Imperial fault has an estimated rate of 15 to 40 mm/yr, with paleoseismic trench data indicating 5 m of slip occurred between the 1940 and 1690 fault ruptures (Thomas and Rockwell, 1996). The UCERF3 model uses an input range of 35 ± 5 mm/yr for the Cerro Prieto fault (Table B-1), which is geodetically based, whereas the modeled mean rates are lower, ranging from 11 to 15 mm/yr (Field *et al*., 2013). Given the very large uncertainty, this study uses a broad slip rate distribution of: 15 mm/yr (weighted 0.25), 20 mm/yr (weighted 0.35), 35 mm/yr (weighted 0.25), 40 mm/yr (weighted 0.15).

Southern San Andreas Fault Zone

The right-lateral strike-slip San Andreas fault zone is the most significant structure accommodating North American-Pacific plate motion, accounting for up to 70% of the relative plate motion along most of its length. The southern San Andreas fault zone includes the section of the fault south of the creeping segment in central California (Figure 4). This part of the fault has generated two large historical earthquakes, the 1857 **M** 7.8 to 8 Ft. Tejon that ruptured the Parkfield through Mojave South sections, and an **M** ~7½ earthquake in 1812 that ruptured the North San Bernardino and Mojave South and possibly Mojave North sections. In addition, the northernmost Parkfield section has experienced numerous moderate earthquakes (**M** ~6) in the historical period, the most recent of which occurred in 2004.

The Working Group on California Earthquake Probabilities (WGCEP) (Field *et al*., 2008) developed a new characterization of the San Andreas fault as part of the Uniform California Earthquake Rupture Forecast (UCERF)2 that differs considerably from that of previous working groups (e.g., WGCEP, 1988; 1995; Cao *et al*., 2003). We use a simplified version of their fault characterization and earthquake recurrence models to model the southern San Andreas fault. They include three alternative deformation models to describe how slip is distributed between the southern San Andreas and other faults in the area including the San Jacinto fault; we use only their preferred model. UCERF3 was released in 2013 by Field *et al*. (2013) but we have not adopted this model because of issues regarding fault segmentation and multi-segment ruptures that we cannot agree with because we find earthquake scenarios in the model that are not supported by paleoseismic data.

Changes in the UCERF2 model (Field *et al*., 2008) from the 2002 model of Cao *et al.* (2003) include modification to the sectioning, geometry, recurrence and slip rates on the fault. Field *et al.* (2008) divide the southern San Andreas fault zone into 10 sections, a departure from earlier working groups who divided it into six rupture segments (e.g., WGCEP, 1988, 1995; Cao *et al.*, 2003). The sections defined by the Field *et al.* (2008) are not necessarily rupture segments and do not imply a specific earthquake model; rather, they are defined based on distinct geological characteristics that may or may not relate to earthquake rupture characteristics. We have adopted the divisions of UCERF2, with the following sections: Parkfield (PK), a 36-km-long section extending from Parkfield to the town of Cholame; Cholame (CH), extending southeast 62 km from Cholame; Carrizo (CC), a 59-km-long segment extending to the southern end of the

Carrizo Plain; Big Bend (BB), a 50-km-long stretch ending at the intersection with the east-west-striking Garlock fault; Mojave North (NM), which extends 40 km from the Garlock fault to Elizabeth Lake, the northern end of the “Mojave segment” used by previous working groups; Mojave South (SM), a 100-km-long section similar to the former “Mojave segment”, that traverses the southeastern edge of the Mojave desert from Elizabeth Lake to near Cajon Pass, about halfway between Wrightwood and Lost Lake; San Bernardino Mountains North (NSB), which extends about 35 km southeast from Cajon Pass to the intersection with the Mill Creek fault and the northern end of an region of structural complexity called the San Gorgonio Pass knot (Field *et al.*, 2008); San Bernardino South (SSB) and San Gorgonio Pass-Garnet Hill, also referred to as Banning-Garnet Hill (BG), which pass through the complex San Gorgonio Pass region and are northwest-striking strike-slip and slightly more west-striking reverse oblique-slip faults, respectively; and last, Coachella Valley (CO), which starts at the junction with the Mission Creek fault where the SAF again regains its northwest strike, and ends at the Salton Sea (Field *et al.*, 2008).

Slip rates on several of the newly defined sections also have changed in the UCERF2 model, reflecting both the new sectioning and more recent geologic and geodetic data. The San Andreas fault zone has the highest slip rate of any fault in California. On the Parkfield, Cholame, Carrizo and Big Bend sections, the average late Holocene slip rate is about 34 to 35 mm/yr, consistent with previous estimates (Sieh and Jahns, 1984; Sims, 1994). The slip rate decreases southward as more slip is transferred to other structures of the San Andreas fault system, especially the San Jacinto fault. As a consequence, the average slip rate on the southern sections of the fault decreases from about 27 ± 7 mm/yr in the Mojave North section to about 20 ± 6 mm/yr on the southernmost Coachella Valley section.

Field *et al*. (2008) used the recurrence interval data determined from paleoseismic studies and a method of assessing the probability that a specific rupture scenario is consistent with the paleoseismic record to determine a rupture recurrence rate for each of the ten sections. They used slip rates to moment balance the *a priori* recurrence rates to develop final moment-balanced rupture rates for all possible rupture scenarios. These rates have been adopted for use in the model. The table of rupture rates appears in Table 3b.

5.1.2 Crustal Background Earthquakes

In state-of-the-practice seismic hazard evaluations, the hazard from background earthquakes is addressed. Background earthquakes are those events that do not appear to be associated with known geologic structures. They occur on crustal faults that exhibit no surficial expression (buried faults) or are unmapped due to inadequate studies. In this source characterization, we address the hazard from background earthquakes through: (1) a gridded seismicity model, where locations of past seismicity appear to be likely locations of future seismicity (stationarity); and (2) the use of a regional seismic source zone for the SBR, where earthquakes are assumed to occur randomly (“uniform” model; Figure 14). For both approaches, the background earthquakes are assumed to occur uniformly from 2 km to the bottom of the seismogenic crust.

The maximum depths of the seismogenic crust is the same distribution used for the crustal faults (Section 5.1.1).

Earthquake recurrence estimates in the Project region are required in order to assess the hazard from background earthquakes. A declustered SBR background zone catalog was developed by Wong *et al*. (2013) and updated for this report (Section 3.2; Figure 14). The declustering was performed using the approach of Youngs *et al*. (2000). Details of the catalog processing can be found in Wong *et al*. (2013). The SBR zone, as defined in this report, incorporates seismicity from the SBR and a portion of the Transition Zone (as defined by Peirce [1984]), because the number of earthquakes in each of these two zones was deemed insufficient to independently determine earthquake recurrence parameters. The recurrence parameters for the SBR were developed using the historical seismicity record for the period of 1830 through September 2019.

Completeness intervals were adopted from Wong *et al*. (2017). These completeness intervals were modified from Thomas *et al.* (2015) and Wong *et al.* (2008) by developing Stepp (1972) plots using an earthquake catalog the updated through April 2017 (Wong *et al*., 2017). These plots were developed by calculating the average annual number of independently occurring events in each half-magnitude increment for the SBR catalog (Figure 15). Completeness estimates and number of earthquakes within each interval used in the recurrence calculations are listed below in Table 4.

In the western U.S., the conventional approach has been to assume that the minimum threshold for surface faulting represents the upper size limit for background earthquakes. In the Basin and Range Province, this threshold ranges from **M** 6 to 6.75 (e.g., dePolo, 1994). It is believed that larger earthquakes will be accompanied by surface rupture, and repeated events of this size will produce recognizable fault-related geomorphic features. We have adopted a maximum magnitude distribution of **M** 6.2 [0.101], **M** 6.35 [0.244], **M** 6.5 [0.310], **M** 6.65 [0.244], and **M** 6.8 [0.101] for the SBR. This distribution is consistent with previous site-specific PSHAs completed in central and southern Arizona where all known Quaternary faults within the region are modeled (e.g., Wong *et al*., 2008; Thomas *et al.,* 2015).

Note that the USGS NSHM distribution of maximum magnitude extends to larger magnitudes, but is designed in part to account for the fact that the NSHM model only includes faults for which sufficient paleoseismic history has been established. Our range of background maximum magnitudes in the Basin and Range Province is similar to what is used in other areas of the western U.S. that possess a moderate to high level of heat flow and hence moderate to high crustal temperatures that constrain the thickness of the seismogenic crust to less than 15 to 20 km (e.g., Wong and Chapman, 1990). A rather unique feature of southern Arizona is the presence of short Quaternary faults (< 20 km) with prominent fault scarps (e.g., Sugarload fault zone). The lengths of these faults suggest maximum magnitudes of **M** 6.5 or less. This observation supports the maximum magnitude distribution for background earthquakes stated above.

We estimated recurrence for the background earthquakes for the gridded seismicity model and the uniform model. In both cases, recurrence parameters (*b*-values and rates) were calculated using the program ABSMOOTH (LCI proprietary software; EPRI/DOE/NRC, 2012). The ABSMOOTH program computes a *b*-value for the source zone then divides the source zone into cells of a selected size (0.2-degree cells in this report) and calculates the rate in each cell using the likelihood function of the data in that cell along with penalty functions that smooth the cell-to-cell variation in the rate. The program outputs both mean values and eight alternative sets ("realizations") of the recurrence parameters in order to characterize epistemic uncertainty in the rates and *b*-values (EPRI/DOE/NRC, 2012). This approach is based on the Markov Chain Monte Carlo techniques to generate multiple realizations from a multi-dimensional probability distribution – in this case, the rate, *b*-value and uncertainty in those parameters. The equally-weighted eight alternative maps of rates and *b*-value represent the central tendency and statistical uncertainty in the recurrence parameters and are selected using the Latin Hypercube sampling technique. Eight realizations are used to provide a good representation of the underlying distributions (EPRI/DOE/NRC, 2012) (Figure 5).

Figure 16 shows the gridded seismicity results generated from ABSMOOTH for the SBR. Recurrence parameters for the uniform seismic source zone were adopted from the eight realizations generated for the gridded seismicity, such that the total rates generated for each realization were assumed to apply uniformly across the SBR zone (Figure 5).

In general, earthquake recurrence for the SBR zone is not well constrained. There are few earthquakes (58 independent events of **M** 3.0 or greater, after declustering and accounting for completeness; Table 4) and the historical record is short (< 200 years). Because of the limited seismographic coverage of the SBR, the recurrence is highly uncertain. To incorporate uncertainty into the hazard analysis, we implemented the eight realizations (which include eight *b*-values and rates) generated by ABSMOOTH, with equal weight applied to each realization (Figure 5).

Table 5 provides the rates of events for **M** 5 and above for the corresponding *b*-values for use in the PSHA. Figure 17 shows the resulting recurrence curves for **M** ≥ 5.0 and the range of *b*-values and rates and the mean maximum magnitude of **M** 6.5 compared to the historical seismicity. There is an apparent change in slope for the historical data between **M** 4.5 and **M** 5.0 (Figure 17). Recurrence curves that incorporate the **M** 3.0 to **M** 3.5 historical data tend to result in high *b*-values and curves that appear to underestimate the rate of **M** 5.0 and greater (curves not shown). To avoid this possible underestimation, recurrence calculations for the SBR were performed using only data for **M** 3.5 and greater, with the resulting curves shown in Figure 17.

An inspection of the resulting recurrence intervals for **M** 5 and 6 events was performed to check the reasonableness of the eight *b*-values and rates for the SBR (Figure 17). Using the mean maximum magnitude and the mean of the eight realizations of the recurrence parameters, the resulting recurrence intervals were evaluated. The mean rate at **M** 5.0 was 0.0626, or a recurrence interval of approximately 16 years, and the mean rate at **M** 6.0 was 0.0072, or a recurrence interval of 138 years. The mean *b*-value of the eight realizations was 0.73.

The use of the uniform and gridded seismic source zones were weighted 0.4 and 0.6, respectively (Figure 5). Recent seismicity may be considered more likely representative of seismicity occurring in the next 100 years. However, given the short nearly 190-year long and incomplete historical record the possibility exists that the catalog is not representative of the long-term record of seismicity and thus significant weight is given to the uniform seismicity model.

5.2 Site Characterization

The proposed area of the TSF consists mainly of Quaternary alluvium which overlays Tertiary conglomerate (KCB, 2019). The hazard has been defined at the top of the conglomerate. According to KCB (2019), the conglomerate consists of gravels and cobbles that are generally cemented by an arkosic sandstone and siltstone matrix. In November 2018, HGI performed P-wave seismic refraction surveys at the TSF site and measured P-wave velocities (V_P) of 8,800 to 9,200 ft/sec (2,682 to 2,804 m/sec) that they thought represented the Gila conglomerate. Assuming a range of Poisson's ratio of 0.30 to 0.35 typical of soft to firm rock would result in a V_S range of 1,300 to 1,500 m/sec. We believe this must represent the upper end of V_S for the Gila conglomerate. At the Near West site, MASW (multi-channel-analysis-of-surface waves) surveys were performed in the Gila conglomerate. A range of 700 to 1,050 m/sec was used for the V_S30 input for Near West site for the site category that included the Gila conglomerate and Pinal schist (Wong *et al*., 2017). In the first site-specific seismic hazard evaluation of Resolution Copper's proposed TSF sites, a V_S30 of 500 ± 100 m/sec was used based on V_S surveys performed at another site located on Gila conglomerate. The differences in V_S30 values for the Gila conglomerate probably reflect actual variability in the unit. For this study, we adopt a V_S30 range of 700 to 1,000 m/sec similar to the recent range for the Near West site.

5.3 Ground Motion Models

To estimate the ground motions for crustal earthquakes in the PSHA and DSHA, we have used GMMs appropriate for tectonically active crustal regions. The crustal GMMs, developed as part of the NGA-West2 Project sponsored by PEER Center Lifelines Program, were published in the journal of *Earthquake Spectra*.

The NGA-West2 GMMs were developed based on an expanded strong motion database compared to the initial NGA database. A number of more recent well recorded earthquakes were added to the NGA-West2 database including the Wenchuan, China, numerous moderate magnitude California events down to **M** 3.0, and several Japanese, New Zealand, and Italian earthquakes. Four of the five NGA-West2 GMMs were used in the PSHA and DSHA: Chiou and Youngs (2014), Campbell and Bozorgnia (2014), Abrahamson *et al*. (2014), and Boore *et al*. (2014) (Figure 5). We did not include the model of Idriss (2014) due its lack of a hanging wall model and it is not applicable for V_S30 less than 450 m/sec. The four NGA-West2 GMMs model the effect of larger ground motions on the hanging wall side of a dipping fault using various distance metrics.

The NGA-West2 models, however, are not as well constrained for extensional normal faulting due to a general sparsity of strong motion data for normal faulting earthquakes, particularly for **M** ≥ 6, used in the development of the models. Hence for normal faulting seismic sources, we also considered recent GMMs, developed for Europe, which are based on datasets that contain more normal faulting events. Specifically, we considered the models of Akkar *et al*. (2014) and Bindi *et al*. (2014). These models are based on data where 47% of the records are from normal faulting. Review of the Bindi *et al*. (2014) model indicates that it does not extrapolate well for magnitudes greater than **M** 7 (GeoPentech, 2015). As a result, it is not used in this study.

The four NGA-West2 models and the Akkar *et al.* (2014) model are weighted equally in the PSHA and DSHA for the normal faults within Arizona and the background seismicity (Figure 5). For the large, distant, strike-slip faults, only the four NGA-West2 models are used (equally-weighted), as the Akkar *et al.* (2014) model is based on data with relatively few strike-slip data and is only valid to distances of 200 km. Note that the published distance ranges for the four NGA-West2 GMMs used in this study are up to 300 km (Abrahamson et al., 2014; Chiou and Youngs, 2014; Campbell and Bozorgnia, 2014) or 400 km (Boore et al., 2014). However, distance scaling out to the larger distances of the California sources in these models was examined as part of the Southwestern United States Ground Motion Characterization Study and found to be appropriate (GeoPentech, 2015).

The Akkar *et al.* (2014) model is not defined for periods greater than 4 sec, and so, for longer periods, the model is not used and the logic tree branch weight assigned to Akkar *et al.* (2014) is equally distributed to the remaining four GMMs.

The aleatory variability in the five GMMs used in this analysis is generally a function of period, magnitude, and V_S30. Details of the individual aleatory variability models can be found in the respective references. For example, for the Abrahamson *et al*. (2014) model and a V_S30 of 760 m/sec, sigma varies from 0.67 to 0.81, 0.65 to 0.72 and 0.62 to 0.69 for **M** 5, 6, and 7, respectively. Note that the aleatory variability in the GMMs represents ergodic sigma, which includes site-to-site variability. This analysis assumes the TSF is founded on rock and there is no need for a site response analysis. If a site response analysis is performed in the future and variability in site amplification is included, then there is some double-counting of site aleatory variability. If the results of the firm rock PSHA with the fully ergodic sigma are used, then use of only mean amplification factors from site response analysis should be considered as an approach to avoid double counting site variability.

A range in V_S30 of 700 to 1,000 m/sec was used in the NGA models for the Gila conglomerate (see Section 4.3). Other input parameters for the NGA-West2 GMMs include $Z_{2.5}$, the depth of a V_S of 2.5 km/sec (a proxy for basin effects) which is only used in one model, Campbell and Bozorgnia (2014). Abrahamson *et al.* (2014) and Chiou and Youngs (2014) use $Z_{1.0}$ the depth to the V_S of 1.0 km/sec. We adopted the default values for $Z_{2.5}$ and $Z_{1.0}$ using equations provided by the authors based on the V_S30 at the site. Other parameters such as depth to the top of rupture (zero for all surficial faults unless specified otherwise), dip angle, and rupture width are specified for each fault or calculated within the PSHA code.

As noted by Al Atik and Youngs (2014), the development of the NGA-West2 models was a collaborative effort with many interactions and exchanges of ideas among the developers and the developers indicated that an additional epistemic uncertainty needs to be incorporated into the median ground motions in order to more fully represent an appropriate level of epistemic uncertainty on the median. The three-point distribution and model of Al Atik and Youngs (2014) was applied. The model is a function of magnitude, style of faulting and spectral period.

6.0 SEISMIC HAZARD RESULTS

The hazard results for ground motions are described below and shown in Figures 18 to 42.

6.1 PSHA RESULTS

The results of the PSHA are presented in terms of ground motion as a function of annual exceedance frequency (AEF). AEF is the reciprocal of the average return period. The results for a V_S30 of 700 m/sec are presented. Results for V_S30 of 1,000 m/sec are similar, but slightly lower. Figure 18 shows the mean, median (50th percentile), 5th, 15th, 85th, and 95th percentile hazard curves for peak horizontal ground acceleration (PGA). The range of uncertainty between the 5th and 95th percentile (fractiles) is about a factor of 3.0 at a return period of 10,000 years. These fractiles indicate the range of epistemic uncertainty about the mean hazard. The 1.0 sec horizontal spectral acceleration (SA) hazard is shown on Figure 19. At the return periods of 475, 2,500, 5,000, and 10,000 years, the mean and fractile PGA and 1.0 sec SA values are listed in Table 6. The hazard can be characterized as low to moderate even at a long return period of 10,000 years.

The contributions of the various seismic sources to the mean PGA and 1.0 sec SA hazard are shown on Figures 20 to 23. At PGA, the contribution from the SBR background earthquakes dominates the hazard due to the absence of any nearby Quaternary faults (Figures 20 and 21). At 1.0 sec SA, the background seismicity controls the hazard for return periods greater than 100 to 200 years, but there are also contributions from the relatively distant Cerro Prieta fault and southern San Andreas fault due to the absence of active local faults (Figures 22 and 23).

The hazard can also be deaggregated in terms of the joint magnitude-distance-epsilon probability conditional on the ground motion parameter (PGA or SA exceeding a specific value). Epsilon is the difference between the logarithm of the ground motion amplitude and the mean logarithm of ground motion (for that M and R) measured in units of standard deviation (ε). Thus positive epsilons indicate larger than average ground motions. By deaggregating the PGA and 1.0 sec SA hazard by magnitude, distance and epsilon bins, we can illustrate the contributions by events at various periods. Figures 24 to 27 illustrate the contributions by events for return periods of 475, 2,500, 5,000 and 10,000 years. At PGA and all return periods, background earthquakes within about 120 km of the site dominate the hazard (Figures 24 and 25). At 1.0 sec SA, the contributions from the more distant faults, Cerro Prieta and San Andreas, are shown in Figures 26 and 27. Note that the peaks for these two distant sources in these figure represent a combined contribution of about 40% to the 1.0 sec SA hazard at the 475-year return period with decreasing contribution as return period increases (Figure 23).

Based on the magnitude and distance bins (Figures 24 to 27), the controlling earthquakes as defined by the mean magnitude (M-bar) and modal magnitude (M*) and mean distance (D-bar) and modal distance (D*) can be calculated. Table 7 lists the M-bar, M*, D-bar, and D* for the four return periods (475, 2,500, 5,000, and 10,000 years) and for PGA and 1.0 sec horizontal SA. Mean epsilons are also provided in Table 7.

In Figure 28, the UHS are shown for V_S30 700 m/sec and a suite of return periods from 475 to 10,000 years. A UHS depicts the ground motions at all spectral periods with the same annual exceedance frequency or return period. The UHS for V_S30 of 1,000 m/sec are lower at all periods, and so the UHS for V_S30 700 m/sec are selected as the final UHS. Table 8 provides the mean UHS for the suite of return periods from 475 to 10,000 years.

6.1.1 Hazard Sensitivities

In this section, sensitivities to the hazard due to the GMMs and major components of the seismic source model are examined. Sensitivities were performed for a V_S30 of 700 m/sec, but the relative results are applicable to all site conditions.

In these sensitivity analyses, the total mean hazard curves are conditioned on specific nodes in the logic tree having a full weight of 1.0. Figure 29 illustrates the sensitivity of the mean PGA hazard from Arizona sources to the choice of GMMs. At the 10,000-year return period, there is a factor of 2.3 difference between the models giving the largest and smallest ground motion. This is a typical value for current GMMs in tectonically active regions and is a significant source of uncertainty in the PGA and 1.0 sec horizontal SA hazard. Similarly, Figure 30 illustrates the sensitivity of the mean PGA hazard from the distant Southern and Baja California sources to the GMMs. Note that the Akkar et al. (2014) GMM is not used for the distant Southern and Baja California sources, as described in Section 5.3. The PGA hazard from these sources is very low. Figures 31 and 32 illustrate the sensitivity of the 1.0 sec SA hazard to GMMs. There is significant uncertainty in the 1.0 sec SA hazard from the large distant sources due to the suite of GMMs (Figure 32).

On Figures 33 and 34, the sensitivity in the PGA and 1.0 sec SA hazard is shown between the gridded and the uniform background zone which were weighted 0.6 and 0.4, respectively, in the PSHA. The hazard is higher for the gridded seismicity background zone model due to the site being located in an area of above average seismicity for the SBR (Figures 2 and 16).

Figures 35 and 36 show the sensitivity in hazard to the Mmax for the background earthquakes. There is some increase in the PGA hazard for the range of Mmax (Figure 35), but more increase in the 1.0 sec SA hazard (Figure 36). The 1.0 sec SA hazard is more sensitive to larger magnitude earthquakes than at PGA.

Figures 37 and 38 show the sensitivity to the differences in the gridded seismicity rates computed by ABSMOOTH. There are significant differences between the different rates with realization 8 giving much lower hazard. This reflects the large uncertainties incorporated into the rates for the background seismicity due to the short and incomplete historical record (Figure 16).

Tornado plots are provided to summarize the sensitivity analyses. The plots show the effects of the dominant seismic hazard model components (on vertical axis) on the total mean hazard specified in terms of the ground motion at a given return period. For each key element of the seismic hazard model, sensitivity analyses are performed assigning a weight of 1.0 to one of the epistemic alternatives (nodes on the logic tree) for that element of the seismic hazard model, as discussed above. The ground motion (PGA and 1.0 sec SA) at 10,000-year return period is computed from each sensitivity analysis. The tornado plot shows the ratio of these ground motions to the ground motion from the full analysis using the entire logic tree.

Figures 39 and 40 show tornado plots at a return period of 10,000 years. At PGA, the gridded seismicity rates and GMMs for Arizona seismic sources are the sources of the largest uncertainty in the hazard. There is also significant uncertainty from the approach to background seismicity, with the gridded seismicity giving higher hazard (Figures 34 and 39). At 1.0 sec SA, the GMMs for both the Arizona sources and the Southern and Baja California sources, are the largest source of uncertainty (Figure 40). Mmax of the background earthquakes is not that significant to the mean hazard (Figures 39 and 40).

6.2 Comparison with National Seismic Hazard Maps

In 1996, the USGS released a "landmark" set of National Hazard Maps for earthquake ground shaking, which was a significant improvement from previous maps they had developed (Frankel *et al*., 1996). These maps have been revised and updated, and the most current version was released in 2014 (Petersen *et al*., 2014). These maps were the result of the most comprehensive analyses of seismic sources and ground motion prediction ever undertaken on a national scale and they make use of the five NGA-West2 models. The 2014 maps are the basis for the current International Building Code. The maps are for NEHRP site class B/C (firm rock) or V_S30 of 760 m/sec.

For a 2,475-year return period, the 2014 USGS National Seismic Hazard Maps indicate a firm rock PGA and 1.0 sec SA of 0.14 and 0.076 g, respectively, for the Project site compared to the site-specific values of 0.078 and 0.051 g for a V_S30 of 700 m/sec (Table 9). The difference is due mainly to the difference in the treatment of the hazard from the background seismicity, and to a lesser extent a difference in GMMs. The USGS uses a minimum rate or floor for the region covered by the SBR based on uniform smoothing of seismicity. The region for which the background rates are computed is much larger and includes higher seismicity regions to the north. In addition, the USGS uses a higher maximum magnitude (**M** 7.45) and a large smoothing kernel (50 km) in their Gaussian smoothing approach. The USGS uses the NGA-West2 GMMs.

In order to examine the reasons for the differences, the hazard was rerun using the Mmax and fault type distribution for the background seismicity used by the USGS. The resulting PGA and 1.0 sec SA of 0.095 and 0.070 g are much closer to the USGS values of 0.14 and 0.076 (Table 9). The remaining differences are likely largely due to the minimum floor the USGS uses for the entire basin and range region, and to a lesser extent the difference in GMMs.

6.3 DSHA Results

The most significant seismic source to the Project in a deterministic sense is the Whitlock Wash fault, although this fault is approximately 52 km to the southeast (Figure 3). Figure 41 shows the median and 84th percentile 5%- damped horizontal acceleration response spectra and the individual spectra from each of the GMMs for the 84th percentile. Tables 10 and 11 provide the inputs and results of the DSHA, respectively.

Figure 42 shows comparisons of the horizontal deterministic spectra with UHS for a range of return periods. The 84th percentile spectra has an equivalent return period similar to the 2,500-year UHS at spectral periods less than 0.2 sec and similar to the 5,000-year UHS for periods reater than about 0.49 sec (Figure 42). The median deterministic spectra has an equivalent return period between 475 and 2,500 years. The equivalent return period of the deterministic ground motions is controlled both by the level of the probabilistic hazard at the site. For this site, the ground motions for the distant Whitlock Wash fault are relatively low compared to the seismicity around the site resulting in relatively short equivalent return periods for the deterministic ground motions.

7.0 DEVELOPMENT OF TIME HISTORIES

In consultation with KCB, we developed nine horizontal-component time histories for the UHS at a return period of 10,000 years. Because the response spectrum of a time history has peaks and valleys that deviate from the design response spectrum (target spectrum), it is necessary to modify the motion to improve its response spectrum compatibility. The procedure proposed by Lilhanand and Tseng (1988), as modified by Al Atik and Abrahamson (2010) and contained in the computer code RSPMatch2009, was used to develop the acceleration time histories through spectral matching to the target spectrum.

Recorded time histories used as input for spectral matching are referred to as “seed” records. Seed records were selected such that they have a scaled spectral shape similar to the target spectrum, and that they originate from magnitudes and distances similar to those that contribute most to the target spectrum, as determined from the deaggregation performed in Section 6 (Table 7). A similar spectral shape minimizes the changes required by the spectral matching program, and improves the overall quality of the matched record (e.g., Grant *et al.*, 2008).

Time-domain approaches to spectral matching such as the one taken in *RSPMatch2009* are preferable to frequency-domain approaches because the resulting adjustments to the time history are more localized in time (Lilhanand and Tseng, 1988); the matched acceleration, velocity, and displacement time histories more closely resemble those of the seed record (Lilhanand and Tseng, 1988); and because frequency-domain approaches can cause large changes to the overall energy content of the time history (Naeim and Lew, 1995).

Figure 43 compares the response spectra of the selected seed time histories scaled to the target spectrum. Table 12 lists the seed time histories and they are shown on Figures 44 to 52. The spectral matches and the resulting time histories are shown on Figures 53 to 70 with the response spectra calculated from the matched time histories. Shown with each set of acceleration, velocity and displacement time histories is the normalized Arias intensity or Husid plot, which provides an appropriate duration measure independent of the absolute amplitude level of the acceleration time history. The properties of the spectrally-matched time histories are listed in Table 13.

The duration of strong ground motion is related to the time required for the release of accumulated strain energy by rupture along the fault. Trifunac and Brady (1975) defined the “significant duration” of a time history as the time interval between the points at which 5% and 95% of the total energy (represented by I_a) has been recorded. The target 5 to 95% duration for the time histories was calculated using the model of Abrahamson and Silva (1996) for a **M** 6.1 at 30 km, based on the deaggregation of the hazard at the 10,000-year return period. The target duration is 9.3 sec with a ±1σ range of 5.7 to 15.2 sec. The spectrally-matched time histories have durations ranging from 8.3 to 16.6 sec with an average of 11.7 sec (Table 13).

Arias intensity (I_a) is a ground motion parameter defined by Arias (1970) as the integral of the square of acceleration over the duration of a time series record, as follows:

$$I_a = \frac{\pi}{2g} \int_0^{\infty} a(t)^2 \, dt \tag{14}$$

where $a(t)$ is acceleration and g is the acceleration of gravity. Studies show that I_a correlates well with the damage potential of earthquakes (Travasarou *et al.*, 2003).

The target I_a for horizontal time histories is 0.2 m/sec with a ±1σ range of 0.14 to 0.29 m/sec, computed using the equally weighted models of Abrahamson *et al.* (2016) and Watson-Lamprey and Abrahamson (2006). The modified horizontal time histories have I_a ranging from 0.20 to 0.28 m/sec with an average of 0.20 m/sec (Table 13).

8.0 REFERENCES

Abrahamson, N.A. and Silva, W.J., 1996, Empirical ground motion models: Report to Brookhaven National Laboratory.

Abrahamson, C., Hao-Jun, M.S. and Yang, B., 2016, Ground-motion prediction equations for Arias intensity consistent with the NGA-West2 ground-motion Models: PEER Report No. 2016/05, Pacific Earthquake Engineering Research Center, University of California, Berkeley, 42 p.

Abrahamson, N.A. and Silva, W.J., and Kamai, R., 2014, Summary of the ASK14 ground-motion relation for active crustal regions: Earthquake Spectra, v. 30, p. 1025-1055.

Aki, K., 1983, Seismological evidence in support of the existence of “Characteristic Earthquakes”: Earthquake Notes, v. 54, p. 60-61.

Al Atik, L. and Youngs, R., 2014, Epistemic uncertainty for NGA-West2 models: Earthquake Spectra: v. 30, p. 1301-1318.

Al Atik, L. and Abrahamson, N., 2010, An improved method for nonstationary spectral matching: Earthquake Spectra: v. 26, p. 601-617.

Anderson, J.G., 1979, Estimating the seismicity from geological structure for seismic risk studies: Bulletin of the Seismological Society of America, v. 69, p. 135-158.

Arias, A., 1970, A measure of earthquake intensity: Seismic Design for Nuclear Power Plants, R.J. Hansen, ed., MIT Press, Cambridge, Massachusetts, pp.438-483.

Bausch, D. and Brumbaugh, D.A., 1997, Relocation study of early Arizona earthquakes: Events of 1906, 1910, and 1912: unpublished report prepared for Arizona Division of Emergency Management, Earthquake Program, 65 p. + Appendices.

Boore, D.M., Stewart, J.P., Seyhan, E., Atkinson, G.M., 2014, NGA-West2 equations for predicting PGA, PGV, and 5%-damped PSA for shallow crustal earthquakes: Earthquake Spectra, v. 32, p. 979-1004.

Brumbaugh, D. S., 1987, A tectonic boundary for the Southern Colorado Plateau: Tectonophysics, v. 136, p. 125-136.

Campbell, K.W. and Bozorgnia, Y., 2014, NGA-West2 ground motion model for the average horizontal components of PGA, PGV, and 5%-damped linear acceleration response spectra: Earthquake Spectra, v. 30, p. 1087-1115.

Cao, T.C., Bryant, W.A., Rowshandel, B., Branum, D., and Wills, C.J., 2003, The revised 2002 California probabilistic seismic hazard maps, June 2003: California Geological Survey website.

Chiou, B-S.J. and Youngs, R.R., 2014, Update of the Chiou and Youngs NGA ground motion model for average horizontal component of peak ground motion and response spectra: Earthquake Spectra, v. 30, p. 1117-1153.

Cornell, C.A., 1968, Engineering seismic risk analysis: Bulletin of the Seismological Society of America, v. 58, p. 1583-1606.

Cornwall, H.R., Banks, N.G., and Phillips, C.H., 1971, Geologic map of the Sonora quadrangle, Pinal and Gila Counties, Arizona: U.S. Geological Survey, Geological Quadrangle Map GQ-1021, 1:24,000 scale.

Cornwall, H.R. and Krieger, M.H., 1978, Geologic map of the El Capitan Mountain quadrangle, Gila and Pinal Counties, Arizona: U.S. Geological Survey, Geological Quadrangle Map GQ-1442, 1:24,000 scale.

dePolo, C.M., 1994, The maximum background earthquake for the Basin and Range Province, western North America: Bulletin of the Seismological Society of America, v. 84, p. 466-472.

DuBois, S.M., Smith, A.W., Nye, N.K., and Nowak, T.A., 1982, Arizona earthquakes, 1776- 1980: Arizona Bureau of Geology and Mineral Technology Bulletin, v. 192, 456 p.

EPRI/DOE/NRC, 2012, Technical Report: Central and Eastern United States Seismic Source Characterization for Nuclear Facilities. EPRI, Palo Alto, CA, U.S. DOE, and U.S. NRC: 2012.

Field, E.H., Biasi, G.P., Bird, P., Dawson, T.E., Felzer, K.R., Jackson, D.D., Johnson, K.M., Jordan, T.H., Madden, C., Michael, A.J., Milner, K.R., Page, M.T., Parsons, T., Powers, P.M., Shaw, B.E., Thatcher, W.R., Weldon, R.J., II, and Zeng, Y., 2013, Uniform California Earthquake Rupture Forecast, Version 3 (UCERF3) – The Time-Independent Model: U.S. Geological Survey Open-File Report 2013-1165, California Geological Survey Special Report 228, and Southern California Earthquake Center Publication 1792.

Grant, D. N., Greening, P. D., Taylor, M. L., and Ghosh, B., 2008, Seed record selection for spectral matching with RSPMatch2005. 14th World Conference on Earthquake Engineering, Beijing, China.

Hanks, T.C. and Kanamori, H. 1979, A moment magnitude scale: Journal of Geophysical Research, v. 84, p. 2348-2350.

KCB Consultants Ltd., 2019, Skunk Camp site investigation, doc. # CCC.03-81600-EX-REP-00012 – Rev. 0 prepared for Resolution Copper Mining LLC.

Keefer, D.I. and Bodily, S.E., 1983, Three-point approximations for continuous random variables: Management Science, v. 26, p. 595-609.

Lilhanand, K. and Tseng, W.S., 1988, Development and application of realistic earthquake time histories compatible with multiple-damping design spectra: Proceeding of the 9th World Conference on Earthquake Engineering, Tokyo-Kyoto, Japan.

Lockridge, J.S., Fouch, M.J., and Arrowsmith, J.R., 2012, Seismicity within Arizona during the deployment of the EarthScope USArray Transportable Array: Bulletin of the Seismological Society of America, v. 102, p. 1850-1863.

Lund, W.R., 2012, Basin and Range Province Earthquake Working Group II Recommendations to the U.S. Geological Survey National Seismic Hazard Mapping Program for the 2014 Update of the National Seismic Hazard Maps: Utah Geological Survey Open-File Report 591, 17 p.

Mack, G.H., Seager, W.R., and Leeder, M.R., 2003, Synclinal-horst basins: examples from the southern Rio Grande rift and southern transition zone of southwestern New Mexico: Basin Research, v. 15, p. 365-377.

McQuarrie, N., and Wernicke, B.P., 2005, An animated tectonic reconstruction of southwestern North America since 36 Ma: Geosphere, v. 1, p. 147–172.

Menges, C.M. and McFadden, L.D., 1981, Evidence for the latest-Miocene to Pliocene transition from Basin-Range tectonic to post-tectonic landscape evolution in southeastern Arizona: Arizona Geological Society Digest, v. 13, p. 151-160.

Menges, C.M. and Pearthree, P.A., 1983, Map of Neotectonic (Latest Pliocene-Quaternary) deformation in Arizona: Arizona Geological Survey Open-File Report 83-22, 48 p. with four plates, 1:500,000, 1:133,830, and 1:121,000 scales.

Menges, C.M. and Pearthree, P.A., 1989, Late Cenozoic tectonism in Arizona and its impact on regional landscape evolution: *in* Geologic Evolution of Arizona, Arizona Geological Society, Digest No. 17, p. 649–680.

Molnar, P., 1979, Earthquake recurrence intervals and plate tectonics: Bulletin of the Seismological Society of America, v. 69, p. 115-133.

Morgan, P., and Swanberg, C.A., 1985, on the Cenozoic uplift and tectonic stability of the Colorado Plateau: Journal of Geodynamics, v. 3, p. 39-63.

Naeim, F. and Lew, M., 1995, On the Use of Design Spectrum Compatible Time Histories. Earthquake Spectra, 11(1), p. 111-127.

Pearthree, P.A., 1998, Quaternary fault data and map of Arizona: Arizona Geological Survey Open-File Report 98-24, 122 p.

Pearthree, P.A., Menges, C.M., and Mayer, L., 1983, Distribution, recurrence, and possible tectonic implications of late Quaternary faulting in Arizona: Arizona Bureau of Geologic Mineral Technical Open-File Report 83-20, 51 p.

Peirce, H.W., 1984, The Mogollon escarpment: Arizona Bureau of Geology and Mineral Technology Fieldnotes, v. 4, p. 8-11.

Petersen, M.D., Frankel, A.D., Harmsen, S.C., Mueller, C.S., Haller, K.M., Wheeler, R.L., Wesson, R.L., Zeng, Y., Boyd, O.S., Perkins, D.M., Luco, N., Field, E.H., Wills, C.J., and Rukstales, K.S., 2008, Documentation for the 2008 update of the United States National Seismic Hazard Maps: U.S. Geological Survey Open-File Report 2008-1128, 61 p.

Peterson, N., 1961, Geology of the Pinal Ranch quadrangle, Arizona: U.S. Geological Survey, Bulletin 1141-H, 1:24,000 scale.

PhotoSat Information Ltd., 2019, PhotoSat stereo satellite surveying project report for Resolution Copper Mining, Arizona: Reference No. 4039, May 31, 2019.

Piety, L.A. and Anderson, L.W., 1991, The Horseshoe fault--Evidence for prehistoric surface- rupturing earthquakes in central Arizona: Arizona Geology, v. 21, no. 3, p. 1, 4-8.

Richard, S.M. and Spencer, J.E., 1998, Compilation geologic map of the Ray-Superior area, central Arizona: Arizona Geological Survey Open-File Report 98-13, 50 p. with three plates, 1:24,000 scale.

Schwartz, D.P. and Coppersmith, K.J., 1984, Fault behavior and characteristic earthquakes-- examples from the Wasatch and San Andreas fault zones: Journal of Geophysical Research, v. 89, p. 5681-5698.

Sieh, K.E. and Jahns, R.H., 1984, Holocene activity of the San Andreas fault at Wallace Creek, California: Geological Society of America Bulletin, v. 95, p. 883-896.

Sims, J.D., 1994, Stream channel offset and abandonment and a 200-year average recurrence interval of earthquakes on the San Andreas fault at Phelan Creek, Carrizo Plain, California, *in* Prentice, C.S., Schwartz, D.P., and Yeats, R.S. (eds.), Proceedings of the workshop on paleoseismology: U.S. Geological Survey Open-File Report 94-568, p. 170-172.

Stepp, J.C., 1972, Analysis of completeness of the earthquake sample in the Puget Sound area and its effect on statistical estimates of earthquake hazard: Proceedings of the International Conference on Microzonation, v. 2, 897-910.

Stirling, M., Rhoades, D., and Berryman, K., 2002, Comparison of earthquake scaling relations derived from data of the instrumental and preinstrumental era: Bulletin of the Seismological Society of America, v. 92, p. 812-830.

Suter, M. and Contreras, J., 2002, Active tectonics of northeastern Sonora, Mexico (southern Basin and Range Province) and the 3 May 1887 MW 7.4 earthquake: Bulletin of the Seismological Society of America, v. 92, p. 581-589.

Thomas, P.A., Wong, I.G., and Abrahamson, N., 2010, Verification of probabilistic seismic hazard analysis software programs: PEER Report 2010/106, Pacific Earthquake Engineering Research Center, College of Engineering, University of California, Berkeley, 173 p.

Thomas, A.P. and Rockwell, T.R., 1996, A 300- to 550-year history of slip on the Imperial fault near the U.S.-Mexico border-Missing slip at the Imperial fault bottleneck: Journal of Geophysical Research, v. 101, p. 5987-5997.

Travasarou, T., Bray, J.D., and Abrahamson, N.A., 2003, Empricial attenuation relationship for Arias intensity: Earthquake Engineering and Structural Dynamics, v. 32, p. 1133-1155.

Trifunac, M. D. and Brady, A.G., 1975, On the correlation of seismic intensity scales with the peaks of recorded strong ground motion: Bulletin of the Seismological Society of America, v. 65, p. 139-162.

United States Geological Survey (USGS) and Arizona Geological Survey (AZGS), 2019, Quaternary Fault and Fold Database of the United States, accessed November 11, 2019 at http//earthquakes.usgs.gov/regional/qfaults.

Watson-Lamprey, J. and Abrahamson, N., 2006, Selection of ground motion time series and limits on scaling: Soil Dynamics and Earthquake Engineering, v. 26, p. 477-482.

Wells, D.L. and Coppersmith, K.J., 1994, New empirical relationships among magnitude, rupture length, rupture width, rupture area, and surface displacement: Bulletin of the Seismological Society of America, v. 84, p. 974-1002.

Wesnousky, S.G., 1986, Earthquakes, Quaternary faults, and seismic hazard in California: Journal Geophysical Research, v. 91, p. 12,587-12,631.

Wesnousky, S.G., 2008, Displacement and geometrical characteristics of earthquake surface ruptures-issues and implications for seismic-hazard analysis and the process of earthquake rupture; Bulletin of the Seismological Society of America, v. 98, p. 1609-1632.

WGCEP (Working Group on California Earthquake Probabilities), 1988, Probabilities of large earthquakes occurring in California on the San Andreas fault: U.S. Geological Survey Open- File Report 88-398, 62 p.

WGCEP (Working Group on California Earthquake Predictions), 1995, Seismic hazards in southern California: probable earthquakes, 1994 to 2024: Bulletin of the Seismological Society of America, v. 95, p. 379-439.

Wong, I.G. and Humphrey, J.R., 1989, Contemporary seismicity, faulting, and the state of stress in the Colorado Plateau: Geological Society of America Bulletin, v. 101, p. 1127-1146.

Wong, I.G. and Chapman, D.S., 1990, Deep intraplate earthquakes in the western U.S. and their relationship to lithospheric temperatures: Bulletin of the Seismological Society of America, v. 80, p. 589-599.

Wong, I., Pezzopane, S., and Dober, M., 2008, Site-specific seismic hazard analyses for Miami Tailing Dams, Claypool, Arizona: unpublished report prepared for Freeport-McMoran Copper and Gold Miami Operations.

Wong, I.G., Nemser, E., Dober, M., Olig, S., Bott, J., and Terra, F., Darragh, R., and Silva, W., 2013, Site-specific seismic hazard analyses for the Resolution Mining Company tailings storage facilities options, Southern Arizona: unpublished report prepared for Resolution Copper Mining.

Wong, I.G., Thomas, P., Lewandowski, N., Lindvall, S., and Seifried, A., 2017, Updated site-specific seismic hazard and development of time histories for the Resolution Copper's New West site, Southern Arizona: unpublished report prepared for Resolution Copper.

Youngs, R.R. and Coppersmith, K.J., 1985, Implications of fault slip rates and earthquake recurrence models to probabilistic seismic hazard estimates: Bulletin of the Seismological Society of America, v. 75, p. 939-964.

Youngs, R.R., Swan, F.H., Power, M.S., Schwartz, D.P., and Green, R.K., 2000, Probabilistic analysis of earthquake ground shaking hazard along the Wasatch Front, Utah, in P.L. Gori and W.W. Hays (eds.), Assessment of Regional Earthquake Hazards and Risk Along the Wasatch Front, Utah: U.S. Geological Survey Professional Paper 1500-K-R, p. M1-M74.

Tables

Table 1. Summary of GPS Waypoint Locations, Observations, and Interpretations from Reconnaissance-Level Fault Investigation

WAYPOINT	COORDINATES	DESCRIPTION	INTERPRETATION
WP-01	N 33.16105° W 110.90905°	View north from south side of unnamed canyon to fault contact mapped by Cornwall *et al.* (1971) juxtaposes Dripping Spring quartzite (ds) on the west against Escabrosa limestone (Me) on the east.	No geologic or geomorphic evidence observed for Quaternary faulting in unnamed canyon from Dripping Spring Wash upstream to WP-01.
WP-02	N 33.16518° W 110.90510°	Quaternary pediment (Qp) mapped by Cornwall *et al.* (1971) shows weak desert pavement, little to no desert varnish, and no carbonate nodules at the ground surface.	No geomorphic evidence observed for Quaternary faulting of this pediment surface.
WP-03	N 33.17220° W 110.90512°	Quaternary pediment (Qp) mapped by Cornwall *et al.* (1971) shows weak desert pavement, minor desert varnish, and no carbonate nodules at the ground surface.	No geomorphic evidence observed for Quaternary faulting of this pediment surface.
WP-04	N 33.18128° W 110.91802°	View southwest from dirt road of ~30-m-high, ~200-m-long, north-facing canyon wall exposure of heavily vegetated Tertiary conglomerate (Tcg) through which Cornwall *et al.* (1971) map an unnamed fault strand as a solid line.	No evidence observed for faulting in canyon wall exposure, although beds cannot be confidently traced along entire length of exposure to definitively preclude faulting at this location.
WP-05	N 33.18072° W 110.91840°	Weakly bedded Tertiary conglomerate (Tcg) exposed along base of unnamed creek, dips shallowly eastward. Near location where Cornwall *et al.* (1971) map an unnamed fault strand as a solid line.	No geologic evidence observed for faulting of ~100-m-long creek-bottom exposure of Tcg.
WP-06	N 33.18143° W 110.91672°	View west-southwest from dirt road of exposure described in WP-04.	Same as WP-04.
WP-07	N 33.18219° W 110.91758°	Quaternary pediment (Qp) mapped by Cornwall *et al.* (1971) shows weak desert pavement, minor desert varnish, and no carbonate nodules at the ground surface.	No geomorphic evidence observed for Quaternary faulting of this pediment surface.
WP-08	N 33.22387° W 110.93458°	Unnamed bedrock fault near Walnut Spring mapped by Cornwall *et al.* (1971) juxtaposes Dripping Spring quartzite (ds) against Precambrian diabase (db). Directly east of this location, Cornwall *et al.* (1971) map a short section of the Dripping Spring fault as a	No geologic or geomorphic evidence observed for Quaternary faulting.

WAYPOINT	COORDINATES	DESCRIPTION	INTERPRETATION
		solid line in active wash deposits (Qal) of Walnut Canyon.	
WP-09	N 33.21329° W 110.93528°	View south from Quaternary pediment (Qp) along tonal and topographic lineament identified in air photos and site topographic data.	No geomorphic evidence observed for Quaternary faulting of this pediment surface.
WP-10	N 33.21236° W 110.93520°	Contact between Precambrian diabase (db) and Tertiary conglomerate (Tcg) exposed in channel.	No geologic or geomorphic evidence observed for Quaternary faulting. Interpreted as geologic, as opposed to fault, contact.
WP-11	N 33.20875° W 110.93613°	View southeast along Quaternary pediment (Qp) across tonal and topographic lineament identified in air photos and site topographic data. Surface shows weak desert pavement, little to no desert varnish, and no carbonate nodules at the ground surface.	No geomorphic evidence observed for Quaternary faulting of this pediment surface.
WP-12	N 33.20866° W 110.93534°	Weathered Precambrian diabase (db) outcrop largely obscured by thin veneer of slope-wash material; was mapped as Tertiary conglomerate (Tcg) by Cornwall *et al.* (1971).	No geomorphic evidence observed for Quaternary faulting. Lineament appears to be erosional feature associated with geologic contact between db and Tcg.
WP-13	N 33.20745° W 110.93372°	View northwest along Quaternary pediment (Qp) across tonal and topographic lineament identified in air photos and site topographic data. Surface shows weak desert pavement, little to no desert varnish, and no carbonate nodules at the ground surface.	No geomorphic evidence observed for Quaternary faulting of this pediment surface.
WP-14	N 33.24755° W 110.94492°	Near unnamed, northwest-striking fault mapped by Richard and Spencer (1998). Fault is mapped in Miocene-age conglomerate (Tc) and is concealed beneath Pleistocene to Late Miocene basin-fill deposits (QTs).	No geologic or geomorphic evidence observed for Quaternary faulting.
WP-15	N 33.25774° W 110.96127°	Road cut exposure of unnamed, northwest-striking fault in Tertiary dacite (Td) mapped by Peterson (1963), expressed as highly weathered zone in Td.	No geologic or geomorphic evidence observed for Quaternary faulting.
WP-16	N 33.25779° W 110.95852°	View northeast along strike of unnamed fault mapped by Peterson (1963). Fault juxtaposes bedded tuffaceous sandstone (QTgt) on the northwest against basin-fill deposits (QTg).	No geologic or geomorphic evidence observed for Quaternary faulting.

WAYPOINT	COORDINATES	DESCRIPTION	INTERPRETATION
WP-17	N 33.25806° W 110.95835°	View northeast along strike of fault described in WP-16.	Same as WP-16.

Table 2. Fault Parameters

FAULT NO.[2]	FAULT NAME	DISTANCE TO SITE (km)	RUPTURE MODEL	MAXIMUM RUPTURE LENGTH[3] (km)	MAXIMUM MAGNITUDE[4] (M)	FAULT DIP[5] (degrees)	FAULT TYPE[6]	APPROXIMATE AGE OF YOUNGEST OFFSET	PROBABILITY OF ACTIVITY[7]	SLIP RATE[8] (mm/yr)	COMMENTS
941	Alma Mesa fault	172	Independent (1.0)	16	6.3 (0.2) 6.6 (0.6) 6.9 (0.2)	45 E (0.2) 60 E (0.6) 75 E (0.2)	N	< 1.6 Ma	1.0	0.005 (0.5) 0.02 (0.5)	This north-northeast striking normal fault is near the northwestern margin of the Alma basin along the Arizona - New Mexico border (Menges and Pearthree, 1983; Houser, 1994). The Alma Mesa fault is characterized by 10- to 20-m-high fault scarps on deeply dissected Plio-Pleistocene alluvial fan remnants. Our maximum slip rate assumes 20 m of vertical displacement occurred since 1 Ma whereas the minimum rate assumes 10 m occurred since 2 Ma.
	Anderson	183	Independent (1.0)	26	6.5 (0.2) 6.8 (0.6) 7.1 (0.2)	35 SW (0.2) 50 SW (0.6) 65 SW (0.2)	N	< 1.6 Ma	1.0	0.001 (0.2) 0.01 (0.6) 0.1 (0.2)	Northwest-striking fault is modified from Pearthree (2013, written communication) and was classified as a potential Quaternary fault in seismic source characterization for Palo Verde Nuclear Generating Station (LCI, 2015). Fault has not yet been included in USGS Quaternary Fault and Fold Database.
2093	Animas Valley faults	204	Independent (1.0)	20	6.4 (0.2) 6.7 (0.6) 7.0 (0.2)	45 W (0.2) 60 W (0.6) 75 W (0.2)	N	< 15 ka	1.0	0.005 (0.2) 0.02 (0.6) 0.2 (0.2)	Our characterization here is the same as in our previous study for Chino Mine (Wong *et al.*, 2006). These faults extend along the eastern margin of Animas Valley and the west side of the Pyramid Mountains (Machette *et al.*, 1986). Preferred slip rate is based on observations of 2 to 3 m scarps on late Pleistocene fans (Machette *et al.*, 1998).
	Agua Prieta (MX)	257	Independent (1.0)	41	6.7 (0.2) 7.0 (0.6) 7.3 (0.2)	35 E (0.2) 50 E (0.6) 65 E (0.2)	N	< 1.6 Ma	1.0	0.001 (0.2) 0.01 (0.6) 0.1 (0.2)	Fault expressed in bedrock and classified as a potential Quaternary fault in seismic source characterization for Palo Verde Nuclear Generating Station (LCI, 2015). The fault is located in northern Sonora, Mexico and along strike of the Quaternary Pedrogosa fault in southeast Arizona.
Not included in USGS database	Big Burro Mountains fault	184	Independent (1.0)	38	6.7 (0.2) 7.0 (0.6) 7.3 (0.2)	45 W (0.2) 60 W (0.6) 75 W (0.2)	N	< 1.6 Ma?	0.7	0.001 (0.5) 0.01 (0.5)	This northwest-striking, southwest-dipping, normal fault along the southwest flank of the Big Burro Mountains is not included in the USGS Quaternary Fault and Fold Database, but we include it as a potential fault source based on mapping of potential Quaternary fault scarps by Machette *et al.* (1986). They estimate tens of meters of slip in Plio-Pleistocene deposits, but little else is known about this poorly understood fault. Based on its poorer geomorphic expression, we assumed a maximum slip rate similar to the preferred rate of the Gold Hill fault zone to the southeast. We assumed 1 to 2 m of slip occurred since ~1 Ma for the minimum rate. We assigned a slightly lower probability of activity of 0.7 because evidence for repeated Quaternary movement is not as strong as other faults in the region that were included by Machette *et al.* (1998) in their Quaternary fault compilation.

FAULT NO.[2]	FAULT NAME	DISTANCE TO SITE (km)	RUPTURE MODEL	MAXIMUM RUPTURE LENGTH[3] (km)	MAXIMUM MAGNITUDE[4] (M)	FAULT DIP[5] (degrees)	FAULT TYPE[6]	APPROXIMATE AGE OF YOUNGEST OFFSET	PROBABILITY OF ACTIVITY[7]	SLIP RATE[8] (mm/yr)	COMMENTS
951	Big Chino fault	229	Independent (1.0)	63	6.9 (0.2) 7.2 (0.6) 7.5 (0.2)	35 SW (0.2) 50 SW (0.6) 65 SW (0.2)	N	<15 ka 10-15 ka	1.0	0.05 (0.2) 0.12 (0.6) 0.3 (0.2)	Slip rates based on 8 m vertical displacement of upper Pleistocene alluvium (80-100 ka): 0.1 – 0.08 mm/yr., and 18 to 25 m vertical displacement of mid Pleistocene (200-400 ka) alluvium: 0.05-0.1 mm/yr (Euge *et al.*, 1992). Maximum value assumes a 3 m event and 10,000 year recurrence interval: 2-0.3 mm/yr. Preferred maximum magnitude based on surface rupture length of 46 km (Pearthree, 1998) and average displacements per event of 1.8 to 2.7 m (Euge *et al.*, 1992).
	Bootlegger	183	Independent (1.0)	32	6.6 (0.2) 6.9 (0.6) 7.2 (0.2)	35 SW (0.2) 50 SW (0.6) 65 SW (0.2)	N	< 1.6 Ma	1.0	0.001 (0.2) 0.01 (0.6) 0.1 (0.2)	Northwest-striking fault is modified from Pearthree (2013, written communication) and was classified as a potential Quaternary fault in seismic source characterization for Palo Verde Nuclear Generating Station (LCI, 2015). Fault has not yet been included in USGS Quaternary Fault and Fold Database.
927	Bunk Robinson	232	Independent (1.0)	14	6.3 (0.2) 6.6 (0.6) 6.9 (0.2)	35 W (0.2) 50 W (0.6) 65 W (0.2)	N	<1.6 Ma	1.0	0.001 (0.2) 0.01 (0.6) 0.1 (0.2)	Fault zone consists of four north- to northwest-trending faults on the eastern side of the San Bernardino Valley in southeastern Arizona. Upper Pliocene basalt flows are displaced 20–150 m. Because there is no definitive evidence of middle to late Quaternary faulting, activity of these faults may have been associated with the basaltic eruptions in the late Pliocene or early Quaternary.
937	Cactus Flats faults	115	Independent (1.0)	9	6.1 (0.2) 6.4 (0.6) 6.7 (0.2)	50 E (0.2) 65 E (0.6) 80 E (0.2)	N	< 750 ka	0.9	0.001 (0.3) 0.004 (0.4) 0.04 (0.3)	This northwest-striking series of normal faults and fractures in basin-fill and terrace gravels of the Gila River are located in the hanging wall of the Safford fault zone and are unusually straight. Because of this and their relatively short length (< 10 km), we assigned a slightly lower probably of activity of 0.9 as they may be non-tectonic subsidence features or secondary to the Safford fault zone. We assumed slightly steeper dips than typical range-bounding normal faults because of their intrabasin location and very straight traces (Houser, 1994). Preferred slip rate is based on 0.5 m offset since 130 ka, whereas the maximum rate is based on 100 m of offset of a 2.5-Ma volcanic tuff (Machette *et al.*, 1986; 1998). The minimum rate assumes 0.5 m of slip occurred since 500 ka.
933	California Wash fold and faults	115	Independent (1.0)	16	6.3 (0.2) 6.6 (0.6) 6.9 (0.2)	45 E (0.2) 60 E (0.6) 75 E (0.2)	N	< 1.6 Ma?	0.6	0.03 (0.2) 0.008 (0.6) 0.003 (0.2)	These short (6 to 8 km long) homoclinal folds and minor faults trend north-northwest along the west side of San Pedro Valley. Middle Pleistocene fan sediments may be deformed but geomorphic expression is very subtle. Plio-Pleistocene basin-fill deposits may be offset by as much as 15 m (Menges and Pearthree, 1983; Lindsay *et al.*, 1990), suggesting comparable preferred slip rates to the Huachuca fault zone. Therefore, we assumed a similar slip rate distribution but assigned a lower probability of activity due to the short length and poor geomorphic expression in Quaternary deposits.

FAULT NO.[2]	FAULT NAME	DISTANCE TO SITE (km)	RUPTURE MODEL	MAXIMUM RUPTURE LENGTH[3] (km)	MAXIMUM MAGNITUDE[4] (M)	FAULT DIP[5] (degrees)	FAULT TYPE[6]	APPROXIMATE AGE OF YOUNGEST OFFSET	PROBABILITY OF ACTIVITY[7]	SLIP RATE[8] (mm/yr)	COMMENTS
947	Carefree Fault Zone	107	Independent (1.0)	11	6.2 (0.2) 6.5 (0.6) 6.8 (0.2)	35 W (0.2) 50 W (0.6) 65 W (0.2)	N	< 750 ka	1.0	0.002 (0.2) 0.01 (0.6) 0.02 (0.2)	Northwest-striking, west side-down normal faults that divide a Precambrian granite pediment from tilted Tertiary volcanic rocks to the west in the McDowell Mountains. Scarps < 3 m high along a contact between the granite bedrock and middle Pleistocene alluvium. Skotnicki *et al.* (1997) interpret middle Pleistocene deposits are faulted but Holocene and late Pleistocene deposits are not displaced. Slip rate is based on < 3 m offset in middle Pleistocene (~300 ka) and older deposits (Pearthree, 1998).
960	Casner Cabin	208	Independent (1.0)	10	6.1 (0.2) 6.4 (0.6) 6.7 (0.2)	35 W (0.2) 50 W (0.6) 65 W (0.2)	N	< 750 ka	1.0	0.001 (0.2) 0.01 (0.6) 0.1 (0.2)	This fault zone forms two fairly sharply defined, narrow grabens on Paleozoic bedrock and Pliocene volcanic rocks. Total vertical displacement is at least 40 m. Middle to late Quaternary faulting is likely because a middle Pleistocene alluvial fan in one of the grabens is probably displaced at least 3 m.
	Chavez Mtn	167	Independent (1.0)	40	6.7 (0.2) 7.0 (0.6) 7.3 (0.2)	35 NE (0.2) 50 NE (0.6) 65 NE (0.2)	N	< 1.6 Ma	1.0	0.001 (0.2) 0.01 (0.6) 0.1 (0.2)	The Chavez Mountain fault strikes north-northwest and forms a series of east-facing scarps. Fault is modified from Pearthree (2013, written communication) and was classified as a potential Quaternary fault in seismic source characterization for Palo Verde Nuclear Generating Station (LCI, 2015). Fault has not yet been included in USGS Quaternary Fault and Fold Database.
929	Chiricahua	217	Independent (1.0)	29	6.6 (0.2) 6.9 (0.6) 7.2 (0.2)	35 E (0.2) 50 E (0.6) 65 E (0.2)	N	< 750 ka	1.0	0.001 (0.2) 0.01 (0.6) 0.1 (0.2)	This is a fault zone with probable Quaternary activity that extends for about 30 km along the east side of the Chiricahua Mountains in southeasternmost Arizona. The mountain front is steep and fairly linear, however, fault scarps are poorly preserved, are not very high, and are formed only on lower to middle Pleistocene alluvial fans. These relations suggest that this fault has a fairly low middle and late Quaternary slip rate and has not ruptured in the latest Quaternary.

FAULT NO.[2]	FAULT NAME	DISTANCE TO SITE (km)	RUPTURE MODEL	MAXIMUM RUPTURE LENGTH[3] (km)	MAXIMUM MAGNITUDE[4] (M)	FAULT DIP[5] (degrees)	FAULT TYPE[6]	APPROXIMATE AGE OF YOUNGEST OFFSET	PROBABILITY OF ACTIVITY[7]	SLIP RATE[8] (mm/yr)	COMMENTS
939, 2090, and 2091	Clifton-Rimrock-Pearson Mesa faults	137 146 165 170	Linked (0.2) Not linked (0.8) Clifton faults Rimrock fault Pearson Mesa fault	36 (floating over total length of 67 km) 16 6 8	6.7 (0.2) 7.0 (0.6) 7.3 (0.2) 6.3 (0.2) 6.6 (0.6) 6.9 (0.2) 5.9 (0.2) 6.2 (0.6) 6.5 (0.2) 6.0 (0.2) 6.3 (0.6) 6.6 (0.2)	45 W (0.2) 60 W (0.6) 75 W (0.2)	N N N N	< 130 ka < 1.6 Ma	1.0	0.005 (0.2) 0.02 (0.6) 0.1 (0.2) 0.003 (0.2) 0.01 (0.6) 0.1 (0.2) 0.005 (0.2) 0.02 (0.6) 0.1 (0.2) 0.003 (0.2) 0.009 (0.6) 0.1 (0.2)	These northwest-striking faults were considered as potentially linked because they are all down-to-the-southwest normal faults along the northeastern margin of Duncan Basin (Machette *et al.*, 1998; Pearthree, 1998). Our depiction here includes additional potential Quaternary fault scarps not shown in the USGS database based on mapping by Machette *et al.* (1986).
1014	Conocho	176	Independent (1.0)	47	6.8 (0.2) 7.1 (0.6) 7.4 (0.2)	55 NE (0.2) 70 NE (0.6) 85 NE (0.2)	N/SS	< 750 ka	1.0	0.015 (0.2) 0.03 (0.6) 0.06 (0.2)	Northwest-trending, discontinuous system of probable sinistral and oblique-normal slip faults that cuts the northeastern part of the Pliocene-Pleistocene Springerville volcanic field in east-central Arizona. Faults displace Mesozoic bedrock and upper Pliocene to lower Pleistocene basalt flows in a down-to-the-northeast sense. An early Pleistocene cinder cone has been displaced vertically about 30 m by the fault. The faults have probably been active in the middle or late Quaternary, but the age of youngest movement is not well constrained.
1015	Coyote Wash	183	Independent (1.0)	42	6.7 (0.2) 7.0 (0.6) 7.3 (0.2)	55 SW (0.2) 70 SW (0.6) 85 SW (0.2)	SS/N	< 750 ka	1.0	0.001 (0.2) 0.01 (0.6) 0.1 (0.2)	Similar to nearby Concho fault, the Coyote Wash fault is a generally northwest-trending, discontinuous system of probable sinistral and oblique-slip faults. The topographic scarp along fault zone evidently is not sharply defined, suggesting faults have probably been active in the middle or late Quaternary, but the age of youngest movement is not well constrained.

FAULT NO.[2]	FAULT NAME	DISTANCE TO SITE (km)	RUPTURE MODEL	MAXIMUM RUPTURE LENGTH[3] (km)	MAXIMUM MAGNITUDE[4] (M)	FAULT DIP[5] (degrees)	FAULT TYPE[6]	APPROXIMATE AGE OF YOUNGEST OFFSET	PROBABILITY OF ACTIVITY[7]	SLIP RATE[8] (mm/yr)	COMMENTS
	El Chile	212	Independent (1.0)	17	6.3 (0.2) 6.6 (0.6) 6.9 (0.2)	35 E (0.2) 50 E (0.6) 65 E (0.2)	N	< 1.6 Ma	1.0	0.001 (0.2) 0.01 (0.6) 0.1 (0.2)	Fault is located in northern Mexico and expressed in bedrock and classified as a potential Quaternary fault in seismic source characterization for Palo Verde Nuclear Generating Station (LCI, 2015).
	Fronteras	252	Independent (1.0)	79	7.0 (0.2) 7.3 (0.6) 7.6 (0.2)	35 W (0.2) 50 W (0.6) 65 W (0.2)	N	< 1.6 Ma	1.0	0.001 (0.2) 0.01 (0.6) 0.1 (0.2)	This normal fault is located in northern Sonora, Mexico and one valley west of the 1887 earthquake rupture of the Pitaycachi fault. Suter and Contreras (2002) considers Quaternary age based on local range front morphology and probable association with seismicity.
2094a and 2094b	Gold Hill fault zone	222	Linked (1.0)	24	6.5 (0.2) 6.8 (0.6) 7.1 (0.2)	45 W (0.2) 60 W (0.6) 75 W (0.2)	N	< 130 ka	1.0	0.002 (0.2) 0.01 (0.6) 0.09 (0.2)	Our characterization for this fault zone is from Wong *et al.* (2006). This normal fault bounds the southwestern flank of the Big Burro Mountains. We assumed a linked rupture model for the northern (2094a) and southern (2094b) sections based on their short individual lengths and kinematic compatibility. Reconnaissance scarp studies found evidence of repeated Quaternary activity with scarps 6 to 8.5 m high on older alluvial fan surfaces (Machette *et al.*, 1986). Preferred slip rate based on 2.9 m of surface offset measured on surfaces estimated to be 200 to 500 ka (Machete *et al.*, 1998).
2095	Gray Ranch	245	Independent (1.0)	20	6.4 (0.2) 6.7 (0.6) 7.0 (0.2)	45 E (0.2) 60 E (0.6) 75 E (0.2)	N	< 15 ka	1.0	0.004 (0.2) 0.04 (0.6) 0.4 (0.2)	The Gray Ranch fault zone is marked by three en echelon, discontinuous, east-facing, south-trending scarps along the eastern flank of a south-central part of the Peloncillo Mountains, an elongate range that straddles the Arizona/New Mexico state boundary. The scarps record evidence of multiple faulting events during or before the middle Pleistocene and at least one event in the late Pleistocene (Vincent and Krider, 1997).
946	Horseshoe Fault Zone	114	Independent (1.0)	21	6.4 (0.2) 6.7 (0.6) 7.0 (0.2)	35 NE (0.2) 50 NE (0.6) 65 NE (0.2)	N	< 15 ka	1.0	0.01 (0.3) 0.04 (0.6) 0.1 (0.1)	Nearly perpendicular normal faults along the western and southern margins of the Horseshoe Basin, an asymmetric graben in the upland region between the Mazatzal Mountains and Humboldt Mountain. Trenches, scarp analyses and mapping indicate latest Pleistocene and Holocene faulting along the entire zone and two or more episodes of faulting since 300 ka. Scarp analyses, soil development, topographic relations, and fault trench results indicate a slip rate of about 0.04 ± 0.03 mm/yr; displacements of about 1.5 to 2 m, and recurrence intervals of approximately 100 kyr (Pearthree, 1998). Piety and Anderson (1991) estimate the paleoearthquakes were magnitude 6.5 to 7. Fault dip is generalized as NE, a combination of E on the northern section and N on southern section. Slip rate is based on < 5 ± 2.5 m of vertical displacement in the past 150 kyr (northern section) and < 2 m of vertical displacement in the past 200 to 300 kyr on the southern section (Pearthree 1998). (~2 to 7.5m/150yr = 0.03 ± 0.02 mm/yr) (2m/200 to 300 kyr = 0.04 ± 0.03 mm/yr).

FAULT NO.[2]	FAULT NAME	DISTANCE TO SITE (km)	RUPTURE MODEL	MAXIMUM RUPTURE LENGTH[3] (km)	MAXIMUM MAGNITUDE[4] (M)	FAULT DIP[5] (degrees)	FAULT TYPE[6]	APPROXIMATE AGE OF YOUNGEST OFFSET	PROBABILITY OF ACTIVITY[7]	SLIP RATE[8] (mm/yr)	COMMENTS
2100 and 2102	Hot Spring and Walnut Springs faults	316	Linked (1.0)	44	6.8 (0.2) 7.1 (0.6) 7.4 (0.2)	35 W (0.2) 50 W (0.6) 65 W (0.2)	N	< 1.6 Ma	1.0	0.004 (0.2) 0.02 (0.6) 0.06 (0.2)	These normal faults bound the margin between the Engle Basin to the west and the Caballo block to the east. We linked these faults because they overlap considerably and are kinematically compatible with each other, and show similar geomorphic expression and age of activity. However, little is known about either of them. Although the Hot Spring fault offsets 2 to 3 Ma basalts by as much as 90 m (Machette, 1987), it does not appear to offset Rio Grande terrace deposits older than 150 ka (Foley *et al.*, 1988), suggesting that rates of activity decreased since mid-Quaternary time. Significant (but unquantified) offsets of the Palomas Formation also supports early Pleistocene activity along both faults (Machette *et al.*, 1998). Our maximum rate assumes 90 m of offset occurred since 2 Ma and our preferred rate allows for as much as 2 m of undetected slip since 150 ka, whereas the minimum rate assumes only 2 m of slip occurred since 700 ka.
932	Huachuca fault zone	190	Independent (1.0)	25	6.5 (0.2) 6.8 (0.6) 7.1 (0.2)	45 E (0.2) 60 E (0.6) 75 E (0.2)	N	130 to 750 ka	1.0	0.03 (0.2) 0.008 (0.6) 0.003 (0.2)	This north-striking, east-dipping, normal fault zone parallels the Huachuca Mountains, but is 3 to 8 km east of the embayed range front. It is characterized by 2- to 3-m-high scarps on lower and middle Pleistocene fan deposits (Demsey and Pearthree, 1994). Preferred slip rate assumes 3 m of vertical slip occurred since 440 ka; maximum rate assumes 3 m occurred since 130 ka, and minimum rates assume only 2 m occurred since 750 ka.
935	Little Rincon Mountains fault	103	Independent (1.0)	17	6.3 (0.2) 6.6 (0.6) 6.9 (0.2)	45 E (0.2) 60 E (0.6) 75 E (0.2)	N	< 1.6 Ma?	0.9	0.009 (0.5) 0.06 (0.5)	Quaternary movement is suspected on two short sections of this fault that defines the western margin of the San Pedro structural trough east of the Rincon Mountains. Fairly sharp 40-m-high scarps on basin deposits of unknown age (Plio-Pleistocene?) suggests Quaternary activity (Pearthree *et al.*, 1988). Our maximum rate assumes 40 m of offset occurred since early Pleistocene (750 ka) whereas our minimum rate assumes 40 m of offset occurred since early Pliocene (~5 Ma).
2013, 2012, and 2011	Mockingbird Hill fault zone and Mogollon fault	201	Linked (0.5)	72	7.0 (0.2) 7.3 (0.6) 7.6 (0.2)	45 W (0.2) 60 W (0.6) 75 W (0.2)	N	< 750 ka	1.0	0.02 (0.2) 0.08 (0.6) 0.7 (0.2)	Our characterization for these fault is from Wong *et al.* (2006). These normal faults are assumed to be linked due to their adjacent, nearly continuous, along-strike position, kinematic compatibility along the eastern margin of the Mangas graben, and individual short lengths. Preferred slip rate based on 110 m of offset of Clum Mine pediment gravels, which are believed to be Plio-Pleistocene (assumed ~1.6 Ma).

FAULT NO.[2]	FAULT NAME	DISTANCE TO SITE (km)	RUPTURE MODEL	MAXIMUM RUPTURE LENGTH[3] (km)	MAXIMUM MAGNITUDE[4] (M)	FAULT DIP[5] (degrees)	FAULT TYPE[6]	APPROXIMATE AGE OF YOUNGEST OFFSET	PROBABILITY OF ACTIVITY[7]	SLIP RATE[8] (mm/yr)	COMMENTS
		192 194	Independent (0.5) Mockingbird Hill-Mogollon faults	22	6.5 (0.2) 6.8 (0.6) 7.1 (0.2)	45 W (0.2) 60 W (0.6) 75 W (0.2)	N	< 1.6 Ma	1.0	0.02 (0.2) 0.08 (0.6) 0.7 (0.2)	
			Unnamed faults east of Alma	12	6.2 (0.2) 6.5 (0.6) 6.8 (0.2)	55 W (0.2) 70 W (0.6) 85 W (0.2)	N	< 1.6 Ma	1.0	0.003 (0.5) 0.02 (0.5)	These north-striking normal faults along the western flank of the Mogollon Mountains are characterized by lineaments and possible scarps on high level alluvial surfaces formed on the Plio-Pleistocene basin fill of the Gila Conglomerate (Ratte, 1981). Our maximum rate assumes as much as 10 m of offset occurred since 500 ka, whereas our minimum rate assumes 5 m of offset occurred since 1.6 Ma.
979	Mormon Lake	194	Independent (1.0)	15	6.3 (0.2) 6.6 (0.6) 6.9 (0.2)	45 W (0.2) 60 W (0.6) 75 W (0.2)	N	< 1.6 Ma	0.5	0.001 (0.2) 0.01 (0.6) 0.2 (0.2)	Over 60 m of displacement on this northwest-trending normal fault zone have produced steep and linear, west-facing escarpment that bounds the east side of topographic low containing Mormon Lake (Menges and Pearthree, 1983). No definitive offset of Quaternary units has been documented.
931	North Swisshelm	193	Independent (1.0)	25	6.5 (0.2) 6.8 (0.6) 7.1 (0.2)	35 NE (0.2) 50 NE (0.6) 65 NE (0.2)	N	< 1.6 Ma	1.0	0.001 (0.2) 0.01 (0.6) 0.1 (0.2)	The fault forms a fairly short, but high and and locally steep, northwest-trending scarp formed on late Cenozoic alluvium on the northeast side of the Swisshelm Mountains. Probable Quaternary age, but no evidence of activity since early Pleistocene (Duke, 1979).
	Oak Creek North	221	Independent (1.0)	17	6.3 (0.2) 6.6 (0.6) 6.9 (0.2)	35 E (0.2) 50 E (0.6) 65 E (0.2)	N	< 1.6 Ma	1.0	0.0025 (0.2) 0.025 (0.6) 0.25 (0.2)	The fault is a major north- to northeast-striking east-side-down normal fault bounding the west side of Oak Creek Canyon and extending north to the southern flank of the San Francisco Mountains. Unfaulted Pliocene rocks preclude Quaternary activity on southern two-thirds of fault, however, northern portion of fault displaces lower Pleistocene (1.0 – 1.6 Ma) volcanic rocks by about 25 m.

FAULT NO.[2]	FAULT NAME	DISTANCE TO SITE (km)	RUPTURE MODEL	MAXIMUM RUPTURE LENGTH[3] (km)	MAXIMUM MAGNITUDE[4] (M)	FAULT DIP[5] (degrees)	FAULT TYPE[6]	APPROXIMATE AGE OF YOUNGEST OFFSET	PROBABILITY OF ACTIVITY[7]	SLIP RATE[8] (mm/yr)	COMMENTS
928	Pedregosa	230	Independent (1.0)	27	6.5 (0.2) 6.8 (0.6) 7.1 (0.2)	35 E (0.2) 50 E (0.6) 65 E (0.2)	N	< 750 ka	1.0	0.001 (0.2) 0.01 (0.6) 0.1 (0.2)	Fault forms discontinuous north to northeast-trending 5- to 15-m-high scarps on early to middle Pleistocene fans on the northeast side of the Pedrogosa Mountains, but a younger basalt flow crosses the fault and is not displaced. This implies fault was last active in the early to middle Pleistocene.
982	Phone Booth	227	Independent (1.0)	11	6.2 (0.2) 6.5 (0.6) 6.8 (0.2)	35 NE (0.2) 50 NE (0.6) 65 NE (0.2)	N	< 1.6 Ma	1.0	0.0005 (0.2) 0.005 (0.6) 0.05 (0.2)	This zone of faults forms a narrow graben and horst in volcanic rocks of the San Francisco field. Total surface displacement on Miocene and Pliocene volcanic rocks is about 30 m (Pearthree, 1996). The moderately sharp geomorphic expression suggest possible Quaternary activity.
126	Pitaycachi fault zone	258	Independent (1.0)	102	7.1 (0.2) 7.4 (0.6) 7.7 (0.2)	35 W (0.2) 50 W (0.6) 65 W (0.2)	N	1887	1.0	0.01 (0.25) 0.02 (0.5) 0.1 (0.25)	Rupture of this complex north-striking fault zone along the western edge of the Sierra Madre Occidental Plateau was responsible for the ~**M** 7.5 1887 Sonora, Mexico earthquake, the largest normal-slip crustal event to have occurred historically in the southern Basin and Range (Suter, 2006; 2015), if not the world (Yeats *et al.*, 1997). Suter (2015) reports a maximum net slip of 5.2 m, a surface rupture length of 101.8 km, and an average surface offset of 2.60 m. Although this zone includes multiple faults that may behave as independent segments (for example, Otates, Teras and Pitaycahi), for simplicity and because of its great distance to the site, we only characterized it as a single independent fault source, which is supported by the 102 km-long 1887 rupture that included portions of all three main segments (Suter, 2015). Late Cenozoic net slip rate estimates range from 0.03 to 0.08 mm/yr along the fault zone, which appears slightly higher than Quaternary estimates of ~0.02 mm/yr (Suter, 2015), based on offsets of 9 to 13 m of early Pleistocene alluvial surfaces (Bull and Pearthree, 1988; Pearthree *et al.*, 1990). Absolute age constraints are lacking so we judged a wider distribution of weights may better account for the large uncertainties.
949	Prescott Valley grabens	217	Independent (1.0)	9	6.1 (0.2) 6.4 (0.6) 6.7 (0.2)	60 W (0.2) 90 (0.4) 60 E (0.4)	N	<750 ka	1.0	0.01 (0.3) 0.06 (0.4) 0.15 (0.3)	Upper Pleistocene deposits may be faulted. Slip rate is based on 4 m displacement in 70-110 kyr, and < 11 m displacement in 110 to 700 kyr (Pearthree, 1998). Crustal dip uncertain but steeper and east dips favored given linear trace geometry and location along the western margin of a basin (Pearthree, 1998).

FAULT NO.[2]	FAULT NAME	DISTANCE TO SITE (km)	RUPTURE MODEL	MAXIMUM RUPTURE LENGTH[3] (km)	MAXIMUM MAGNITUDE[4] (M)	FAULT DIP[5] (degrees)	FAULT TYPE[6]	APPROXIMATE AGE OF YOUNGEST OFFSET	PROBABILITY OF ACTIVITY[7]	SLIP RATE[8] (mm/yr)	COMMENTS
2087a and 2087b	Red Hills fault	317	Linked (1.0)	14	6.3 (0.2) 6.6 (0.6) 6.9 (0.2)	35 W (0.2) 50 W (0.6) 65 W (0.2)	N	< 130 ka	1.0	0.01 (0.2) 0.04 (0.6) 0.2 (0.2)	This normal fault bounds the eastern margin of Palomas Basin and has significant structural relief. It merges with the Caballo fault to the north and abuts the Derry Hills fault to the south. We assumed the northern (2087a) and southern (2087b) sections of Machette *et al.* (1998) were linked due to their individual short lengths, continuous along-strike geometry, and kinematic compatibility. We assumed the Red Hills fault behaves independently from the Caballo fault because the former does not appear to have ruptured 1 or 2 times during the Holocene like the Caballo fault. Prominent scarps were observed on late Pleistocene surfaces (Seager *et al.*, 1982) and Machette *et al.* (1998) categorized the slip rate as <0.2 mm/yr based on 3 to 5 m scarps on these surfaces. Our preferred rate assumes 4 m of vertical slip occurred since 130 ka. Our maximum rate assumes 5 m of slip occurred since 30 ka, whereas our minimum rate assumes 3 m of slip occurred since 250 ka.
	Rock House South	215	Independent (1.0)	26	6.5 (0.2) 6.8 (0.6) 7.1 (0.2)	35 NE (0.2) 50 NE (0.6) 65 NE (0.2)	N	< 1.6 Ma	1.0	0.001 (0.2) 0.01 (0.6) 0.1 (0.2)	Renamed fault from one of the Leupp faults, a group of northwest-trending normal faults are at the easternmost edge of and beyond the Pliocene-Quaternary San Francisco volcanic field in north-central Arizona. These faults cut Paleozoic and Mesozoic bedrock, locally middle Pleistocene basalt, and Quaternary alluvium.
936a and 936b	Safford fault zone (northern and southern sections)	115	Linked (1.0)	31	6.6 (0.2) 6.9 (0.6) 7.2 (0.2)	45 E (0.2) 60 E (0.6) 75 E (0.2)	N	< 15 ka	1.0	0.005 (0.2) 0.015 (0.6) 0.1 (0.2)	This northwest-striking, northeast-dipping normal fault extends along the base of the Pinaleno Mountains and is characterized by fault scarps showing recurrent Quaternary movement (Menges and Pearthree, 1983; Machette *et al.*, 1986). We linked the northern and southern sections because of their individual short lengths, similar scarp morphology and age of youngest movement. Our preferred slip rate is based on 5 to 10 m of vertical displacement on middle and late Quaternary deposits (Machette *et al.*, 1986) assumed to be ~500 ka. Maximum and minimum rate assumed to be similar to the Rimrock fault (2090).
943	Sand Tank	161	Independent (1.0)	23	6.5 (0.2) 6.8 (0.6) 7.1 (0.2)	35 NW (0.2) 50 NW (0.6) 65 NW (0.2)	N	< 130 ka	1.0	0.001 (0.2) 0.01 (0.6) 0.03 (0.2)	The fault forms a short (~3 km) , low (<2 m) fault scarp trending north to northwest in Pleistocene alluvium along the western piedmont of the Sand Tank Mountains. The length of this fault source is based on subtle air photo lineaments that extend farther north and southwest with no discernable offset on Pleistocene fan surfaces. Trenching by Demsey and Pearthree (1990) strongly suggest only one surface rupture in the past 70-200 ka and that this late Pleistocene earthquake produced 1.5 to 2 m of vertical displacement.

FAULT NO.[2]	FAULT NAME	DISTANCE TO SITE (km)	RUPTURE MODEL	MAXIMUM RUPTURE LENGTH[3] (km)	MAXIMUM MAGNITUDE[4] (M)	FAULT DIP[5] (degrees)	FAULT TYPE[6]	APPROXIMATE AGE OF YOUNGEST OFFSET	PROBABILITY OF ACTIVITY[7]	SLIP RATE[8] (mm/yr)	COMMENTS
934	Santa Rita fault zone	129	Independent (1.0)	52	6.8 (0.2) 7.1 (0.6) 7.4 (0.2)	30 W (0.2) 50 W (0.6) 65 W (0.2)	N	< 130 ka	1.0	0.08 (0.2) 0.025 (0.6) 0.008 (0.2)	This fault is characterized by discontinuous late Quaternary scarps that trend north to northeast along the base of the Santa Rita Mountains. A trench near Madera Canyon exposed late Pleistocene alluvium displaced ~2 m and middle Pleistocene alluvium displaced ~3.5 m (Pearthree and Calvo, 1987). This is generally consistent with scarp studies that indicate 3-m-scarps on late Pleistocene alluvial fans and terraces, whereas scarps are as high as 5 m on late-middle Pleistocene alluvium (~200 to 300 ka) (Pearthree and Calvo, 1987). Our preferred slip rate of 0.025 mm/yr is based on 2 to 3 m of late Pleistocene slip, and 3 to 5 m of slip since 200 to 300 ka. Our minimum rate of 0.008 mm/yr assumes only 3 m of slip occurred since ~500 ka and our maximum is about 3 times our preferred rate. This addresses uncertainties in rates given possible temporal clustering, the lack of absolute age constraints, and the limited recurrence information. We assumed shallower dips than typical basin and range normal faults based on interpretation of seismic-reflection data (e.g., Johnson and Loy, 1992). However, we did not assume dips as shallow as 20° as suggested by Johnson and Loy (1992) based on arguments against such shallow dips for earthquake ruptures discussed by Wong *et al.* (1995).
945	Sugarloaf Fault Zone	78	Independent (1.0)	8	6.0 (0.2) 6.3 (0.6) 6.6 (0.2)	35 NE (0.2) 50 NE (0.6) 65 NE (0.2)	N	< 130 ka	1.0	0.005 (0.3) 0.02 (0.6) 0.05 (0.1)	Northwest-striking normal fault that forms an asymmetric graben along the western flank of the Mazatzal Mountains. East-facing scarps are low but sharp and as much as 5 m high between granite bedrock and basin-fill deposits. Natural exposures and two trenches revealed late and latest Pleistocene deposits are offset, but middle Pleistocene to Holocene deposits are not faulted. Slip rate is based on < 1 m vertical displacement in the past 50 to 100 kyr Pearthree (1998).
2097	Unnamed faults west of the Pyramid Mountains	204	Independent (1.0)	16	6.3 (0.2) 6.6 (0.6) 6.9 (0.2)	35 W (0.2) 50 W (0.6) 35 W (0.2)	N	< 130 ka	0.9	0.009 (0.2) 0.03 (0.6) 0.17 (0.2)	These poorly-studied normal faults bound the western flank of the Pyramid Mountains, and are subparallel to the Animas Valley faults (2093), but have more subdued scarps. Based on this and because these faults may be associated with the Animas Valley faults (Machette *et al.*, 1998), we assumed similar slip rates to the Animas Valley faults, but a slightly lower probability of activity.
948	Verde	172	Independent (1.0)	8	6.0 (0.2) 6.3 (0.6) 6.6 (0.2)	60 E (0.3) 75 E (0.4) 90 (0.3)	N	< 130 ka	1.0	0.001 (0.2) 0.02 (0.6) 0.2 (0.2)	The Verde fault zone is the master, steeply northwest-dipping fault on the southwestern margin of the Verde Valley, which is a large, asymmetric, southwest-tilted graben in the Basin and Range province near the margin of the Colorado Plateaus. The fault forms a high, relatively linear, steep, northeast-facing mountain front. Morphologic analysis of alluvial fan scarp profiles suggests an early to middle Holocene time of youngest movement (Pearthree et al., 1983); however, if the steep slope elements of these scarps are due to local erosion, then the youngest faulting may be late Pleistocene (Euge et al., 1992).

FAULT NO.[2]	FAULT NAME	DISTANCE TO SITE (km)	RUPTURE MODEL	MAXIMUM RUPTURE LENGTH[3] (km)	MAXIMUM MAGNITUDE[4] (M)	FAULT DIP[5] (degrees)	FAULT TYPE[6]	APPROXIMATE AGE OF YOUNGEST OFFSET	PROBABILITY OF ACTIVITY[7]	SLIP RATE[8] (mm/yr)	COMMENTS
1016	Vernon	165	Independent (1.0)	59	6.9 (0.2) 7.2 (0.6) 7.5 (0.2)	55 NE (0.2) 70 NE (0.6) 85 NE (0.2)	SS/N	< 750 ka	1.0	0.001 (0.2) 0.01 (0.6) 0.1 (0.2)	This fault zone is a generally northwest-trending, probable sinistral and oblique-slip system of faults that cuts through the middle of the Pliocene-Pleistocene Springerville volcanic field in east-central Arizona. Basalts as young as Pleistocene are deformed by the fault zone.
2092	Washburn Ranch	221	Independent (1.0)	12	6.2 (0.2) 6.5 (0.6) 6.8 (0.2)	35 E (0.2) 50 E (0.6) 65 E (0.2)	N	< 15 ka	1.0	0.001 (0.2) 0.01 (0.6) 0.1 (0.2)	This zone of en echelon faults bound the western margin of the Animas Valley and eastern margin of the Peloncillo Mountains, an elongate range that straddles the Arizona/New Mexico state boundary. The fault has fresh scarps that appear to be Holocene in age on the basis of their morphology.
940	Whitlock Wash Fault	52	Independent (1.0)	23	6.5 (0.2) 6.8 (0.6) 7.1 (0.2)	60 W (0.2) 75 W (0.6) 90 (0.2)	N	< 1.6 Ma	0.9	0.001 (0.2) 0.01 (0.6) 0.1 (0.2)	Discontinuous north- to northwesrt-striking, W-down normal faults along the eastern side of San Pedro Valley. Quaternary activity is suspected based on a prominent escarpment and faulting in Pliocene basin-fill deposits. No evidence of Quaternary movement has been found. Mapping on the southern zone revealed lower to middle Quaternary deposits that are not faulted. Probability of activity is assumed to be 0.9, as evidence for Quaternary activity is equivocal (Pearthree, 1998). The slip rate is unknown, but probably < 0.02 mm/yr (Pearthree1998).

Table 3A. Southern California and Baja California Fault Sources Included in Analysis

Fault Name fm2.1 (0.5) [1] fm 2.2 (0.5)	P(a)[2]	Rupture Length (km)	Slip Rate (mm/yr)	SR unc.[3]	Aseismic Slip Factor[4]	Paleoseismic Recurrence Interval (yrs)	Sense of Slip[5]	Downdip Width (km)	Width unc.	Rupture Top (km)	Rupture Bottom (km)	Dip (degrees)	Dip Direction	Preferred Mmax □ 0.3[6]
San Andreas Fault Zone [segmented (0.9)]														
San Andreas-1906 rupture	1.0	473.0	24.0	3.0	0	300	rl-ss	13.0	2	0	13.0	90		7.9
San Andreas Parkfield	1.0	36.4	34.0	5.0	0	24.5	rl-ss	10.2	2	0	10.2	90		6.7
San Andreas-Cholame	1.0	62.5	34.0	5.0	0	155	rl-ss	12.0	2	0	12.0	90		7.0
San Andreas-Carrizo	1.0	59.0	34.0	3.0	0	175	rl-ss	15.1	2	0	15.1	90		7.1
San Andreas-Big Bend	1.0	49.7	34.0	3.0	0	175	rl-ss	15.1	2	0	15.1	90		7.0
San Andreas-Mojave N	1.0	36.9	27.0	7.0	0	155	rl-ss	15.1	2	0	15.1	90		6.8
San Andreas-Mojave S	1.0	97.6	29.0	7.0	0	130	rl-ss	13.1	2	0	13.1	90		7.3
San Andreas-San Bernardino N	1.0	35.3	22.0	6.0	0	175	rl-ss	12.8	2	0	12.8	90		6.8
San Andreas-San Bernardino S	1.0	43.4	16.0	6.0	0	200	rl-ss	12.8	2	0	12.8	90		6.9
San Andreas-San Gorgonio Pass/Garnet Hill	1.0	55.9	10.0	6.0	0	225	rl-ss	19.3	2	0	16.4	58	N	7.0
San Andreas-Coachella	1.0	69.4	20.0	5.0	0	212	rl-ss	11.1	2	0	11.1	90		7.1
Rupture Scenarios (see SoSAF Table 2b)														
San Jacinto - Imperial Fault Zone [segmented (0.9)]														
Imperial	1.0	45.8	20.0	5.0	0	□	rl-ss	14.7	2	0	14.6	82	N	6.9
Superstition Hills	1.0	36.2	4.0	2.0	0	□	rl-ss	12.6	2	0	12.6	90		6.8
Superstition Mountain	1.0	26.3	5.0	3.0	0	395	rl-ss	12.4	2	0	12.4	90		6.6
San Jacinto-Borrego	1.0	34.2	4.0	2.0	0	130	rl-ss	13.1	2	0	13.1	90		6.7
San Jacinto-Coyote Creek	1.0	42.9	4.0	2.0	0	375	rl-ss	15.9	2	0	15.9	90		6.9
San Jacinto-Clark	1.0	46.8	14.0	6.0	0	240	rl-ss	16.8	2	0	16.8	90		7.0
San Jacinto-Anza	1.0	46.1	18.0	6.0	0	240	rl-ss	16.8	2	0	16.8	90		7.0
San Jacinto-Anza stepover	1.0	24.2	9.0	4.0	0	□	rl-ss	16.8	2	0	16.8	90		6.6
San Jacinto-SJV stepover	1.0	24.2	9.0	4.0	0	□	rl-ss	16.8	2	0	16.8	90		6.6
San Jacinto- San Jacinto Valley	1.0	18.5	18.0	6.0	0	□	rl-ss	18.5	2	0	18.5	90		6.5
San Jacinto-San Bernardino	1.0	45.1	6.0	4.0	0	200	rl-ss	16.1	2	0	16.1	90		6.9
Rupture Scenarios (see Table 2c)														
Cerro Prieto[7] (Scenario A-0.6, Scenario B-0.4)	1.0	See Below[8]	20[9]	See below[9]	0.0	□	rl-ss	13.3	2	0	13.3	90		7.1[10] (-0.3, +0.5)

Table 3B. Maximum Magnitudes and Rupture Rates for the Southern San Andreas Fault*

	Rupture Name (segments involved)	Area (km^2)	Ells-B Mag	H&B Mag	A-Prior	Ells-B Rate	H&B Rate	Comments
	Weight				0.	0.25	0.2	
1	PK	78	6.09	5.87	3.46E-02	2.49E-02	5.26E-02	Rupture area is reduced from fault by 0.79 aseismic factor
2	CH	750.2	7.08	6.9	5.00E-05	5.21E-05	5.46E-05	
3	CC	891.2	7.15	7	3.00E-04	1.60E-04	5.74E-05	
4	BB	751	7.08	6.9	3.00E-04	5.68E-04	5.26E-04	
5	NM	556.5	6.95	6.73	2.00E-04	1.05E-04	1.44E-04	
6	SM	1279	7.31	7.21	5.00E-04	6.45E-04	6.78E-04	
7	NSB	451.9	6.86	6.64	7.00E-04	7.12E-04	6.64E-04	
8	SSB	555.5	6.94	6.73	5.00E-05	5.10E-05	5.17E-05	
9	BG	843	7.13	6.97	5.00E-04	1.88E-04	1.35E-05	
10	CO	693.4	7.04	6.86	2.50E-03	6.70E-03	1.21E-02	Rupture area is reduced from fault by 0.1 aseismic factor
11	PK+CH	828.2	7.12	6.96	1.60E-03	4.36E-03	7.01E-03	
12	CH+CC	1641.4	7.42	7.36	3.00E-04	2.39E-04	2.15E-04	
13	CC+BB	1642.2	7.42	7.36	0	5.02E-06	5.07E-06	
14	BB+NM	1307.5	7.32	7.23	0	1.01E-06	1.01E-06	
15	NM+SM	1835.4	7.46	7.42	7.00E-04	4.95E-06	5.04E-06	
16	SM+NSB	1730.9	7.44	7.39	6.00E-04	8.79E-04	8.90E-04	
17	NSB+SSB	1007.4	7.2	7.07	8.00E-04	1.05E-03	1.22E-03	
18	SSB+BG	1398.5	7.35	7.26	9.00E-04	5.03E-06	4.95E-06	
19	BG+CO	1536.4	7.39	7.32	7.00E-04	2.83E-04	4.10E-04	
20	PK+CH+CC	1719.4	7.44	7.38	7.00E-04	4.26E-04	4.19E-04	
21	CH+CC+BB	2392.4	7.58	7.58	0	9.94E-07	9.93E-07	
22	CC+BB+NM	2198.7	7.54	7.53	0	1.00E-06	1.01E-06	
23	BB+NM+SM	2586.4	7.61	7.62	2.50E-04	1.88E-04	2.67E-04	
24	NM+SM+NSB	2287.4	7.56	7.55	1.00E-04	7.24E-05	6.69E-05	
25	SM+NSB+SSB	2286.4	7.56	7.55	4.00E-04	6.05E-04	7.55E-04	
26	NSB+SSB+BG	1850.4	7.47	7.43	4.00E-04	2.22E-04	3.05E-05	
27	SSB+BG+CO	2091.9	7.52	7.5	4.00E-04	2.23E-04	2.48E-04	
28	PK+CH+CC+BB	2470.4	7.59	7.59	4.00E-04	8.20E-04	8.34E-04	
29	CH+CC+BB+NM	2948.8	7.67	7.7	0	9.91E-07	9.99E-07	

30	CC+BB+NM+SM	3477.7	7.74	7.79	4.00E-04	1.95E-04	4.99E-06	
31	BB+NM+SM+NSB	3038.4	7.68	7.71	0	9.95E-07	1.00E-06	
32	NM+SM+NSB+SSB	2842.9	7.65	7.68	2.00E-04	1.04E-04	1.02E-04	
33	SM+NSB+SSB+BG	3129.4	7.7	7.73	3.00E-04	2.92E-04	1.97E-04	
34	NSB+SSB+BG+CO	2543.8	7.61	7.61	4.00E-04	2.23E-04	2.17E-04	
35	PK+CH+CC+BB+NM	3026.9	7.68	7.71	7.00E-04	1.54E-03	1.66E-03	
36	CH+CC+BB+NM+SM	4227.8	7.83	7.9	5.00E-04	4.16E-04	2.67E-04	
37	CC+BB+NM+SM+NSB	3929.6	7.79	7.86	1.00E-04	8.64E-05	5.55E-05	
38	BB+NM+SM+NSB+SSB	3593.9	7.76	7.81	5.00E-05	4.92E-05	5.42E-05	
39	NM+SM+NSB+SSB+BG	3685.9	7.77	7.83	1.00E-04	6.19E-05	3.29E-05	
40	SM+NSB+SSB+BG+CO	3822.8	7.78	7.85	4.00E-04	3.58E-04	4.16E-04	
41	PK+CH+CC+BB+NM+SM	4305.9	7.83	7.92	2.00E-03	1.04E-03	6.43E-04	
42	CH+CC+BB+NM+SM+NSB	4679.8	7.87	7.96	0	9.91E-07	9.89E-07	
43	CC+BB+NM+SM+NSB+SSB	4485.1	7.85	7.94	1.00E-04	9.04E-05	6.76E-05	
44	BB+NM+SM+NSB+SSB+BG	4436.9	7.85	7.93	0	1.01E-06	1.01E-06	
45	NM+SM+NSB+SSB+BG+CO	4379.2	7.84	7.93	1.00E-04	6.01E-05	3.90E-05	
46	PK+CH+CC+BB+NM+SM+NSB	4757.8	7.88	7.97	5.00E-04	4.21E-04	3.49E-04	
47	CH+CC+BB+NM+SM+NSB+SSB	5235.3	7.92	8.03	5.00E-05	5.00E-05	5.09E-05	
48	CC+BB+NM+SM+NSB+SSB+BG	5328.1	7.93	8.04	5.00E-05	4.44E-05	3.00E-05	
49	BB+NM+SM+NSB+SSB+BG+CO	5130.2	7.91	8.02	5.00E-05	4.50E-05	4.70E-05	
50	PK+CH+CC+BB+NM+SM+NSB+SSB	5313.3	7.93	8.04	1.00E-04	1.00E-04	1.09E-04	
51	CH+CC+BB+NM+SM+NSB+SSB+BG	6078.2	7.98	8.12	0	9.95E-07	1.01E-06	
52	CC+BB+NM+SM+NSB+SSB+BG+CO	6021.5	7.98	8.11	1.00E-05	9.66E-06	9.24E-06	
53	PK+CH+CC+BB+NM+SM+NSB+SSB+BG	6156.3	7.99	8.12	5.00E-05	4.65E-05	4.09E-05	
54	CH+CC+BB+NM+SM+NSB+SSB+BG+CO	6771.6	8.03	8.18	0	1.01E-06	9.93E-07	
55	PK+CH+CC+BB+NM+SM+NSB+SSB+BG+CO	6849.7	8.04	8.18	1.00E-04	8.29E-05	6.59E-05	
Total					5.42E-02	4.88E-02	8.37E-02	

PK Parkfield
CH Cholame
CC Carrizo
BB Big Bend
NM Mojave North
SM Mojave South
NSB San Bernardino North

SSB San Bernardino South
BG San Gorgonio Pass-Garnet Hill (aka Banning-Garnet Hill)
CO Coachella
*From Table 3, Appendix G, WGCEP (2008)

Table 3C. Maximum Magnitudes and Rupture Rates for the San Jacinto Fault*

	Rupture Name (segments involved)	Area (km^2)	Ells-B Mag	H&B	A-Prior	Ells-B Rate	H&B Rate	Comments
	Weight				0.5	0.25	0.2	
1	SBV	725.7	7.06	6.88	2.31E-03	4.39E-04	4.42E-04	
2	SJV (SJV+SJV stepover sections)	686.7	7.04	6.85	2.43E-03	4.50E-04	4.49E-04	
3	A (A+A stepover sections)	1193.9	7.28	7.17	0	8.83E-05	8.82E-05	
4	C	786.1	7.1	6.93	0	8.87E-05	8.98E-05	
5	CC	681.5	7.03	6.85	8.89E-04	4.50E-04	4.48E-04	
6	B	403.6	6.81	6.59	4.82E-03	4.45E-04	4.43E-04	Rupture area is reduced from fault by
7	SM	325.8	6.71	6.49	1.09E-03	1.50E-03	4.01E-03	Rupture area is reduced from fault by
8	SBV+SJV	1412.4	7.35	7.27	1.32E-03	4.49E-04	4.41E-04	
9	SJV+A	1880.6	7.47	7.44	0	4.41E-04	4.50E-04	
10	A+C	1980.1	7.5	7.47	3.15E-03	1.21E-03	1.16E-03	
11	A+CC	1875.4	7.47	7.43	0	8.82E-05	9.00E-05	
12	CC+B	1085.1	7.24	7.12	8.89E-04	4.50E-04	4.47E-04	
13	B+SM	729.4	7.06	6.89	1.09E-03	4.40E-04	4.43E-04	
14	SBV+SJV+A	2606.4	7.62	7.62	0	4.47E-04	4.48E-04	
15	SJV+A+C	2666.8	7.63	7.64	0	4.48E-04	4.51E-04	
16	SJV+A+CC	2562.2	7.61	7.61	0	8.91E-05	8.93E-05	
17	A+CC+B	2279.1	7.56	7.55	0	9.02E-05	8.95E-05	
18	CC+B+SM	1411	7.35	7.27	8.89E-04	4.48E-04	4.40E-04	
19	SBV+SJV+A+C	3392.5	7.73	7.78	1.05E-03	4.49E-04	4.41E-04	
20	SBV+SJV+A+CC	3287.9	7.72	7.76	0	8.94E-05	9.03E-05	
21	SJV+A+CC+B	2965.8	7.67	7.7	0	8.82E-05	8.89E-05	
22	A+CC+B+SM	2604.9	7.62	7.62	0	8.93E-05	8.96E-05	
23	SBV+SJV+A+CC+B	3691.5	7.77	7.83	0	8.80E-05	8.97E-05	
24	SJV+A+CC+B+SM	3291.6	7.72	7.76	0	8.94E-05	9.03E-05	
25	SBV+SJV+A+CC+B+SM	4017.3	7.8	7.88	0	8.90E-05	8.82E-05	
Total					*1.99E-02*	*9.04E-03*	*1.15E-02*	

SBV	San Bernardino Valley
SJV	San Jacinto Valley
A	Anza
C	Clark
CC	Coyote Creek
B	Borrego Mountain
SM	Superstition Mountain

Note: Does not include Imperial or Superstition Hills faults

Table 4. Completeness Estimates and Number of Earthquakes in Each Magnitude Interval

Magnitude Range (M)	Year of Completeness	Number of Earthquakes
3.0 – 3.49	1980	41
3.5 – 3.99	1959	30
4.0 – 4.49	1939	13
4.5 – 4.99	1940	3
5.0 – 5.49	1880	10
5.5 – 5.99	1880	1
≥ 6.0	1880	1

Table 5. Recurrence Parameters for the SBR Background Zone

Realization	b-value	N (M ≥ 5)	Weight
1	0.66	0.06513	0.125
2	0.77	0.06027	0.125
3	0.75	0.06871	0.125
4	0.81	0.04485	0.125
5	0.70	0.07190	0.125
6	0.67	0.06505	0.125
7	0.60	0.11131	0.125
8	0.89	0.03754	0.125

Table 6. Summary of Probabilistic Ground Motions

Return period (years)	PGA (g) Mean [5th, 95th percentiles]	0.2 Sec SA (g) Mean [5th, 95th percentiles]	1.0 Sec SA (g) Mean [5th, 95th percentiles]
475	0.024 [0.012 – 0.042]	0.06 [0.026 – 0.095]	0.023 [0.015 – 0.032]
2,500	0.079 [0.036 – 0.13]	0.19 [0.086 – 0.30]	0.051 [0.032 – 0.072]
5,000	0.11 [0.055 – 0.18]	0.29 [0.13 – 0.44]	0.070 [0.043 – 0.10]
10,000	0.26 [0.080 – 0.24]	0.42 [0.20 – 0.63]	0.096 [0.058 – 0.14]

Table 7. Magnitude, Distance, and Epsilon Deaggregation

Distance (km)	PGA						1.0 Sec SA					
	M*[1]	D*[1]	ε[1]	M-bar[2]	D-bar[2]	ε[2]	M*[1]	D*[1]	ε[1]	M-bar[2]	D-bar[2]	ε[2]
475-Year Return Period												
All	5.1	25	-0.43	-	-	-	7.3	350	1.57	-	-	-
< 200	-	-	-	5.73	57.6	-0.17	-	-	-	6.0	66	0.35
> 200	-	-	-	6.8	250	2.02	-	-	-	7.3	379	1.54
2,500-Year Return Period												
All	5.1	15	0.22	-	-	-	5.9	15	-0.11	-	-	-
< 200	-	-	-	5.7	30.8	0.36	-	-	-	6.1	44	0.64
> 200	-	-	-	7.1	235	2.47	-	-	-	7.5	381	2.06
5,000-Year Return Period												
All	5.3	15	0.40	-	-	-	6.1	15	-0.02	-	-	-
< 200	-	-	-	5.7	25.6	0.58	-	-	-	6.1	36.3	0.75
> 200	-	-	-	7.2	235	2.5	-	-	-	7.5	379	2.19
10,000-Year Return Period												
All	5.5	15	0.55	-	-	-	6.1	15	0.36	-	-	-
< 200	-	-	-	5.8	21.9	0.80	-	-	-	6.1	29.6	0.87
> 200	-	-	-	7.3	235	2.5	-	-	-	7.6	374	2.3

[1] Modal magnitude and distance are based on full hazard results for all magnitudes and distances. Epsilon is mean epsilon for modal M-D bin.

[2] Mean magnitudes and distances are computed for hazard from events at distances less than and greater than 200 km due to the bimodal nature of the hazard. Hazard from events at less than 200 km are from background seismicity and local faults. Hazard from events greater than 200 km are from faults in Southern California and northern Mexico. Epsilons are mean epsilon for hazard < 200 km and > 200 km.

Table 8. Mean UHS

Period (sec)	Spectral Acceleration (g)			
	475-Year Return Period	2,500-Year Return Period	5,000-Year Return Period	10,000-Year Return Period
0.01	0.036	0.079	0.11	0.16
0.03	0.044	0.095	0.15	0.21
0.05	0.058	0.12	0.19	0.28
0.10	0.081	0.18	0.28	0.41
0.15	0.08	0.20	0.30	0.44
0.20	0.078	0.19	0.29	0.42
0.25	0.069	0.17	0.25	0.37
0.30	0.061	0.15	0.23	0.33
0.40	0.049	0.12	0.17	0.25
0.50	0.041	0.097	0.14	0.20
0.75	0.031	0.069	0.097	0.14
1.00	0.023	0.051	0.070	0.096
2.00	0.013	0.025	0.033	0.044
3.00	0.009	0.017	0.021	0.027
4.00	0.007	0.013	0.016	0.020
5.00	0.006	0.010	0.013	0.015
7.50	0.004	0.007	0.010	0.012
10.0	0.003	0.006	0.008	0.011

Table 9. Comparison with 2014 USGS NSHMs

	This Study	Ratio of This Study to 2014 USGS	Sensitivity Analysis using 2014 USGS Mmax and fault type for Background Zone	Ratio of Sensitivity Analysis to 2014 USGS	2014 USGS[1]
	700 m/sec Mean, [5th, 95th percentiles]		**760 m/sec Mean, [5th, 95th percentiles]**		**760 m/sec Mean**
PGA	0.078 g [0.035 – 0.12 g]	0.56	0.095 g [0.042 – 0.15 g]	0.68	0.14 g
1.0 Sec SA	0.051 g [0.031 – 0.071g]	0.67	0.070 g [0.037 – 0.11 g]	0.92	0.076 g

[1] 2014 USGS v. 4.1.4 (Unified Hazard Tool (https://earthquake.usgs.gov/hazards/interactive/) accessed 10/27/19)

Table 10. DSHA Inputs

INPUT PARAMETER	INPUT PARAMETER DEFINITION	WHITLOCK WASH FAULT
M	Moment magnitude	6.9
R_{RUP}	Closest distance to coseismic rupture (km)	52.0
R_{JB}	Closest distance to surface projection of coseismic rupture (km)	51.2
R_X	Horizontal distance from top of rupture measured perpendicular to fault strike (km)	10.1
R_{y0}	The horizontal distance off the end of the rupture measured parallel to strike (km)	51.0
U	Unspecified-mechanism factor: 1 for unspecified; 0 otherwise	0
F_{RV}	Reverse-faulting factor: 0 for strike slip, normal, normal-oblique; 1 for reverse, reverse-oblique and thrust	0
F_N	Normal-faulting factor: 0 for strike slip, reverse, reverse-oblique, thrust and normal-oblique; 1 for normal	1
F_{HW}	Hanging-wall factor: 1 for site on down-dip side of top of rupture; 0 otherwise	1
Z_{TOR}	Depth to top of coseismic rupture (km)	0.0
Dip	Average dip of rupture plane (degrees)	75
V_{S30}	The average shear-wave velocity (m/s) over a subsurface depth of 30 m	700 – 1,000
$F_{Measured}$		1
Z_{HYP}	Hypocentral depth from the earthquake	
$Z_{1.0}$	Depth to Vs=1 km/sec	Default
$Z_{2.5}$	Depth to Vs=2.5 km/sec	Default
W	Fault rupture width (km)	15.5
Region	Specific Regions considered in the models	Global

Table 11. Median and 84th Percentile Deterministic Response Spectra

	M 6.9 Whitlock Wash Fault	
Period (sec)	Median (g)	84th Percentile (g)
0.01	0.049	0.091
0.02	0.050	0.093
0.03	0.054	0.10
0.05	0.065	0.13
0.075	0.079	0.16
0.10	0.089	0.18
0.15	0.10	0.20
0.20	0.11	0.21
0.25	0.10	0.20
0.30	0.098	0.19
0.40	0.084	0.17
0.50	0.073	0.15
0.75	0.053	0.11
1.0	0.040	0.082
1.5	0.026	0.054
2.0	0.019	0.039
3.0	0.011	0.024
4.0	0.008	0.016
5.0	0.005	0.011
7.5	0.003	0.005
10.0	0.002	0.003

Table 12. Properties of Seed Time Histories

RSN	Year	Earthquake Name	Station Name	Mag	ClstD (km)	V_S30 (m/s)	Comp	PGA (g)	PGV (cm/s)	PGD (cm)	AI (m/sec)	5-95% Dur (sec)
31	1966	Parkfield	Cholame - Shandon Array #8	6.2	12.9	257	320	0.27	8.9	3.6	0.40	13.1
68	1971	San Fernando	LA - Hollywood Stor FF	6.6	22.8	316	90	0.22	21.8	11.6	0.70	13.4
162	1979	Imperial Valley-06	Calexico Fire Station	6.5	10.5	231	225	0.28	16.9	9.3	0.90	14.8
172	1979	Imperial Valley-06	El Centro Array #1	6.5	21.7	237	140	0.13	16.1	7.7	0.30	19.5
319	1981	Westmorland	Westmorland Fire Sta	5.9	6.5	194	90	0.38	44.2	15.5	1.76	6.9
322	1983	Coalinga-01	Cantua Creek School	6.4	24	275	360	0.29	26.3	10.5	1.16	11.7
2935	1999	Chi-Chi, Taiwan-04	TTN051	6.2	37.6	665	N51E	0.07	6.5	4.3	0.04	11.0
4472	2009	L'Aquila, Italy	Celano	6.3	21.4	613	E	0.08	4.9	3.1	0.04	6.6
8136	2011	Christchurch, New Zealand	SWNC	6.2	25.5	296	N24E	0.19	13.4	5.6	0.24	8.9

RSN Record Sequence Number from NGA-West2 Database
Mag moment magnitude
ClstD closest distance
Comp component
PGA peak horizontal ground acceleration
PGV peak horizontal ground velocity
PGD peak horizontal ground displacement
AI Arias intensity
Dur duration

Table 13. Properties of Spectrally-Matched Time Histories

RSN	Year	Earthquake Name	Station Name	Mag	ClstD (km)	V_S30 (m/s)	Comp	PGA (g)	PGV (cm/s)	PGD (cm)	AI (m/sec)	5-95% Dur (sec)
31	1966	Parkfield	Cholame - Shandon Array #8	6.2	12.9	257	320	0.16	8.0	5.0	0.20	12.9
68	1971	San Fernando	LA - Hollywood Stor FF	6.6	22.8	316	90	0.15	9.6	6.4	0.22	12.3
162	1979	Imperial Valley-06	Calexico Fire Station	6.5	10.5	231	225	0.16	10.6	6.4	0.27	12.4
172	1979	Imperial Valley-06	El Centro Array #1	6.5	21.7	237	140	0.15	15.7	5.8	0.28	13.3
319	1981	Westmorland	Westmorland Fire Sta	5.9	6.5	194	90	0.16	11.9	9.0	0.25	7.9
322	1983	Coalinga-01	Cantua Creek School	6.4	24	275	360	0.17	13.8	7.5	0.21	16.6
2935	1999	Chi-Chi, Taiwan-04	TTN051	6.2	37.6	665	N51E	0.15	13.7	13.3	0.24	11.3
4472	2009	L'Aquila, Italy	Celano	6.3	21.4	613	E	0.16	12.7	10.1	0.20	8.3
8136	2011	Christchurch, New Zealand	SWNC	6.2	25.5	296	N24E	0.16	13.6	8.1	0.20	10.6

RSN record sequence number from NGA-West2 database
Mag moment magnitude
ClstD closest distance
Comp component
PGA peak horizontal ground acceleration
PGV peak horizontal ground velocity
PGD peak horizontal ground displacement
AI Arias intensity
Dur duration

Figures

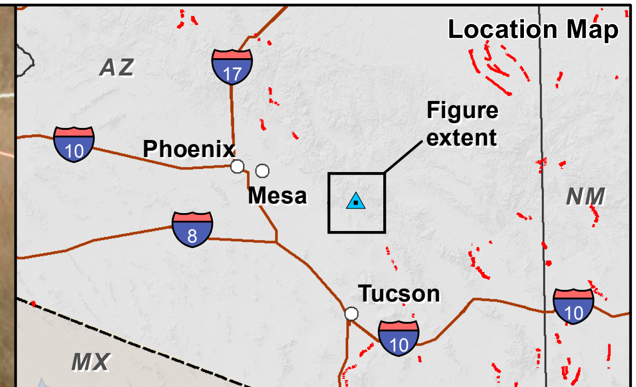

EXPLANATION

Site location

USGS fault; solid where certain, dashed where approximate, dotted where concealed (USGS, 2010)

Source:
Aerial imagery from ESRI

0 2 4 mi
0 4 8 km

Map projection and scale: NAD 1983 UTM Zone 12N, 1:300,000

Project Location Map

RESOLUTION COPPER, SKUNK CAMP TSF SITE

LCI Lettis Consultants International, Inc.

Figure 1

File path: S:\1885\Figures\Figure_01.mxd; Date: 11/01/2019; User: Joshua, LCI; Rev.1

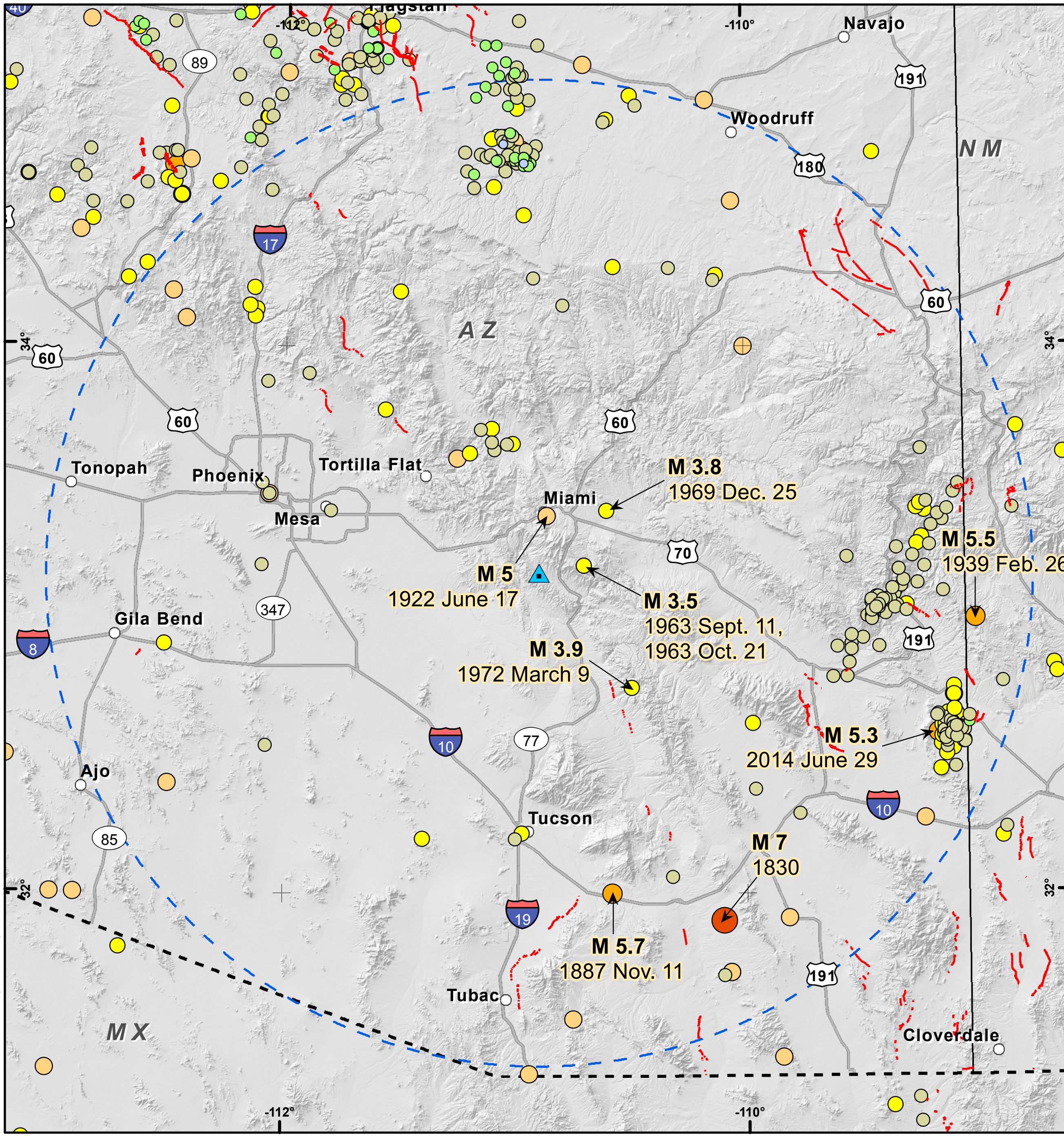

EXPLANATION

- Site location
- 200 km site buffer
- USGS fault; solid where certain, dashed where approximate, dotted where concealed (USGS, 2010)

Seismicity [M]

- ≤ 1.00
- 1.01 - 2.00
- 2.01 - 3.00
- 3.01 - 4.00
- 4.01 - 5.00
- 5.01 - 6.00
- 6.01 - 7.00

Sources:
Seismicity catalog from USGS (2019) and Wong et al. (2008)

0 25 50 mi
0 50 100 km

Map projection and scale: NAD 1983 UTM Zone 12N, 1:2,500,000

Historical Seismicity in the Project Region, 1830 - September 2019

RESOLUTION COPPER, SKUNK CAMP TSF SITE

Lettis Consultants International, Inc. | Figure 2

File path: S:\1885\Figures\Figure_02.mxd; Date: 11/01/2019; User: Joshua, LCI; Rev.1

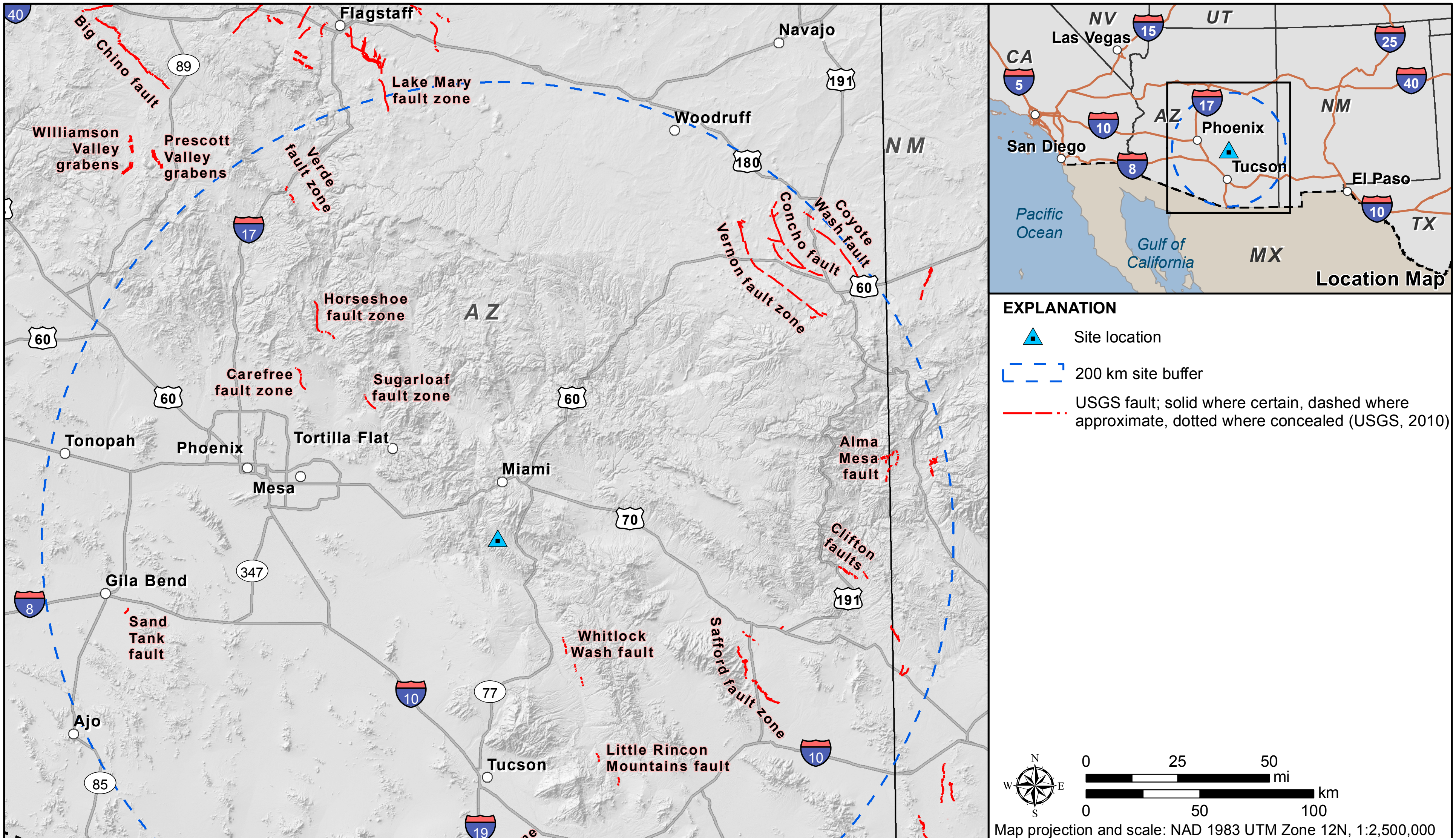

Quaternary Faults in the Project Region

RESOLUTION COPPER, SKUNK CAMP TSF SITE

Lettis Consultants International, Inc. | Figure 3

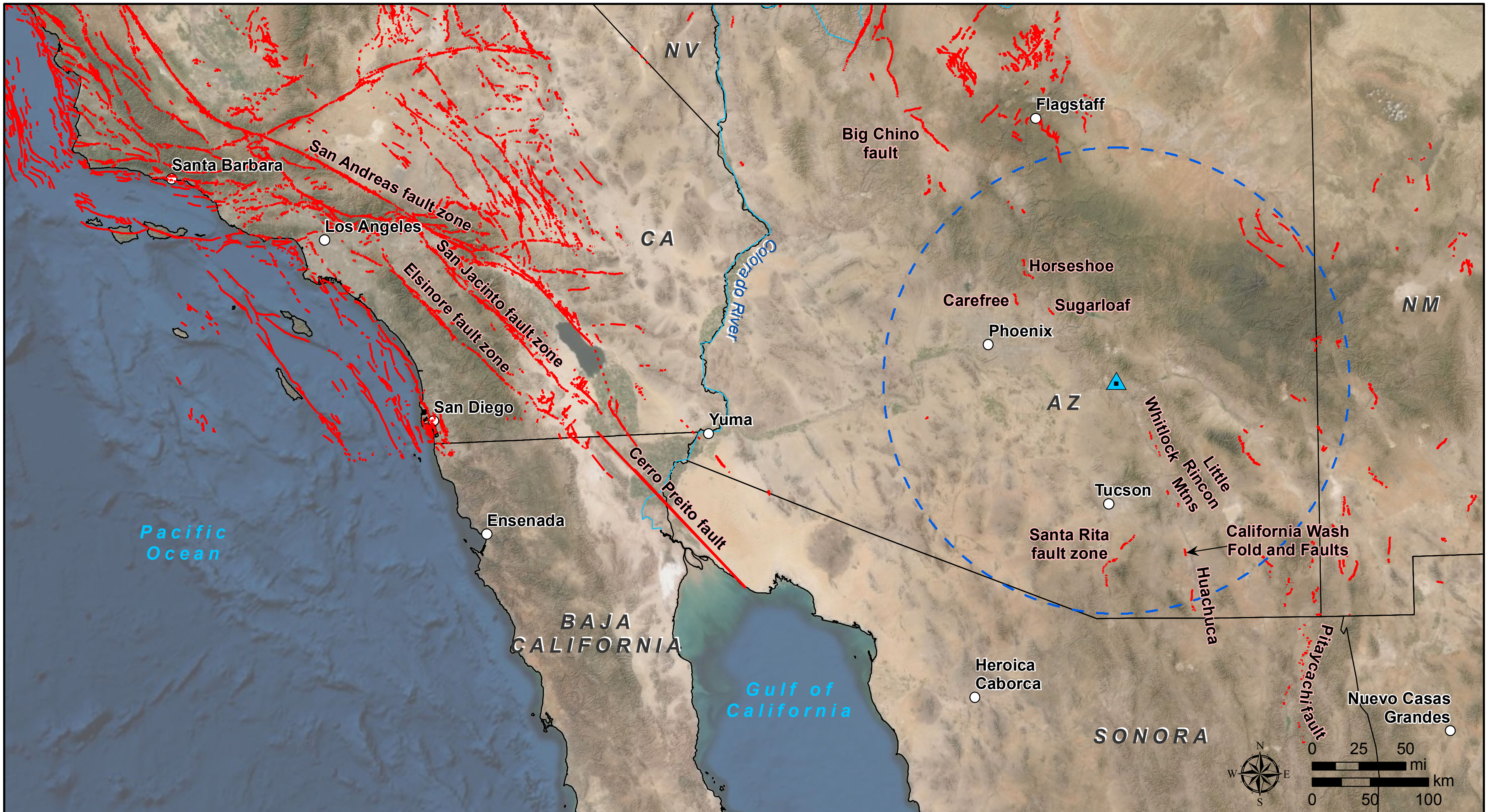

EXPLANATION

Site location

200 km site buffer

USGS fault; solid where certain, dashed where approximate, dotted where concealed (USGS, 2010)

Note:
- USGS fault data does not extend south of the US border

Sources:
- Cerro Prieto trace from UCER3 (Field et al., 2013)
- Aerial imagery from ESRI

Map projection and scale: NAD 1983 UTM Zone 12N, 1:5,000,000

Regional Quaternary Faults

RESOLUTION COPPER, SKUNK CAMP TSF SITE

Lettis Consultants International, Inc.

Figure 4

File path: S:\1885\Figures\Figure_04.mxd; Date: 10/23/2019; User: Javier, LCI; Rev.1

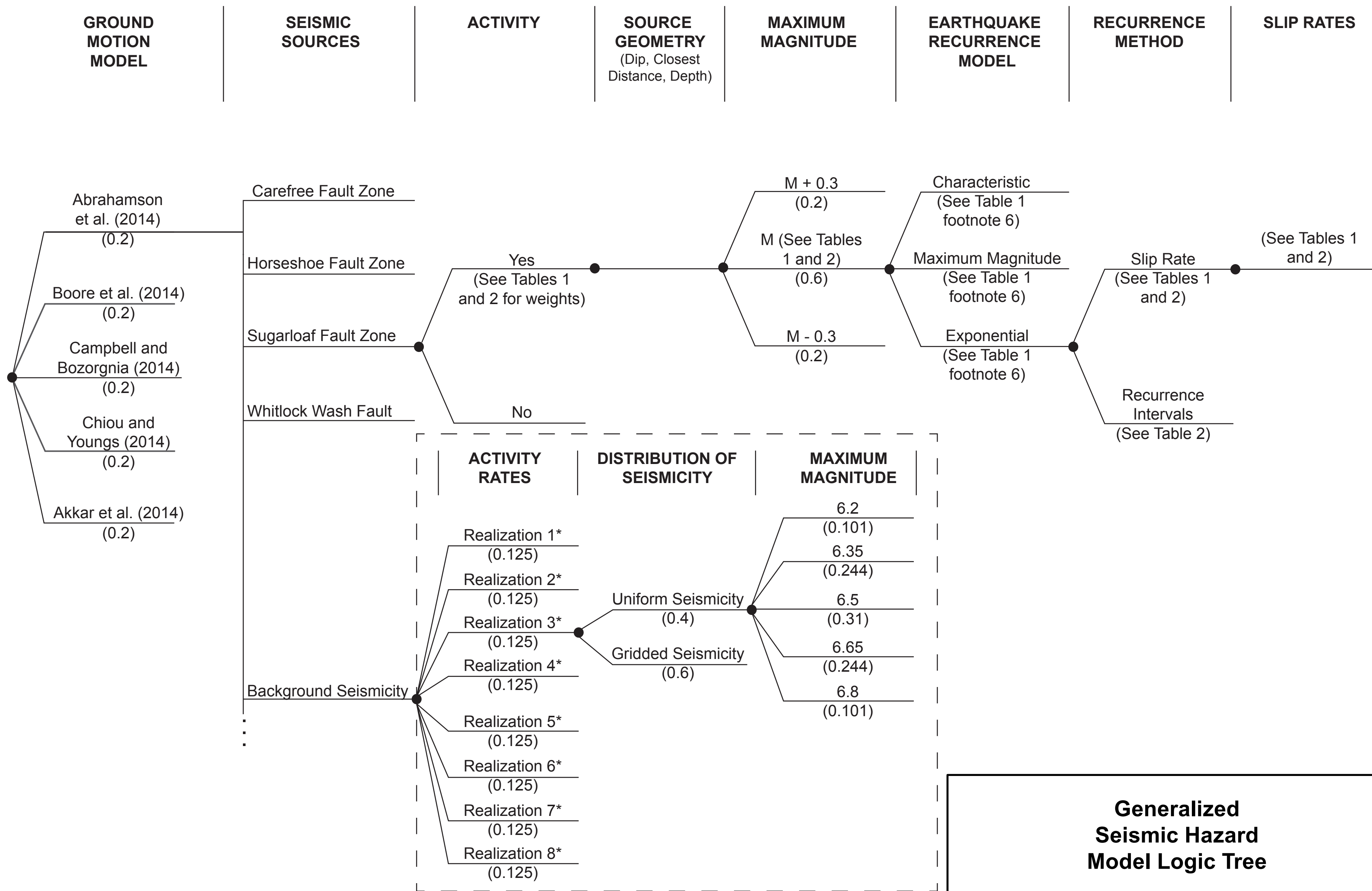

* See Table 4.

File path: S:\1885\Figures\Figure_05.ai: 10/21/2019; User:Jch, LCI.

Generalized Seismic Hazard Model Logic Tree

RESOLUTION COPPER, SKUNK CAMP TSF SITE

LCI Lettis Consultants International, Inc. | Figure **5**

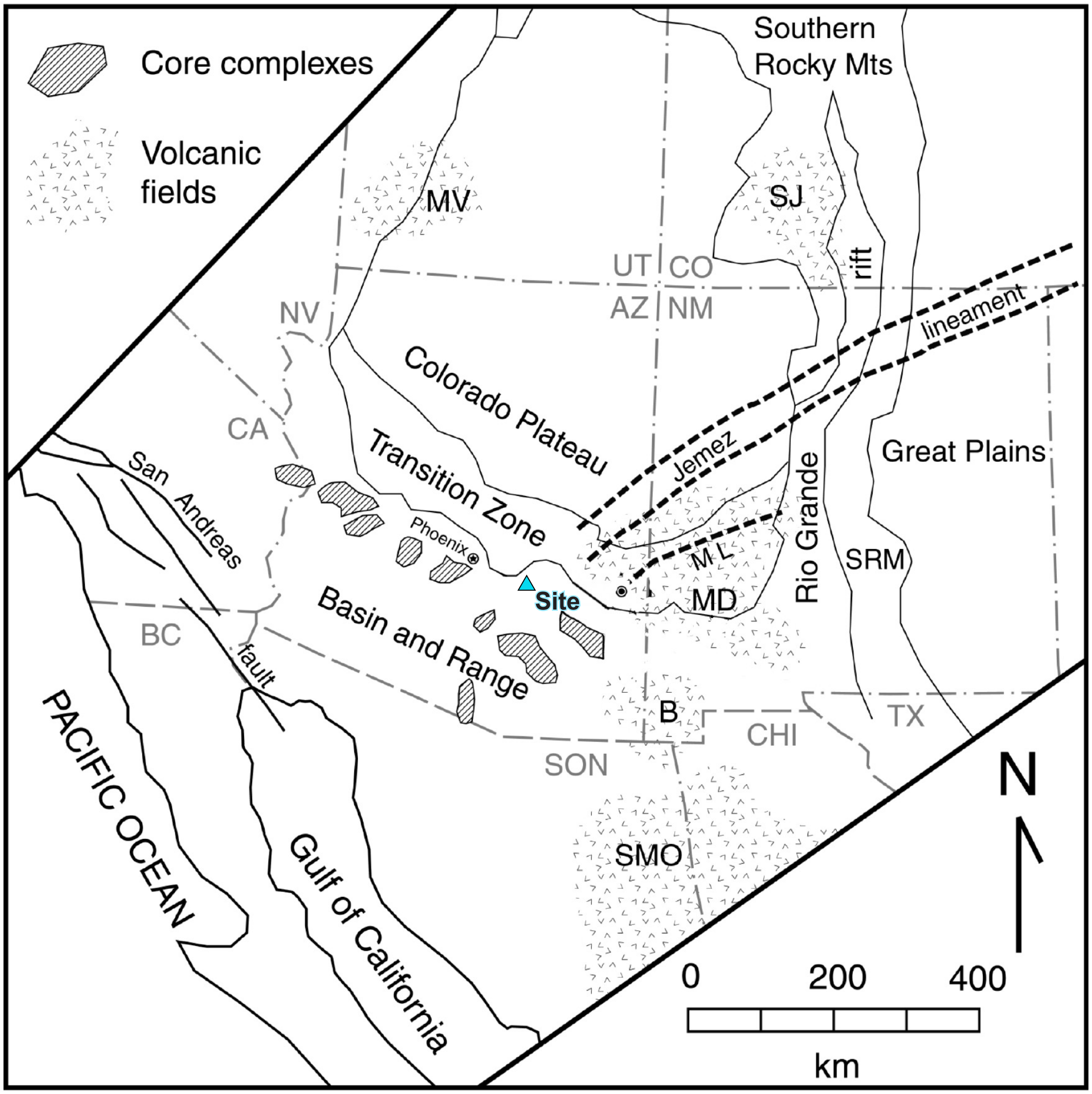

EXPLANATION

△ Site location

Source: Figure modified from Drewes et al. (1985) and Wong et al. (2013)

Seismotectonic Setting

RESOLUTION COPPER, SKUNK CAMP TSF SITE

LCI Lettis Consultants International, Inc. | Figure **6**

File path: S:\1885\Figures\Figure_06.ai; 10/21/2019; User:Jch, LCI.

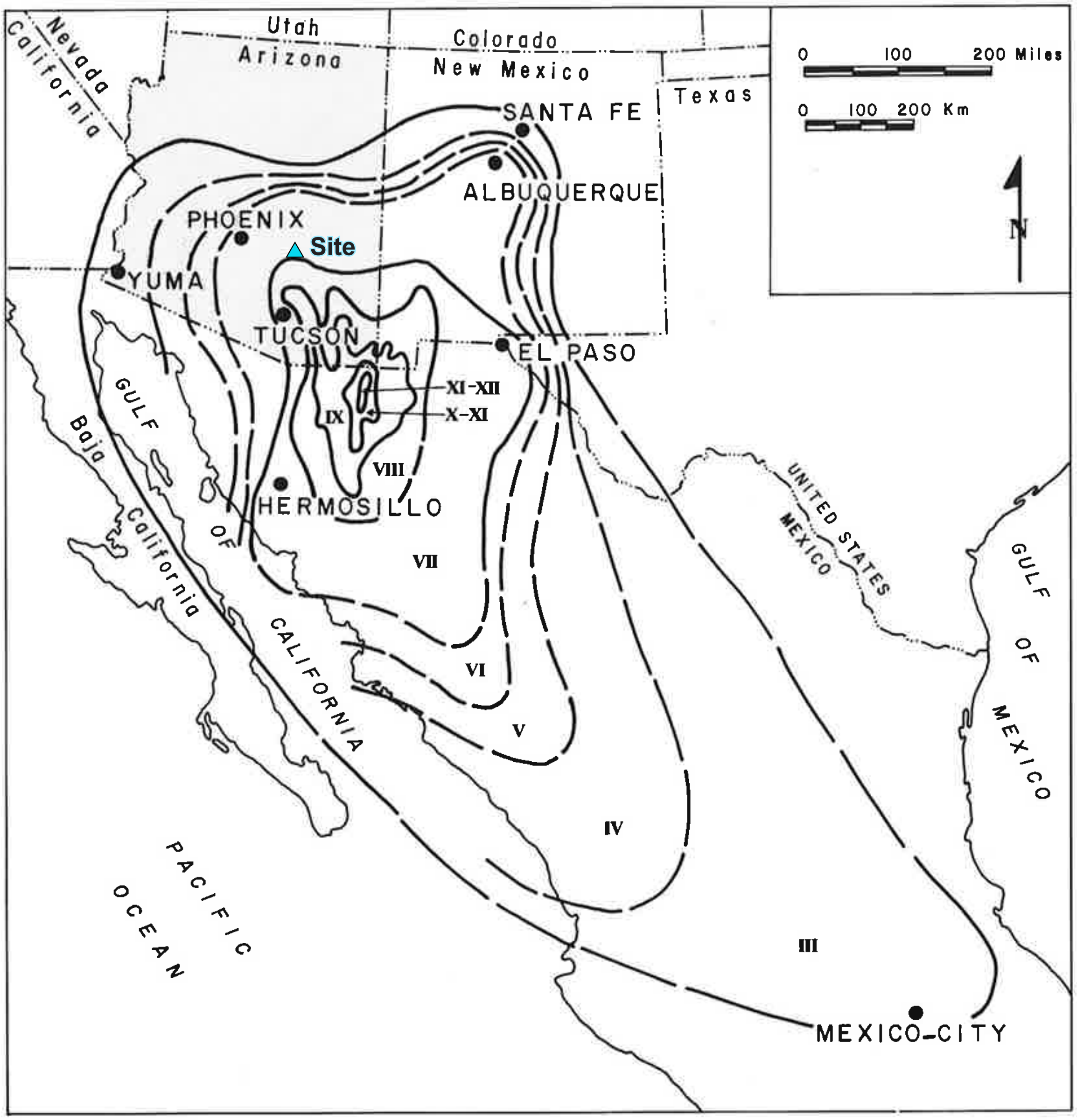

EXPLANATION

△ Site location

Source: Figure modified from DuBois et al. (1982)

Isoseismal Map of 3 May 1887 M 7.4 Sonora, Mexico Earthquake

RESOLUTION COPPER, SKUNK CAMP TSF SITE

Lettis Consultants International, Inc.

Figure **7**

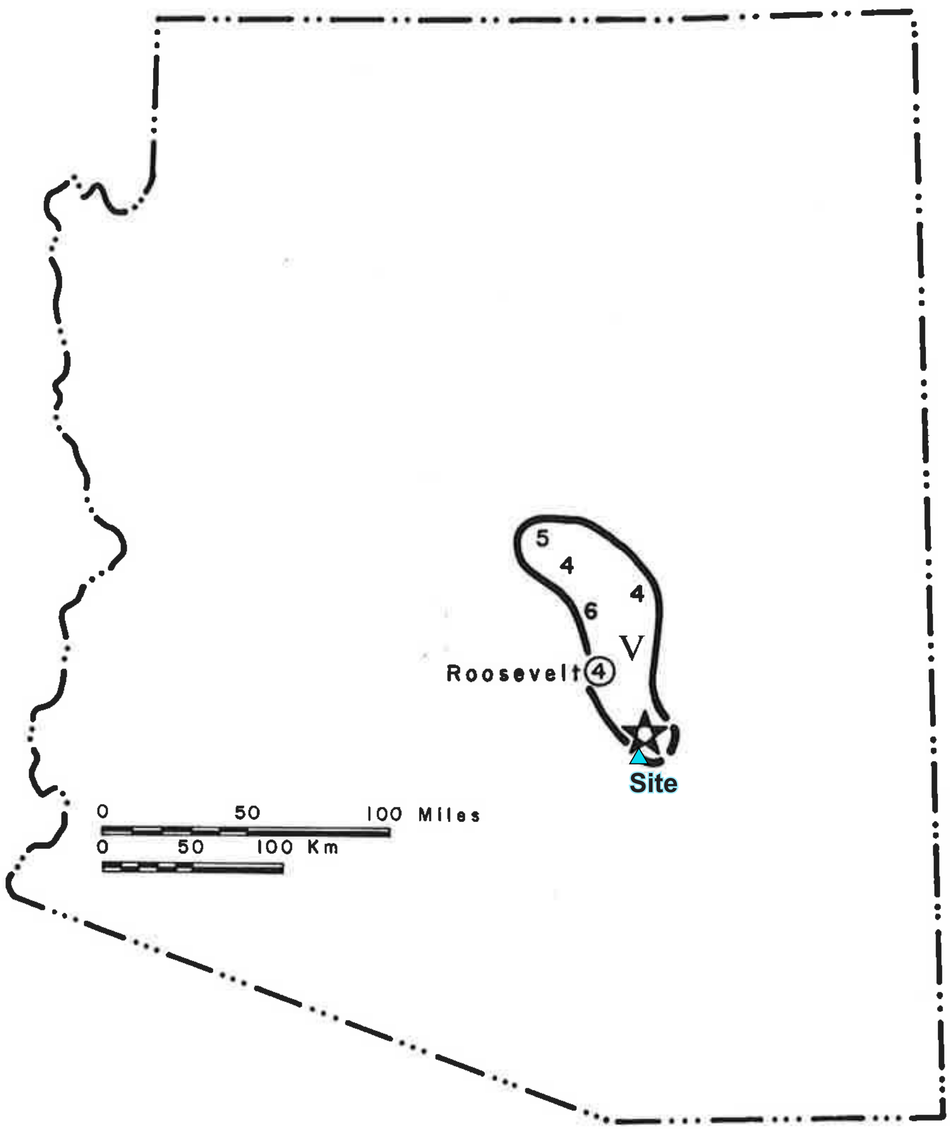

EXPLANATION

△ Site location

Source: Figure modified from DuBois et al. (1982)

Isoseismal Map of the 17 June 1922 M5.0 Miami, Arizona, Earthquake

RESOLUTION COPPER, SKUNK CAMP TSF SITE

Lettis Consultants International, Inc. | Figure **8**

File path: S:\1885\Figures\Figure_08.ai: 10/21/2019; User:Jch, LCI.

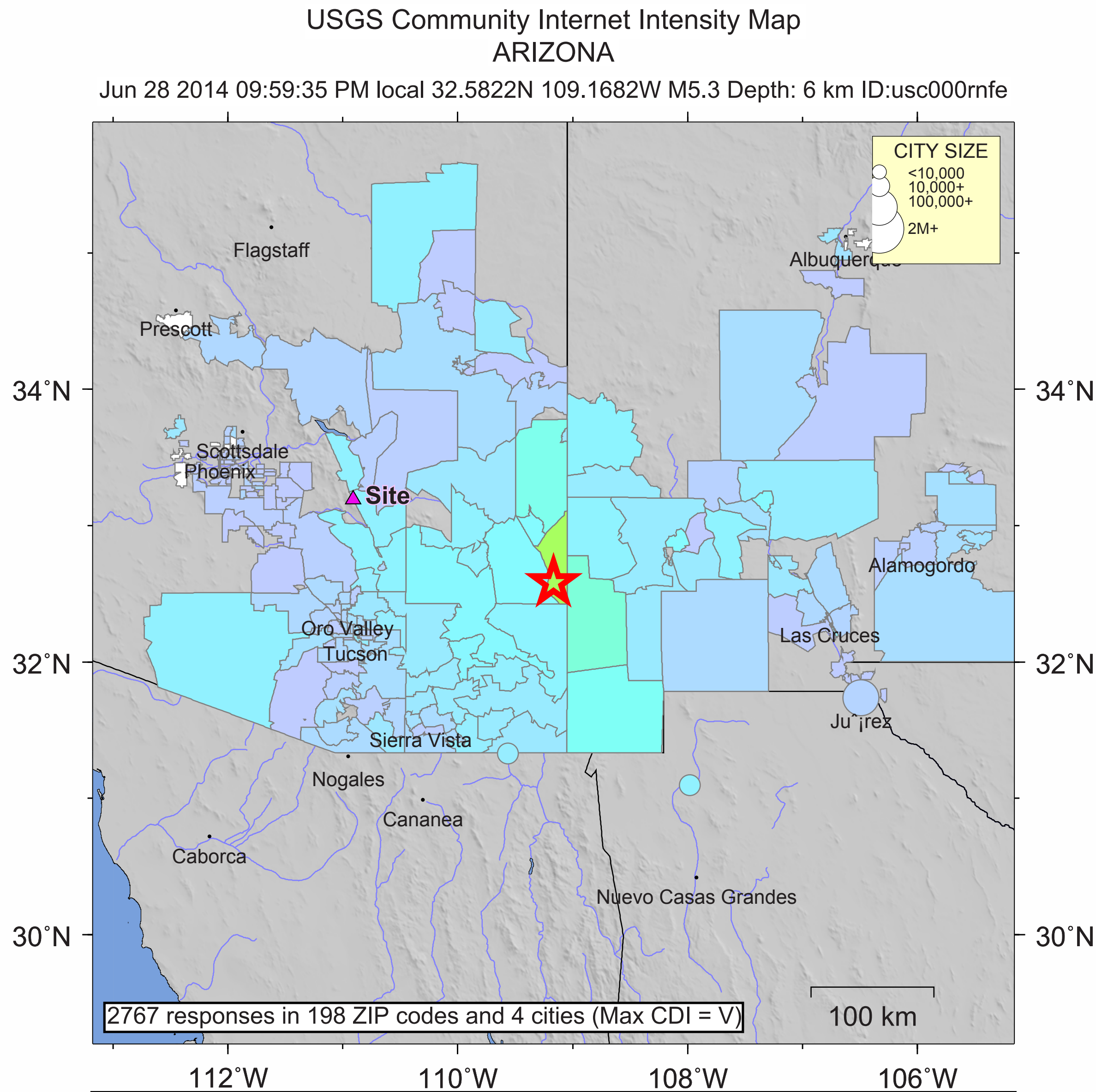

INTENSITY	I	II-III	IV	V	VI	VII	VIII	IX	X+
SHAKING	Not felt	Weak	Light	Moderate	Strong	Very strong	Severe	Violent	Extreme
DAMAGE	none	none	none	Very light	Light	Moderate	Moderate/Heavy	Heavy	V. Heavy

Processed: Fri Jan 22 03:18:23 2016

EXPLANATION

▲ Site location

☆ Earthquake epicenter

Source: Figure modified from USGS (2014)

Did You Feel It Map for the 28 June 2014 M 5.2 Southeastern Arizona Earthquake

RESOLUTION COPPER, SKUNK CAMP TSF SITE

Lettis Consultants International, Inc. | Figure 9

File path: S:\1885\Figures\Figure_09.ai: 10/21/2019; User:Jch, LCI.

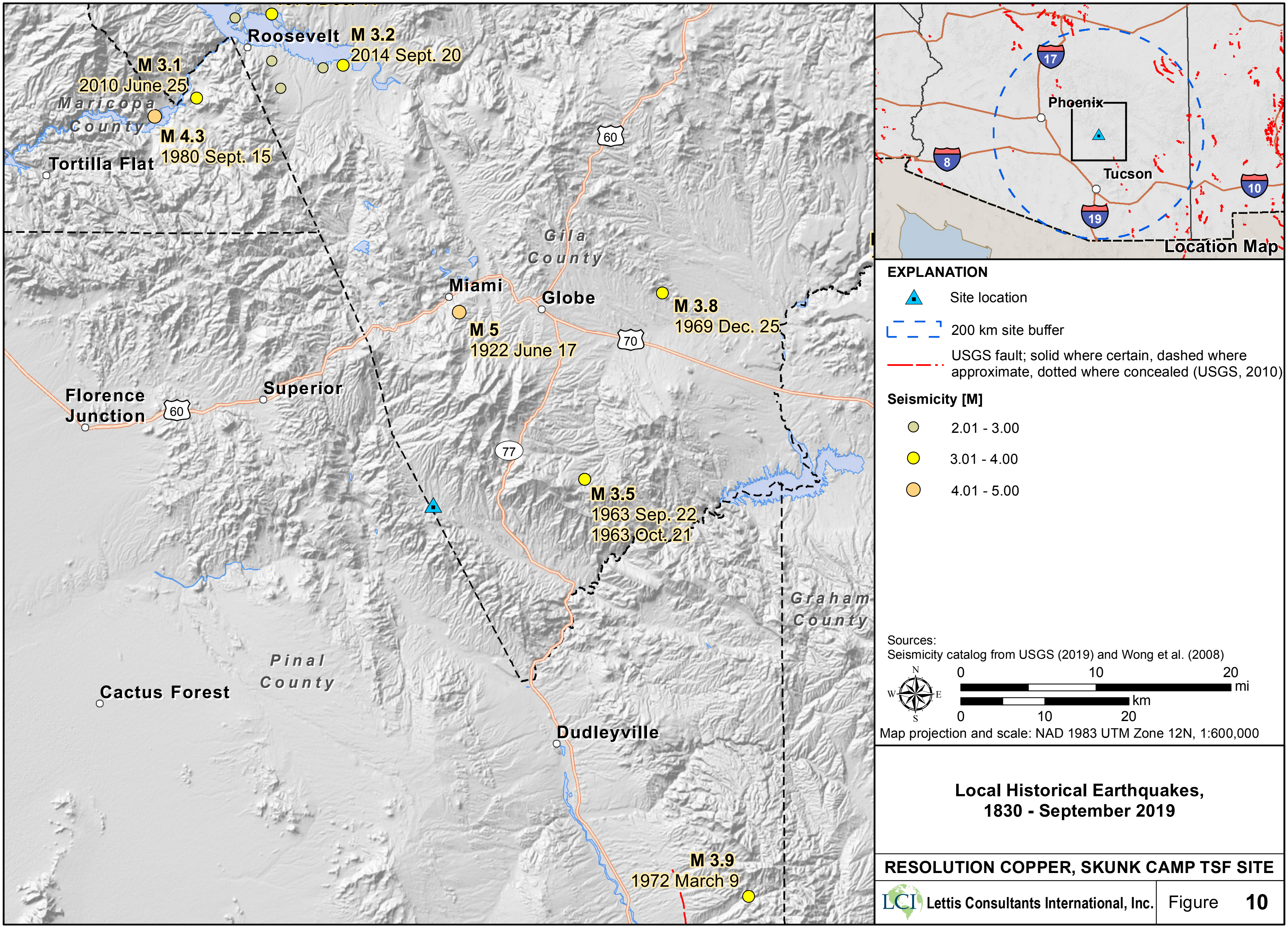

Local Historical Earthquakes, 1830 - September 2019

RESOLUTION COPPER, SKUNK CAMP TSF SITE

Lettis Consultants International, Inc. | Figure **10**

File path: S:\1885\Figures\Figure_10.mxd; Date: 10/29/2019; User: nora, LCI; Rev.1

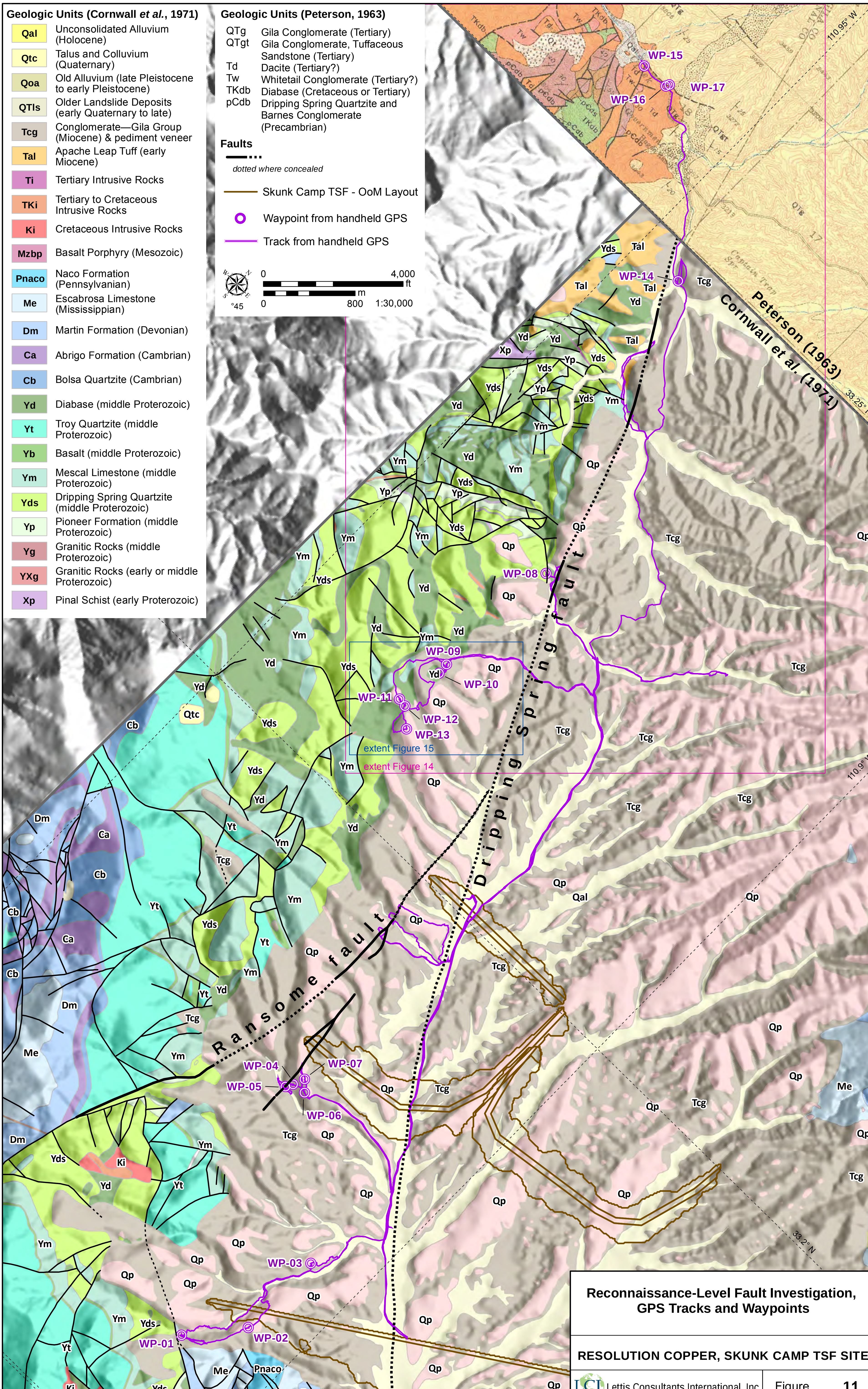

Reconnaissance-Level Fault Investigation, GPS Tracks and Waypoints

RESOLUTION COPPER, SKUNK CAMP TSF SITE

LCI Lettis Consultants International, Inc. | Figure **11**

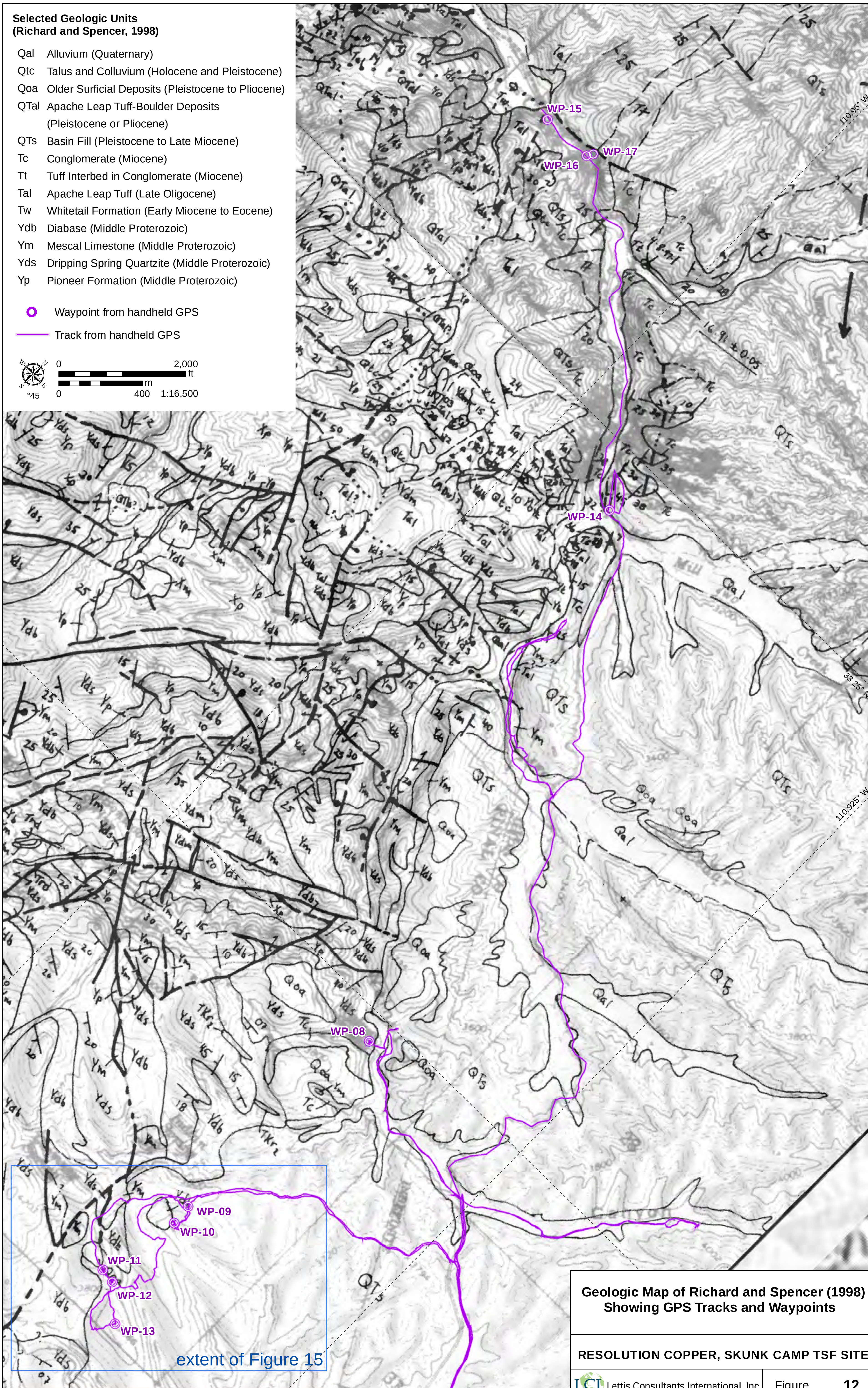

Geologic Map of Richard and Spencer (1998) Showing GPS Tracks and Waypoints

RESOLUTION COPPER, SKUNK CAMP TSF SITE

Lettis Consultants International, Inc. | Figure 12

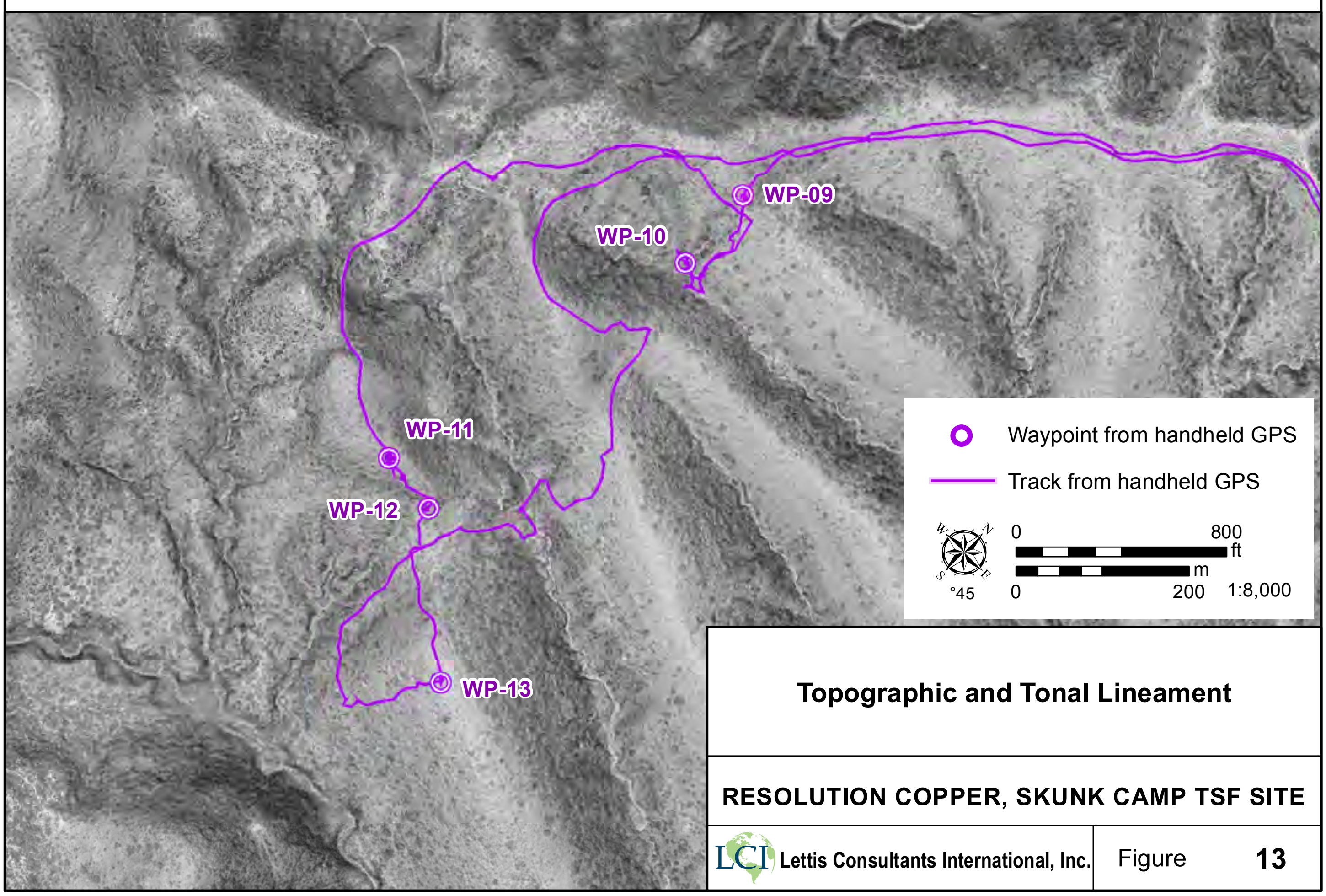

Topographic and Tonal Lineament

RESOLUTION COPPER, SKUNK CAMP TSF SITE

Lettis Consultants International, Inc. | Figure **13**

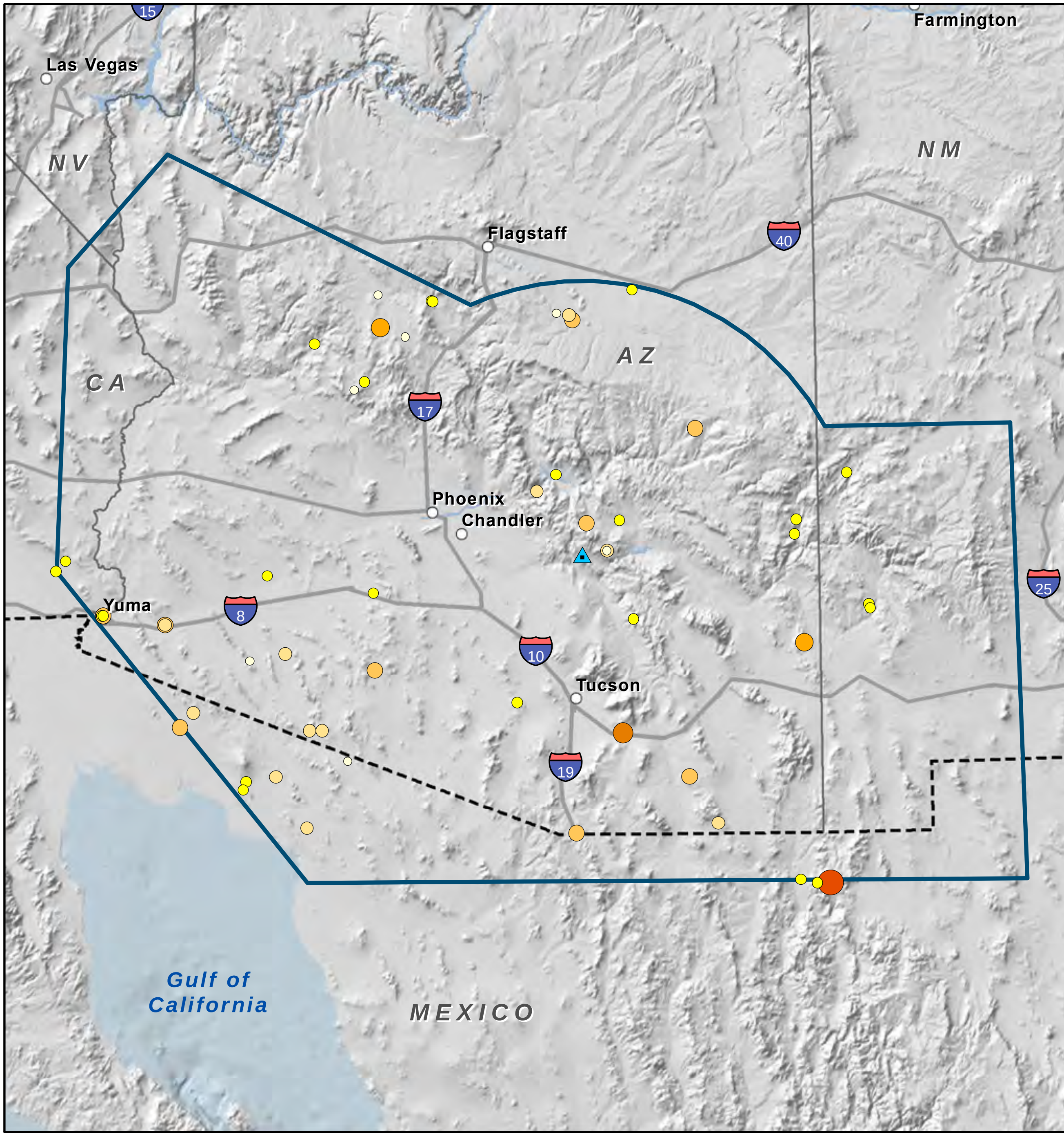

EXPLANATION

Site location

SBR zone

Seismicity [M]

- 3.00 - 3.50
- 3.51 - 4.00
- 4.01 - 4.50
- 4.51 - 5.00
- 5.00 - 5.51
- 5.51 - 6.00
- 6.01 - 6.50
- > 6.50

Sources:
Seismicity catalog from USGS (2019) and Wong et al. (2008)

N W E S

0 25 50 mi

0 50 100 km

Map projection and scale: NAD 1983 UTM Zone 12N, 1:4,500,000

Independent Earthquakes, 1830 - September 2019, in the SBR Seismic Source Zone (M ≥ 3.0)

RESOLUTION COPPER, SKUNK CAMP TSF SITE

LCI Lettis Consultants International, Inc.

Figure **14**

File path: S:\1885\Figures\Figure_14_.mxd; Date: 11/22/2019; User: Whitney, LCI; Rev.1

EXPLANATION

Magnitude bin:

- 3.0 - 3.5
- 3.5 - 4.0
- 4.0 - 4.5
- 4.5 - 5.0
- 5.0 - 5.5
- 5.5 - 6.0
- 6.0 - 6.5
- 6.5 - 7.0

Completness:

- 3.0 - 3.5
- 3.5 - 4.0
- 4.0 - 5.0
- ≥ 5.0

Stepp Plot for the SBR Seismic Source Zone

RESOLUTION COPPER, SKUNK CAMP TSF SITE

LCI Lettis Consultants International, Inc. | Figure **15**

File path: S:\1885\Figures\Figure_15.ai; Date: 11/22/2019; User: Whitney Newcomb, LCI; Rev.0

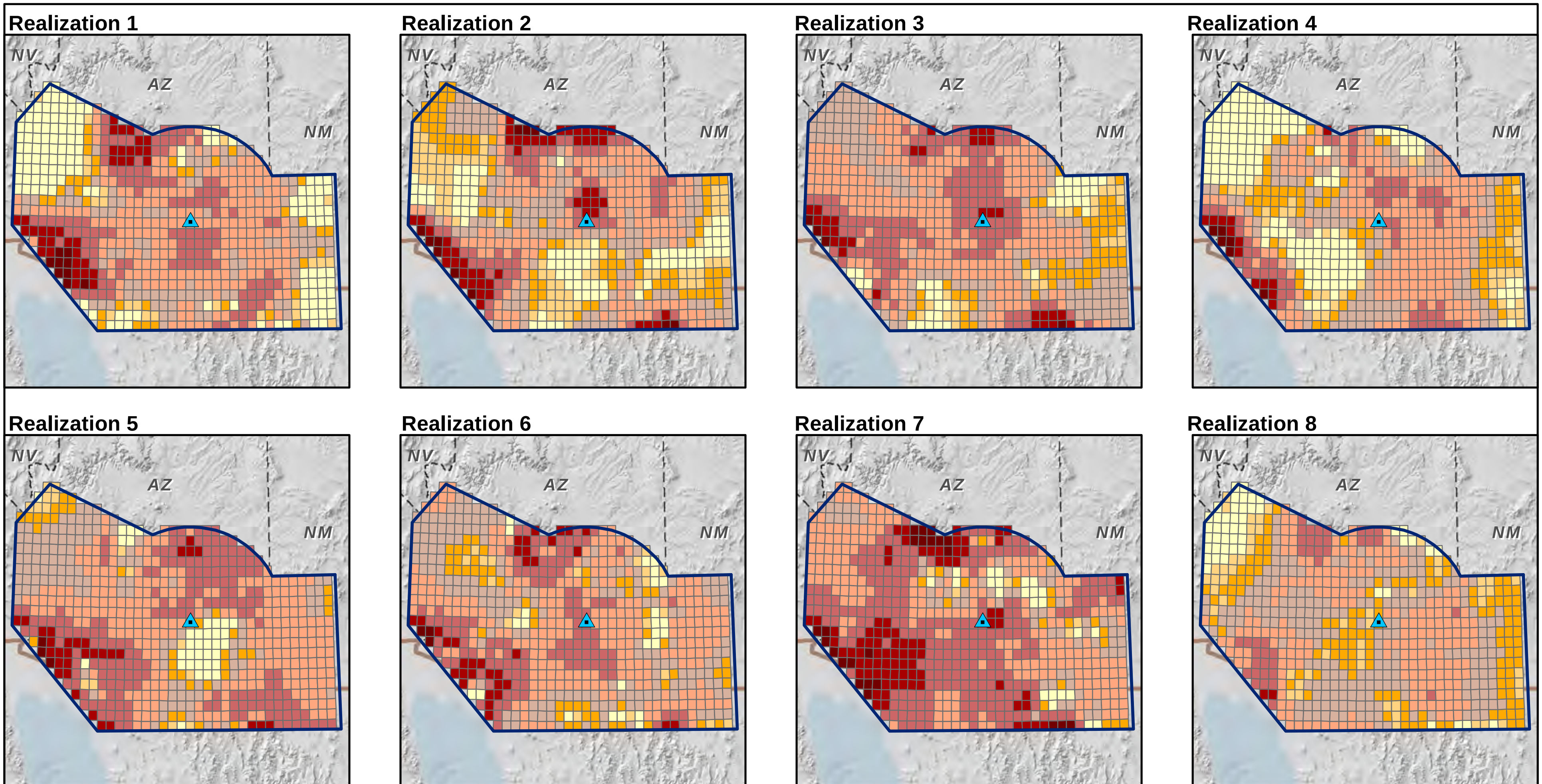

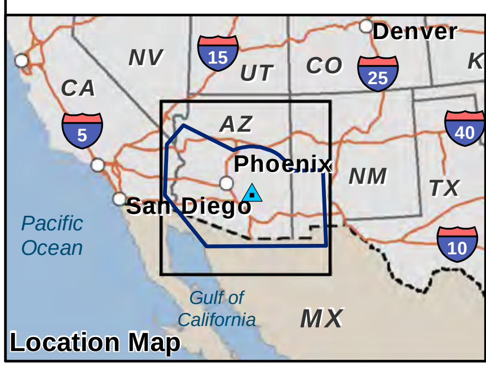

EXPLANATION

Site location

Gridded seismicity data:

SBR zone

Rate

≤ 8.00X10^{-6}	6.31X10^{-5} - 1.30X10^{-4}
8.01X10^{-6} - 1.60X10^{-5}	1.31X10^{-4} - 2.50X10^{-4}
1.61X10^{-5} - 3.10X10^{-5}	2.51X10^{-4} - 5.00X10^{-4}
3.11X10^{-5} - 6.30X10^{-5}	≥ 5.01X10^{-4}

N S W E

0 100 200 mi

0 100 200 km

Map projection and scale: NAD 1983 UTM Zone 12N, 1:13,000,000

Gridded Seismicity for the SBR Seismic Source Zone

RESOLUTION COPPER, SKUNK CAMP TSF SITE

Lettis Consultants International, Inc. | Figure **16**

File path: S:\1885\Figures\Figure_16.mxd; Date: 11/22/2019; User: Whitney, LCI; Rev.1

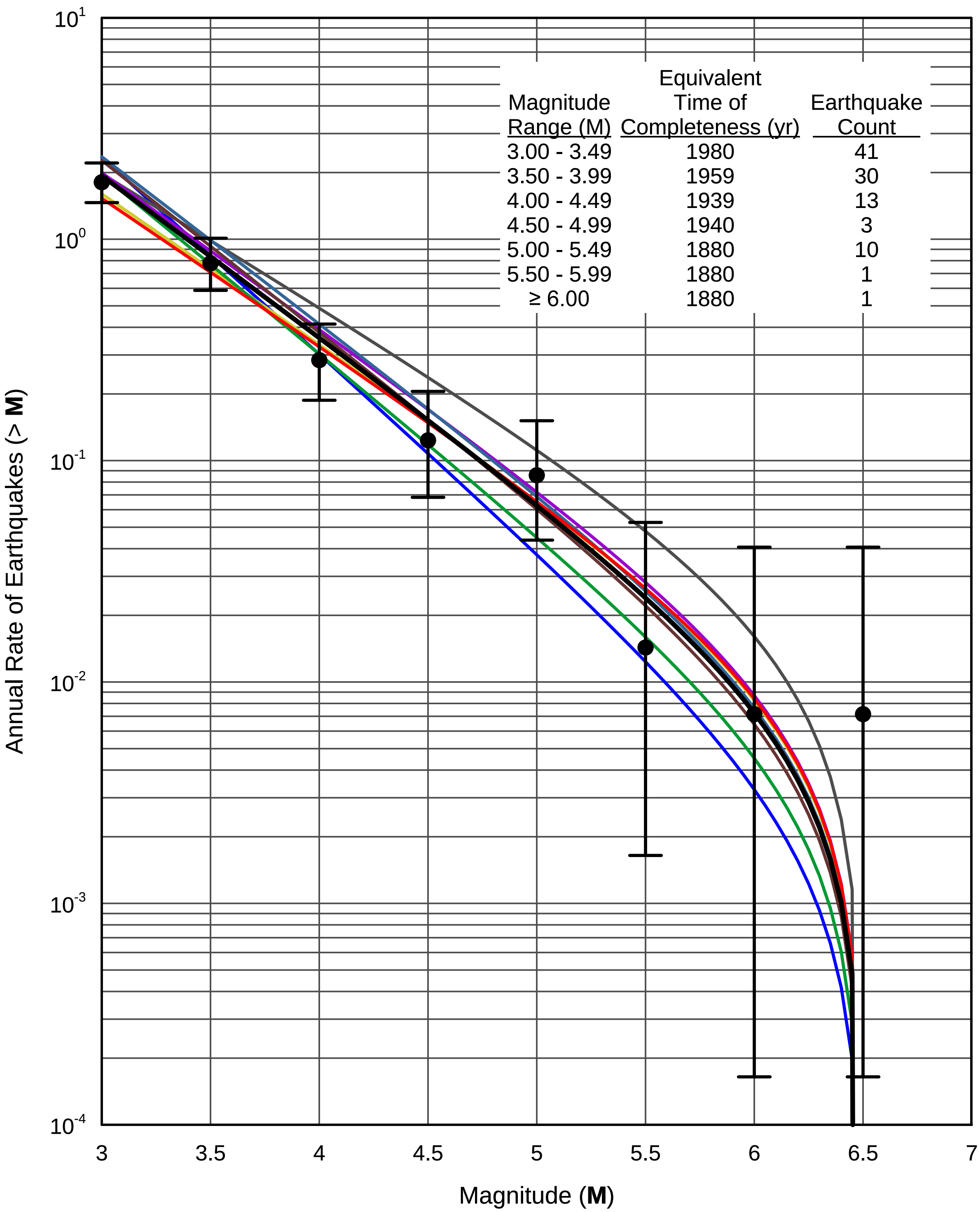

EXPLANATION

● Cumulative earthquake rate

ABSMOOTH Realization

1, 2, 3, 4, 5, 6, 7, 8, Mean

Note: Error bars on cumulative earthquake rate represent two standard deviations.

Cumulative Magnitude-Recurrence Curves for the Southern Basin and Range Province Areal Source Zone for M_{MAX} 6.5

RESOLUTION COPPER, SKUNK CAMP TSF SITE

Lettis Consultants International, Inc.

Figure **17**

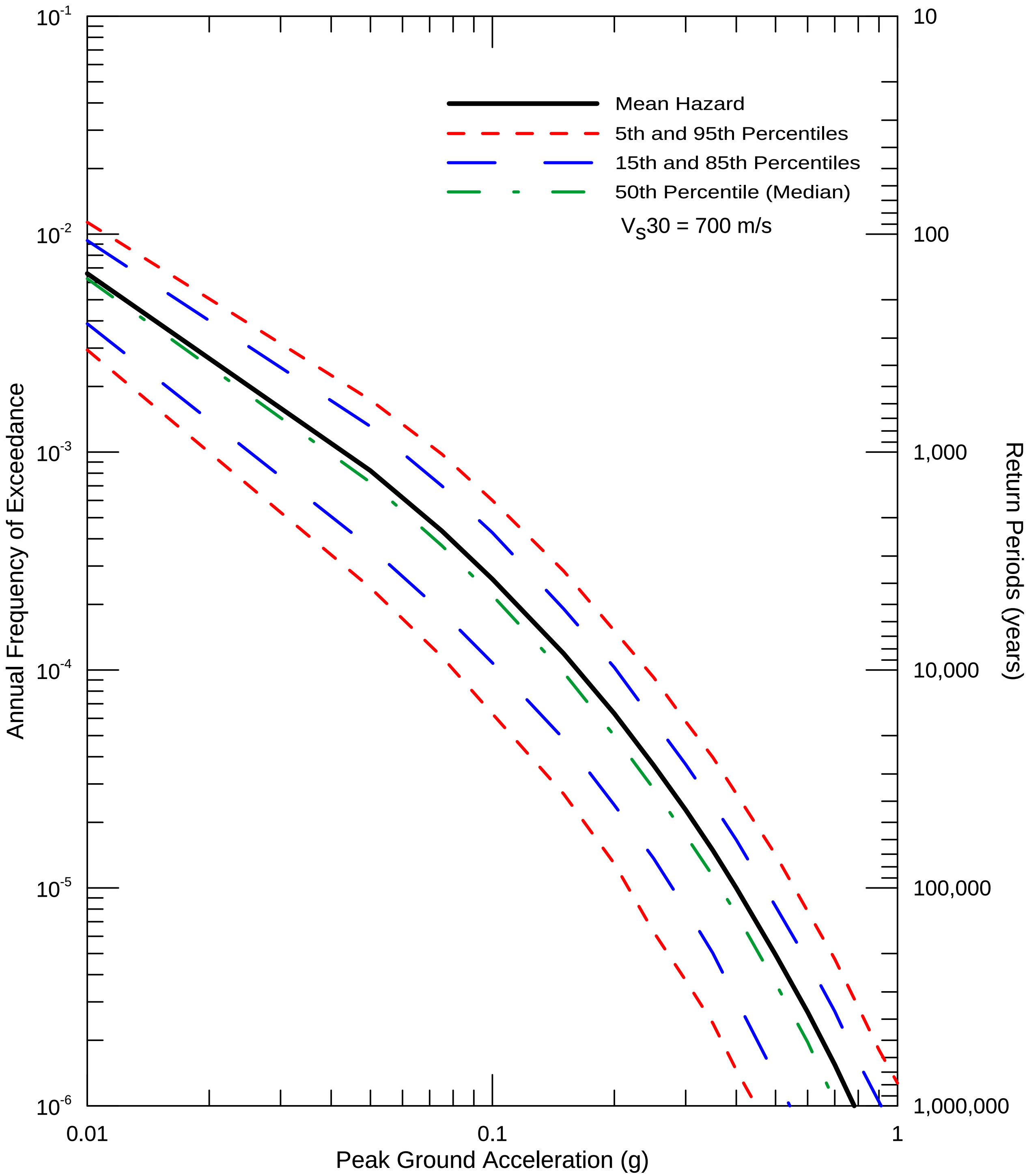

Seismic Hazard Curves
for Peak Horizontal Acceleration

RESOLUTION COPPER, SKUNK CAMP TSF SITE

LCI **Lettis Consultants International, Inc.** Figure **18**

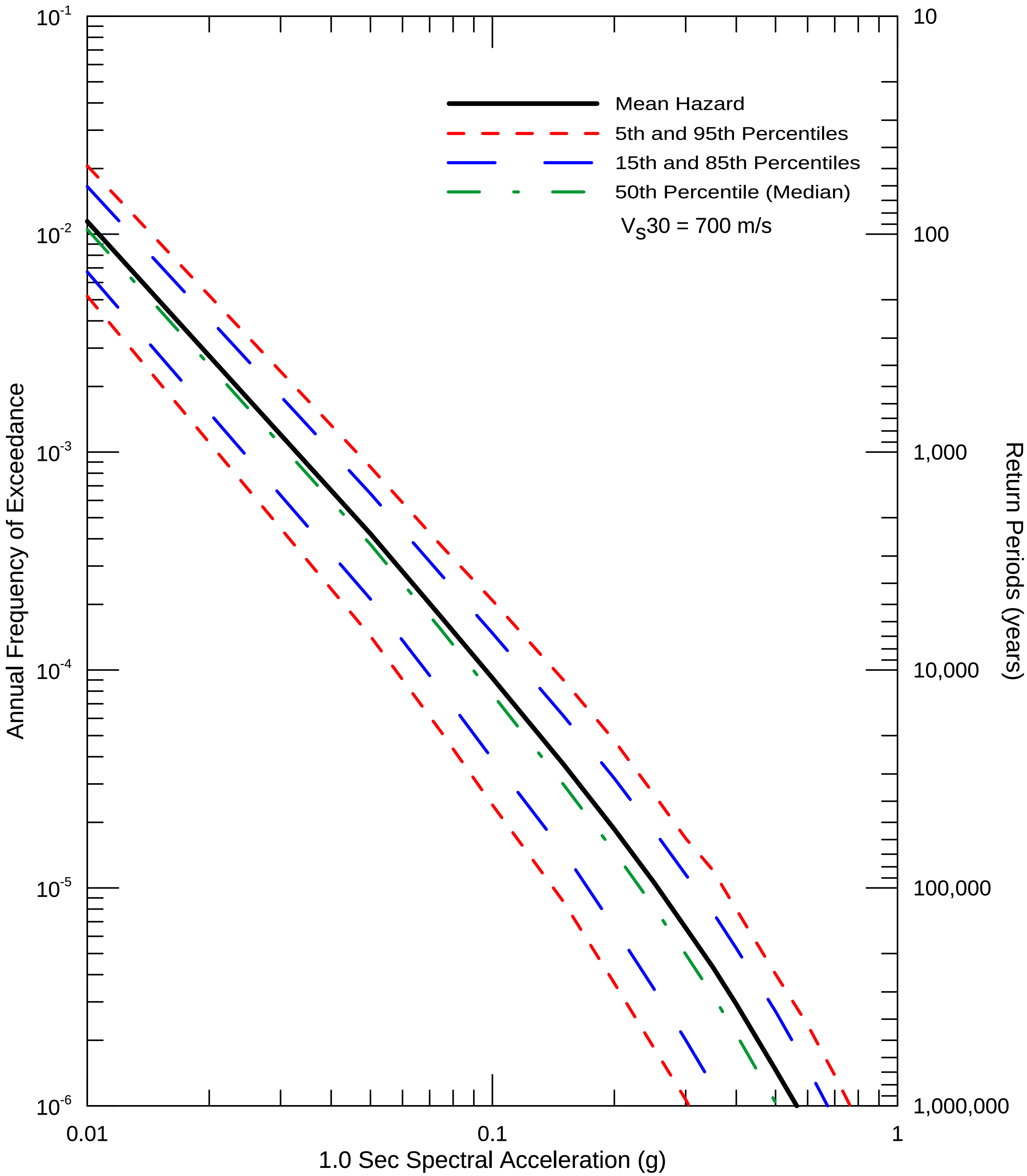

Seismic Hazard Curves for
1.0 Sec Horizontal Spectral Acceleration

RESOLUTION COPPER, SKUNK CAMP TSF SITE

Lettis Consultants International, Inc. | Figure **19**

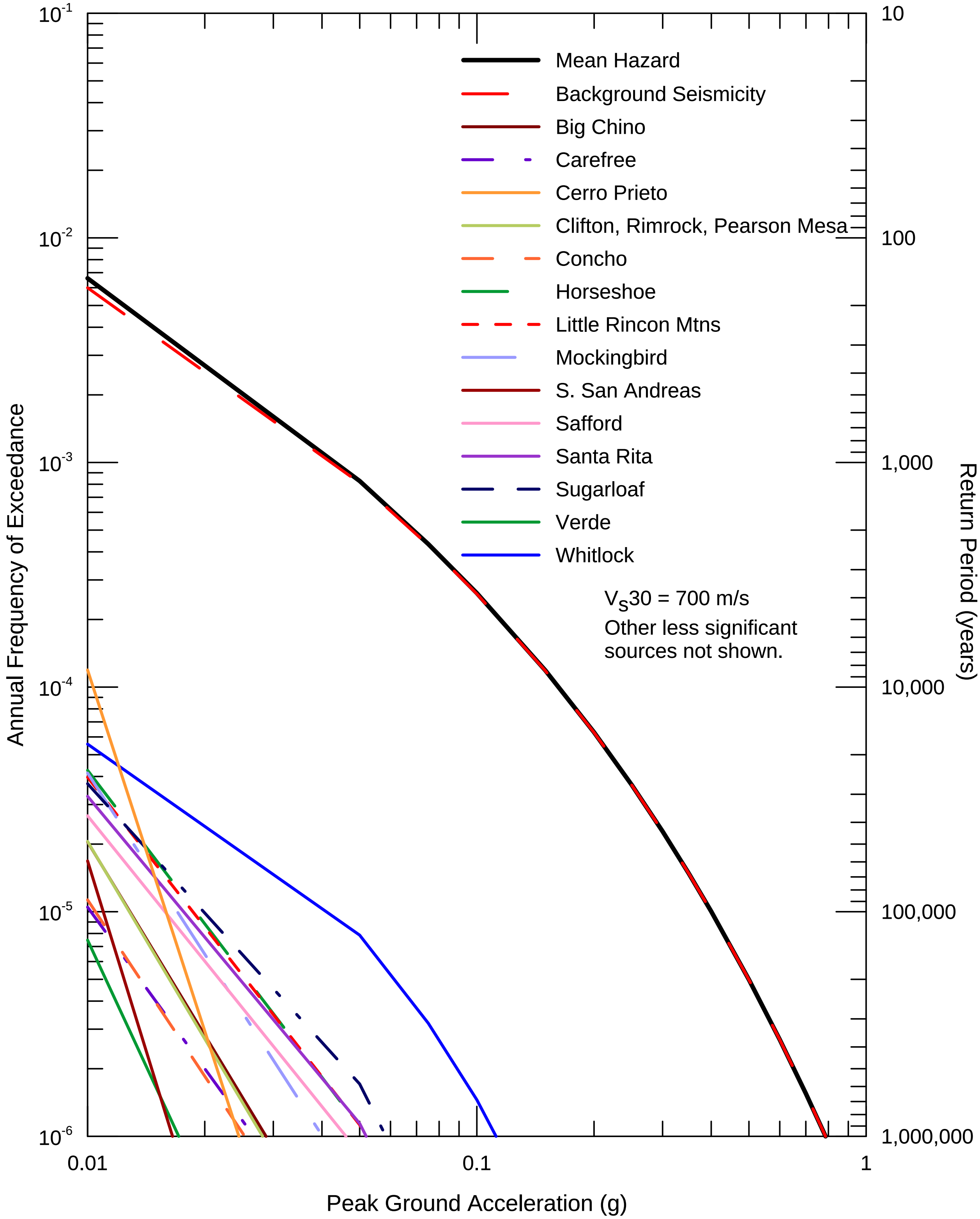

Seismic Source Contributions for Mean Peak Horizontal Acceleration Hazard

RESOLUTION COPPER, SKUNK CAMP TSF SITE

Lettis Consultants International, Inc. | Figure **20**

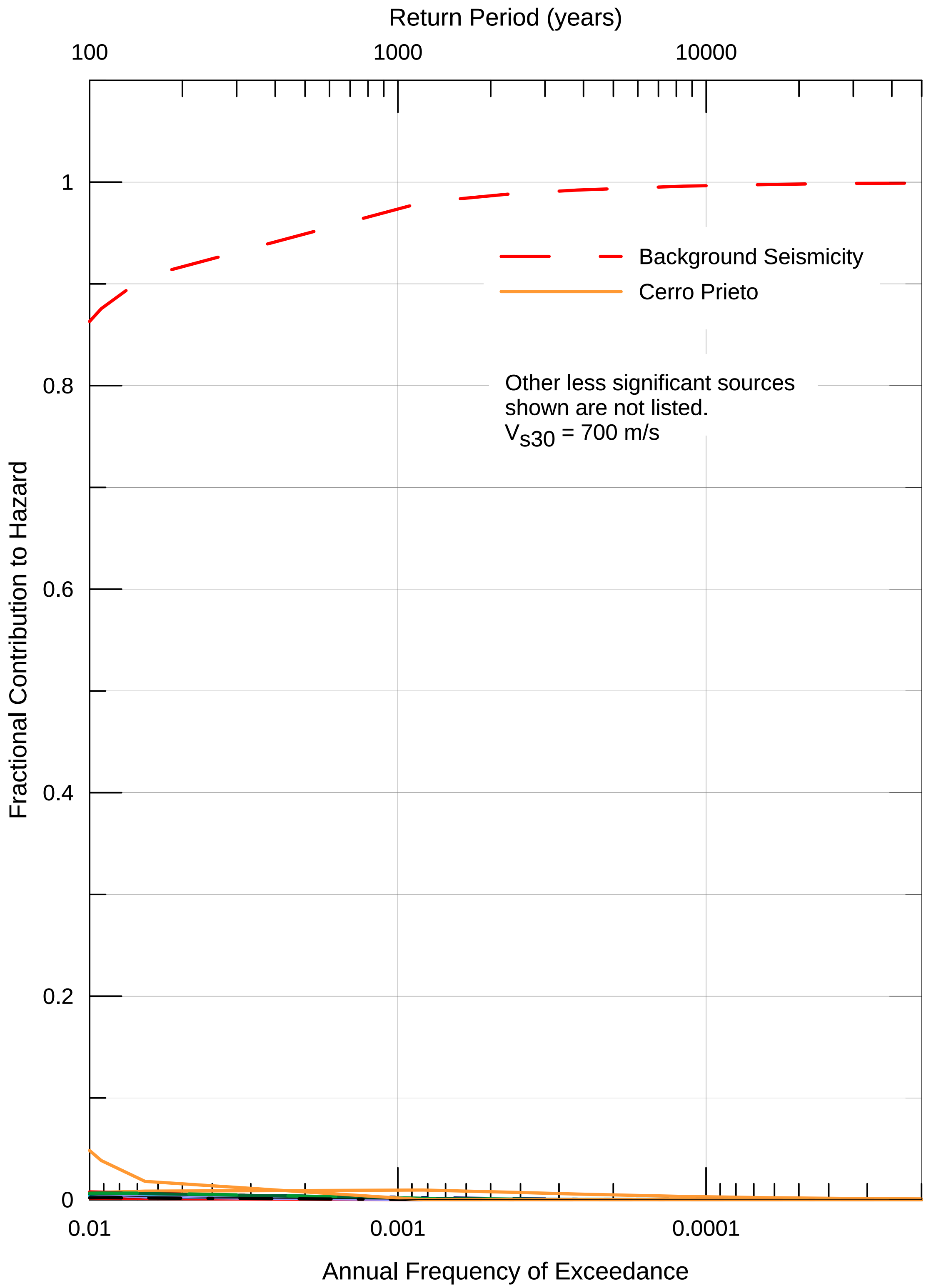

Seismic Source Fractional Contributions for Mean Peak Horizontal Acceleration Hazard

RESOLUTION COPPER, SKUNK CAMP TSF SITE

Lettis Consultants International, Inc.

Figure **21**

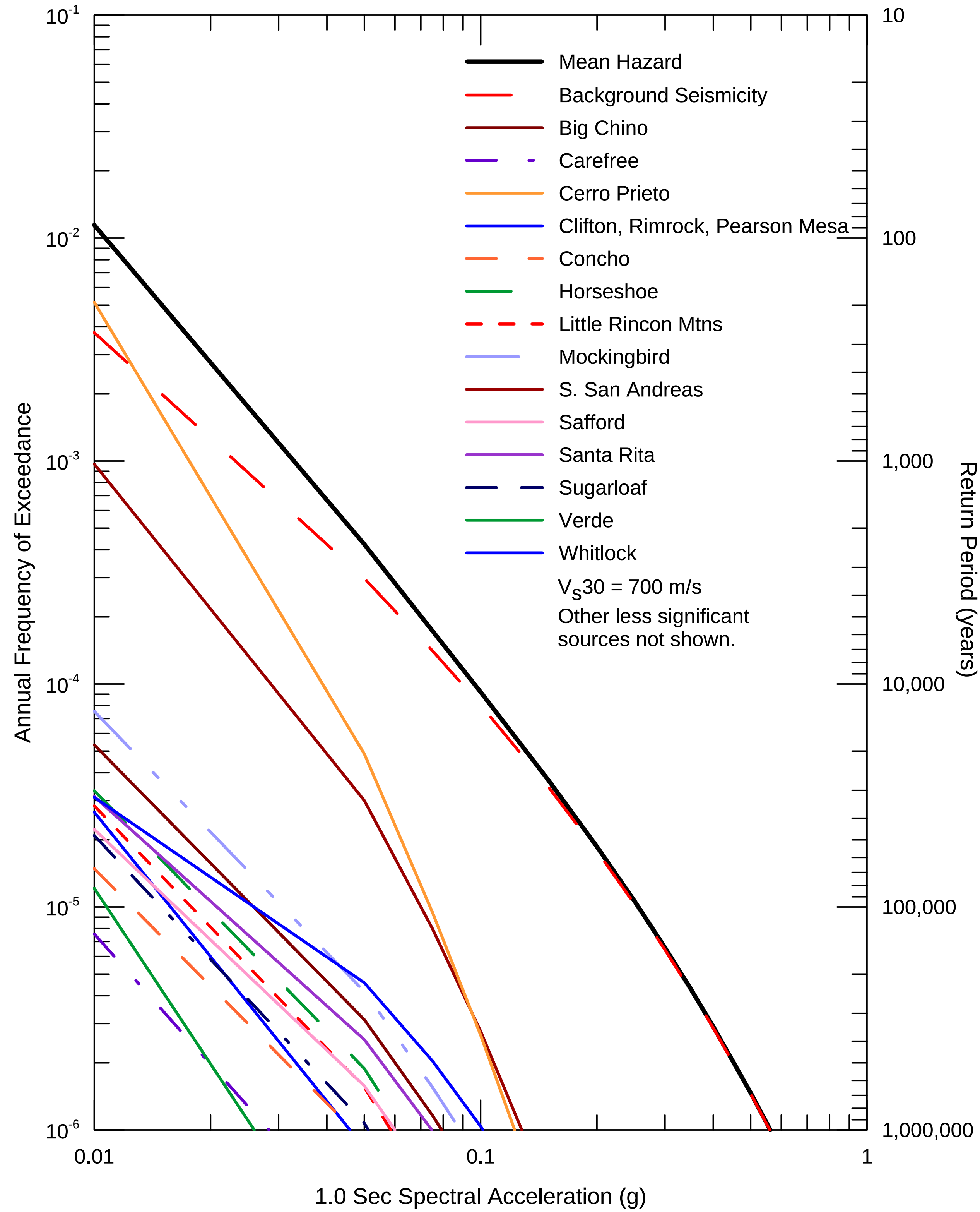

Seismic Source Contributions for Mean 1.0 Sec Horizontal Spectral Acceleration Hazard

RESOLUTION COPPER, SKUNK CAMP TSF SITE

LCI **Lettis Consultants International, Inc.** Figure **22**

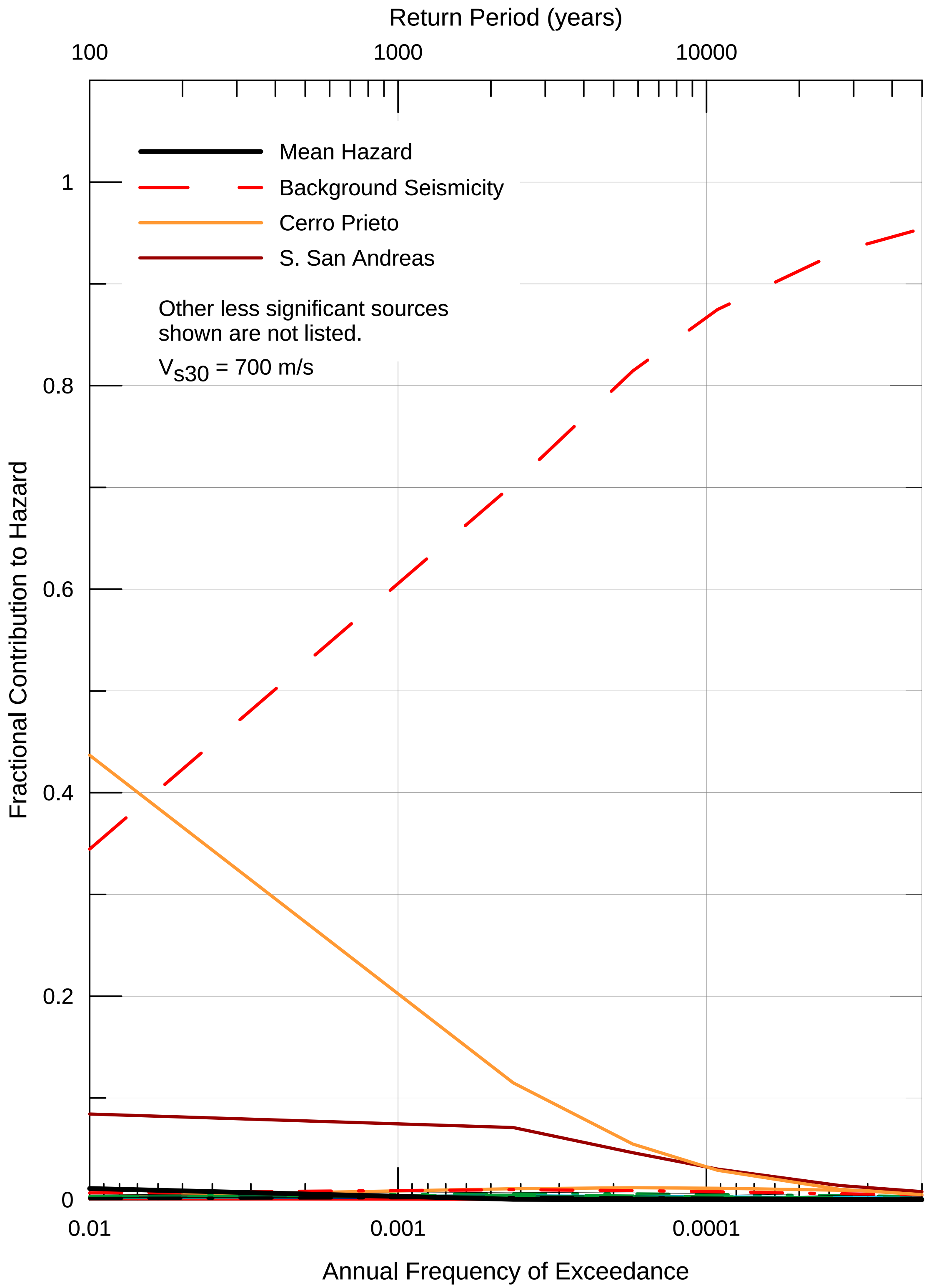

Seismic Source Fractional Contributions for Mean 1.0 Sec Spectral Horizontal Acceleration Hazard

RESOLUTION COPPER, SKUNK CAMP TSF SITE

LCI **Lettis Consultants International, Inc.**

Figure **23**

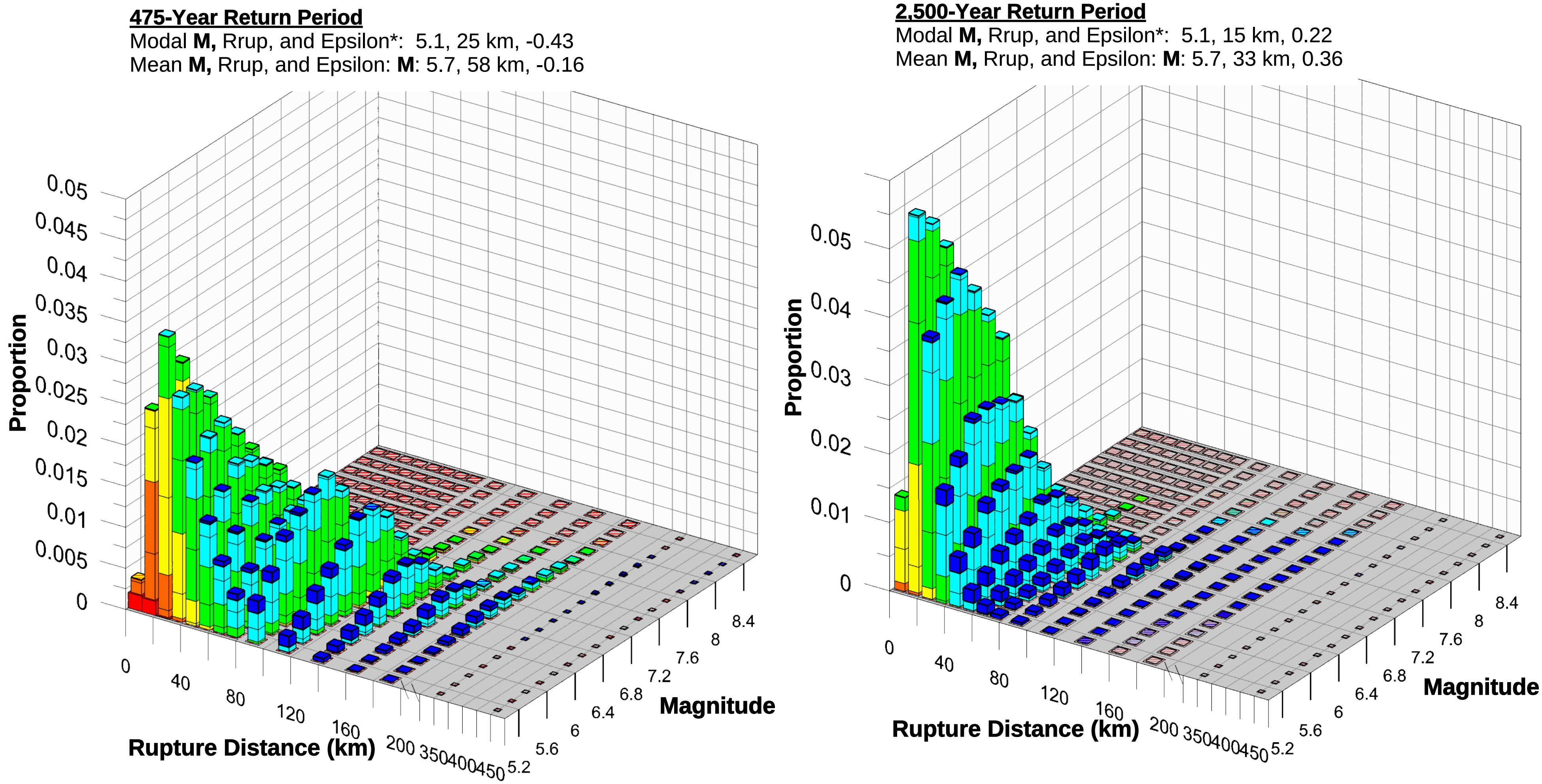

Epsilon

- 2 to 3
- 1 to 2
- 0 to 1
- -1 to 0
- -2 to -1
- < -2

V_s30 = 700 m/s

Epsilon* is mean epsilon for modal magnitude-distance bin

Magnitude and Distance Contributions to the Mean Peak Horizontal Acceleration Hazard at 475 and 2,500-Year Return Periods

RESOLUTION COPPER, SKUNK CAMP TSF SITE

Lettis Consultants International, Inc.

Figure **24**

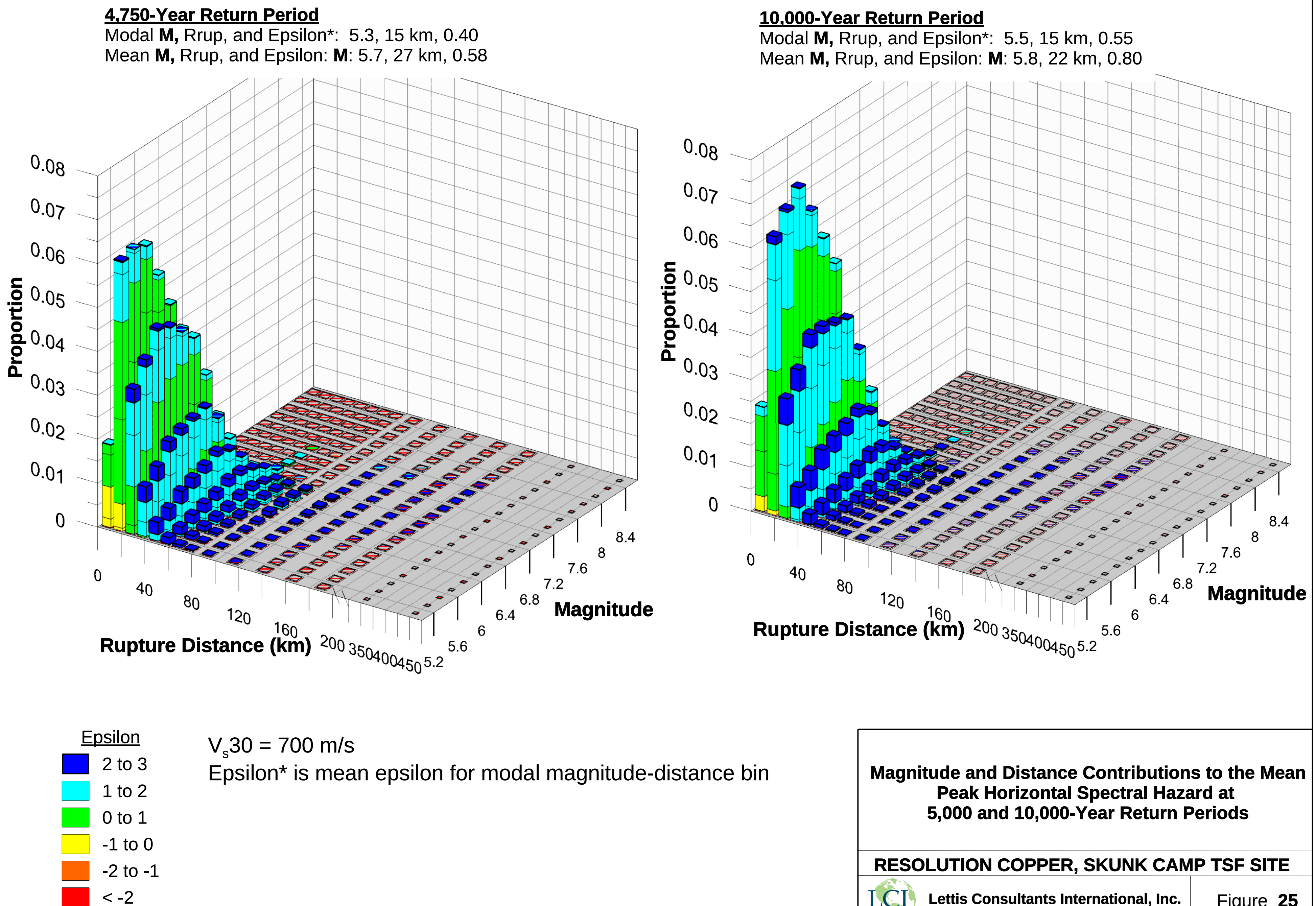

V_s30 = 700 m/s
Epsilon* is mean epsilon for modal magnitude-distance bin

Magnitude and Distance Contributions to the Mean Peak Horizontal Spectral Hazard at 5,000 and 10,000-Year Return Periods

RESOLUTION COPPER, SKUNK CAMP TSF SITE

Lettis Consultants International, Inc.

Figure **25**

475-Year Return Period

Modal **M,** Rrup, and Epsilon*: 7.3, 350 km, 1.57
For sources < 200 km: Mean **M,** Rrup and Epsilon: **M**: 6.0, 66 km, 0.35
For sources > 200 km: Mean **M,** Rrup and Epsilon: **M**: 7.3, 379 km, 1.54

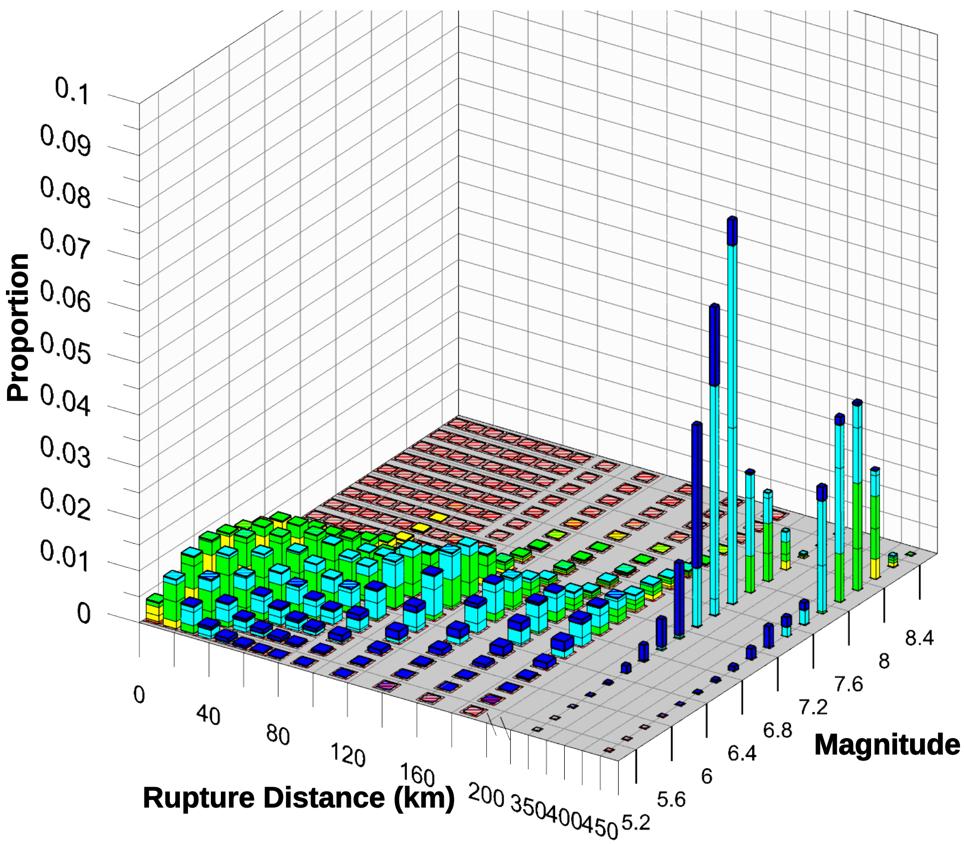

2,500-Year Return Period

Modal **M,** Rrup, and Epsilon: 7.3, 350 km, 1.57
For sources < 200 km: Mean **M,** Rrup, and Epsilon: **M**: 6.0, 66 km, 0.35
For sources > 200 km: Mean **M,** Rrup, and Epsilon: **M**: 7.3, 379 km, 1.54

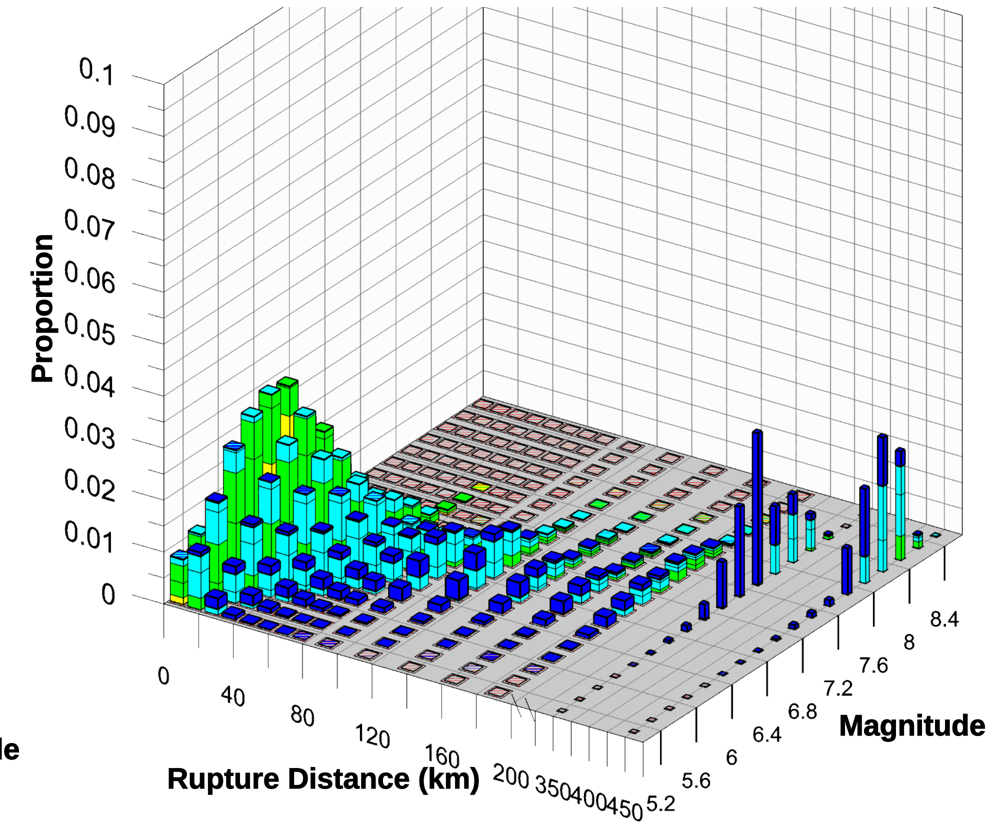

Epsilon

- 2 to 3
- 1 to 2
- 0 to 1
- -1 to 0
- -2 to -1
- < -2

V_s30 = 700 m/s
Epsilon* is mean epsilon for modal magnitude-distance bin.

Magnitude and Distance Contributions to the Mean 1.0 Sec Horizontal Spectral Acceleration Hazard at 475 and 2,500-Year Return Periods

RESOLUTION COPPER, SKUNK CAMP TSF SITE

LCI **Lettis Consultants International, Inc.**

Figure **26**

5,000-Year Return Period
Modal **M,** Rrup, and Epsilon*: 6.1, 15 km, -0.02
For sources < 200 km: Mean **M,** Rrup and Epsilon: **M**: 6.1, 36 km, 0.75
For sources > 200 km: Mean **M,** Rrup and Epsilon: **M**: 7.5, 379 km, 2.19

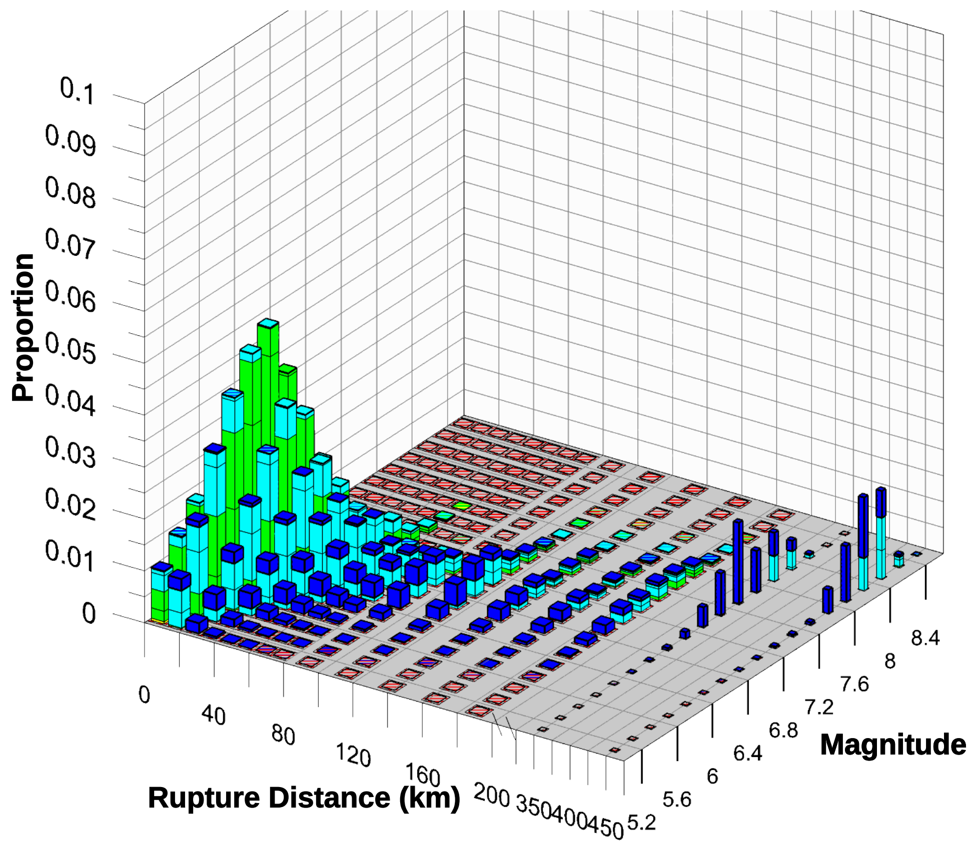

10,000-Year Return Period
Modal **M,** Rrup, and Epsilon: 6.1, 15 km, 0.36
For sources < 200 km: Mean **M,** Rrup, and Epsilon: **M**: 6.1, 30 km, 0.87
For sources > 200 km: Mean **M,** Rrup, and Epsilon: **M**: 7.6, 374 km, 2.30

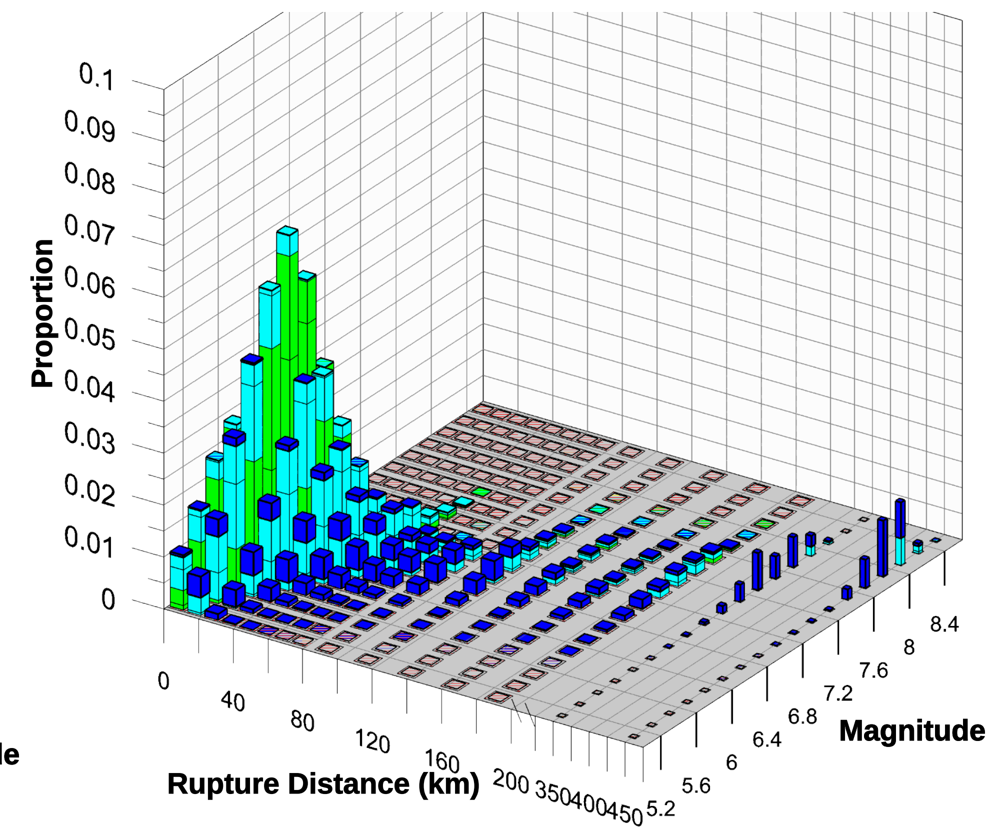

Epsilon
- 2 to 3
- 1 to 2
- 0 to 1
- -1 to 0
- -2 to -1
- < -2

V_s30 = 700 m/s
Epsilon* is mean epsilon for modal magnitude-distance bin.

Magnitude and Distance Contributions to the Mean 1.0 Sec Horizontal Spectral Acceleration Hazard at 5,000 and 10,000-Year Return Periods

RESOLUTION COPPER, SKUNK CAMP TSF SITE

LCI **Lettis Consultants International, Inc.** Figure **27**

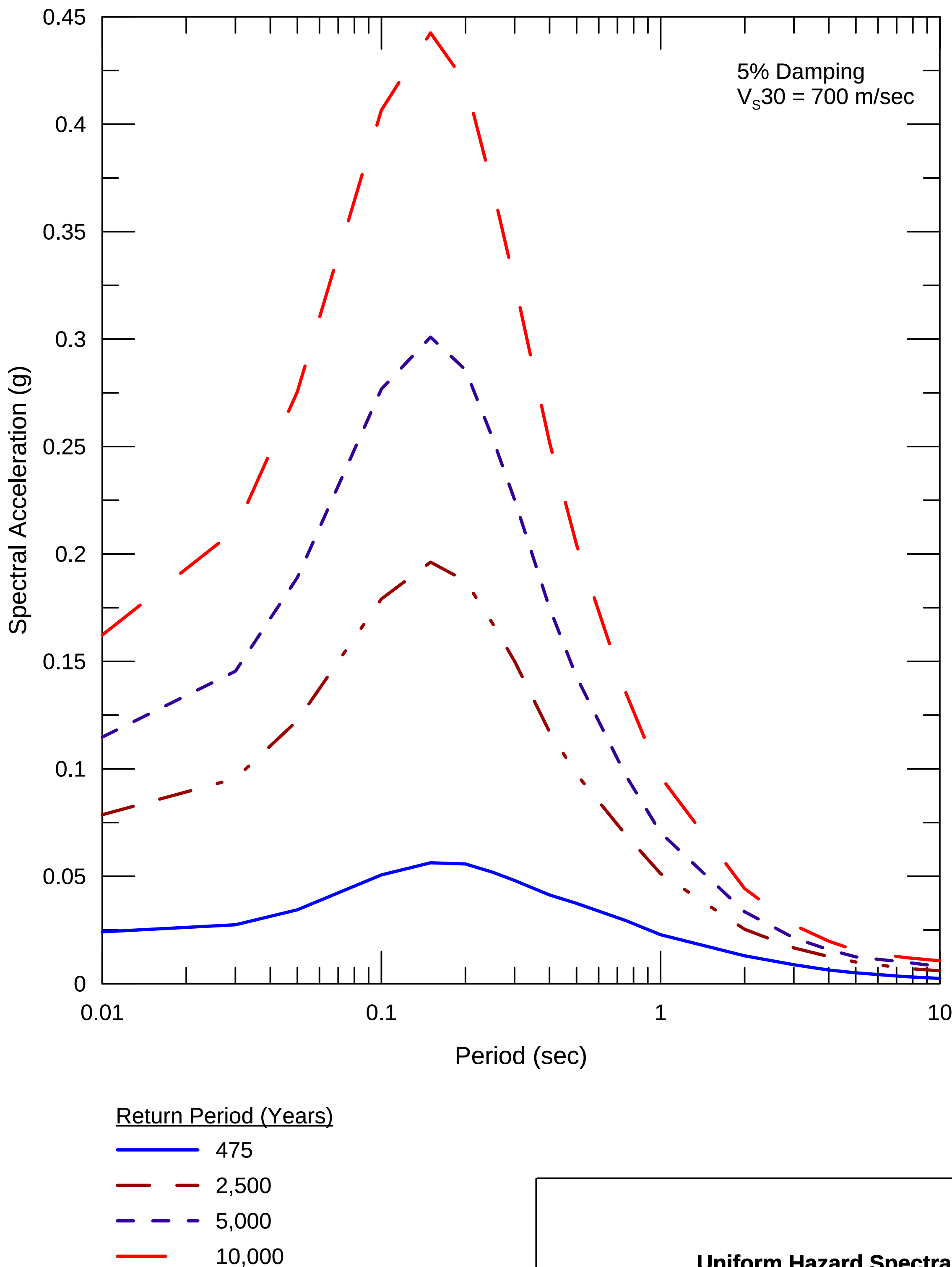

Uniform Hazard Spectra

RESOLUTION COPPER, SKUNK CAMP TSF SITE

LCI **Lettis Consultants International, Inc.** Figure **28**

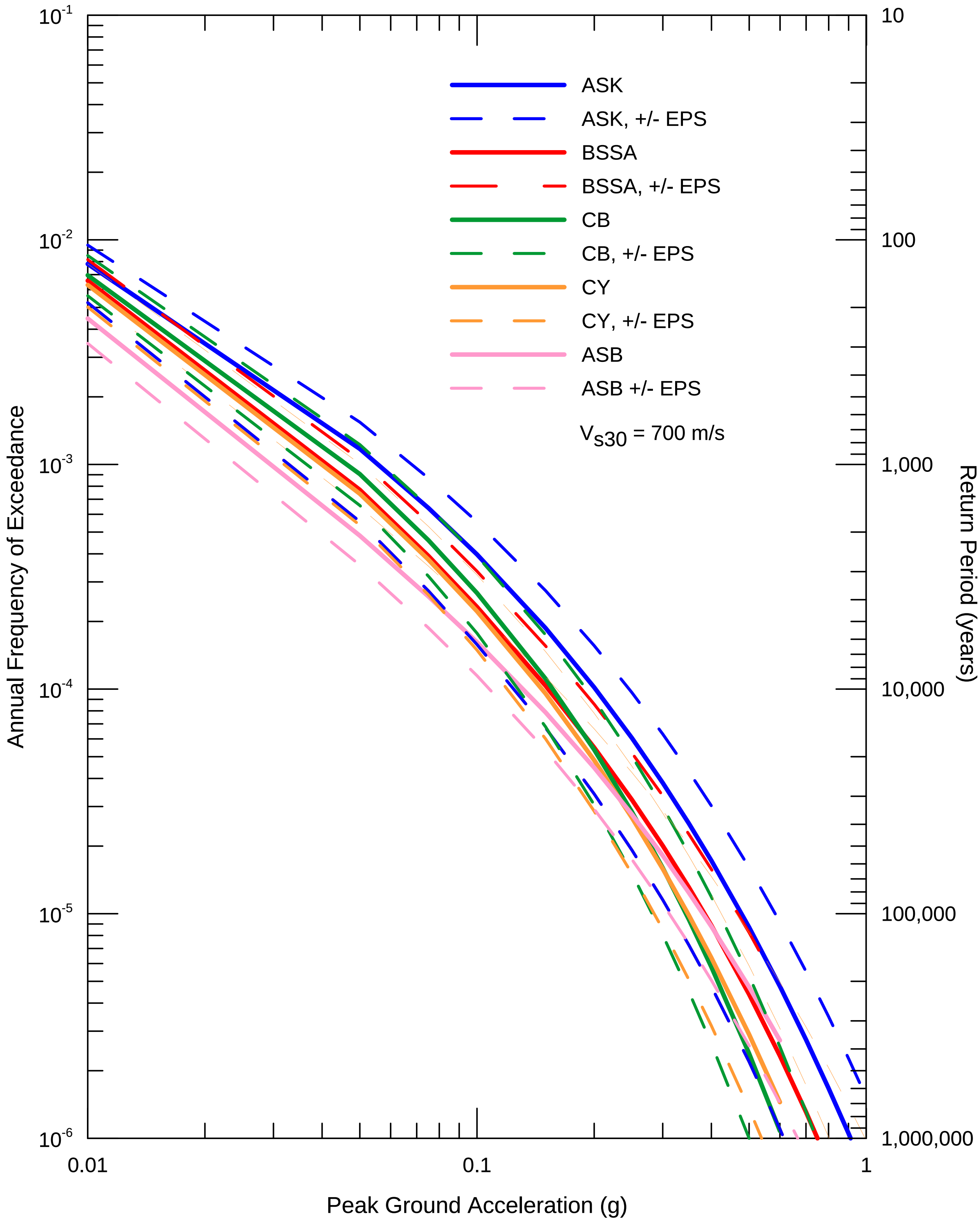

Sensitivity of Mean Peak Horizontal Acceleration Hazard from Arizona Sources to GMMs

RESOLUTION COPPER, SKUNK CAMP TSF SITE

Lettis Consultants International, Inc. | Figure **29**

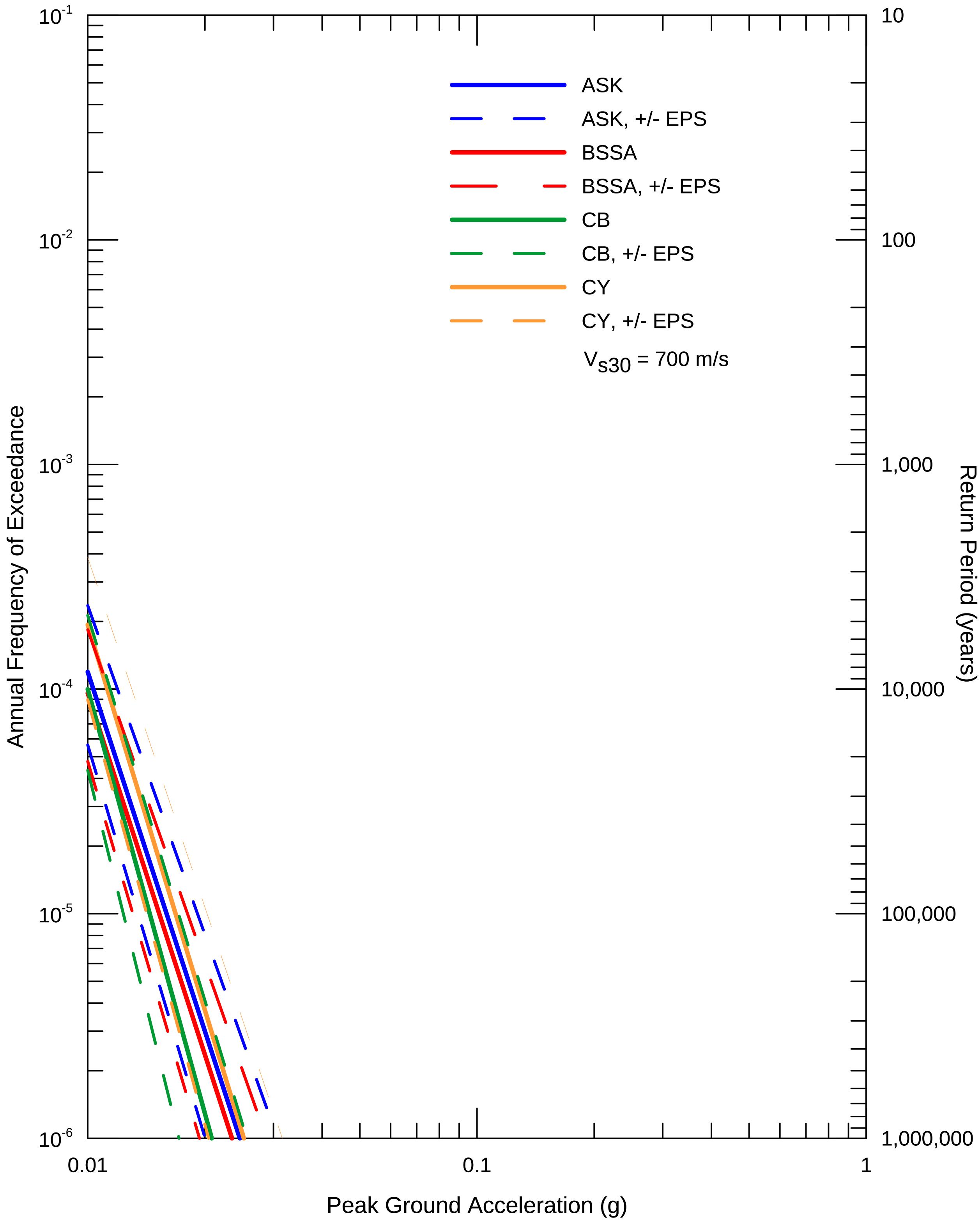

Sensitivity of Mean Peak Horizontal Acceleration Hazard from Southern and Baja California Sources to GMMs

RESOLUTION COPPER, SKUNK CAMP TSF SITE

Lettis Consultants International, Inc. Figure **30**

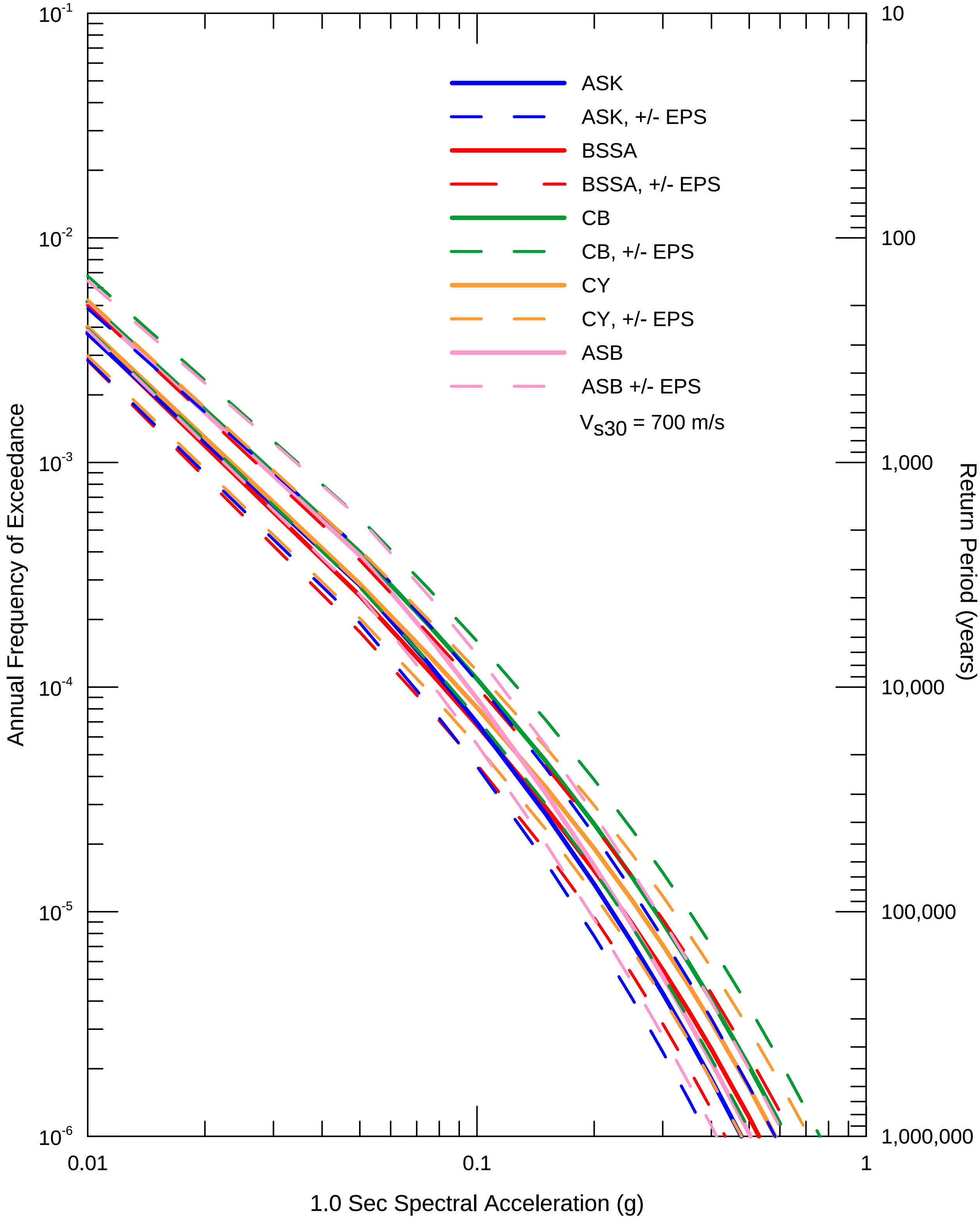

Sensitivity of Mean 1.0 Sec Horizontal Spectral Acceleration Hazard from Arizona Sources to GMMs

RESOLUTION COPPER, SKUNK CAMP TSF SITE

Lettis Consultants International, Inc.

Figure **31**

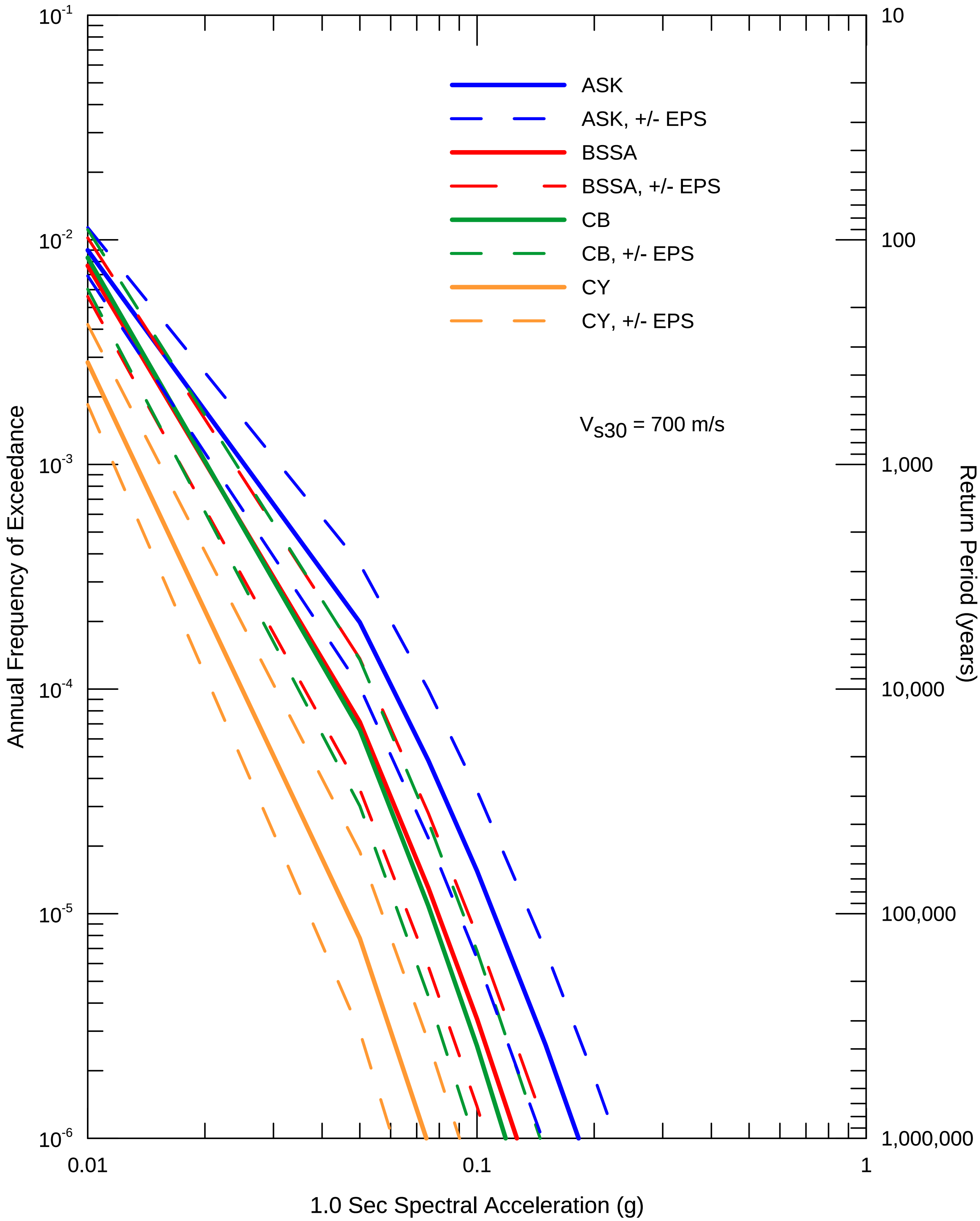

Sensitivity of Mean 1.0 Sec Horizontal Spectral Acceleration Hazard from Southern and Baja California Sources to GMMs

RESOLUTION COPPER, SKUNK CAMP TSF SITE

Lettis Consultants International, Inc. Figure **32**

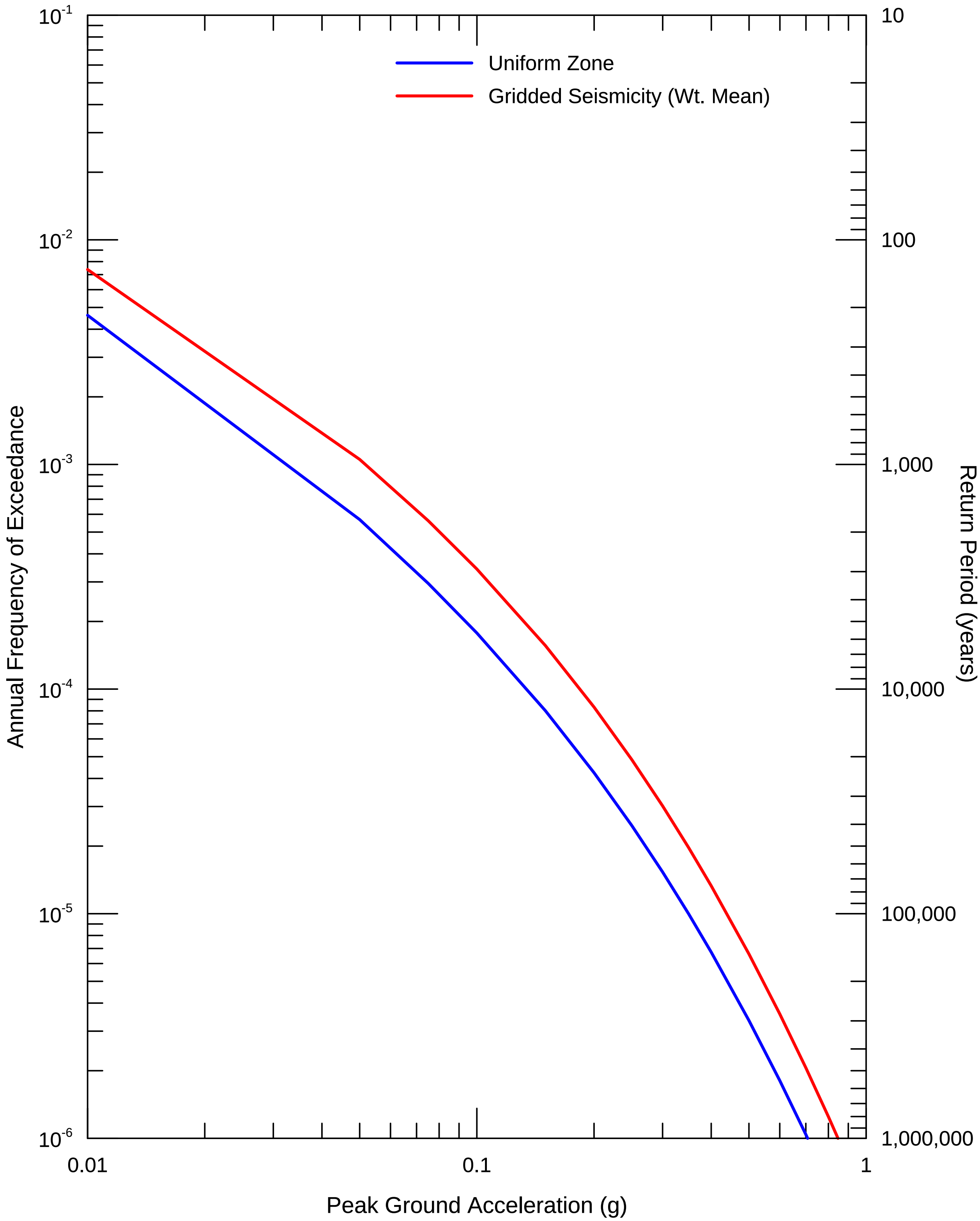

V_S30 = 700 m/s

Hazard Curves shown represent hazard
with end branch weights of 1.0
(e.g. 100% SBR Uniform Background Seismicity)

Sensitivity of Mean Peak Horizontal Acceleration Hazard to Gridded and Uniform Background Seismicity

RESOLUTION COPPER, SKUNK CAMP TSF SITE

Lettis Consultants International, Inc.

Figure **33**

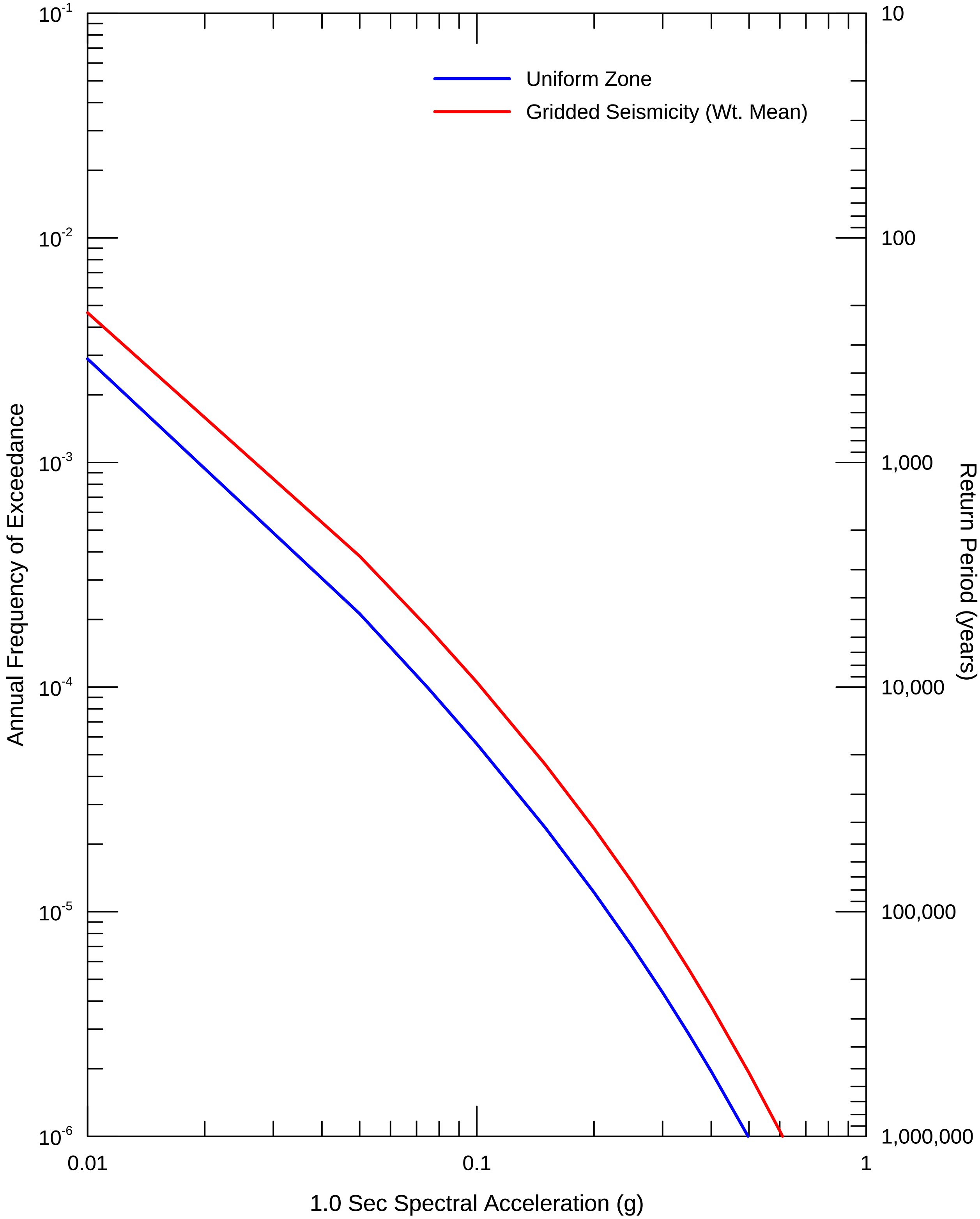

V_S30 = 700 m/s

Hazard Curves shown represent hazard
with end branch weights of 1.0
(e.g. 100% SBR Uniform Background Seismicity)

Sensitivity of Mean 1.0 Sec Horizontal Spectral Acceleration Hazard to Gridded and Uniform Background Seismicity

RESOLUTION COPPER, SKUNK CAMP TSF SITE

LCI **Lettis Consultants International, Inc.**

Figure **34**

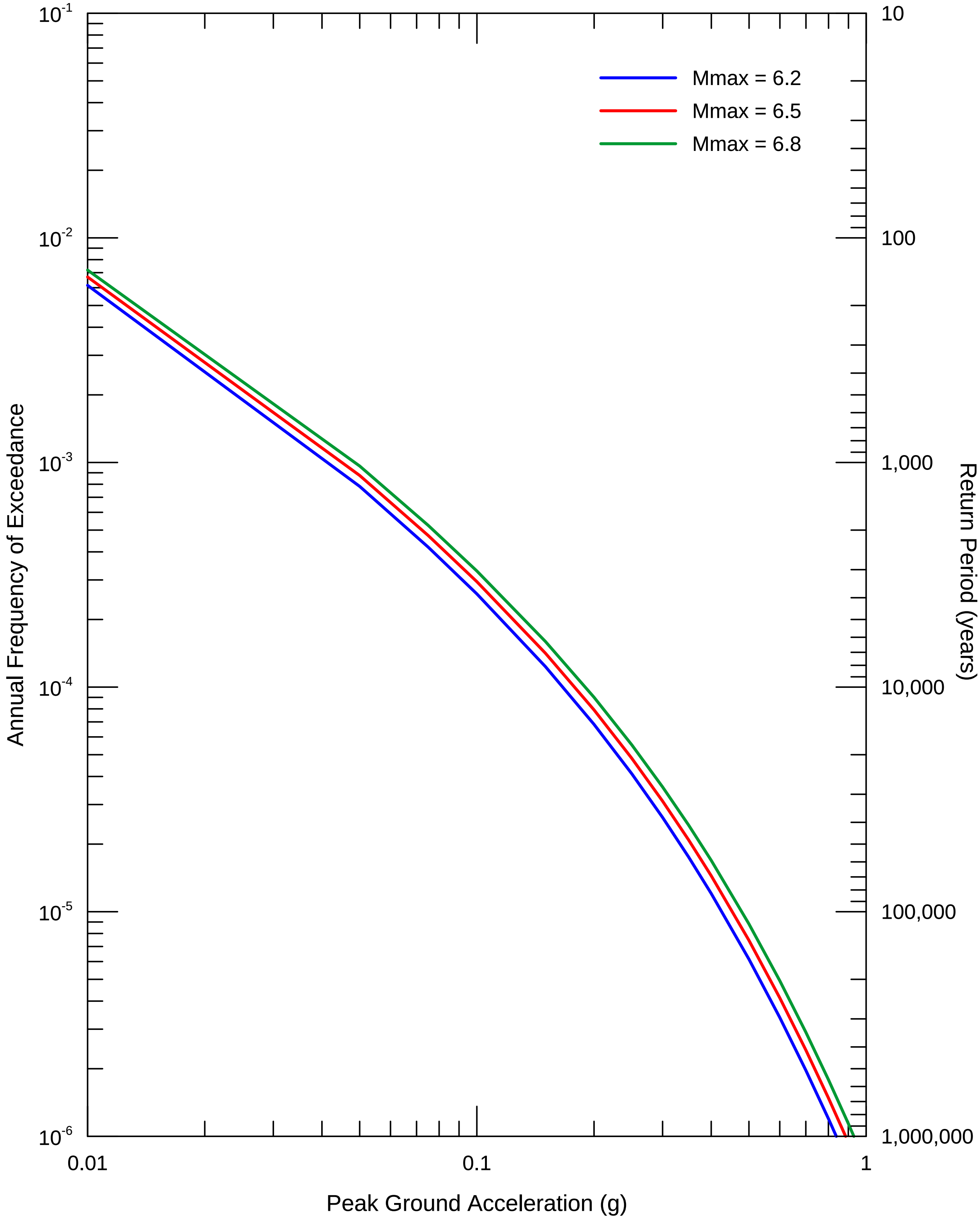

V_S30 = 700 m/s

Hazard Curves shown represent hazard
with end branch weights of 1.0
(e.g. 100% SBR Background Seismicity Mmax = 6.2)

Sensitivity of Mean Peak Horizontal Acceleration Hazard to Mmax for Background Seismicity

RESOLUTION COPPER, SKUNK CAMP TSF SITE

Lettis Consultants International, Inc.

Figure **35**

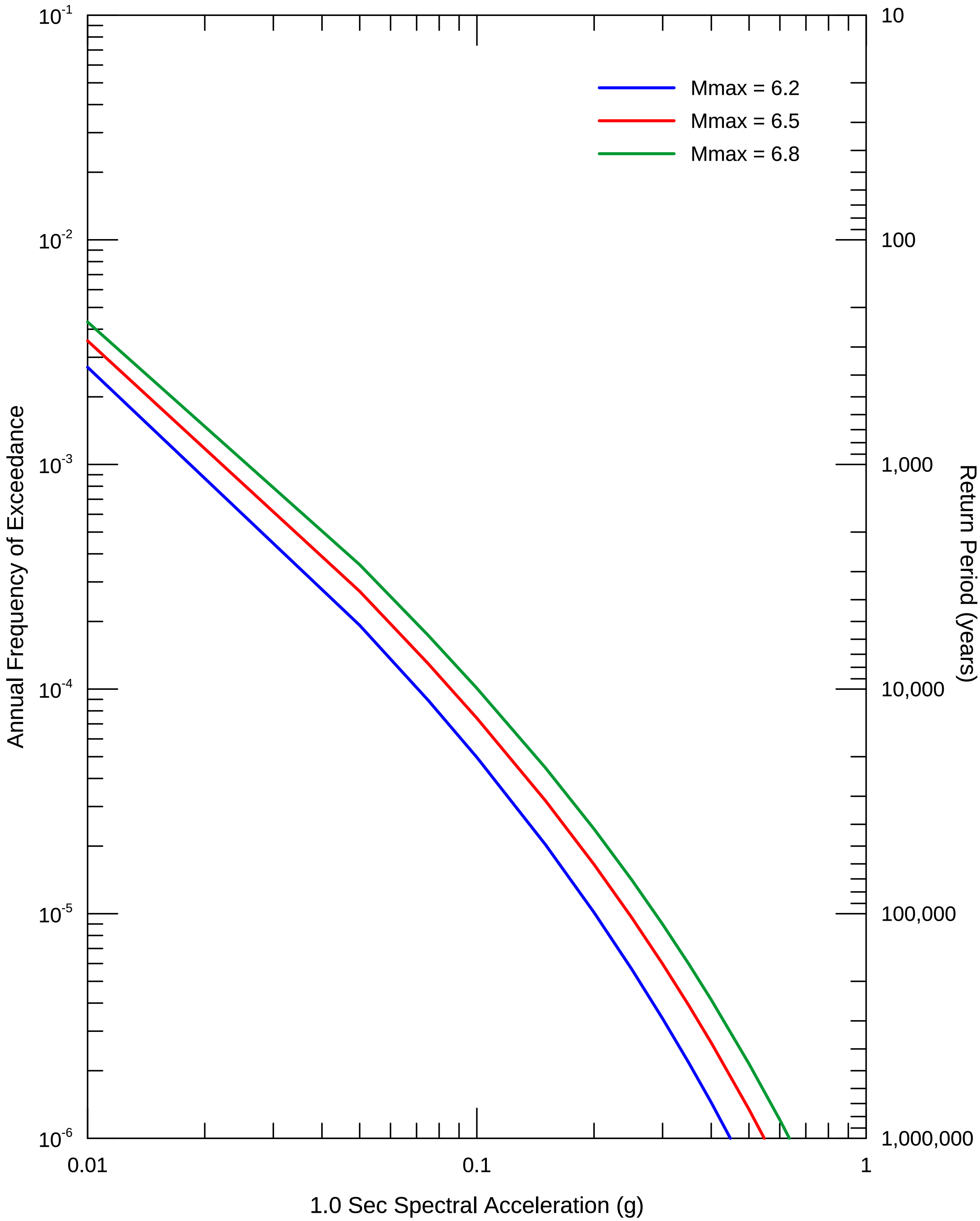

V_S30 = 700 m/s

Hazard Curves shown represent hazard
with end branch weights of 1.0
(e.g. 100% SBR Background Seismicity Mmax = 6.2)

Sensitivity of Mean 1.0 Sec Horizontal Spectral Acceleration Hazard to Mmax for Background Seismicity

RESOLUTION COPPER, SKUNK CAMP TSF SITE

Lettis Consultants International, Inc.

Figure **36**

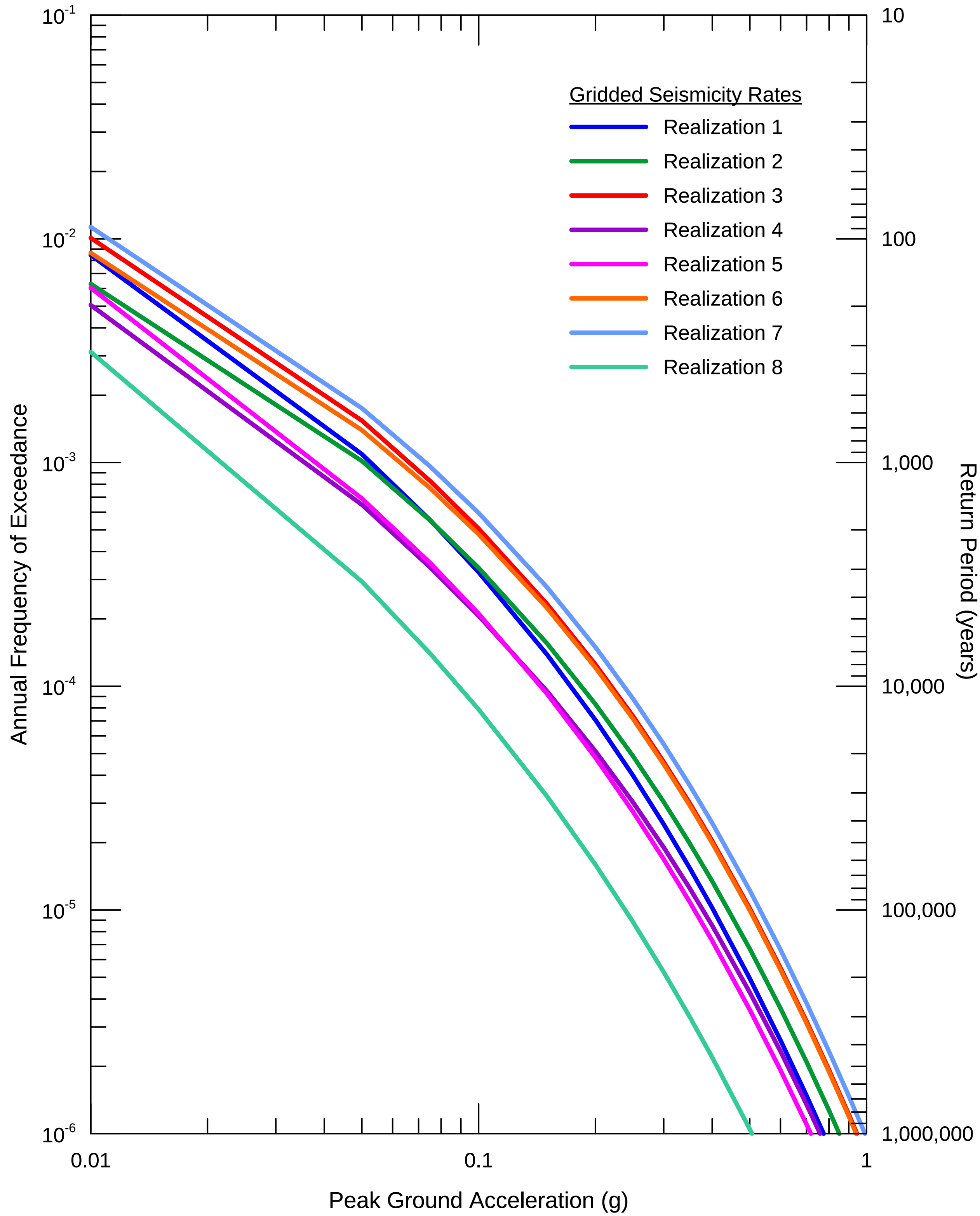

V_S30 = 700 m/s

Hazard Curves shown represent hazard
with end branch weights of 1.0
(e.g. 100% Gridded Seismicity Realization 1)

Sensitivity of Mean Peak Horizontal Acceleration Hazard to Gridded Seismicity Rate Realizations

RESOLUTION COPPER, SKUNK CAMP TSF SITE

Lettis Consultants International, Inc.

Figure **37**

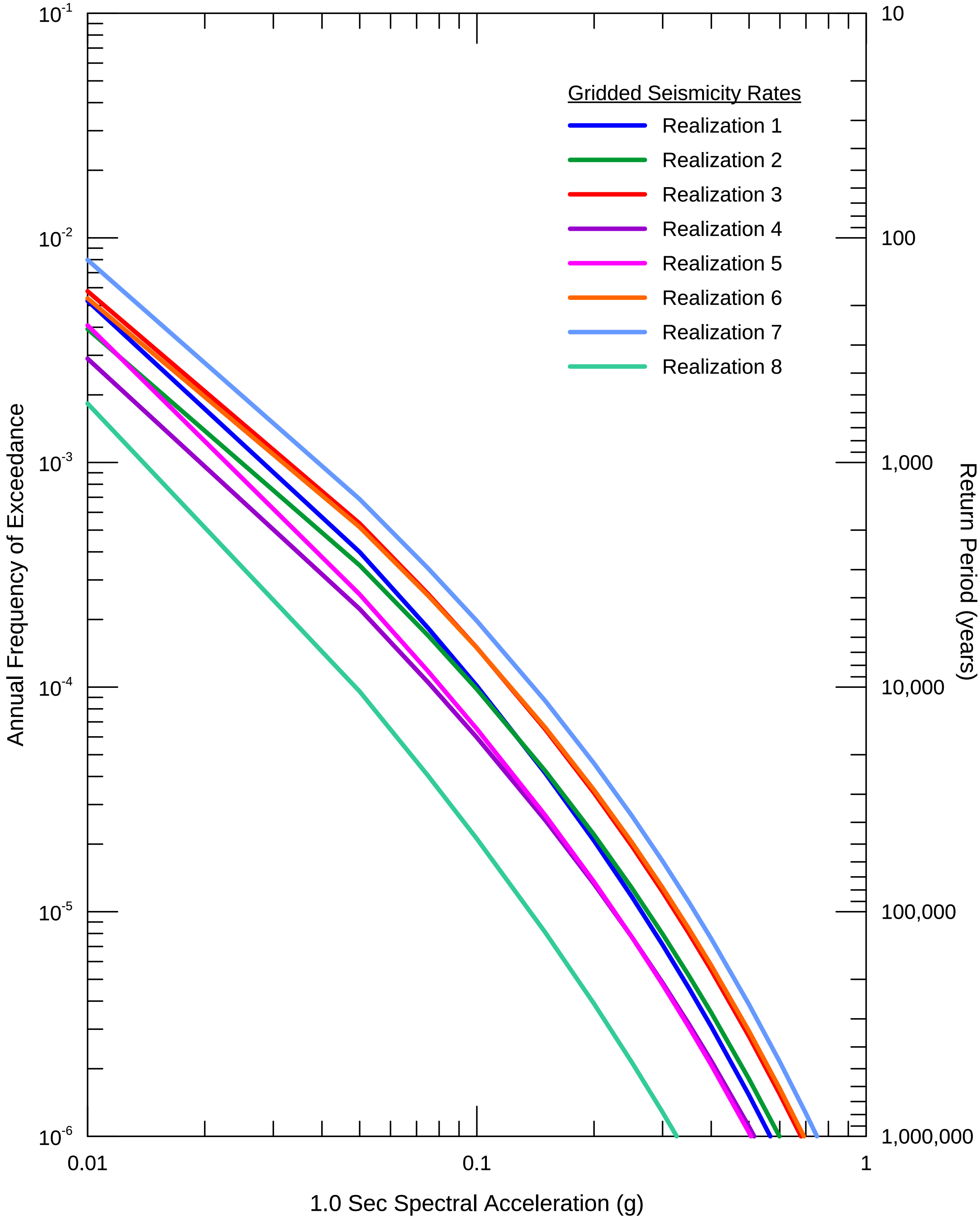

V_S30 = 700 m/s

Hazard Curves shown represent hazard with end branch weights of 1.0 (e.g. 100% Gridded Seismicity Realization 1)

Sensitivity of Mean 1.0 Sec Horizontal Spectral Acceleration Hazard to Gridded Seismicity Rate Realizations

RESOLUTION COPPER, SKUNK CAMP TSF SITE

Lettis Consultants International, Inc. | Figure **38**

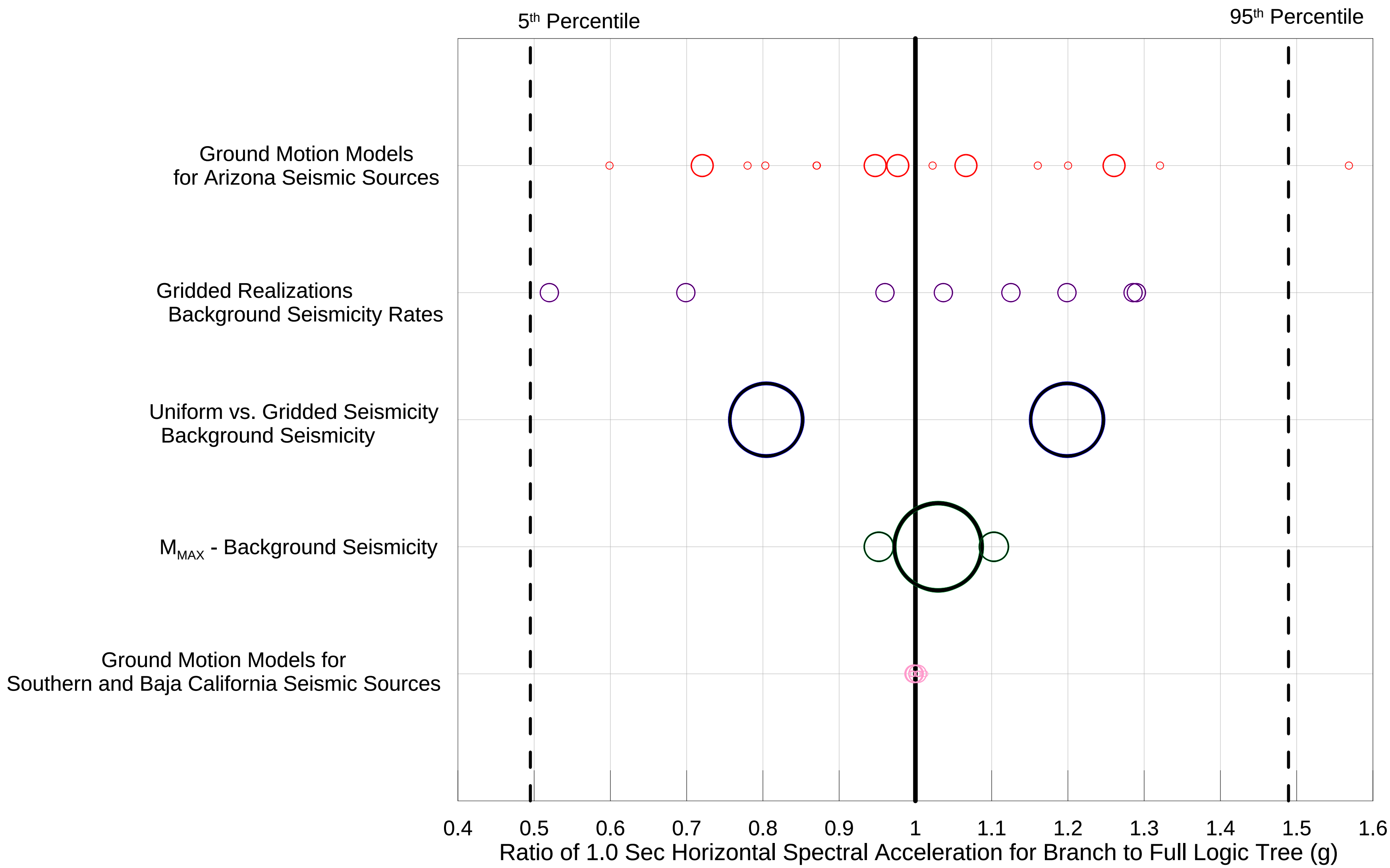

V_S30 = 700 m/sec

Symbol size proportional to logic tree branch weight.

Tornado Plot for Peak Ground Spectral Acceleration at 10,000-Year Return Period

RESOLUTION COPPER, SKUNK CAMP TSF SITE

Lettis Consultants International, Inc. | Figure **39**

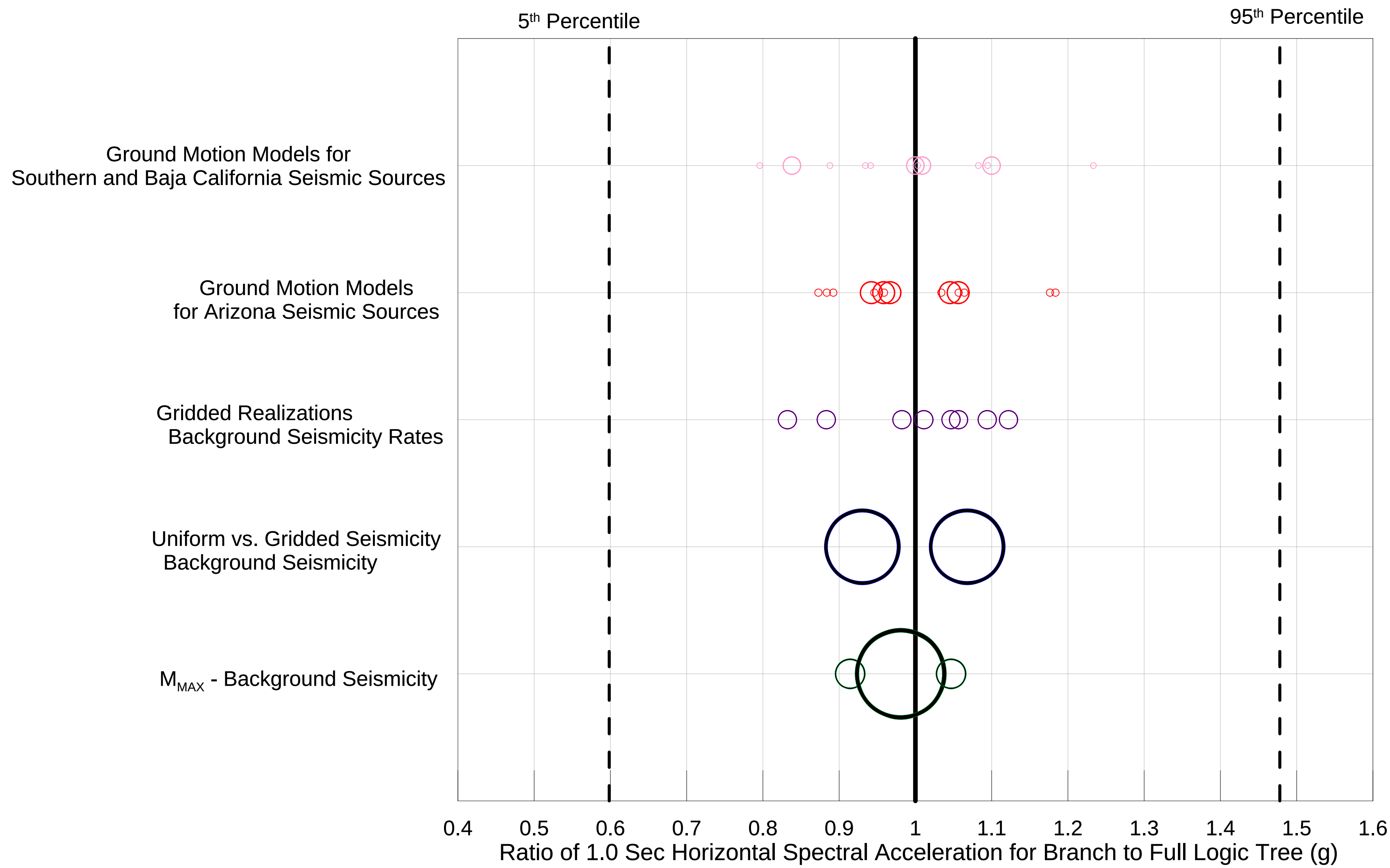

V_S30 = 700 m/sec

Symbol size proportional to logic tree branch weight.

Tornado Plot for 1.0 Sec Horizontal Spectral Acceleration at 10,000-Year Return Period

RESOLUTION COPPER, SKUNK CAMP TSF SITE

Lettis Consultants International, Inc.

Figure **40**

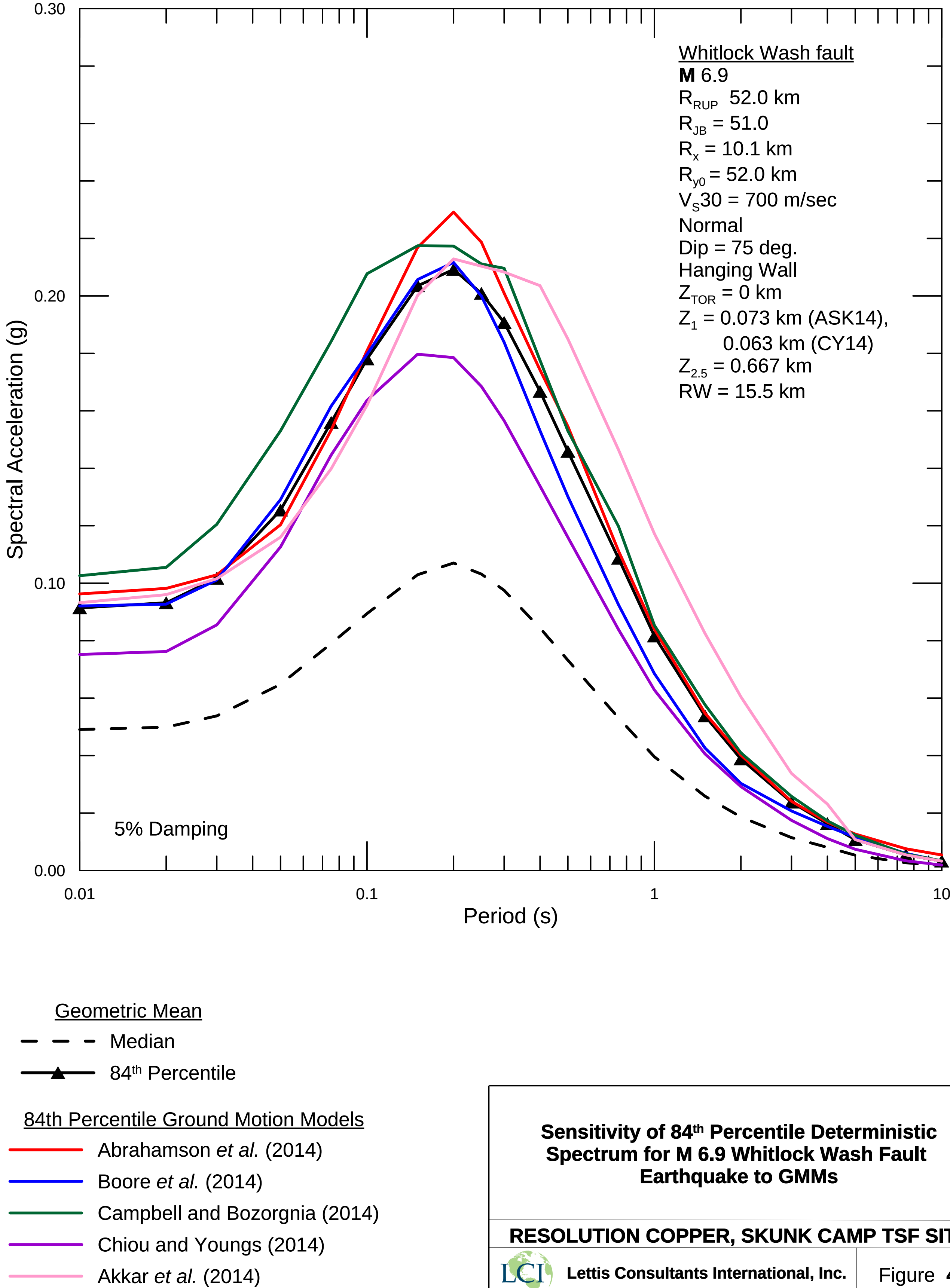

Sensitivity of 84th Percentile Deterministic Spectrum for M 6.9 Whitlock Wash Fault Earthquake to GMMs

RESOLUTION COPPER, SKUNK CAMP TSF SITE

Lettis Consultants International, Inc. | Figure **41**

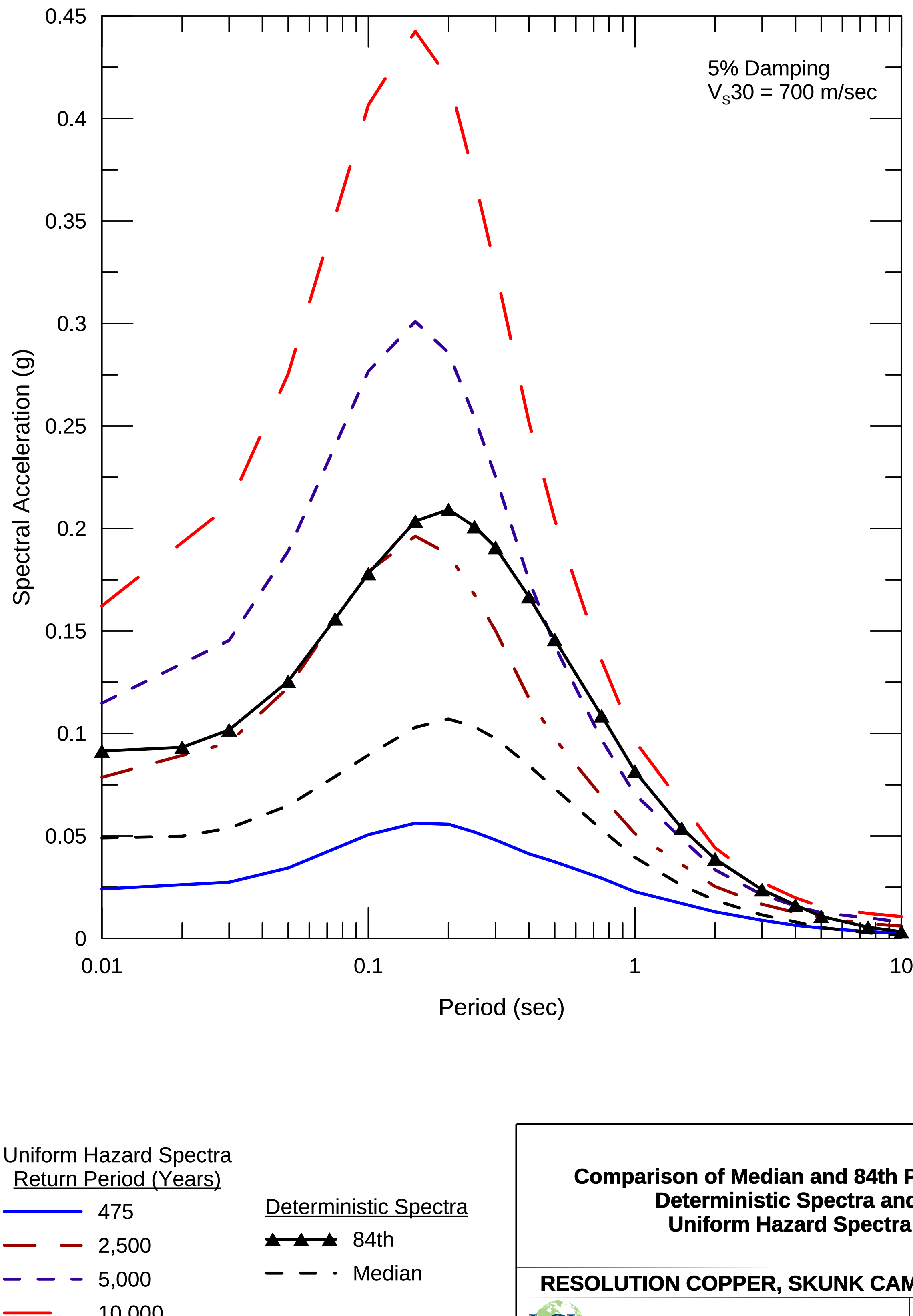

Comparison of Median and 84th Percentile Deterministic Spectra and Uniform Hazard Spectra

RESOLUTION COPPER, SKUNK CAMP TSF SITE

Lettis Consultants International, Inc.

Figure **42**

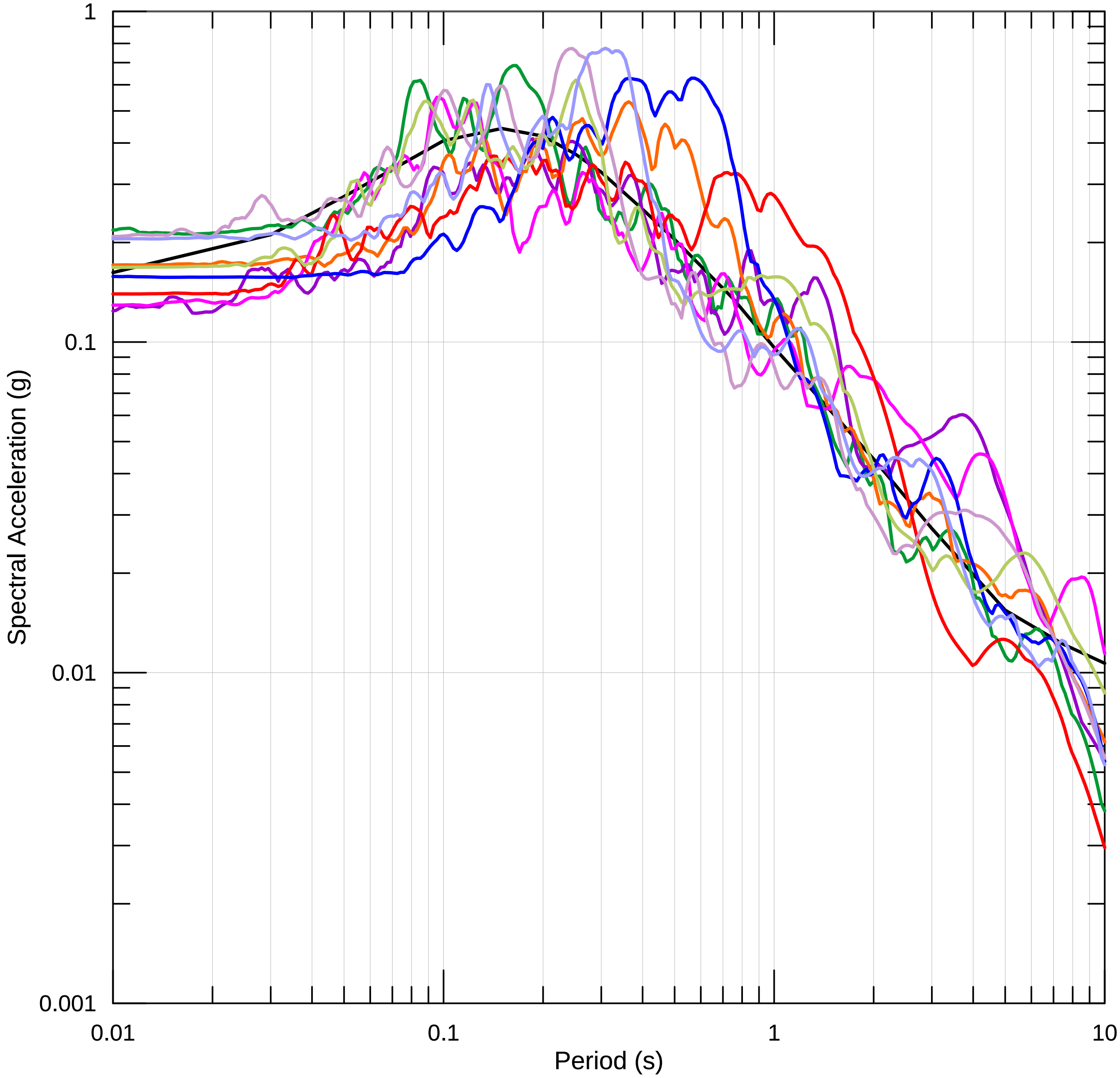

10,000-Year Return Period UHS Target Spectrum and Scaled Seed Time Histories Response Spectra

RESOLUTION COPPER, SKUNK CAMP TSF SITE

LCI **Lettis Consultants International, Inc.**

Figure **43**

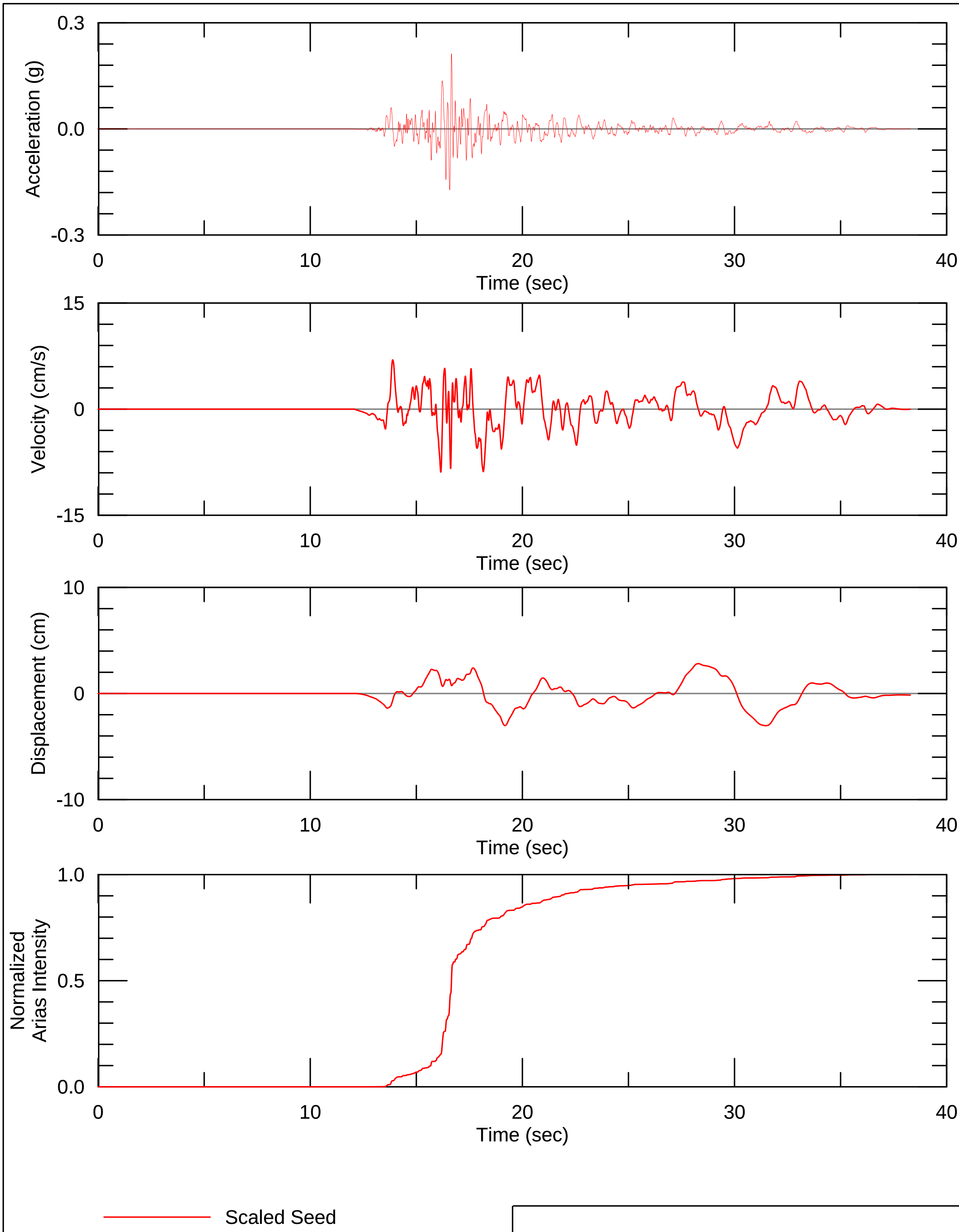

Seed Time History,
1966 M 6.2 Parkfield - Cholame-Shandone Array #8
(320), RSN 31

RESOLUTION COPPER, SKUNK CAMP TSF SITE

Lettis Consultants International, Inc. | Figure **44**

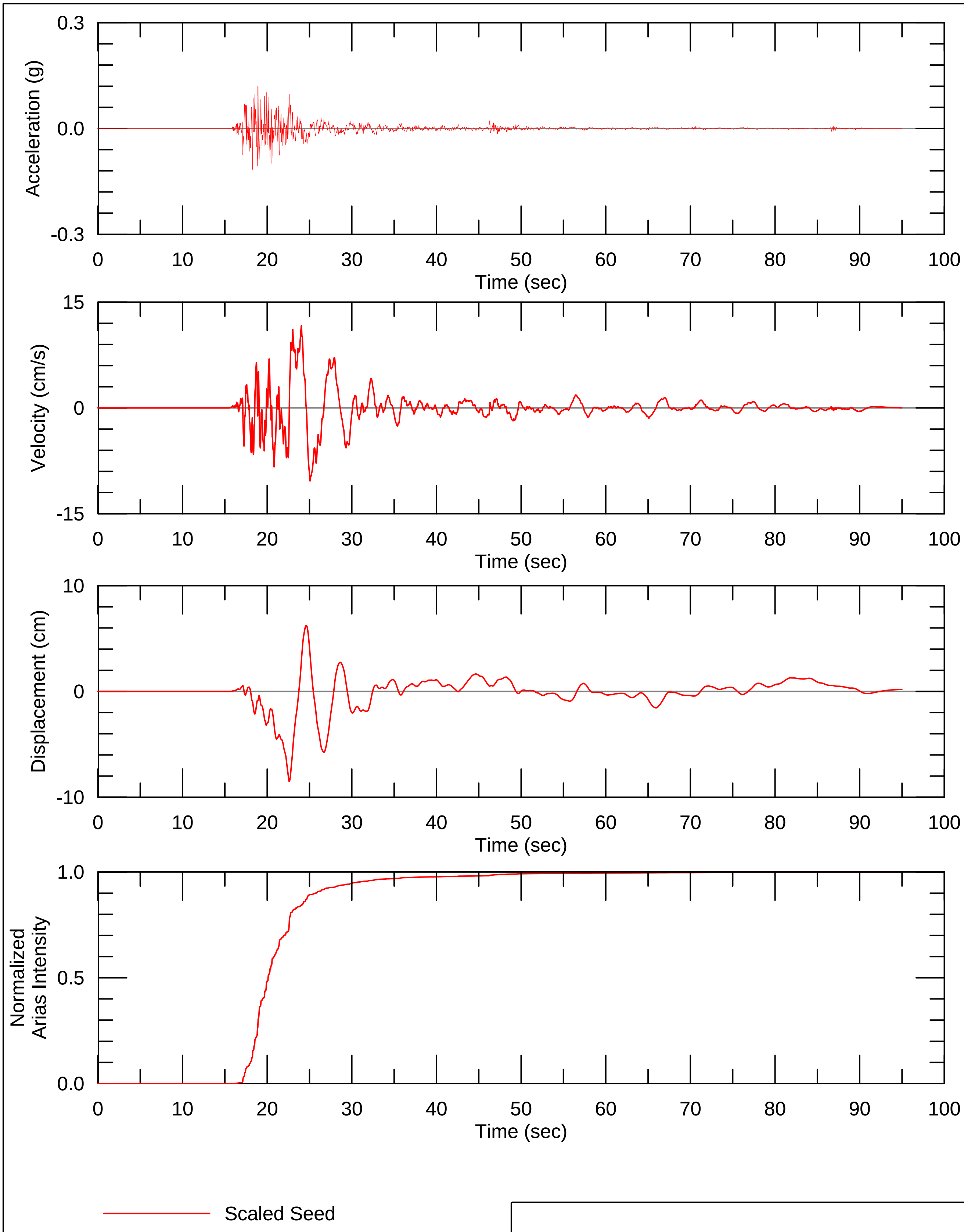

Seed Time History,
1971 M 6.6 San Fernando - LA - Hollywood Stor FF (90), RSN 68

RESOLUTION COPPER, SKUNK CAMP TSF SITE

Lettis Consultants International, Inc. Figure **45**

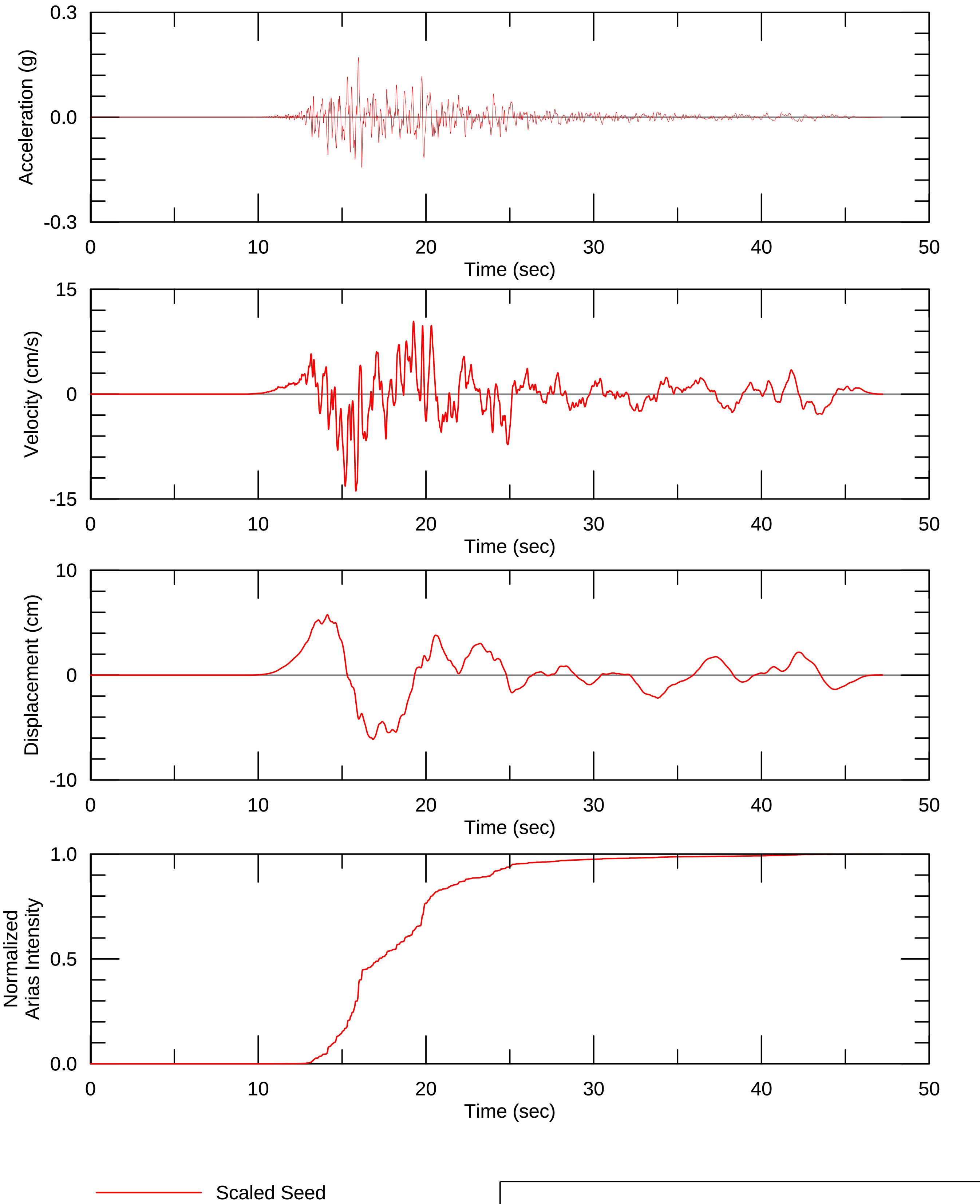

Seed Time History,
1979 M 6.5 Imperial Valley-06 - Calexico Fire Station (225), RSN 162

RESOLUTION COPPER, SKUNK CAMP TSF SITE

Lettis Consultants International, Inc. Figure **46**

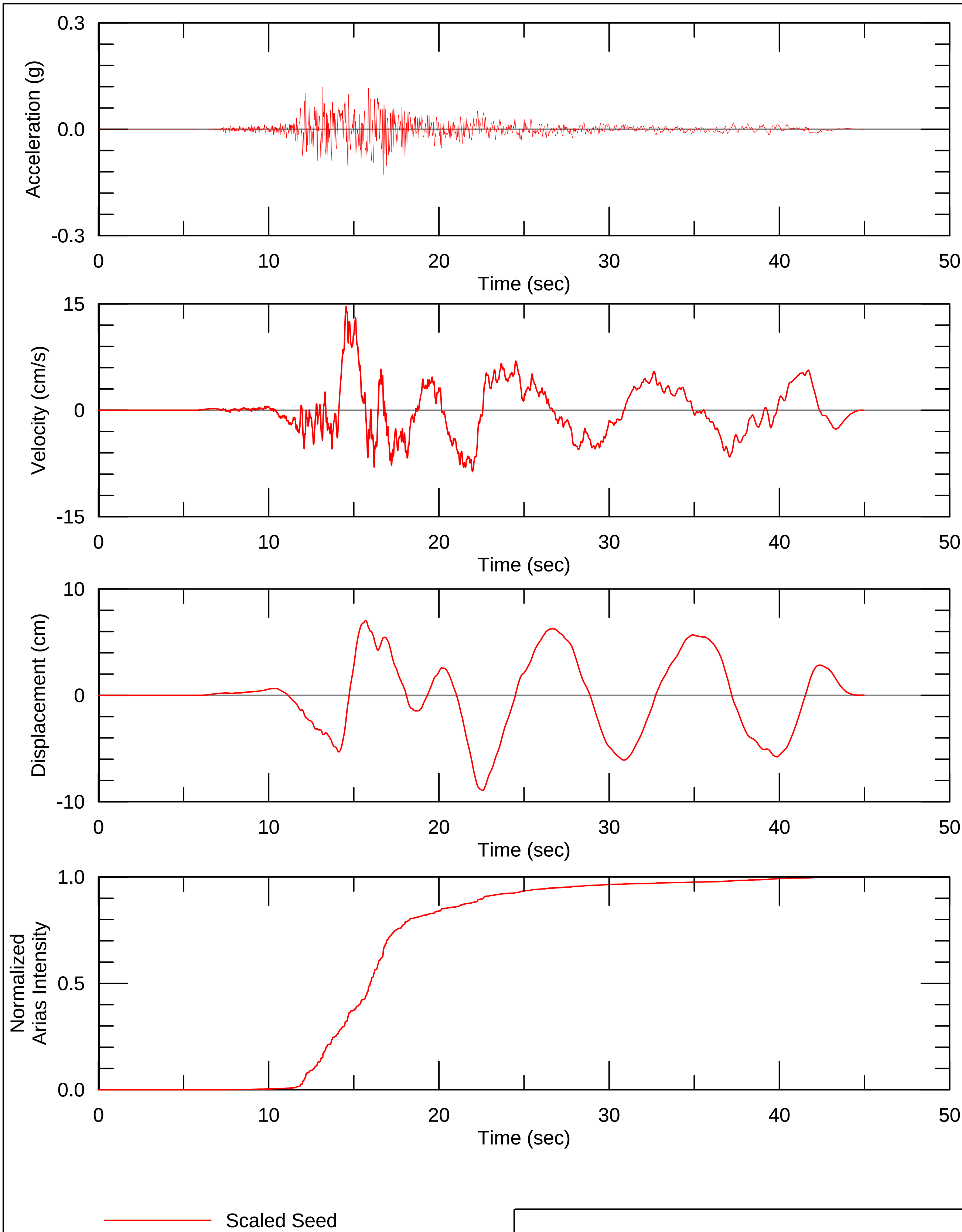

Seed Time History,
1979 M 6.5 Imperial Valley-06 - El Centro Array #1
(140), RSN 172

RESOLUTION COPPER, SKUNK CAMP TSF SITE

LCI **Lettis Consultants International, Inc.** Figure **47**

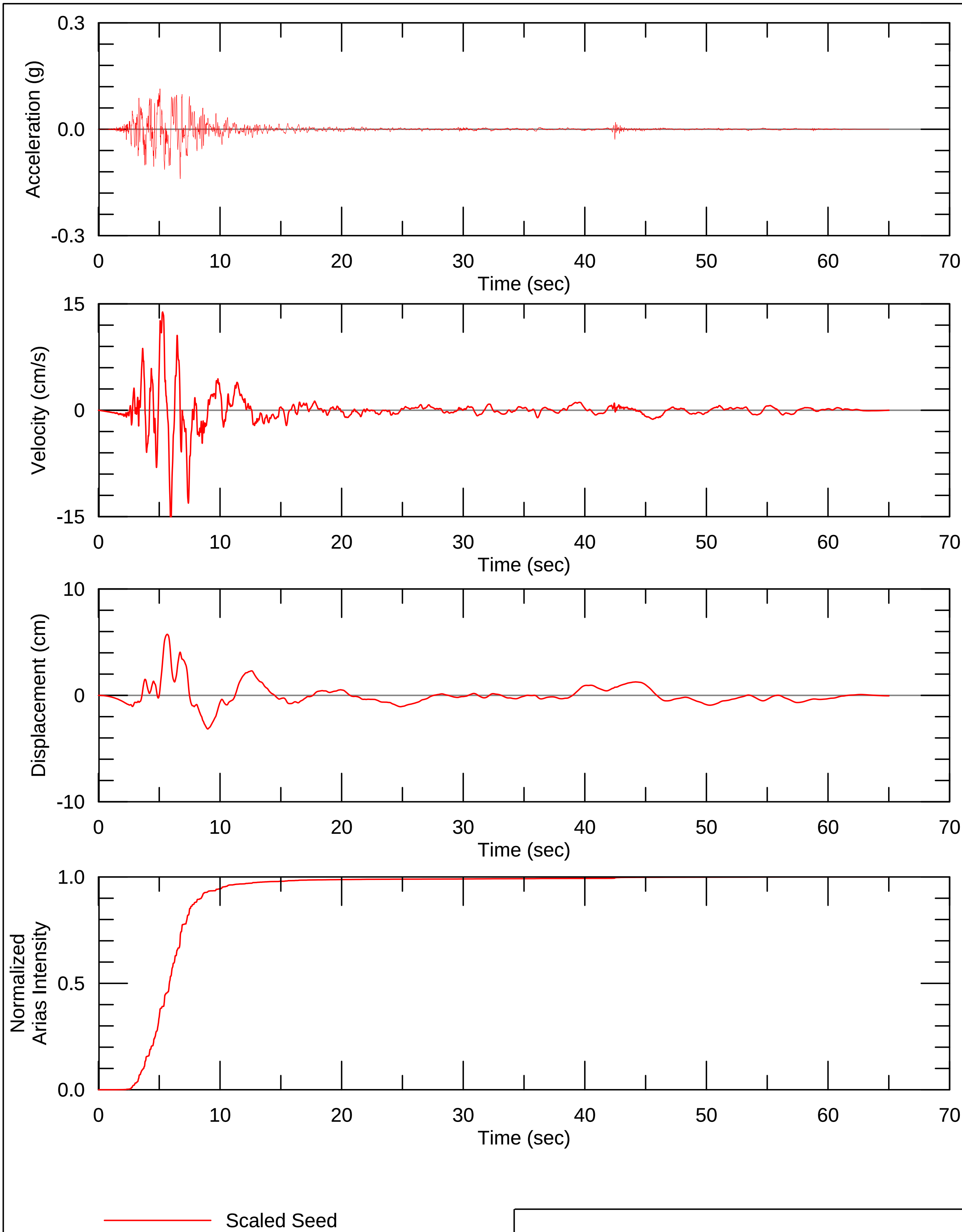

Seed Time History,
1981 M 5.9 Westmorland - Westmorland Fire Station (90), RSN 319

RESOLUTION COPPER, SKUNK CAMP TSF SITE

Lettis Consultants International, Inc.

Figure **48**

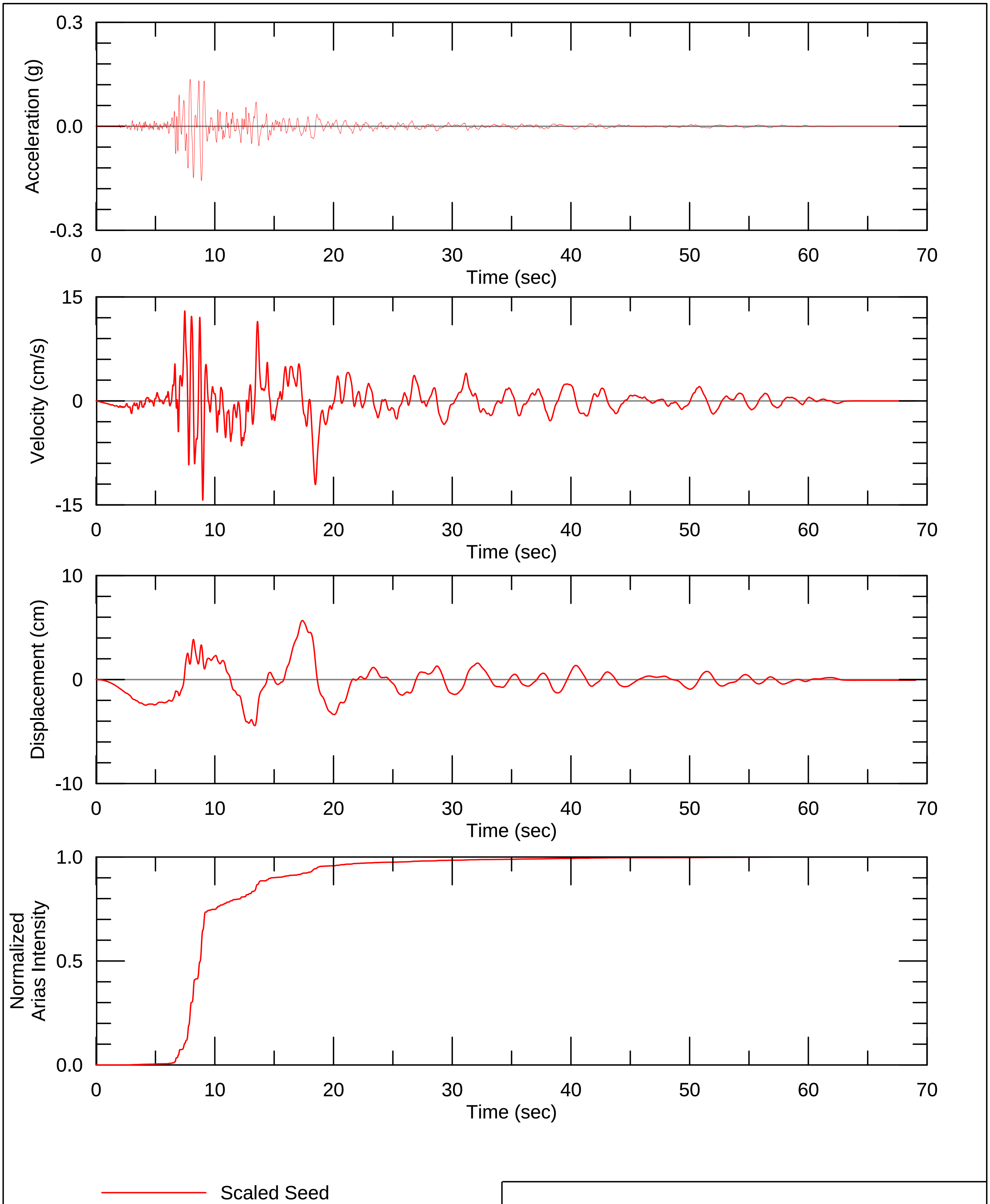

Seed Time History,
1983 M 6.3 Coalinga-01 - Cantua Creek School (360), RSN 322

RESOLUTION COPPER, SKUNK CAMP TSF SITE

Lettis Consultants International, Inc. Figure **49**

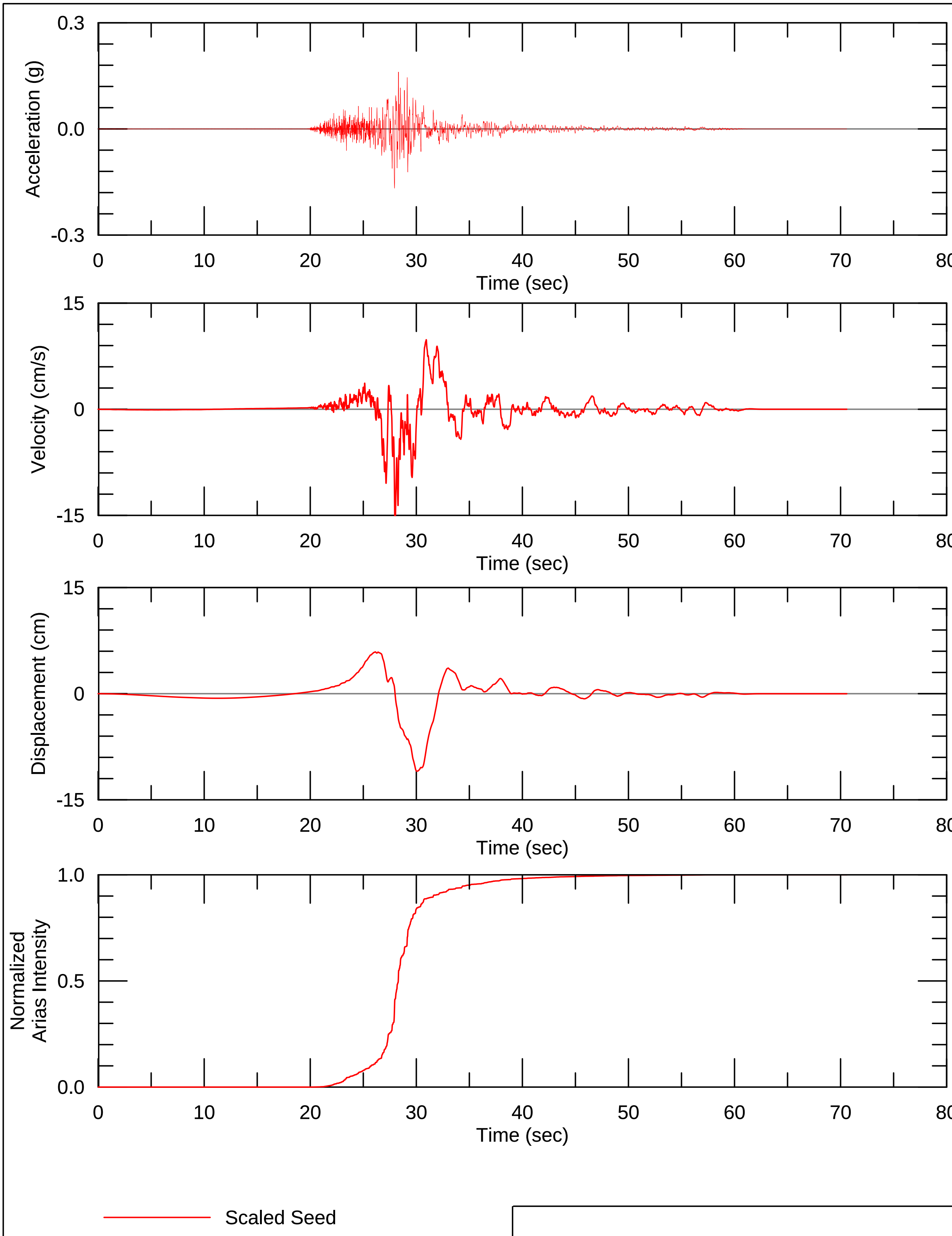

Seed Time History,
1999 Chi-Chi, Taiwan-04 - TTN051 (N51E),
RSN 2935

RESOLUTION COPPER, SKUNK CAMP TSF SITE

LCI **Lettis Consultants International, Inc.** Figure **50**

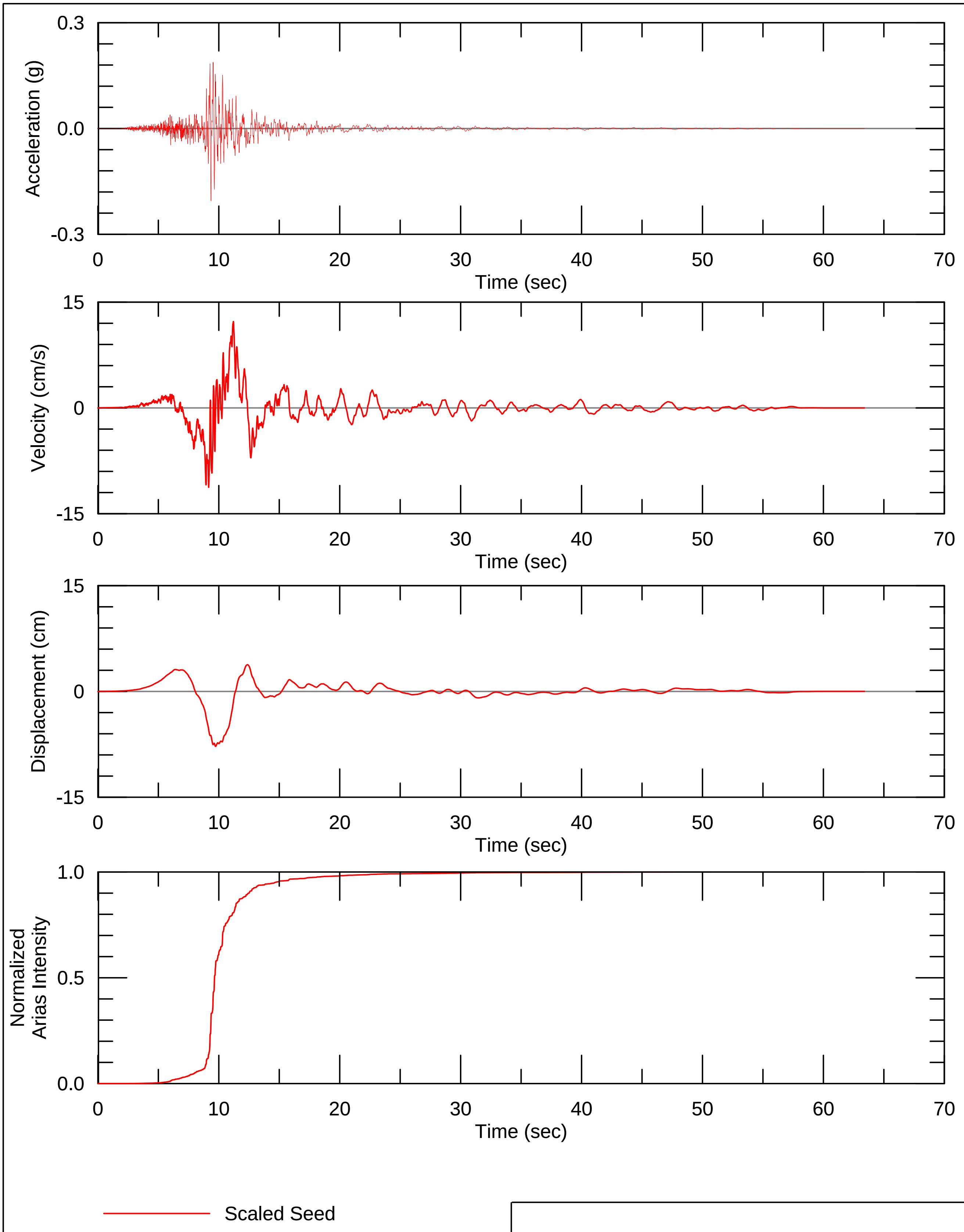

Seed Time History,
2009 L'Aquila, Italy - Celano (E),
RSN 4472

RESOLUTION COPPER, SKUNK CAMP TSF SITE

Lettis Consultants International, Inc. | Figure **51**

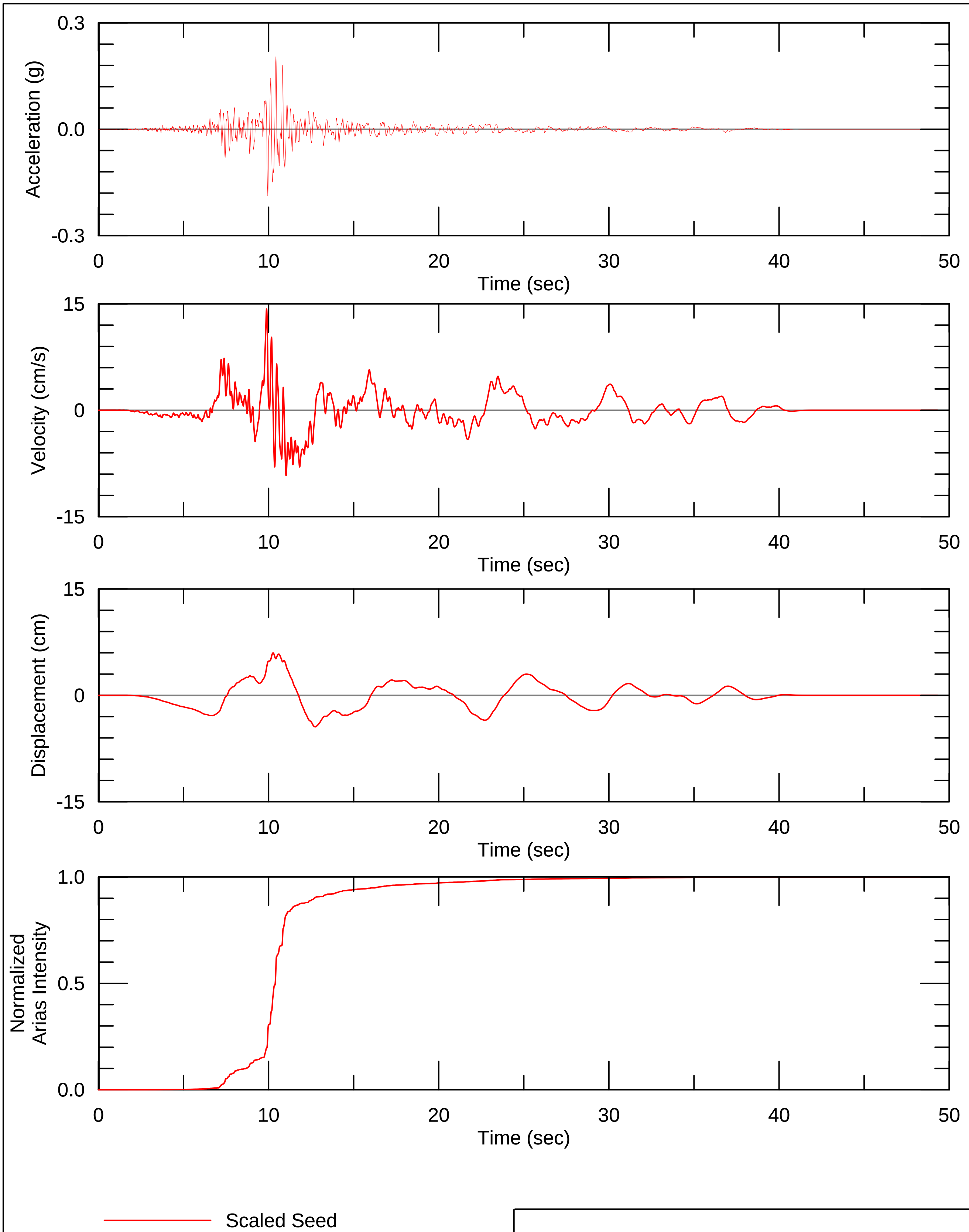

Seed Time History, 2011 M 6.2 Christchurch, New Zealand - SWNC (N24E), RSN 8136

RESOLUTION COPPER, SKUNK CAMP TSF SITE

Lettis Consultants International, Inc. | Figure **52**

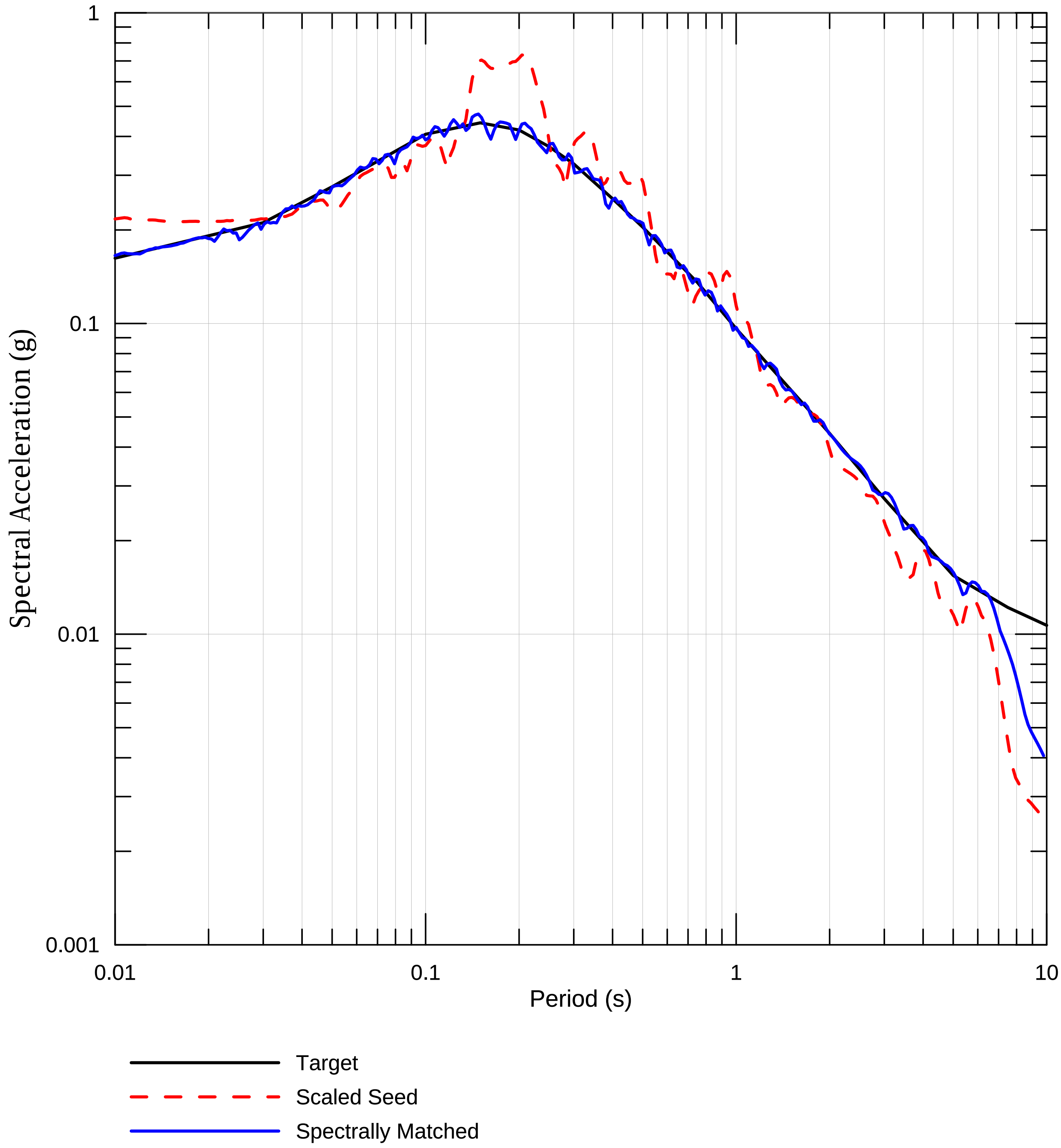

Response Spectra for Time History Spectrally Matched to 10,000-Year Return Period UHS, 1966 M 6.2 Parkfield - Cholame-Shandone Array #8 (320), RSN 31

RESOLUTION COPPER, SKUNK CAMP TSF SITE

Lettis Consultants International, Inc. Figure **53**

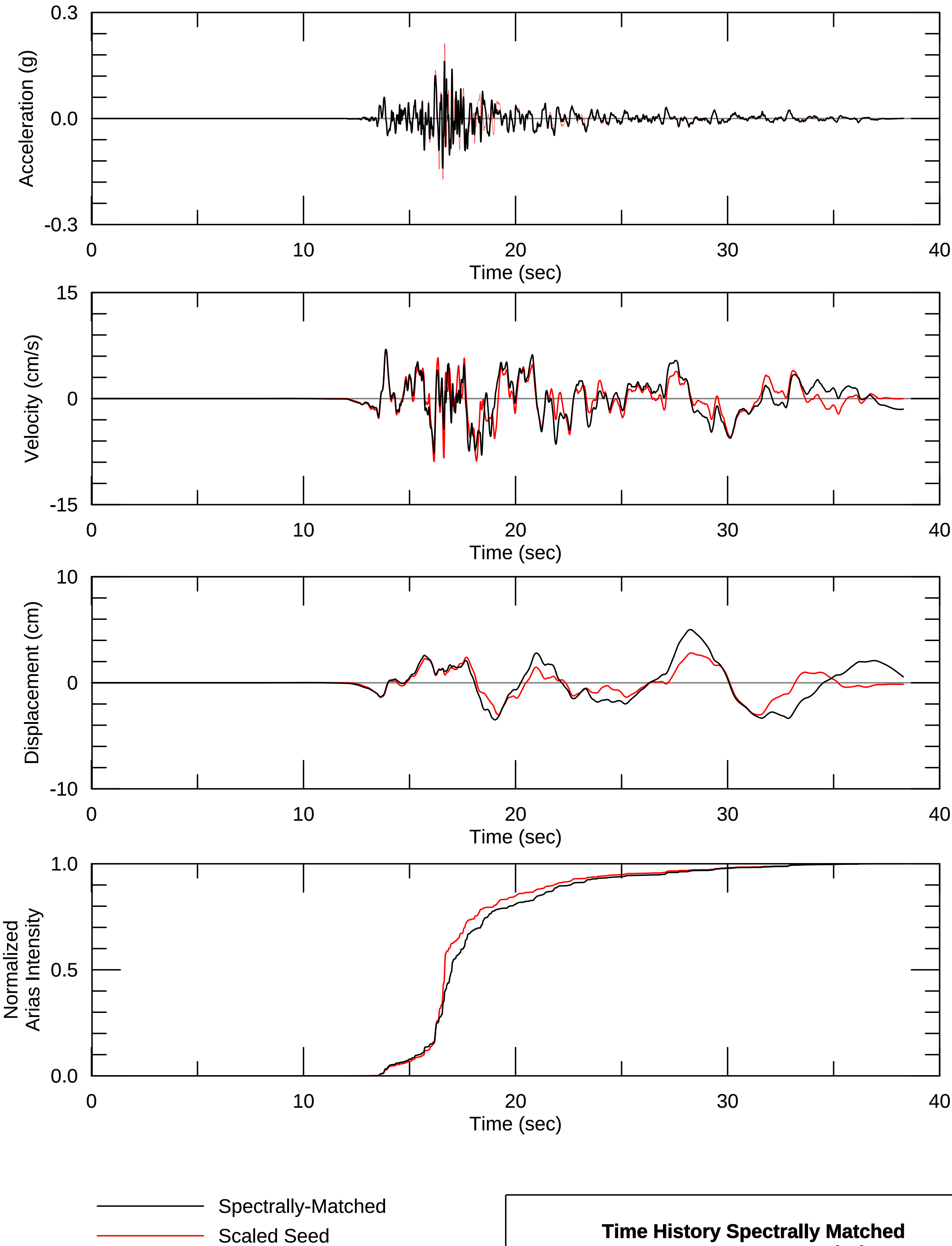

Time History Spectrally Matched to 10,000-Year Return Period UHS, 1966 M 6.2 Parkfield - Cholame-Shandone Array #8 (320), RSN 31

RESOLUTION COPPER, SKUNK CAMP TSF SITE

Lettis Consultants International, Inc. | Figure **54**

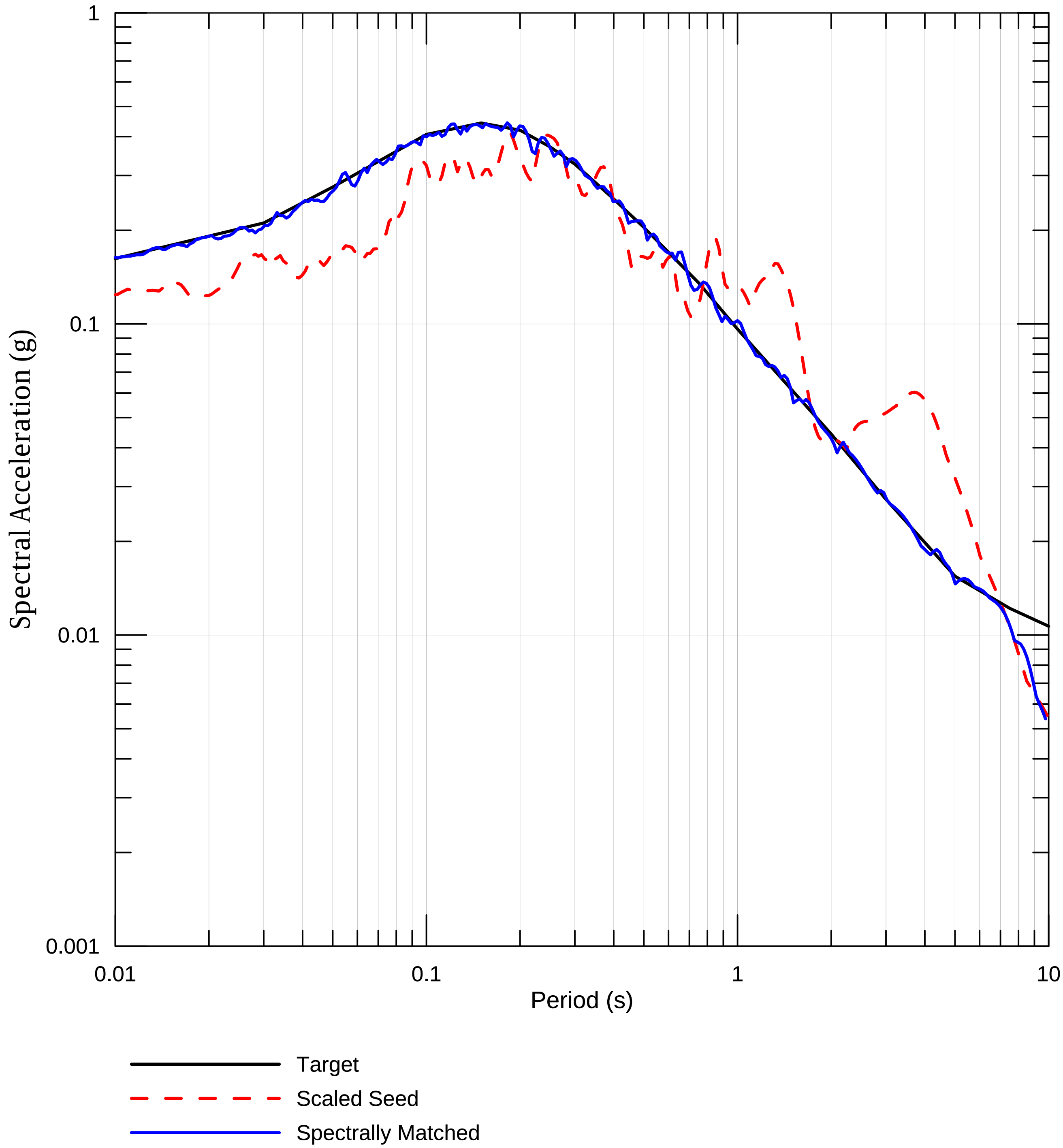

Response Spectra for Time History Spectrally Matched to 10,000-Year Return Period UHS, 1971 M 6.6 San Fernando - LA - Hollywood Stor FF (90), RSN 68

RESOLUTION COPPER, SKUNK CAMP TSF SITE

Lettis Consultants International, Inc.

Figure **55**

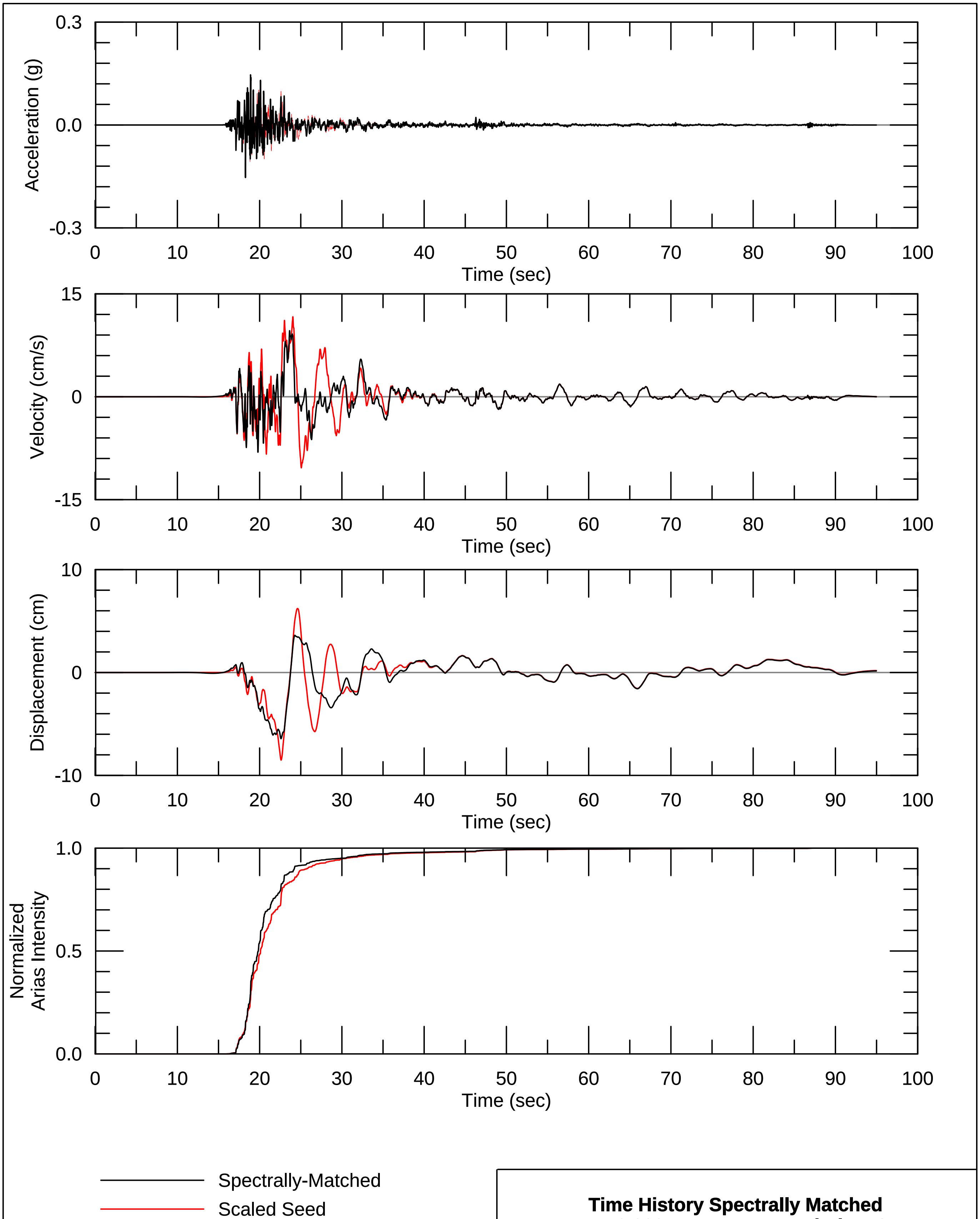

Time History Spectrally Matched to 10,000-Year Return Period UHS, 1971 M 6.6 San Fernando - LA - Hollywood Stor FF (90), RSN 68

RESOLUTION COPPER, SKUNK CAMP TSF SITE

Lettis Consultants International, Inc. | Figure **56**

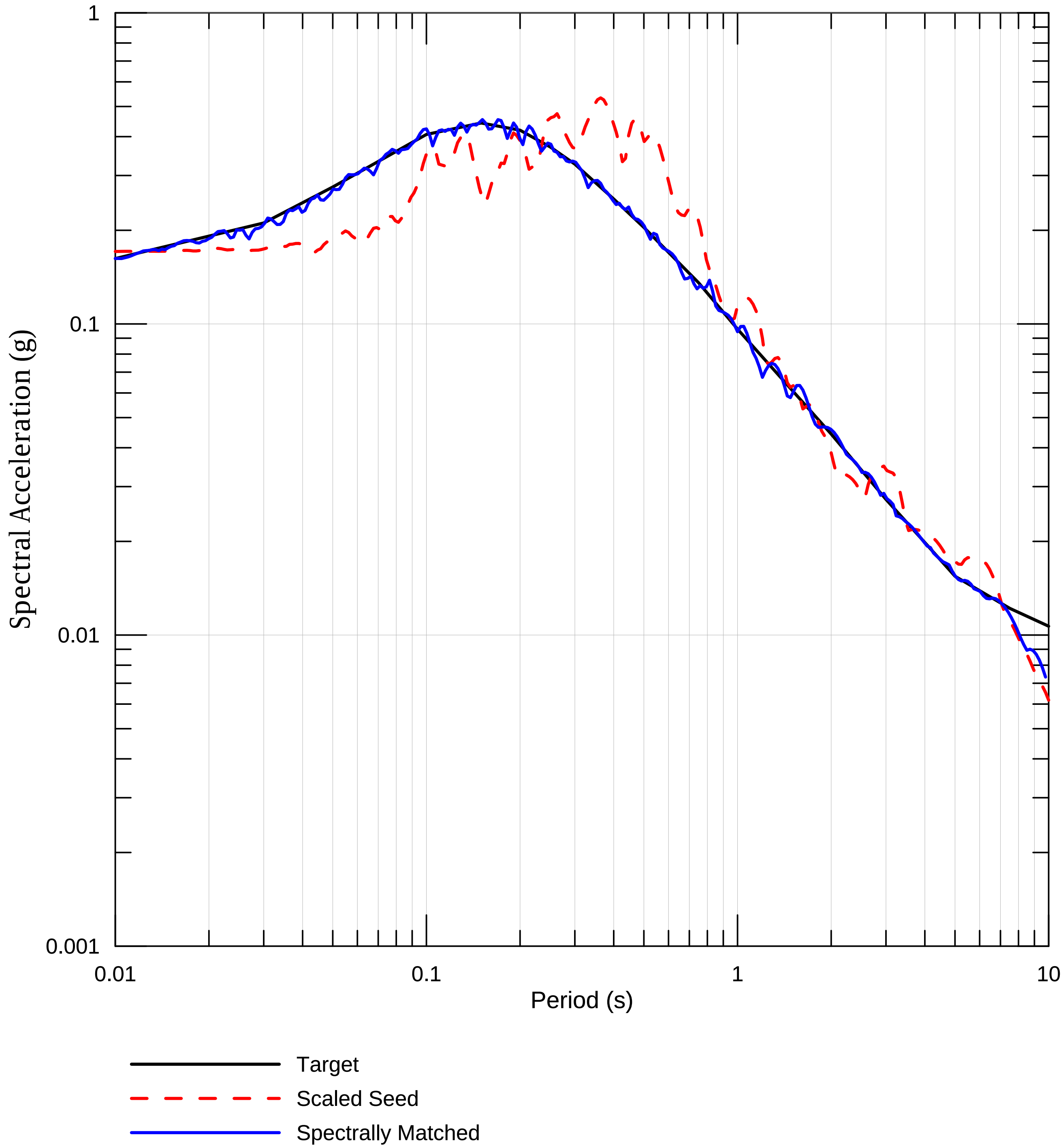

Response Spectra for Time History Spectrally Matched to 10,000-Year Return Period UHS, 1979 M 6.5 Imperial Valley-06 - Calexico Fire Station (225), RSN 162

RESOLUTION COPPER, SKUNK CAMP TSF SITE

LCI **Lettis Consultants International, Inc.** Figure **57**

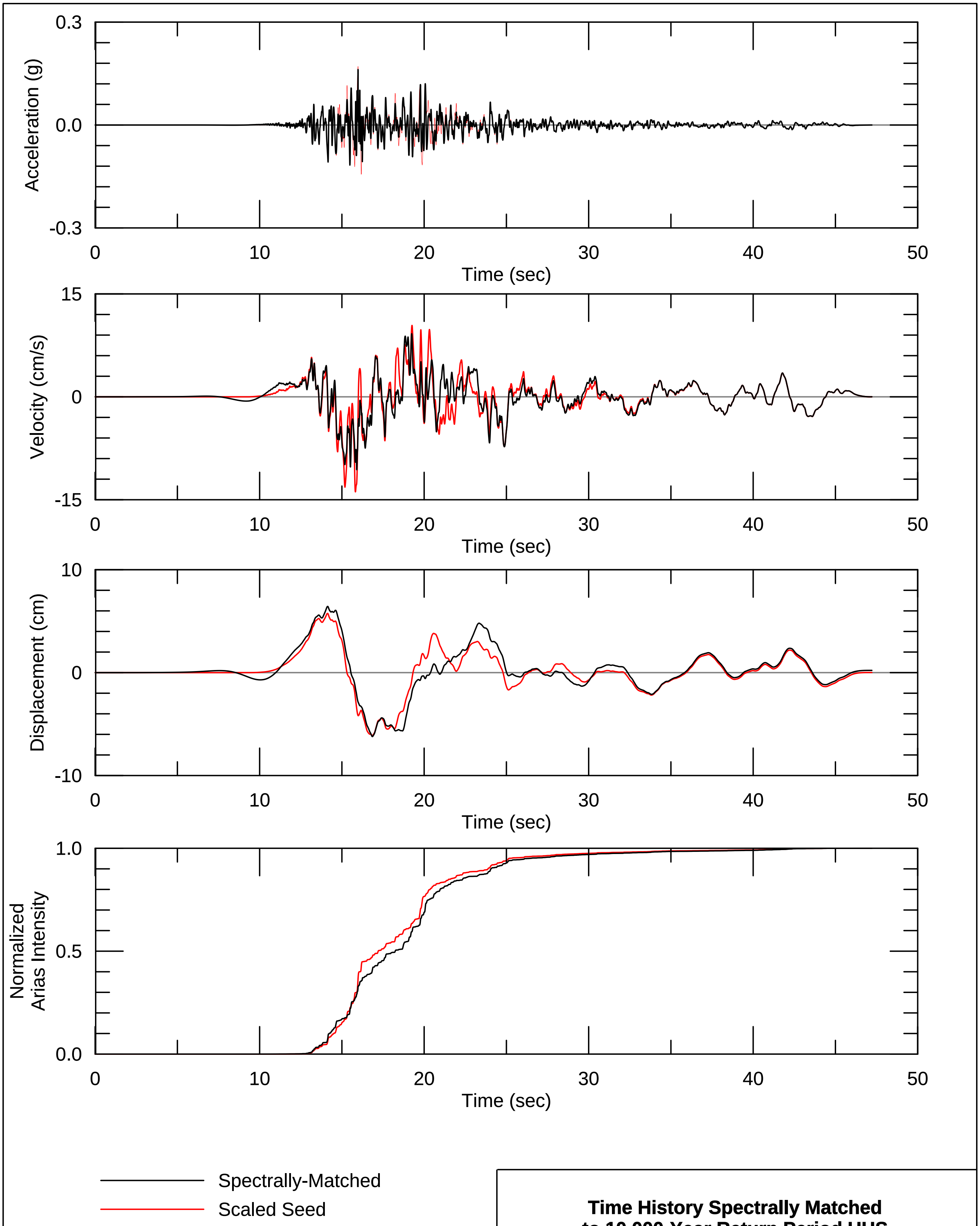

Time History Spectrally Matched to 10,000-Year Return Period UHS, 1979 M 6.5 Imperial Valley-06 - Calexico Fire Station (225), RSN 162

RESOLUTION COPPER, SKUNK CAMP TSF SITE

Lettis Consultants International, Inc. Figure **58**

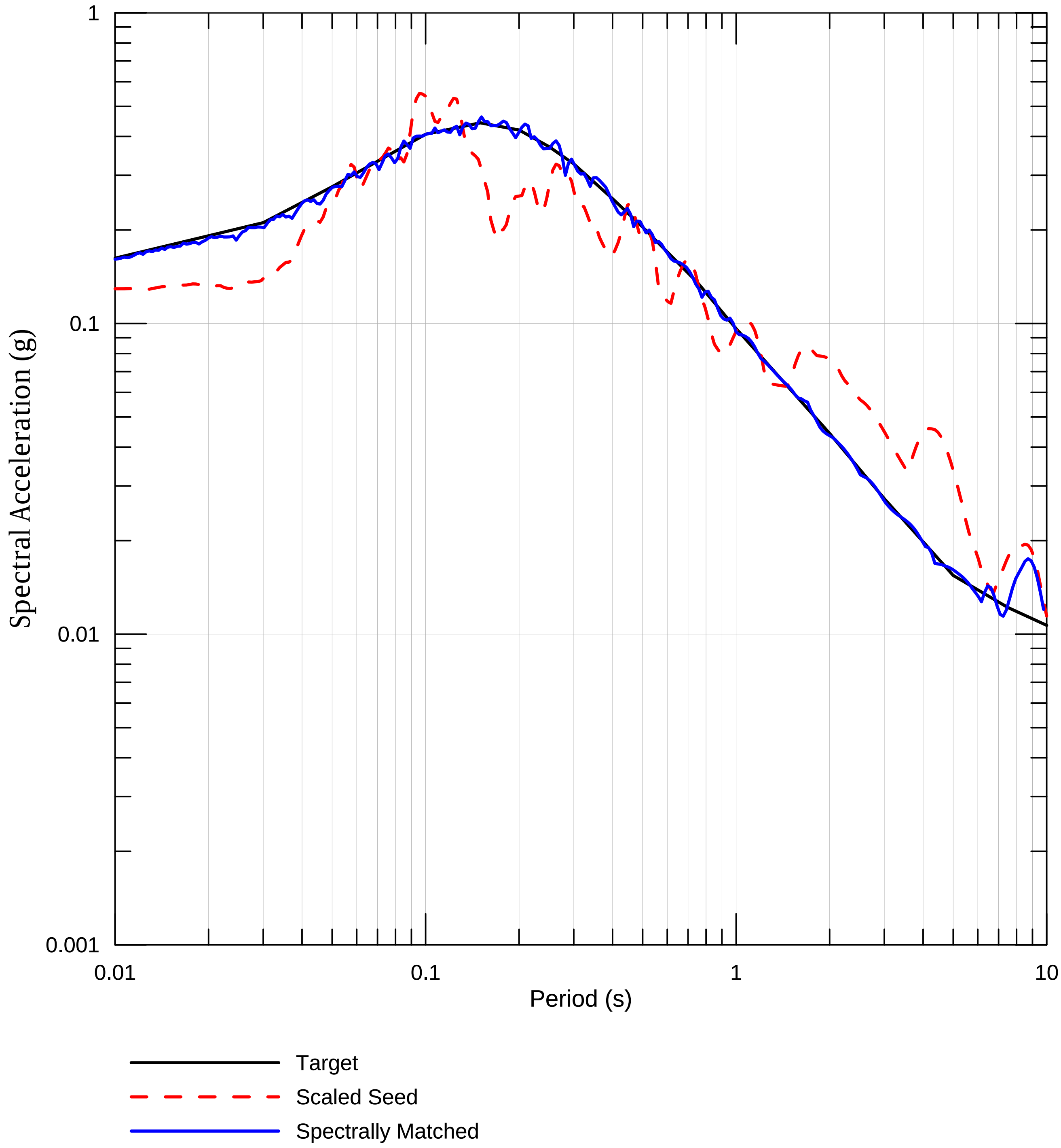

Response Spectra for Time History Spectrally Matched to 10,000-Year Return Period UHS, 1979 M 6.5 Imperial Valley-06 - El Centro Array #1 (140), RSN 172

RESOLUTION COPPER, SKUNK CAMP TSF SITE

Lettis Consultants International, Inc.

Figure **59**

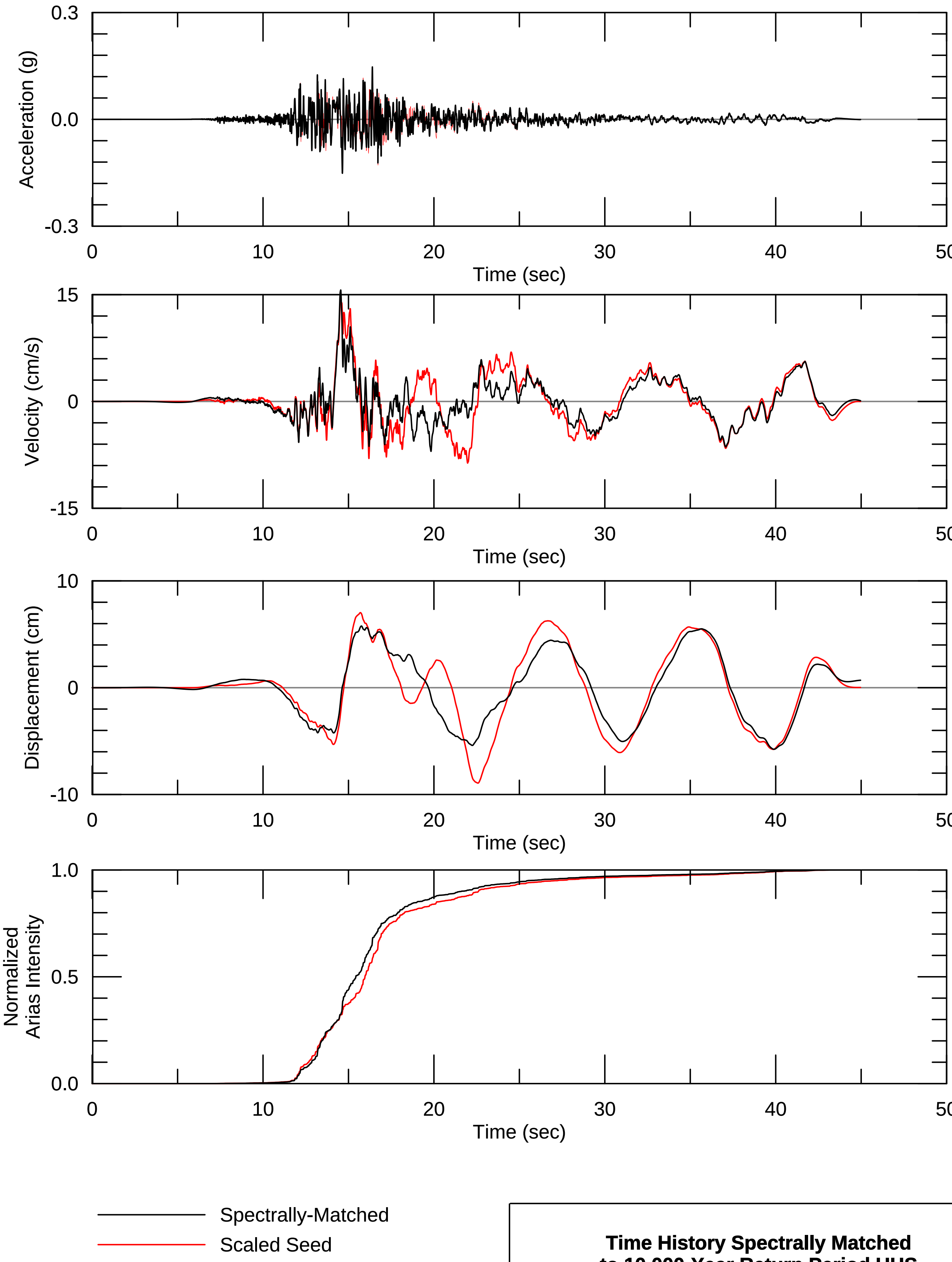

Time History Spectrally Matched to 10,000-Year Return Period UHS, 1979 M 6.5 Imperial Valley-06 - El Centro Array #1 (140), RSN 172

RESOLUTION COPPER, SKUNK CAMP TSF SITE

Lettis Consultants International, Inc. | Figure **60**

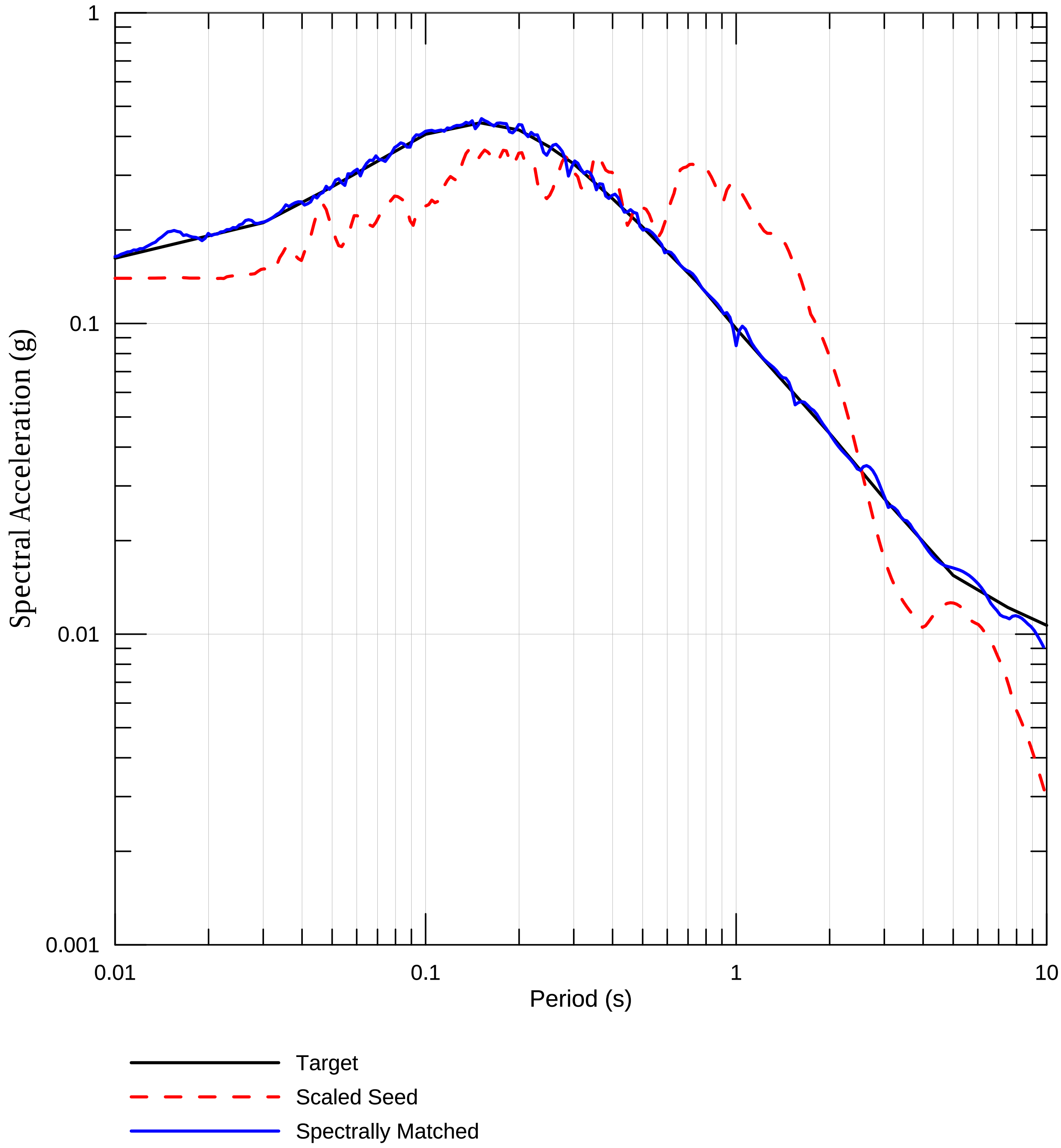

Response Spectra for Time History Spectrally Matched to 10,000-Year Return Period UHS, 1981 M 5.9 Westmorland - Westmorland Fire Station (90), RSN 319

RESOLUTION COPPER, SKUNK CAMP TSF SITE

Lettis Consultants International, Inc. Figure **61**

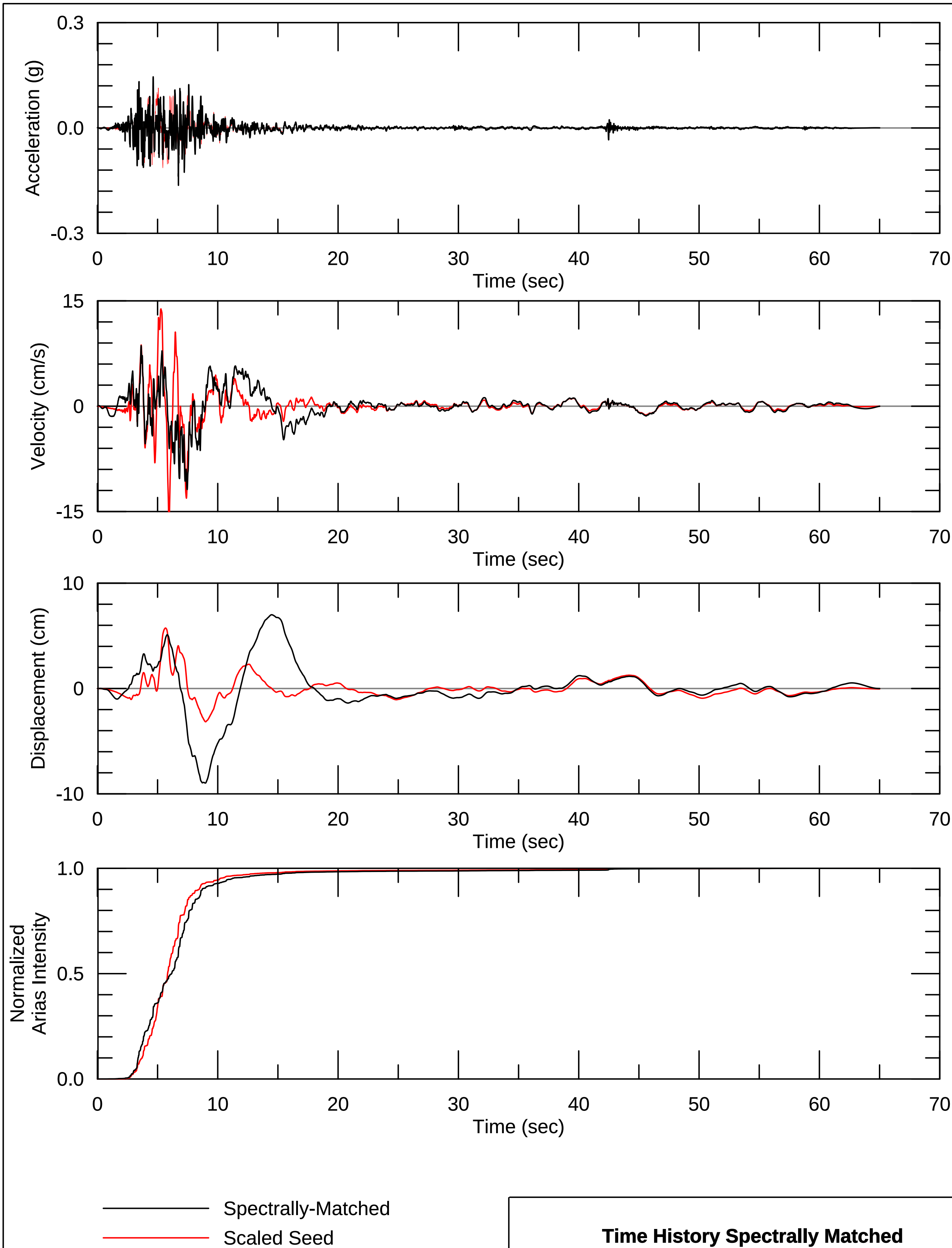

Time History Spectrally Matched to 10,000-Year Return Period UHS, 1981 M 5.9 Westmorland - Westmorland Fire Station (90), RSN 319

RESOLUTION COPPER, SKUNK CAMP TSF SITE

Lettis Consultants International, Inc. | Figure **62**

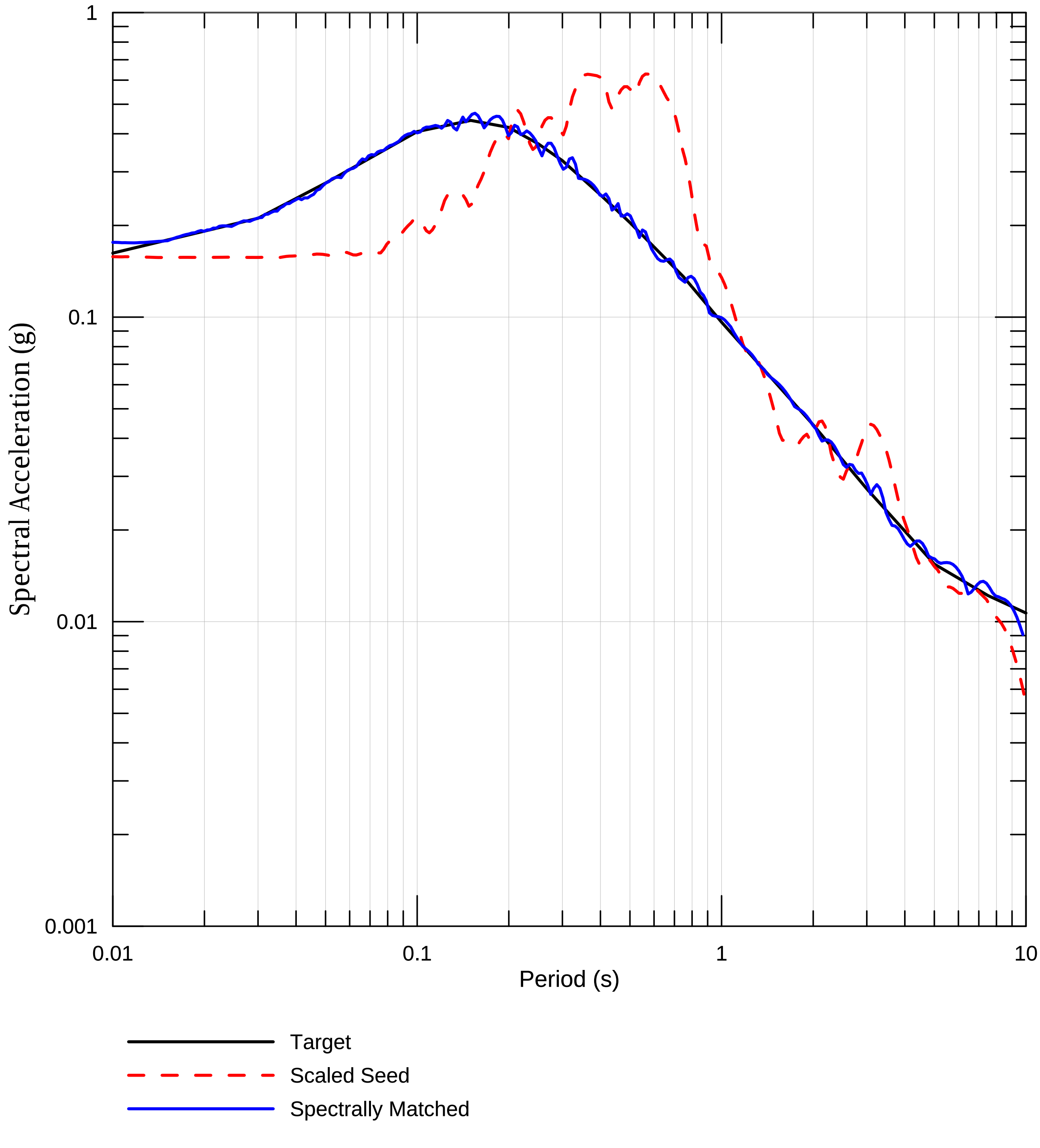

Response Spectra for Time History Spectrally Matched to 10,000-Year Return Period UHS, 1983 M 6.3 Coalinga-01 - Cantua Creek School (360), RSN 322

RESOLUTION COPPER, SKUNK CAMP TSF SITE

Lettis Consultants International, Inc.

Figure **63**

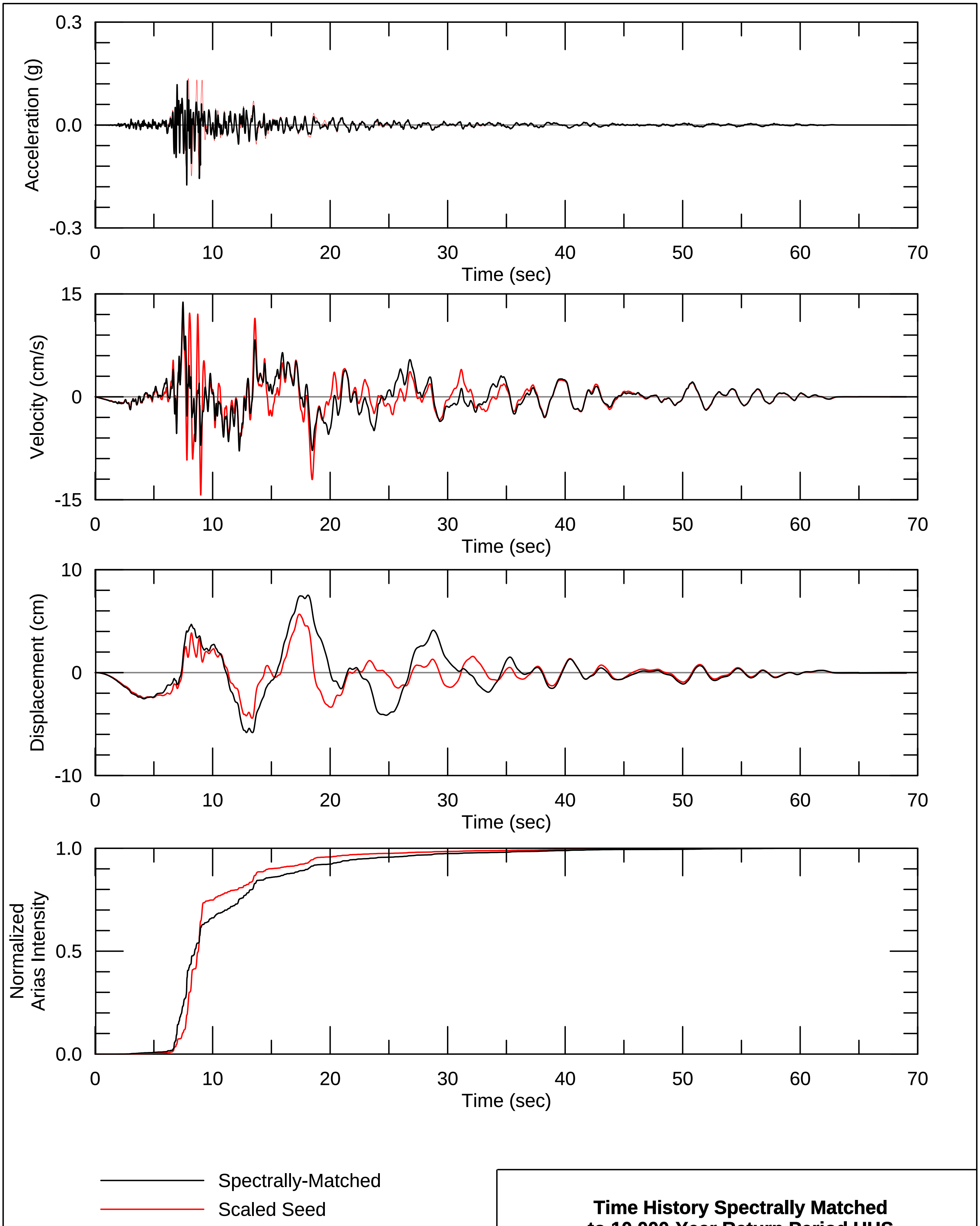

Time History Spectrally Matched to 10,000-Year Return Period UHS, 1983 M 6.3 Coalinga-01 - Cantua Creek School (360), RSN 322

RESOLUTION COPPER, SKUNK CAMP TSF SITE

Lettis Consultants International, Inc. Figure **64**

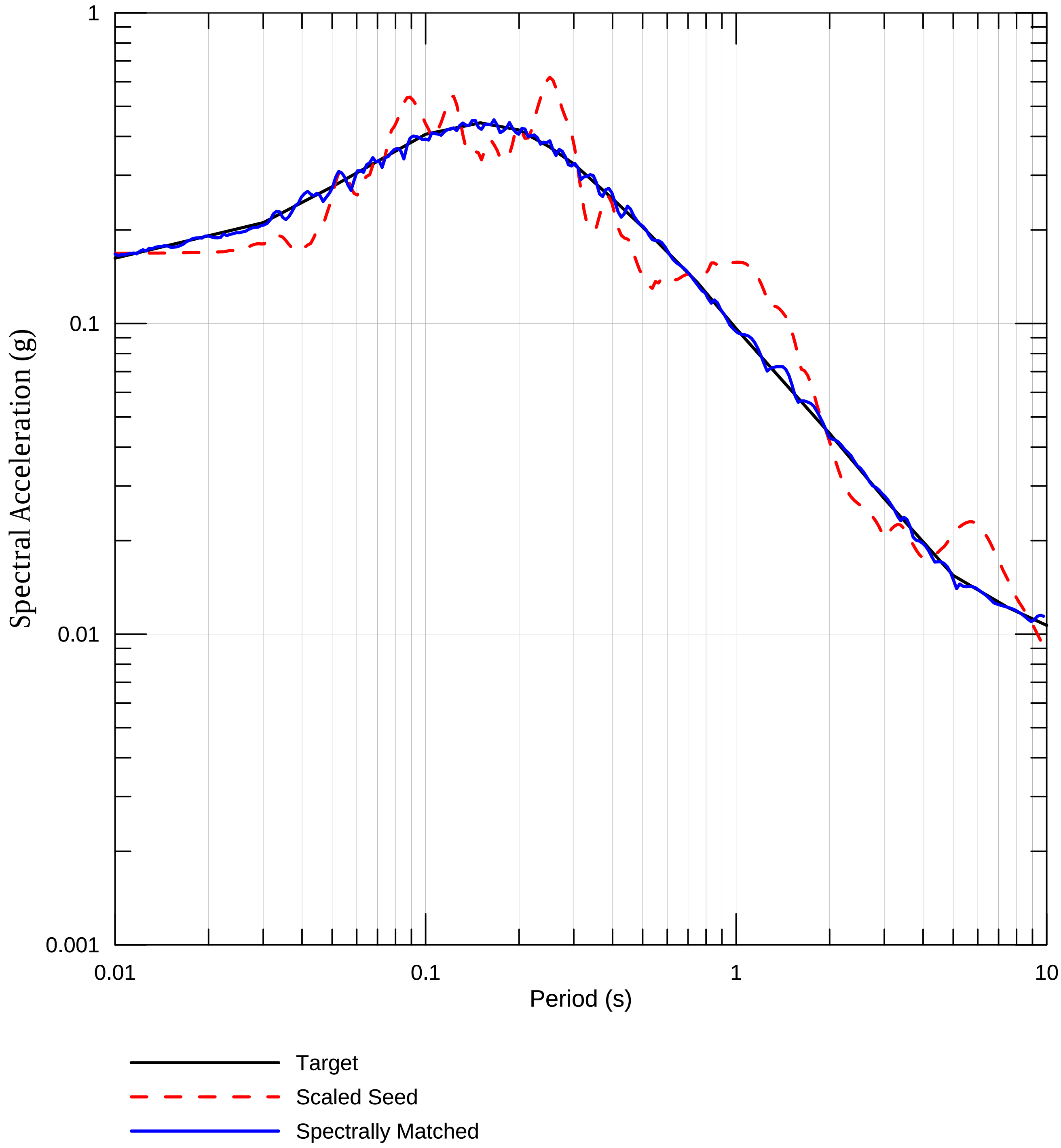

Response Spectra for Time History Spectrally Matched to 10,000-Year Return Period UHS, 1999 Chi-Chi, Taiwan-04 - TTN051 (N51E), RSN 2935

RESOLUTION COPPER, SKUNK CAMP TSF SITE

LCI **Lettis Consultants International, Inc.** Figure **65**

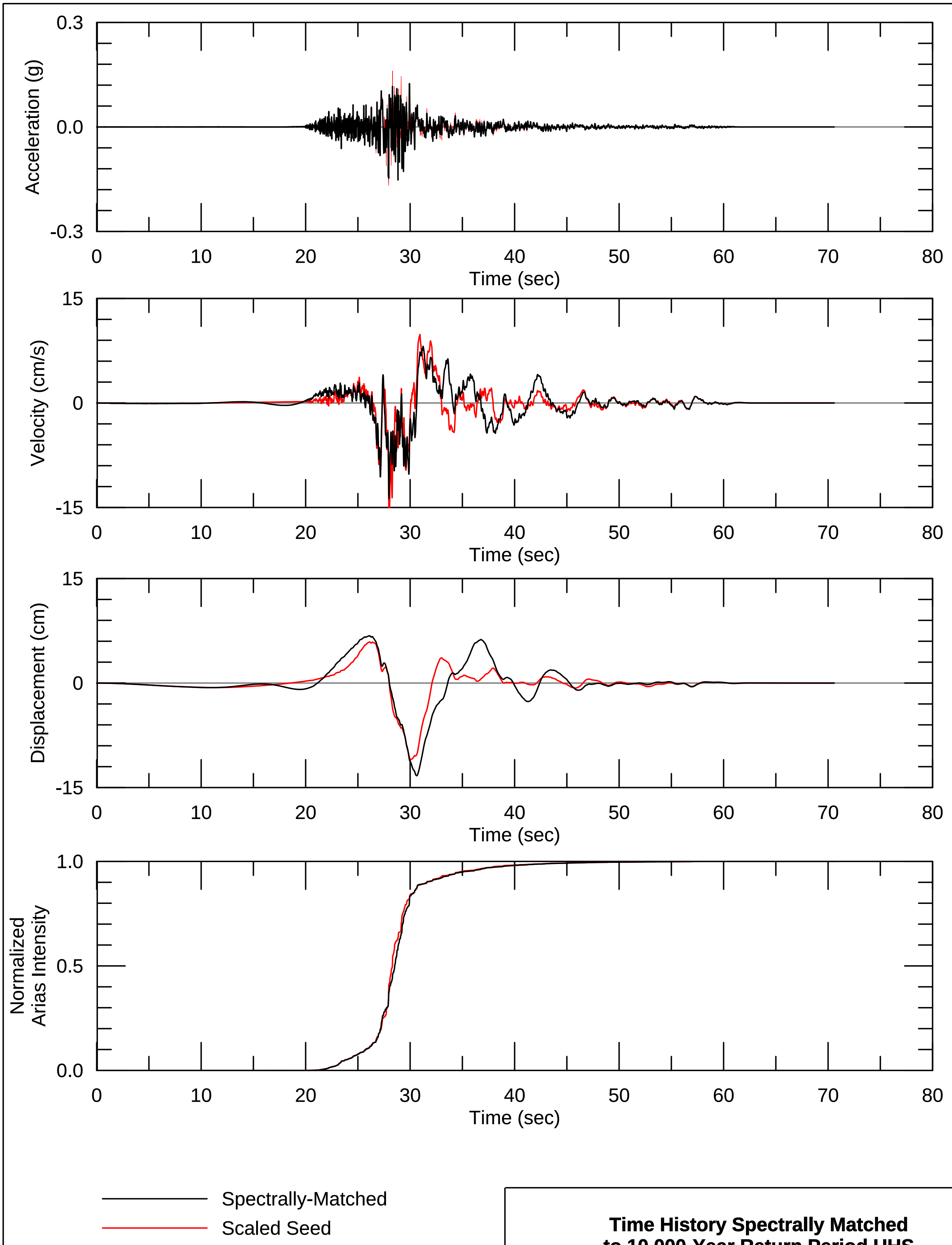

Time History Spectrally Matched to 10,000-Year Return Period UHS, 1999 Chi-Chi, Taiwan-04 - TTN051 (N51E), RSN 2935

RESOLUTION COPPER, SKUNK CAMP TSF SITE

LCI **Lettis Consultants International, Inc.** | Figure **66**

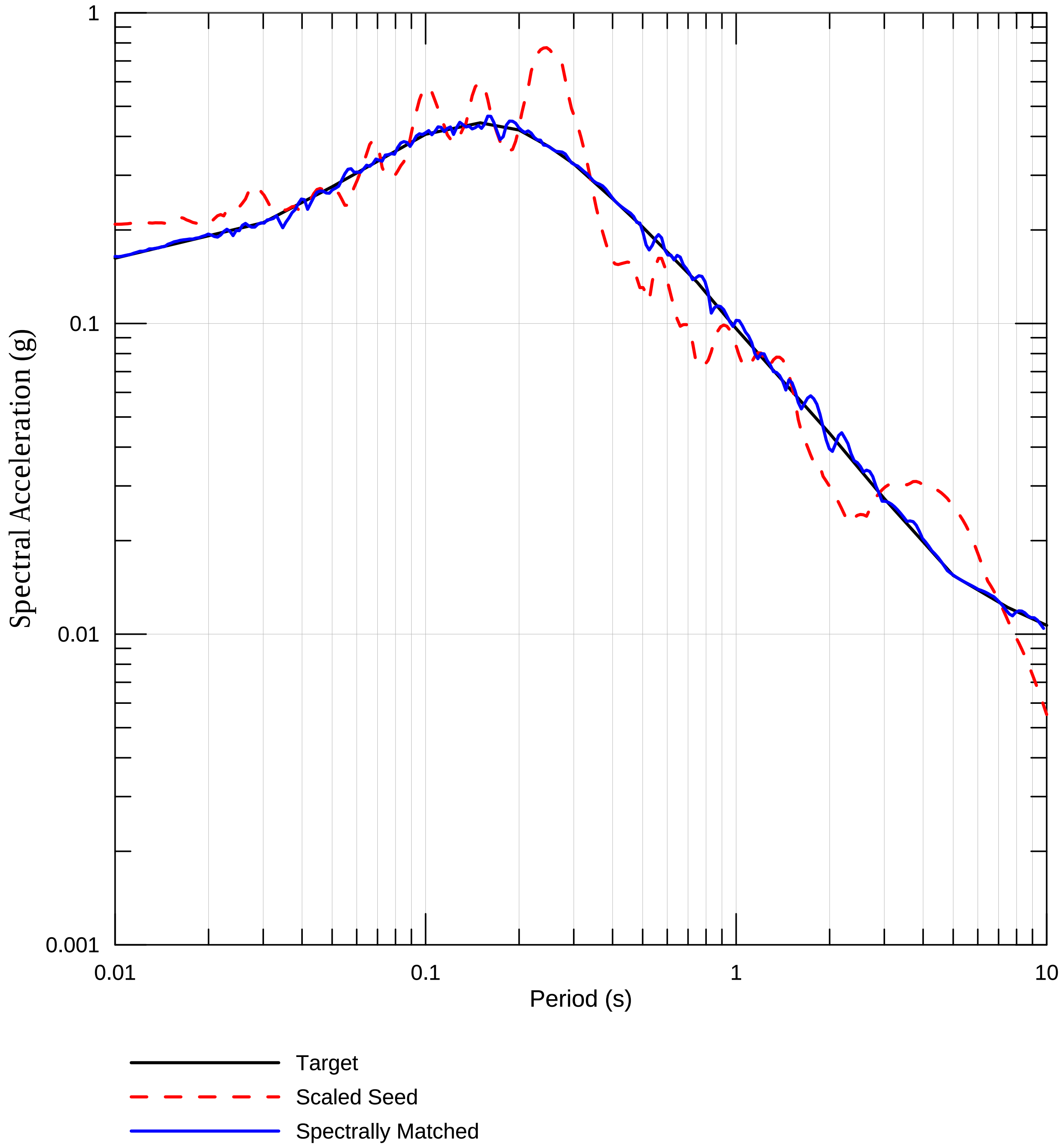

Response Spectra for Time History Spectrally Matched to 10,000-Year Return Period UHS 2009 L'Aquila, Italy - Celano (E), RSN 4472

RESOLUTION COPPER, SKUNK CAMP TSF SITE

Lettis Consultants International, Inc. | Figure **67**

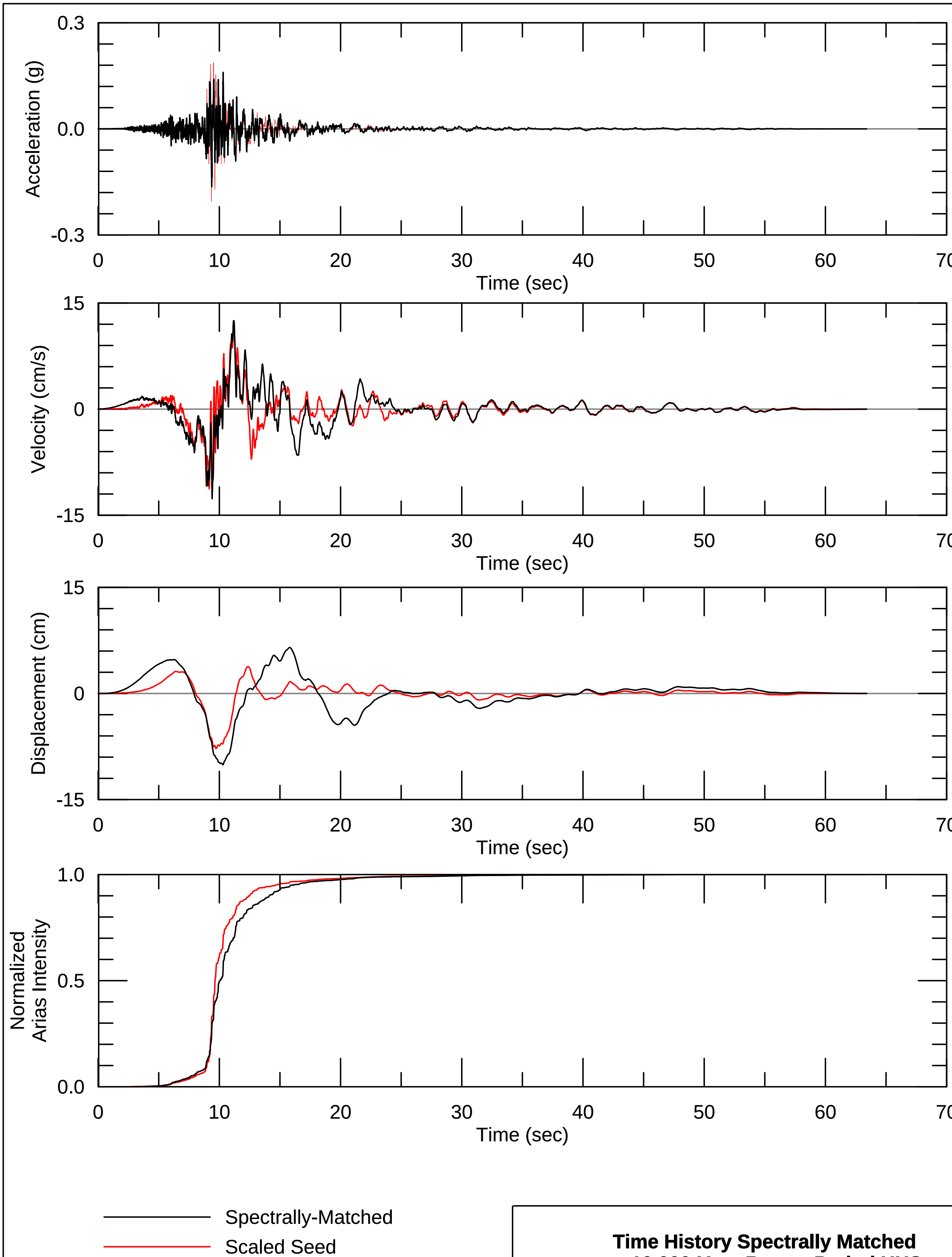

Time History Spectrally Matched to 10,000-Year Return Period UHS, 2009 L'Aquila, Italy - Celano (E), RSN 4472

RESOLUTION COPPER, SKUNK CAMP TSF SITE

Lettis Consultants International, Inc. | Figure **68**

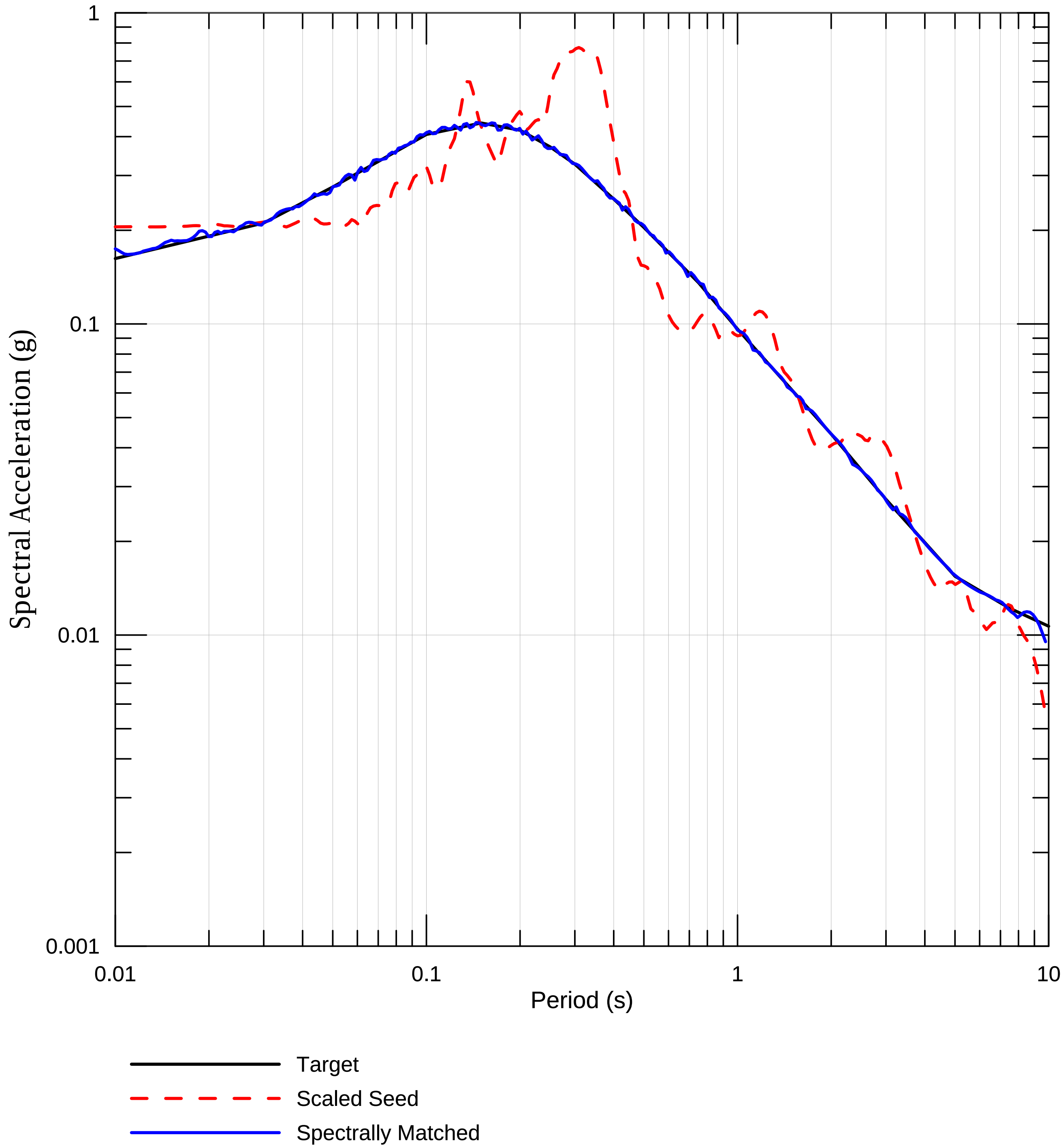

Response Spectra for Time History Spectrally Matched to 10,000-Year Return Period UHS 2011 M 6.2 Christchurch, New Zealand - SWNC (N24E), RSN 8136

RESOLUTION COPPER, SKUNK CAMP TSF SITE

Lettis Consultants International, Inc. | Figure **69**

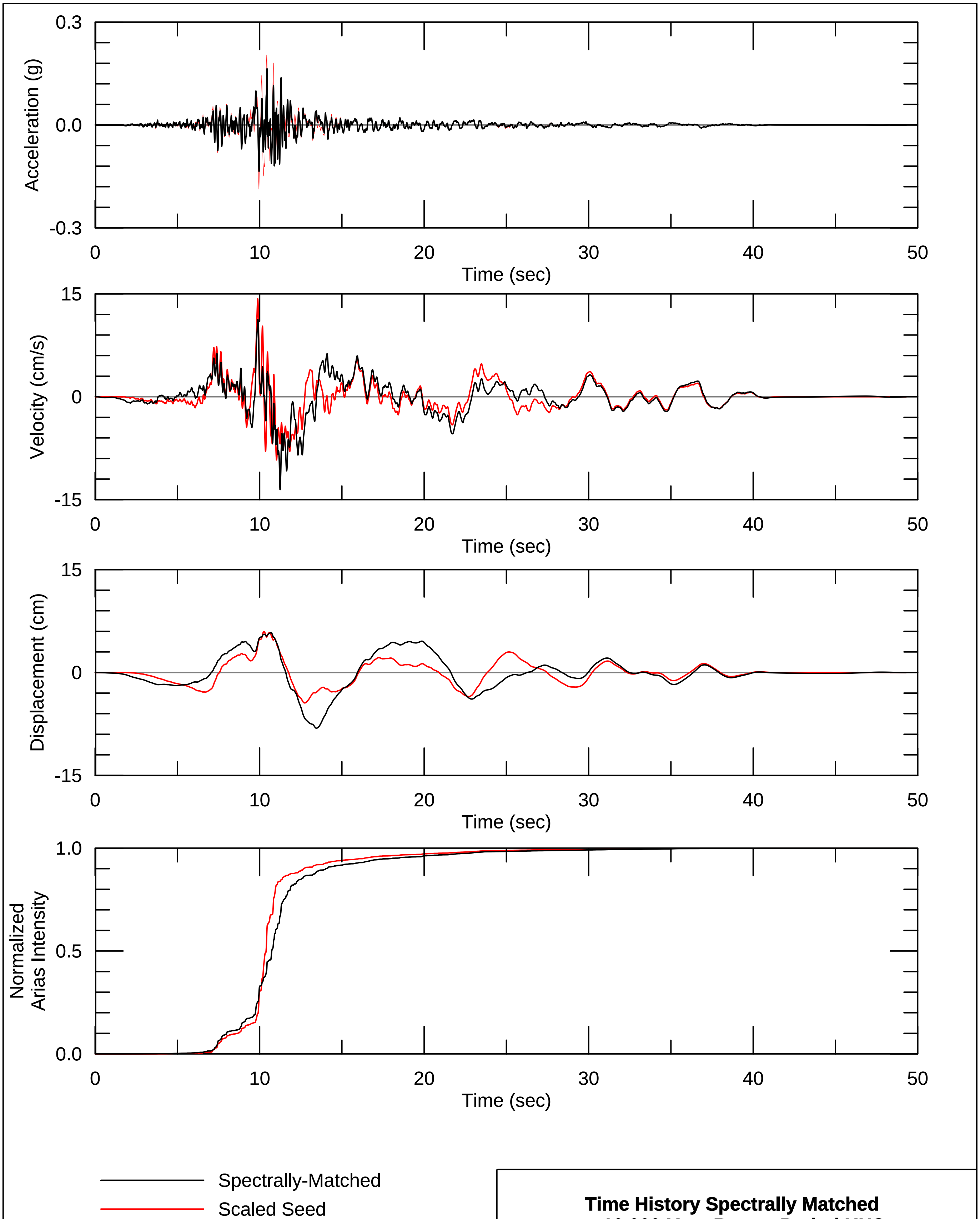

Time History Spectrally Matched to 10,000-Year Return Period UHS, 2011 M 6.2 Christchurch, New Zealand - SWNC (N24E), RSN 8136

RESOLUTION COPPER, SKUNK CAMP TSF SITE

Lettis Consultants International, Inc.

Figure **70**